Molecular Mechanisms of Sec61-Mediated Polytopic Protein Membrane Integration

By David G. Pitonzo

A DISSERTATION

Presented to the Department of Physiology and Pharmacology

and Oregon Health and Sciences University

School of Medicine

in partial fulfillment of

the requirements for the degree of

Doctor of Philosophy

DECEMBER 2007

School of Medicine
Oregon Health and Sciences University

Certificate of Approval

This is to certify the Ph.D. thesis of

David G. Pitonzo

has been approved

[redacted]

Professor in Charge of Thesis

[redacted]

Member

[redacted]

Member

[redacted]

Member

[redacted]

Member

Table of Contents

List of Figures

II. Introduction

III. Results

B. Manuscript 2

C. Manuscript 3

List of Abbreviations

AAA-ATPase	ATPase associated with various cellular activities
ABC	adenosine tri-phosphate binding cassette
Aha1	activator of Hsp90 ATPase
ANB	5-azido-2-nitrobenzoyl
AQP	Aquaporin
ADP	adenosine di-phosphate
ATP	adenosine tri-phosphate
AVP	arginine vasopressin
BiP	binding protein
Calu 3	carcinoma, lung (human) cell line 3
CF	cystic fibrosis
CFTR	cystic fibrosis transmembrane conductance regulator
CHIP	carboxy terminus of Hsp70 binding protein
CHO	Chinese hamster ovary
CNS	central nervous system
CSF	cerebro-spinal fluid
DNA	deoxy-ribonucleic acid
DTSSP	3, 3-dithiobis(sulfosuccinimidylpropionate)
DTT	dithiothreitol
EDEM	ER degradation enhancing α-mannosidase-like protein
EDTA	ethylene-diamine tetra-acetic acid

EM	electron microscopy
ER	endoplasmic reticulum
ERAD	endoplasmic reticulum associated degradation
FPLC	fast protein liquid chromatography
FRET	fluorescence resonance energy transfer
GlpF	glycerol uptake facilitator
GPCR	G-protein coupled receptor
GRP	glucose regulated protein
GTP	guanosine triphosphate
Hop	Hsp70/Hsp90 organizing protein
Hsp(c)	heat shock protein (cognate)
IB	immunoblot
IP	immunoprecipitation
MDCK	Madin-Darby Canine Kidney cells
MDR	multi-drug resistance protein
mRNA	messenger ribonucleic acid
NBD	nucleotide binding domain or 7-nitrobenz-2-oxa-1, 3-diazo-4-yl
NDI	nephrogenic diabetes insipidus
NPA	asparagine-proline-alanine
npl4	nuclear protein localization protein 4
NTP	nucleotide tri-phosphate
ORCC	outward-rectifying chloride channel
OST	oligosaccharyltransferase

PCR	polymerase chain reaction
P-gp	P-glycoprotein
PK	proteinase K
PKA	protein kinase A
PMSF	phenylmethylsulfonyl fluoride
Puro	puromycin
R	regulatory domain
RC	regulatory cap
RNA	ribonucleic acid
RNC	ribosome-nascent chain complex
RRL	rabbit reticulocyte lysate
RTC	ribosome-translocon complex
SDS-PAGE	sodium dodecyl-sulfate polyacrilimide gel electrophoresis
SR	signal sequence receptor
SRP	signal recognition particle
TCA	trichloroacetic acid
TM	transmembrane segment
TMD	transmembrane domain
TRAM	translocating chain associated membrane protein
TRAP	translocon-associated protein
tRNA	transfer ribonucleic acid
TX-100	Triton X-100
UBA	ubiquitin associated

UBC	ubiquitin-conjugating
UBX	ubiquitin regulatory-X
ufd1	ubiquitin fusion domain 1
UV	ultraviolet
V2	vasopressin-2
WT	wild type

Acknowledgements

A great many people have provided support during my time as a graduate student. I would first like to thank the faculty of the Dept. of Physiology and Pharmacology for laying the groundwork and providing excellent advice during my first 2 years. Special thanks also go to Beth Dupriest and Paolo Vianney Rodrigues for comradeship during this time. I would like to especially thank Jon Oberdorf, Heather Sadlish and Colin Daniel for all their help when I first joined the Skach lab. I would also like to thank a great bunch of technicians, Joel Elege, Jamie Knowles, Fred Larabee, Barbara Leighton, Karl Rusterholtz and Zhongying Yang for all their hard work in keeping the lab up and running and, the last three especially, for all their hard work generating the ANB-tRNA probe. Thanks also go to Eric Carlson, Teresa Buck, Toru Shibatani, Presanna Devareneni and Brian Conti for many spiriited discussions about science.

Thank you to my past and present advisory committee members, David Dawson, David Farrens, Bruce Schnapp, Matthew Sachs and Jeff Karpens for sitting through long meetings and providing excellent advice and especially for helping to keep me on track.

Special thanks are due to Bill Skach, my mentor and thesis advisor for putting in long hours every day, always being available to talk and help solve problems and for his faith in my ability to complete this work.

Most importantly, to my family, Beth, Michael and Jesse for supporting me through these past five years and for understanding that I had to miss alot of time with them, I love you all and will make you proud.

Abstract

A major challenge of modern biology is elucidating the mechanisms used by polytopic membrane proteins to achieve native tertiary structure in living cells. This challenge is made more acute because of the increasingly recognized number of diseases caused by the inability of membrane proteins to fold correctly. Early events of polytopic protein folding occur in the membrane of the endoplasmic reticulum and are orchestrated by the ribosome-translocon complex, a >3MD multi-component machine that is responsible for correctly orienting lumenal and cytosolic domains and inserting transmembrane segments into the lipid bilayer. The core component of the translocon is the sec61$\alpha\beta\gamma$ heterotrimer, hypothesized to serve as a passive conduit for translocation and integration via an axial translocation pore and a lateral integration passage. Polytopic proteins have been further hypothesized to independently insert individual TM segments, via the translocon, into the lipid bilayer prior to folding. Here we use a photocrosslinking approach where a photoactive probe is coupled to a modified aminoacyl tRNA engineered to read through a UAG (amber) stop codon. Amber codons are engineered via PCR into cDNA templates and serially truncated to represent progressive points during synthesis. Because these templates contain no termination stop codon, they remain attached to the ribosome, thereby generating a uniform cohort of integration intermediates. We first examine the biogenesis of a complete native polytopic protein, aquaporin (AQP) 4. A series of truncations of AQP4 with probes engineered in one of three consecutive residues in the center of each TM permit us to examine the interaction of each TM with sec61 alpha as it enters and traverses sec61α. This study reveals that each TM initially enters sec61 in a

preferred orientation and is sequentially replaced in this primary site by the downstream TM. Further, TMs can enter into different molecular environments proximal to sec61 as synthesis progresses. As many as 4 TMs can reside in proximity to sec61α simultaneously. We then use a similar approach to examine the early interactions of a TM derived from the second transmembrane domain of the cystic fibrosis transmembrane conductance regulator (CFTR). Here we find that, unlike AQP4 TMs, CFTR TM8 has a prolonged initial contact with sec61 and maintains this proximity even after peptidyl-tRNA cleavage with puromycin. Additionally, this persistent interaction is due to the presence of a charged aspartate residue, D924, in the center of TM8. When energy is depleted by addition of apyrase, release of TM8 from sec61 alpha is significantly delayed. When D924 is replaced with valine, TM8 no longer demonstrates a persistent interaction and leaves the translocon sooner. A third study of full length CFTR using velocity centrifugation gradients reveals that full length CFTR remains in association with the ribosome-translocon complex after completion of synthesis and is slowly released. In oocytes, replacement of fresh oocytosol facilitates release as does the addition of NTPs. These studies demonstrate that multiple TMs of polytopic proteins can remain in the vicinity of sec61 prior to integration and that certain substrates can remain associated with sec61 alpha after release from the ribosome. This suggests that sec61 plays an active role in the biogenesis of membrane proteins and that integration of multispanning proteins is more complex than previously thought.

II. INTRODUCTION

Membrane protein folding is an important but poorly understood area of modern cell biology. Membrane spanning proteins have been estimated to comprise 20-30 % of open reading frames in both prokaryotes and eukaryotes [1]. These gene products code for ion channels, transporters, enzymes, hormone receptors and signaling molecules. Further, it is increasingly recognized that many diseases are caused by improper folding and subsequent degradation or aggregation of aberrant proteins [2]. The pharmacological correction of misfolded proteins is an area of increasing study both academically and commercially. While several compounds have shown promise in correcting membrane protein folding defects in the laboratory [3, 4], little is understood of their mechanism of action. Additionally, despite advances in the pharmacology of protein folding, early biogenesis pathways of membrane proteins remain poorly elucidated. A key question concerns how membrane proteins are initially integrated into the lipid bilayer. Understanding folding pathways of polytopic substrates will be critical in the rational design of therapeutic compounds aimed at both misfolding-prone nascent proteins and/or the machinery that directs the folding process.

A) Protein folding: General considerations:

1) The folding of soluble proteins.

The folding of cytosolic proteins has been extensively studied and is operationally defined as the acquisition of the lowest free energy state accessible on a practical time scale (reviewed in [5]). For aqueous proteins, it is generally accepted that the principal driver of folding is an intramolecular hydrophobic effect; the transfer of non-polar amino

acid side chains into a non-polar environment. This process is energetically driven by loss or gain of polar interactions between water (solvent) molecules. The formation of hydrogen bonds between amino acid side chains and/or backbone atoms is required to further stabilize the interior protein fold [5]. For most proteins this process occurs in several steps. First the formation of secondary structure (i.e. alpha helix, beta sheet), second the acquisition of early tertiary structure ("molten globule"), and lastly compaction into the final native structure by extrusion of water molecules from the protein's interior. The cumulative interplay of hydrogen bonds, van der Waals forces and hydrophobic interactions lead to the lowest free energy state. Interestingly, most soluble proteins possess only marginal stability at room temperature. Therefore, even minor interactions that lower or raise the free energy state can influence overall structure [6].

2) The folding of membrane proteins

Compared to soluble proteins, membrane protein folding is less well understood. Because membrane proteins span a lipid bilayer separating two compartments, lumenal and cytosolic domains must be properly oriented and the transmembrane segments (TMs) integrated into the membrane. Membrane protein folding has therefore been viewed traditionally as a two-step process. Alpha-helical transmembrane segments first equillibrate into the lipid bilayer and helical packing drives native structure acquisition within the membrane lipid environment [7, 8]. Indeed, a number of early studies suggested that TMs enter a lipid-containing environment as soon as they are targeted to the membrane [9, 10] and, in the case of polytopic proteins, that TMs enter the membrane in rapid succession [11]. Critical to this model, though, is the assumption that all TMs are inherently stable in the lipid bilayer. While the two-step model provides an initial

hypothesis to drive investigation, experimental evidence increasingly points toward more complex scenarios. For example, some TMs are unable to integrate as isolated segments due to the presence of polar/charged residues or inadequate length to span the apolar interior of the membrane [12-15]. This leaves two extant models of transmembrane protein integration as it relates to folding, 1) the sequential model, in which TMs enter the lipid bilayer one at a time in the order of synthesis, and, 2) a coordinated/cooperative model, in which TMs accumulate within some non-lipid environment prior to de facto integration.

3) The role of chaperones

Protein folding is essentially the thermodynamic decoding of an amino acid sequence into its tertiary structure. This has traditionally been studied by denaturation of full-length proteins and examining their refolding in dilute solutions. However, because translation proceeds vectorially from N- to C-terminus and proteins emerge progressively through the ribosome tunnel, all regions of a polypeptide are not simultaneously available when folding is initiated in cells. In order to prevent off pathway intermediates, cells utilize chaperone proteins to mask hydrophobic surfaces, improve solubility and prevent aggregation in the crowded milieu of the cytosol. Cytosolic chaperones alter the free energy of folding by slowing folding kinetics and increasing folding efficiency. For example, Hsp70 chaperone proteins represent a ubiquitous family that each contain a binding pocket, access to which is regulated by ATP hydrolysis and various co-factors. ATP binding opens the pocket to enable substrate binding and release (reviewed in [16]). The pocket binds short hydrophobic stretches of amino acids which would normally be

buried in the hydrophobic interior of the folded protein [17]. Repeated cycles of ATP binding and release allow the protein to continually sample folding landscapes both co- and post-translationally. The Hsp90 family is another widely studied group of chaperones which usually functions as part of a large complex. Substrates can be transferred from Hsp70 to Hsp90 by Hop which has binding sites for both chaperones [18].

The lumen of the endoplasmic reticulum possesses its own set of chaperones, including an Hsp70 family member (BiP), an Hsp90 family member (grp94), numerous protein disulfide isomerases and calnexin/calreticulin [19, 20]. Calnexin/calreticulin are lectins that monitor modifications to N-linked glycans to determine whether the substrate should be trafficked or degraded [21]. Chaperones can, therefore, work through different mechanisms, often in response to the unique conditions within different compartments. Membrane folding in the lipid environment is facilitated by a unique complex called the Sec61 translocon. Its primary role is thought to be axial translocation of hydrophilic peptide domains into the ER lumen and the lateral partitioning of hydrophobic TMs into the lipid bilayer. Sec61 is currently thought to act as a passive conduit for translocation and integration, without engaging in specific substrate interactions. However, should Sec61 have chaperone function as suggested in manuscript 3, this might manifest as the stabilization of polar residues within a TM helix to prevent off-pathway interhelical hydrogen bonds in the lipid-transitional environment.

B) The Translocon

1) Structural insights.

The translocation/integration process begins when a translated signal sequence reaches the end of the ribosome exit tunnel and binds the cytosolic signal recognition particle (SRP). This results in translational pausing and subsequent targeting of the ribosome-nascent chain complex (RNC) to the signal sequence receptor (SR), an integral ER membrane protein [22, 23]. Signal sequence release from SRP then occurs through coordinated hydrolysis of GTP by SRP and SR resulting in ribosome transfer to a core component of the translocon, Sec61α, a ten-spanning protein (Figure Intro-1). The signal sequence binds to Sec61α and, in a separate but highly coordinated step, opens the lumenal end of the translocon to allow translocation of the elongating nascent polypeptide [24-26]. The core of the translocon is comprised of an oligomeric arrangement of the Sec61αβγ heterotrimer. Compartmental integrity is proposed to be maintained by ribosome binding at the cytosolic end of the translocon [27] and by BiP [28, 29], an ER lumenal Hsp70 family member, at the lumenal end [30]. In addition, he translocon contains the translocating chain-associated membrane protein (TRAM) which interacts with the N-terminus of certain signal sequences [31, 32] and is necessary for the translocation of certain substrates [33-36]. The translocation-associated protein (TRAPαβγδ) also facilitates translocation of certain substrates [37]. Recently, upregulation of the TRAP heterotetrameric complex was demonstrated under ER stress conditions, accelerating ER degradation and potentially implicating TRAP in the retrotranslocation of misfolded substrates [38]. The translocon-associated oligosaccharyltransferase (OST) complex is responsible for the core glycosylation of

secretory-pathway proteins displaying the NXS/T consensus sequence [39, 40]. Interestingly, affinity of sec61 heterotrimers with OST can vary [41] although the reason for this phenomenon is still under investigation. Therefore, while minimal requirements for protein translocation consist of the signal sequence receptor (SR), sec61α, and, for certain substrates, TRAM [22, 35, 42, 43], functional translocons are more complex and the precise architecture of fully assembled, actively translocating translocon complexes remains unknown (see Figure 1-7).

A major question in membrane protein folding, therefore, is how fully assembled translocons facilitate translocation and integration. Early 3D cryo-EM reconstruction of translocons obtained from digitonin solubilized rough microsomes at 26Å resolution revealed a ~95Å torus with a thickness of ~40 Å and an inner diameter of up to 35 Å. A large central hole suggested the location of the translocating pore (Figure Intro-2). Saturation binding studies of ribosomes with increasing concentrations of sec61 suggested a stoichiometry of 2-4 sec61 heterotrimers per ribosome. The sec61 oligomer appeared to be attached to the large ribosomal subunit by a single tether with a 15-20Å gap [44]. The sec61 stoichiometry was partially validated by Snapp, et al who used fluorescence resonance energy transfer (FRET) to demonstrate the presence of at least two sec61 complexes per translocon [45]. A subsequent study of yeast RTCs at 25 Å resolution in native ER membranes with translocating polypeptides revealed 3-4 ribosomal connections to a translocon about 95 Å in diameter [46]. The gap between ribosome and sec61 was still about 20Å. Further cryo-EM studies of E coli secYEG (sec61αβγ homolog) to 8 Å resolution revealed secYEG dimers without an obvious hole

for a translocation pathway [47]. Finally, a 3.2 Å X-ray crystal structure of SecYEβ from *Methanococcus jannischii* revealed that SecY (the archael sec61α homolog) possessed inverted two-fold symmetry in which a short helix, TM2a, appeared to plug a very narrow 8-10 Å channel. Based on this structure it was proposed that single Sec61αβγ heterotrimers function as the aqueous translocating pathway [48]. A "ring" of hydrophobic residues in the center of the putative pore was proposed to seal the conduit during translocation, thereby preserving the compartmental integrity of the ER (Figure Intro-3). During active translocation, the polypeptide chain was hypothesized to dislocate the plug while TM sequences would insert between secY TMs 2b and 7 for lateral transfer into membrane lipids.

A later cryo-EM study showed intact RTCs to 10 Å resolution [49]. Fitting the previous X-ray crystal structure into the cryo EM images suggested a tetrameric secY arrangement, with dimers arranged in a "back to back" conformation, i.e. lateral gates pointing away from each other (see Figure 1-7). Although the presence of TRAM, SRα and several OST components were identified by western blot, there was no room left for them in the fitted cryo-EM structure. The model showed seven ribosomal connections that precluded the use of all but one of the four sec61 monomers as the active translocation channel (Figure Intro-4). The purpose of the additional channels was purported to be recruitment of other translocon-associated proteins and facilitation of ribosomal binding. Despite the seven ribosome-translocon connections there was still a 7Å gap noted between the ribosome and translocon. Additionally, the previous central "hole" was now seen as a depression which was not aligned with the ribosome exit tunnel

[49]. A subsequent cryo-EM reconstruction of prokaryotic secY bound to a translating ribosome [50] found two secY dimers, this time arranged in a front to front configuration (see Figure 1-7). Notably, only three ribosome connections were noted in this study.

In summary, cryo-EM images of detergent solubilized translocons consistently suggest a gap between sec61 and the ribosome, but, as resolution improves, the width of this gap decreases and the number of connections between ribosome and translocon increases. While these structural translocon studies shed light on how the core complex may be assembled, the true nature of fully assembled functional translocons remains to be elucidated. Further, the location, orientation and stoichiometry of some translocon components (e.g. TRAM, OST) remain entirely unknown. The arrangement of Sec61$\alpha\beta\gamma$ heterotrimers and, therefore, the orientation of the putative lateral integration gates is uncertain at best.

2) Functional insights

Structural studies of static, detergent solubilized complexes present a somewhat different view of translocation than functional studies utilizing intact RTCs. Specifically, fluorescence quenching studies from the Johnson laboratory examining fluorescence lifetimes and iodide quenching of 7-nitrobenz-2-oxa-1,3 diazo 4-yl (NBD) demonstrated that nascent secretory proteins traverse a large aqueous pathway extending through the ribosome and translocon [24]. Translocating nascent polypeptide chains are inaccessible from either cytosol or lumen until at least 70 amino acids are synthesized after which they become accessible only from the ER lumen [25]. As a TM segment is synthesized,

the lumenal pore closes and, over the synthesis of just 2 additional residues, the ribosome translocon junction relaxes to expose the polypeptide to the cytosol [27]. These highly coordinated gating events are mediated by the TM inside the ribosome tunnel [27] (Figure Intro-5). Further, the diameter of the active translocation pathway using collisional quenching agents of varying sizes demonstrated a large aqueous pore that admitted quenching agents between 40-60 Å [51]. Further refinements to the above picture were elucidated using RNCs with either depleted, intact or BiP loaded microsomes, demonstrating that BiP is responsible for closing the lumenal gate prior to relaxation of the ribosome translocon junction [28]. Additionally, different sized quenching agents demonstrated a distinct difference in pore size when BiP sealed the pore [52]. BiP assumes an ADP bound conformation during sealing and an ATP bound conformation when opening the pore [29]. FRET analysis demonstrated that closing and opening of the lumenal and cytosolic ends of the tranlocon occured when the TM folded into helical or near-helical conformation inside the ribosome tunnel [53]. Clearly the narrow pore size noted in the X-ray crystal structure [48] must be reconciled with these extensive biophysical studies of functional translocons.

Because the translocation channel functions to transfer TMs to a lipid-containing environment [9, 10, 14] it has been hypothesized that TM integration might be driven by simple thermodynamic partitioning through the putative lateral gate into the lipid bilayer. An important issue, however, concerns the assembly and integration of multiple TMs as demonstrated for certain proteins. For example, carbonate [54] and urea [55] extraction of TM segments of P-glycoprotein showed that, even after translocon entry and

establishment of a transmembrane orientation, individual TMs were not fully integrated in the membrane. An additional study on a chimeric substrate showed that a shorter hydrophobic TM relied on a longer purportedly stronger signal anchor for integration [56]. One question with major implications for translocon structure and membrane protein folding is whether multiple TMs might reside in the translocon prior to the final stages of integration (e.g. see figure 2-7). How would a translocon be assembled to accommodate multiple TMs? How do these individual TMs integrate?

Topogenic determinants are discrete sequences in a polypeptide that direct translocation and integration events. For example, a "signal anchor" is defined as a TM sequence that targets to the ER membrane and directs translocation of flanking residues. If the N-terminus is translocated, the signal anchor is classified as "type I". Conversely, "type II" signal anchors translocate their C-terminus. Precise mechanisms of how translocation specificity is achieved is unclear (see section 4 below). However, both types of signal anchors open the axial translocon gate. Alternatively, "stop transfer" sequences terminate ongoing translocation and thereby direct C-terminal sequence into the cytosol [184, 207, 219].

The mechanism by which type II signal anchors orient to position their N- and C-termini in the the proper compartment constitutes a key question in translocon function. As translation proceeds, the nascent protein exits from N-to C-terminus. Type II signal anchors must, therefore, rotate in order to achieve their final transmembrane orientation. This rotation is partially driven electrostatically by the "positive inside rule" and

sterically by potentially folded N-terminal domains [57]. Interestingly, it has been demonstrated that rotation may occur inside the translocon for certain substrates, and can be blocked by the glycosylation of an upstream loop [58]. The question then is where within a narrow-pore model could this occur? A related concern is the close spacing of TMs which occurs in many polytopic proteins, i.e 2 consecutive TMs separated by only 1-5 amino acids. For example, in manuscript 2, we show that two closely spaced TMs in aquaporin 4 (TMs 4 and 5) can simultaneously enter and reside near sec61. How does the translocon accommodate entry by two TMs, the concommitant rotation of one of them, plus a loop?

3) The structure/function dilemma.

Cryo-EM and X-ray derived translocon structures must be reconciled with functional translocon studies and the topogenic requirements of substrates. The X-ray structure of secY [48] shows a narrow translation pore and a potential lateral gate which could potentially accommodate, at most, one TM. Because this structure was derived in the closed state, it has been hypothesized that conformational changes occur that could widen the lateral gate during translocation. Even with molecular modeling, however, the potential space within a sec61 monomer is insufficient to accommodate multiple TMs with concommitant rotation of a type II signal anchor [50]. Part of the answer may lie in the orienation of secY/61 dimers, i.e. front to front vs. back to back (see Figure 1-7). If oriented front to front, two heterotrimers could potentially work in tandem, but, to date, the engagement of two sec61 molecules by a single translocating polypeptide has not

been demonstrated. Further, the Hamman study [51], demonstrating an aqueous pore size >40 Å, must be reconciled with the 5-8 Å pore of the x-ray crystal structure.

A second issue concerns the role of the helix 2a plug as a compartmental barrier vs. the role of BiP. Interestingly, studies in *S. cerevisiae* show the plug region to be dispensible [59] whereas studies in *E coli.* suggest the plug is important to maintain a seal [60]. It should be noted that both *Archaea* and *Prokarya* do not posses BiP homologs, therefore, helix 2a may actually perform different functions in different organisms. In eukaryotes, stabilization of sec61 oligomeric assemblies is a hypothesized helix 2a function [61].

4) Gating and the ribosome/translocon complex

Recognition of topogenic information contained within the primary protein sequence must precisely direct axial and lateral translocon gating events. In this regard, evidence indicates a three-way communication amongst the ribosome, translocon and nascent chain in which the ribosome-translocon complex functions as a cohesive machine for the precise orientation of cytosolic, lumenal and transmembrane domains [27, 62, 63].

The structure-function dilemma results in two competing models for axial gating into the ER lumen. Functional studies suggest that a large pore [51] forms by an oligomeric arrangement of sec61 heterotrimers. The cytosolic side is gated by the ribosome and the lumenal side is closed by BiP [24, 25, 28, 29, 51]. As a newly synthesized TM inside the ribosome tunnel forms an alpha helix [27, 53] a conformational change is transmitted to the translocon resulting in lumenal closure by BiP [52]. BiP closure is followed by loosening of the ribosome translocon junction and exposure of the nascent chain to the

cytosol. The tight coupling of lumenal closure and cytosolic accessibility leads to the hypothesis that both compartmental integrity and membrane protein topology might be established by alternating cycles of cytosolic and lumenal gating (Figure Intro-6). This model leaves several unanswered questions. For example, how does the ribosome distinguish the large variety of TM sequences to direct proper gating events? How are gating events precisely regulated as translation proceeds at 5 aa per second? Alternatively, the structural gating model is based upon the cryo-EM and x-ray secY crystal structures [44, 46, 48, 64, 65]. In this model, a gap of 12-15Å exists between the ribosome and translocon, permitting continuous access to the cytosol. The membrane barrier is maintained inside the narrow 8-12Å channel by the pore ring and the helix 2b plug in the closed state. Questions posed by the x-ray-derived structural model include how multiple TMs and loops occupy a translocon simultaneously and how the translating protein is redirected from cytosol to lumen. If Sec61$\alpha\beta\gamma$ stoichiometry is tetrameric, why is only one heterotrimer used for active translocation and what is the function of the other sec61 heterotrimers and co-associated proteins [49, 60]?

There is evidence to suggest that the ribosome may remain bound to the translocon after the completion of synthesis [66]. Ribosomes carrying SRP bound signal sequences can effectively compete-off pre-bound ribosomes. Conversely if a pre-bound ribosome encounters an mRNA for a cytosolic protein lacking a signal sequence, its affinity for the translocon is decreased, leading to dissociation [67, 68]. This raises the question of whether the ribosome plays a continuing role in membrane protein biogenesis after the nascent chain is released, as is suggested in manuscript 3.

C) Integration

1) General considerations - models of integration

The "passive partitioning model" states that TMs move into the lipid bilayer alone or in groups, strictly as a consequence of their physico-chemical properties [14, 69-71]. The translocon, in this model, serves as a passive conduit to allow equilibration and thermodynamic partitioning into lipid, presumably by lateral movement between TM2b and TM7 of the Sec61α subunit. A second model, for which there is mounting evidence [13, 15, 33, 54], proposes that the ribosome-translocon complex controls the release of TMs into lipid in a highly regulated fashion that is partially determined by the state of translation. A critical difference between these models is the role of the translocon as either a passive or active conduit. The passive model also suggests that downstream steps in the folding pathway, i.e. helical packing and tertiary structure acquisition, occur after *de facto* integration into the lipid bilayer, whereas the second models allows the possibility of early helical packing prior to integration. These issues will be further addressed in section II, D and in manuscript 1. Importantly, in both of the above models, release of the polypeptide from the ribosome results in movement of TMs out of the translocon and integration in the bilayer. This occurs upon cleavage of the peptidyl-tRNA bond either by translation termination or addition of puromycin. To date, TM integration has been demonstrated by loss of crosslinking to translocon components, crosslinking to lipids and resistance to extractability of TMs with aqueous perturbants.

2) Cooperative helical interactions

Two early studies using the multi-drug transporter, MDR (P-glycoprotein), illustrate that two or more TMs might accumulate in the translocon prior to membrane integration. The first study demonstrated that TM1 or TM2 could both independently orient with proper topology, but the presence of both TMs was required for integration [54]. The second study showed that up to five TMs could be extracted with urea prior to the termination of synthesis demonstrating that MDR was not fully integrated until released from the ribosome [72].

A study using cystic fibrosis transmembrane conductance regulator (CFTR) TMD2 demonstrated that TM8 requires the presence of TM7 to acquire a transmembrane orientation [15]. Interestingly, this "cooperativity" between TMs was necessitated by the presence of a charged aspartate in the center of TM8. When TM8 was isolated and studied in a chimeric context, it was not recognized by the RTC as a TM segment and was translocated. When the aspartate was replaced with valine, the TM8 sequence terminated translocation and behaved like a *bona fide* stop transfer sequence [15]. Another study using polypeptides derived from leader peptidase showed that a short TM segment continued to crosslink Sec61 (i.e was not integrated) unless a more hydrophobic segment was present to facilitate integration [56]. These studies illustrate two important concepts: TMs do not always integrate individually and sequentially, and, TMs which often need partners in their native context can integrate independently when presented to the translocon in a different context. Again, however, integration always follows release

of the nascent chain from the ribosome either by reaching a termination codon or by peptidyl-tRNA cleavage.

Polytopic proteins have a wide variety of functions in their compartmental membranes. Voltage-gated channels, for example, contain four basic residues in the S4 segment, which acts as the voltage sensor. Such sequence diversity raises the question as to how charged residues in the center of a TM might be stably integrated into lipid [69, 73]. Even a single polar residue can influence TM recognition by the translocon [15]. Further, many TM helices of membrane channels are amphipathic, due to their role as barriers between the lipid bilayer and an aqueous conduit. From a biogenesis standpoint, the energy required for thermodynamic partitioning into lipid must, therefore, be balanced by structural features needed for function.

3) The role of polar/charged residues in helical association

Although the hydrophobic effect is the primary driving force for tertiary structure formation in soluble proteins, hydrogen bonding and helical packing play a greater role in folding within the apolar environment of the lipid bilayer [5]. These two primary types of interactions are driven by polar/charged residues and by the "void and pocket" mechanism [76]. Within each of these two categories, certain interactions are preferred. In the case of H-bonds, these are, in decreasing order of energetics, Asp-Arg, Asp-Lys, Asp-Asn, Asn-Asn, Asp-Tyr, His-His, Lys-Gln, Glu-Lys, Glu-Glu, Lys-Asn and Gln-Arg [76, 78, 79]. These polar residues are also intimately involved in membrane protein

function. In the apolar environment of the lipid bilayer, hydrogen bond formation plays a much greater role in the folding and stabilization of membrane proteins than in the folding of soluble proteins because competition with water molecules is eliminated in the membrane interior [76, 77]. A study of polyleucine sequences demonstrated that residues capable of either donating or accepting a shared hydrogen, i.e. Asn, Asp, Gln, Glu and His, were able to stimulate TM-oligomer formation whereas Ser, Thr, and Tyr were not [80, 81]. Interestingly, while fairly uncommon, charged residues within TM sequences tend to be very strongly conserved within protein families [82].

The role of aspartate and asparagine residues in facilitating helix-helix interactions has been extensively studied. For example, a study of leader peptidase demonstrated that the free energy of partitioning was decreased for a third short hydrophobic segment that included Asp/Asn residues [79]. Similarly, micelles incorporating NBD and tetramethylrhodamine on separate TM segments showed increased energy transfer when Asn residues were included [77]. Asn-Asn or Asp-Asp pairs introduced into TM segments could also drive helical hairpin formation while a polypeptide was still membrane extractable, implying that H-bonds between helices may begin to form within the translocon [78]. While the above studies propose that hydrogen bonding can stabilize native structure, it is unclear exactly how hydrogen bonds stabilize folding *intermediates* and, if so, whether H-bond formation could be chaperoned by translocon proteins. Regarding the possible chaperone function of sec61α, several points should be stressed. First TM the putative lateral passageway into lipid is contained within sec61α [48, 49, 50], second, TMs can contact lipid early in the integration process while still in proximity

to sec61α [9, 10], and, last, multiple TMs can accumulate near sec61α prior to integration [10, 12, 14, 72, 74]. While other translocon proteins such as TRAM [33] and OST [75] have been shown to interact with substrates following the completion of synthesis, this has never been demonstrated with sec61α. If persistent interaction with sec61α could be demonstrated and if this persistent interaction were dependent upon a polar residue, this would strengthen the argument that sec61α might form specific interactions with its substrate. In manuscript 3, we demonstrate polar residue-dependent persistent crosslinking to Sec61α. This suggests an intermolecular helix-helix interaction between CFTR-TM8 and sec61α that may represent a chaperoned folding intermediate.

D) Model proteins used in these studies

1) Aquaporins

Aquaporins (AQPs) constitute a ubiquitously expressed family of six-spanning polytopic proteins that serve as water channels. Two re-entrant loops each containing a canonical NPA motif form a selectivity filter for water and/or glycerol. There are thirteen known human family members which are expressed in a tissue specific manner.

a) Aquaporin structure

A major advance in understanding how water is transported across biological membranes came with the the first 2D cryto-EM structure of human AQP1 to 3.8 Å [83]. This landmark study was the first known structure of a human membrane protein to nearly atomic resolution. A 2.2 Å resolution x-ray crystal structure of the *E. coli* glycerol

channel GlpF soon followed [84]. Further refinement of AQP1 structure came with the 2.2Å x-ray crystal structure of bovine AQP1 [85]. These structures all revealed a 2-fold pseudosymmetric hourglass, narrowing at the selectivity filter (see manuscript 1, fig 1). Sequence homology of the N- and C-terminal halves suggest that the channel arose as the result of gene duplication [86]. TMs were tilted as much as 30 degrees with respect to the membrane normal [87]. Molecular dynamics simulations revealed a mechanism by which water molecules pass in single file through the selectivity filter, hydrogen bonding with asparagine side chains amino groups of the NPA motif [88]. Sequential displacement of water molecules from this site therefore explained high flow rates with exclusion of protons due to 180 degree flipping of the water dipole as it transits the selectivity filter [89]. Although each AQP monomer possesses an independent water pore, aquaporins function as tetramers that form in the ER prior to trafficking [90].

b) Functions and Diseases of Selected Aquaporins

In the kidney, AQP1 is responsible for 50% of water and solute reabsorbtion from the glomerular filtrate [91]. Rare individuals have been identified that contain AQP1 missense/deletion mutations. These patients present with a mild phenotype suggesting that loss of proximal water reabsorption can be partially compensated by more distal nephron segments [91].

AQP 2 is generally found in the distal tubule and collecting duct where it serves as the major regulator of water reabsorption. Regulation of AQP2 involves the insertion of AQP2 molecules into the apical membrane of the renal collecting duct under control of

the vasopressin (AVP)-responsive V2 receptor [92]. Misfolding of either AQP2 or the V2 receptor is implicated in the pathogenesis of nephrogenic diabetes insipidus (NDI), causing excretion of a dilute urine that leads to severe dehydration [95]. Studies in CHO and MDCK cells demonstrate improved trafficking of mutant AQP2 in the presence of glycerol, suggesting that the folding pathway might be amenable to pharmacologic manipulation [93, 94].

AQP4, the model protein studied in manuscript 2, is expressed mainly in the brain and the renal collecting duct, wih lower levels seen in other tissues [96]. AQP4 is expressed in brain astrocytes and is notably localized at the blood-brain and blood-CSF barriers. AQP4 knockout mice have demonstrated the channel's role in water balance, astrocyte migration and signal transduction. The role in water balance is particularly interesting because the knockout phenotype is only apparent after a CNS insult. The AQP4 knockout conferred protection against cytotoxic insults such as that seen in meningitis but led to exacerbation of vasogenic edema as would be seen in brain abscess or tumor [97]. Pharmacologic manipulation of AQP4 expression or function may therefore prove clinically valuable in the treatment of CNS tumors, traumatic brain injury or stroke. More detailed knowledge of the AQP4 folding pathway would aid in this endeavor.

c) AQP Topogenesis

Aquaporins are excellent model proteins due to their relatively simple topology and known structure [98, 99]. For AQP4, its six-spanning topology is established as each TM

exits the ribosome. In contrast, AQP1 topology is acquired non-sequentially and predominantly post-translationally [98, 100]. Specifically, AQP1-TM2 is initially translocated into the ER lumen, TM3 is inserted in a type I transmembrane configuration and TM4 is oriented in the cytosol as the peptide exits the ribosome. Rotation of TM3 to a type II configuration with concomitant insertion of TMs 2 and 4 into their transmembrane orientation occurs only subsequent to the synthesis of TMs 5 and 6. Interestingly, this mechanism is partially driven by polar residues N49/K51 that flank TM2 because replacing corresponding residues from AQP4, M48/L50 enables AQP1-TM 2 to co-translationally terminate translocation and stop in the plane of the membrane [101]. However, the N49M/K51L mutations block AQP1 function by interfering with monomer folding and tetramerization [102]. This illustrates how residues important for function can often impact biogenesis. AQP4 was chosen for initial studies of native polytopic protein integration in manuscript 2 because, unlike AQP1, AQP4 topology is established sequentially and co-translationally.

2) The cystic fibrosis transmembrane conductance regulator (CFTR)

a) Structure

CFTR has also been used to study polytopic protein folding. Cystic fibrosis (CF), caused primarily by misfolding of CFTR, is the most common, lethal inherited disease in the Caucasian population [103, 104]. While over 1500 mutations have been implicated in the CF phenotype, the deletion of a phenylalanine at residue 508 is found in at least one allele in 90% of American patients with clinical disease. CFTR is a 12-spanning

polytopic protein consisting of 2 six-spanning transmembrane domains (TMDs), two nucleotide binding domains (NBDs) and a unique regulatory (R) domain (Figure 3-1A). It is a member of the ABC transporter family and its chloride channel function is regulated by PKA-mediated phosphorylation, ATP binding at the NBD 1/NBD2 dimer interface and hydrolysis at the NBD2 consensus site. While detailed knowledge of the molecular structure of CFTR is lacking because high resolution crystal structures are unavailable, topology studies, hydropathy plots and crystal structures of prokaryotic ABC transporters have aided in developing models of the native structure (Figure 3-1) [103, 105, 106, 107].

CFTR NBD1 has been successfully crytallized as a soluble domain [108]. Interestingly, crystallization of the ΔF508 mutant of NBD1 revealed little change in the overall fold [109]. Studies suggest, however that the ΔF508 mutation interferes with the folding of NBD2, as well as the TMD1-NBD1 interface which may affect both stability and channel gating [110, 111, 112].

b) CFTR Function

CFTR acts as a chloride channel in the apical membrane of epithelial tissues where it facilitates epithelial fluid movement [113]. The primary clinical effects of CF are seen in lung, GI tract, pancreas, sweat glands and reproductive system. In addition, CFTR is thought to regulate the function of other ion channels, including the epithelial sodium channel (ENaC) and the outward-rectifying chloride channel (ORCC) [114, 115]. It may also stimulate bicarbonate secretion via an Na/HCO3 symporter, as seen in human Calu 3

respiratory epithelial cells [116]. The effects of CFTR dysfunction in the lung are the production of inspissated airway secretions, decreased bronchopulmonary clearance, chronic inflammation and repeated infections [117], ultimately resulting in decreased pulmonary function and early death.

c) Folding and disease - CF and the ΔF mutation

The ΔF508-CFTR folding defect results in an unstable molecule that becomes targeted for degradation via the endoplasmic reticulum associated degradation (ERAD) pathway [118-122]. The few ΔF508 molecules that reach the plasma membrane in heterologous expression systems also show decreased $T_{1/2}$ due to more rapid internalization [123, 124] indicating that structural defects persist even after traversing the secretory pathway. ΔF508-CFTR molecules may posses a defect in domain-domain interactions resulting in altered channel gating. During the biogenesis process, both wild type (WT) and ΔF508 CFTR molecules interact with cytosolic chaperones that include Hsp70, Hsp40 and Hsp90 [119, 125]. Previous studies have indicated that Hsp70 is involved in a biogenesis/degradation quality control checkpoint [126] while Hsp90 interactions primarily stabilize CFTR [127]. Consistent with this, a recent study implicated Hsp90 in CFTR biogenesis via a newly identified co-chaperone Aha1 [128]. CFTR molecules that fold successfully are trafficked to the Golgi where they undergo complex glycosylation, whereas those that fail to fold correctly are targeted for proteosomal degradation. In many expression systems up to 70% of WT protein and >99% of ΔF508 CFTR is degraded via the endoplasmic reticulum-associated degradation (ERAD) pathway [129]. However, in certain pulmonary-derived cell lines, WT CFTR processing is >90% efficient [130, 131].

Thus, both WT and ΔF CFTR appear to be particularly difficult folding substrates for the cell. Interestingly, the ΔF508 folding defect is temperature-sensitive and incubation at reduced temperatures (18-27° C) result in increased amounts of ΔF508 CFTR reaching the cell surface in Xenopus oocytes, S9 insect cells and CF bronchial epithelial cells [132, 133]. The small amount of ΔF CFTR that does get to the cell surface, however, is more rapidly turned over at elevated temperatures [134].

Pharmacologic manipulation has resulted in increased levels of ΔF508 CFTR at the cell surface [135] and increased cAMP activated chloride currents in ΔF508 CFTR-transfected human embryonic kidney cells [136]. More recently, high-throughput analyses of large chemical libraries have resulted in the discovery of multiple compounds that increase ΔF508 CFTR folding [137]. While use of these compounds individually results in levels of rescue too low to likely have therapeutic value, use of two compounds concommittantly results in a 2-4 fold increase in cell surface expression [138]. These studies suggest that the folding defect of mutant CFTR is amenable to pharmacologic manipulation. Identification of how such corrector molecules act will require detailed analysis of folding pathways. Because current knowledge in this critical area is extremely limited, CFTR polypeptides are frequently utilized as model integration substrates in studies of the folding pathway.

E. Experimental Strategy - Overview

The primary premise of my thesis is to examine membrane protein integration vis à vis interactions with sec61α. In order to deconvolute the integration of nascent membrane

proteins, the dynamic changes that occur during synthesis were examined using uniform cohorts of static integration intermediates. This is because nascent chains that remain tethered to the ribosome mimic transient stages of the integration process. cDNA templates used in these studies were, therefore, truncated to remove terminal stop codons to prevent interaction with release factors that cleave the peptidyl tRNA bond and release the nascent chain. Thus, all truncated polypeptide chains are trapped at the same stage of synthesis as intact ribosome-nascent chain intermediates (Figure Intro-10). By examining a series of such intermediates in separate experiments, different length truncations provide sequential "snapshots" of the nascent chain environment at progressive points in synthesis. To identify the molecular environment of each TM, a photocrosslinking probe is incorporated into the growing nascent chain using a modified aminoacyl tRNA that has been modified to recognize an amber (UAG) stop codon. By engineering amber stop codons at precise locations in the mRNA and controlling the length of mRNA by truncation, it is possible to ensure that only one photocrosslinking molecule is incorporated in each nascent chain at a precise location along the integration pathway.

1) The Photocrosslinking Probe.

The photocrosslinker used in these studies is an ε-N-5-azido-2-nitro-benzoyl-lysine (ANB-lys). This moiety contains a nitrophenyl azide for UV photolysis in which the optimal activation wavelength is shifted to 320-350 nm by the nitro group. A further advantage is that photolysis reactions can occur at physiologic pH, maintaining the biological integrity of proteins. UV irradiation of the nitrophenyl azide forms a nitrene

that is capable of reacting non-specifically with a variety of active and reactive C–H and N–H bonds (Figure Intro-7).

2) The amber suppressor tRNA and generation of ε-ANB tRNA^{Amb}

To generate the amber suppressor tRNA the anticodon of an E. coli lysine tRNA was mutated to a CUA, in place of the endogenous CUU. This tRNA is transcribed in vitro, ^{14}C-lysine is enzymatically attached and εANB is coupled to the ε-amino group of lysine. Generally, ~85-95% of amber suppressor tRNAs are ^{14}C-lysine coupled. Linking the ANB-NOS probe to ^{14}C-lys-tRNA^{Amb} is accomplished in a precisely timed reaction at pH 8.6 for 14 seconds to minimize hydrolysis of the lysine Cα ester linkage to the tRNA and ensure maximal incorporation of the probe to the ε-amino group of lysine (Figure Intro-8).

3) Engineering mRNA with UAG sites for probe incorporation.

To incorporate the ε-ANB-lys probe into the protein of interest, a unique TAG codon is introduced into the cDNA via PCR overlap extension. In our aquaporin experiments (manuscript 2), we chose incorporation sites near the center of each TM to specifically examine how TMs interact and move through Sec61. A series of truncations for each TAG-containing cDNA is then generated by PCR using antisense primers (Figure Intro-9). Each cDNA thus generated has an engineered TAG codon at a specific site, lacks a terminal stop codon and encodes a specified number of residues. Capped mRNAs are transcribed in vitro with SP6 polymerase and purified by phenol extraction and ethanol precipitation.

4) Generation of integration intermediates.

Integration intermediates are made in a series of in vitro translation reactions using rabbit reticulocyte lysate (RRL) as a source of cytosol, canine rough microsomes (CRM) as a source of ER membrane, ^{35}S-methionine as radioactive tracer and the ε-ANB $tRNA^{Amb}$ probe. When the translating ribosome encounters the UAG codon one of two events occur. Either a cytosolic release factor will cause release of the polypeptide chain, or an ε-ANB-lysine will be incorporated at the site of the UAG codon. The first outcome is referred to as "non-read-through." The second outcome is referred to as "read-through" and results in probe incorporation and continued translation to the end of the truncated mRNA. Because there is no terminal stop codon, the polypeptides thus translated will remain tethered to the ribosome via their peptidyl-tRNA bond to generate a uniform population of molecules at the same stage of synthesis. These ribosome-translocon-nascent chain complexes are referred to as integration intermediates. A series of C-terminal truncations that each incorporate the probe at the same site in the polypeptide, therefore generates a parallel series of static integration intermediates that represent progressive stages of synthesis (Figure Intro-10).

5). Generation of photoadducts.

Integration intermediates are then subjected to UV irradiation to convert the ANB to a reactive nitrene. If an adjacent protein with a suitable reactive group is present within reach of the 12Å spacer arm, a photoadduct is obtained. However, photodduct generation can be quenched by solute molecules and by reactive bonds in the nascent chain itself

that are within reach of the spacer arm. These scenarios are more likely if other proteins are further away or present a less favorable reactive group. Short half-life (10^{-4} sec) also leads to relatively low crosslinking efficiency generally seen using this technique. Alternatively, the advantages of photocrosslinking are minimal change to the polypeptide, precise incorporation at a specific site and less reliance on specific reactive groups (e.g. primary amines or disulphide-producing cysteines).

6). Verification and identification of photoadducts

Each translation is performed with several negative controls to facilitate verification of photoadduct formation. First, an identical mRNA that does not contain a UAG codon is translated side-by-side with a UAG-containing construct. This "minus TAG" polypeptide cannot incorporate a probe and also serves as a reference for the electrophoretic mobility of the read-through band. Next, an equal amount of non-UV exposed translation product is compared to UV exposed material. Finally, the integration intermediate is disrupted by the addition of puromycin, which cleaves the peptidyl-tRNA bond and putatively releases the nascent chain. Photoadducts are visualized via SDS-PAGE and subsequent autoradiography by the appearance of a band that migrates with slower electrophoretic mobility than the read-through band (Figure Intro-10). The ^{35}S tracer enables femtomole quantities of protein to be seen by autoradiography. Finally, photoadducts are identified by immunoprecipitation with antisera against known translocon components.

7) Quantification of relative read-through efficiencies and relative photoadduct formation

In order to compare relative crosslinking efficiencies amongst various samples, equal amounts of translation products are examined by SDS-PAGE. Relative read-through efficiencies of non-UV treated polypeptides are then quantified on a phosphorimager and corrections made for differences in band intensity. SDS-PAGE is then repeated to verify the accuracy of quantitation. Equal amounts of read-through proteins for each sample are then used in immunoprecipitation reactions to enable direct comparison of photocrosslinking efficiencies at different sites and at different stages of synthesis.

F. Aims addressed in this thesis

1) Is AQP4 integrated in a sequential or coordinated/coopoerative fashion?

The first aim of the thesis was to determine whether the co-translational integration of a polytopic membrane protein is accomplished by the sequential, individual integration of TMs or by cooperative integration. This was done by examining the entrance, traversal and exit of all six AQP4 TM segments by photocrosslinking to sec61α (manuscript 2).

To address the integration question, photoactive crosslinking probes were inserted at three consecutive sites in the center of each AQP4 TM. One site and one TM were examined in up to 18 separate constucts. To generate these constructs, mRNAs were truncated by PCR amplification and translated in rabbit reticulocyte lysate to yield uniform populations of molecules, each at a defined stage of synthesis. Crosslinking with UV light yielded photoadducts to sec61α that were verified by quantitative

immunoprecipitation. We find that, as TMs enter sec61α, they reside in a primary binding site until entry of the next TM. Interestingly, TMs did not integrate in a sequential manner. Rather, some TMs (1, 3 and 5) remained proximal to sec61α. and multiple TMs accumulated in the vicinity of sec61α prior to integration, in support of a cooperative integration model. This was somewhat surprising given that each AQP4 TM acquires topology independently and sequentially.

The crosslinking pattern of TMs 1, 3 and 5 suggested that these TMs occupy multiple sec61-proximal environments as AQP4 synthesis proceeds. Many had asymmetric crosslinking efficiencies implying that the nascent chain is not randomly oriented. An alternate explanation is that nearby proteins did not contain a nitrene-reactive group within reach of the 12Å spacer arm. I find this explanation unlikely in that the nitrene is strongly electrophilic and reacts with a wide variety of C–H and C–N bonds (Figure Intro-7).

For AQP4, chains released from the ribosome by addition of puromycin uniformly lost sec61α crosslinks implying that the peptidyl-tRNA tether holds the nascent chain in the translocon and that integration occurs upon release.

2) Does the CFTR-TMD2 integration mechanism differ from AQP4?

The second project of my thesis investigated membrane integration of the second transmembrane domain of CFTR (CFTR-TMD2). Like AQP4, CFTR-TMD2 contains 6 TMs. However, because the amount of CFTR that achieves native conformation varies

depending on the expression system used, CFTR may be an inherently difficult substrate for folding [129, 130, 139, 140]. This suggests that the integration strategy used by CFTR may differ from AQP4. Several previous Skach lab studies [15, 105, 140] determined that polar residues within TM sequences affect how CFTR acquires topology. One study [15] specifically demonstrated that CFTR-TM8 requires the presence of TM7 to stop in the membrane due to the presence of an aspartate residue, D924. Given this unusual behavior, I examined TM8-sec61α interactions using the photocrosslinking approach to discover whether CFTR TM8 behaved differently from the more conventional TMs in AQP4. Surprisingly, TM8 retention within the translocon lasted over the synthesis of at least 70 residues. Most unexpectedly, CFTR TM8-sec61α crosslinks persisted even after peptidyl tRNA cleavage, suggesting a highly unique interaction with sec61α. Given these initial results I asked whether persistent TM8-sec61α interactions were dependent upon an intact ribosome-translocon complex. The answer was yes. I discovered that removal of ribosomes with high salt or EDTA disrupted TM8-sec61α crosslinking, consistent with dependency upon an intact RTC. This was true for both integration intermediates and for released chains.

Because previous studies reported persistent nascent chain crosslinks to OST subunits [75, 141], I asked whether two closely spaced CFTR N-linked glycosylation sites in the lumenal loop between TMs 7 and 8 could be responsible for persistent sec61 interaction. Deletion of consensus sites, both separately and together, showed this not to be the case.

Finally, I followed up on an earlier observation that the polar aspartate residue in the center of TM8 affected TM stop transfer activity [15]. Given that aspartate strongly drives H-bonding between TMs in an apolar environment and that previous studies demonstrated the interaction of nascent chains with lipids while still proximal to sec61 [9, 10] I tested whether the aspartate residue might also be responsible for the persistent crosslinking observed following petidyl-tRNA cleavage. Consistent with this, replacement of the aspartate residue with valine abrogated persistent peptidyl-tRNA-independent sec61 interactions. Moreover, replacing aspartate 924 with glutamate restored persistent crosslinking confirming the hypothesis that nascent chains may form interactions with translocon machinery that are independent of the peptidyl-tRNA bond.

3) Is release of full-length CFTR from the ribosome-translocon complex also delayed?

As detailed in manuscript 4, delayed CFTR release from the RTC is not limited to isolated TM7-8 complexes. In Oberdorf, et al, we showed prolonged interaction of full length CFTR with ER biosynthetic machinery after completion of synthesis. Further, nascent peptide release was stimulated by ATP and cytosol. I therefore asked whether ATP could also facilitate release of TM7-8 polypeptides. When ATP was depleted with apyrase prior to the addition of puromycin, departure of the peptidyl tRNA-cleaved chain from the translocon was significantly slowed.

G) Conclusion

Taken together, the results of these studies have profound implications for the integration process: 1) TMs can accumulate near sec61 prior to integration, and, 2) sec61 proximity can persist after peptidyl-tRNA cleavage and presumptive release from the ribosome. Persistent interactions are sequence-specific and can involve polar residues in TM segments. It is difficult to reconcile a simple two-step model for membrane protein folding with these results. Rather, our results indicate that nascent membrane proteins may remain near sec61 after the completion of synthesis which may provide time for early tertiary structure to form. Dependence of delayed integration on a polar residue also suggests that sec61 may act as a "charged residue chaperone" to prevent off pathway helix-helix interactions and implies an entirely new function for this important translocon protein.

Figure Intro-1

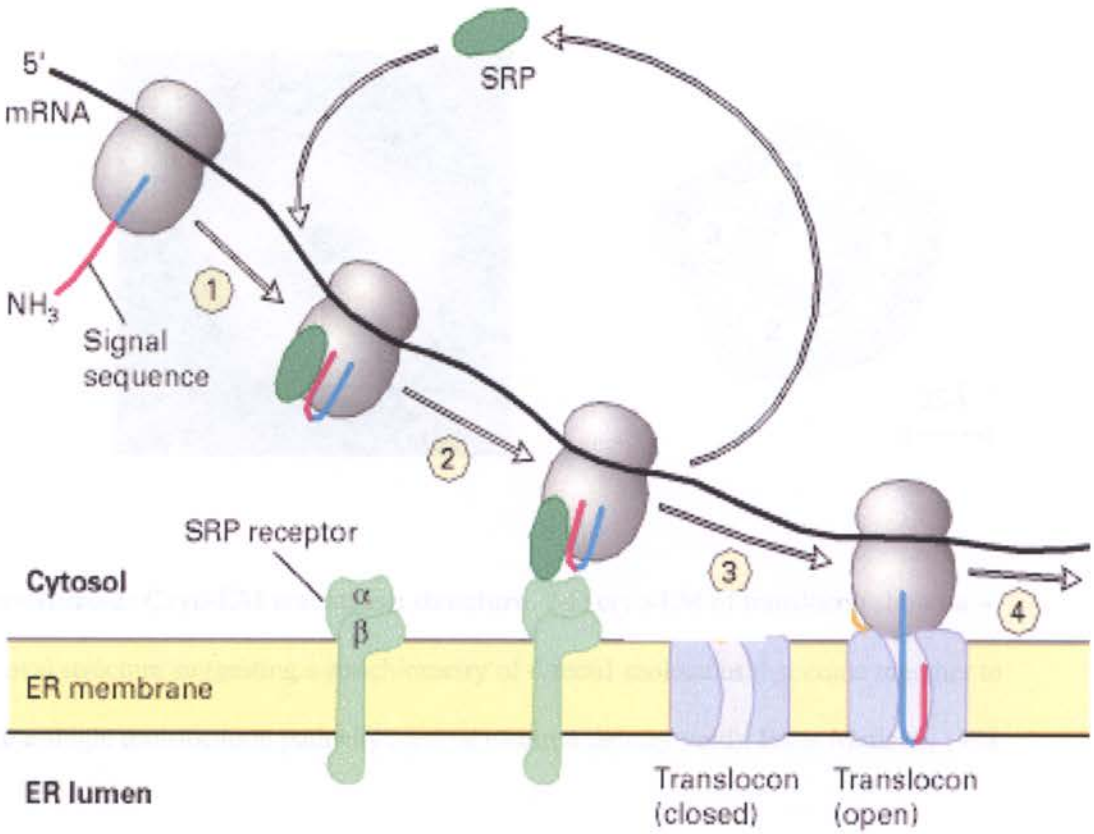

Figure Intro-1 Targeting of membrane protein to ER. Signal sequence binds cytosolic signal recognition particle (SRP) (1) and targets to SRP receptor at ER membrane (2). Ribosome-nascent chain complex is transferred to sec61 (3, purple). adapted from: Molecular Cell Biology. 4th ed. Lodish, Harvey; Berk, Arnold; Zipursky, S. Lawrence; Matsudaira, Paul; Baltimore, David; Darnell, James E. New York: W. H. Freeman & Co.; c2000.

Figure Intro-2

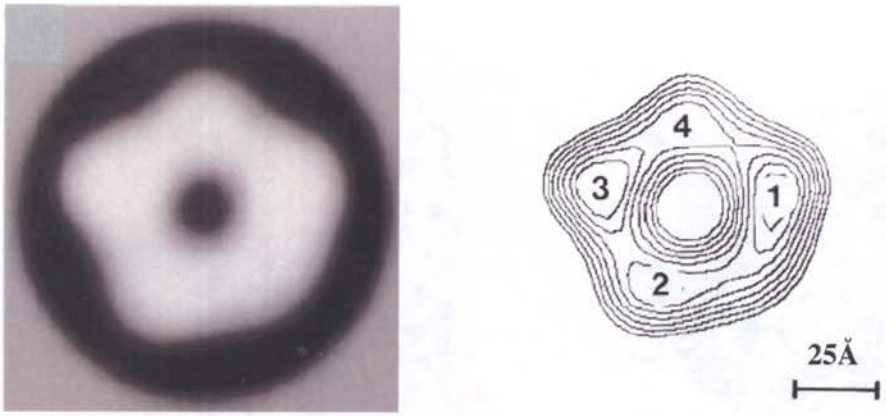

Figure Intro-2: Cryo-EM translocon structure. 2-D cryo-EM of translocon shows a ~ 90Å oval structure suggesting a stoichiometry of 4 sec61 molecules that come together to create a single translocation pathway (central electron density void). From Matlack, 1998

Figure Intro-3

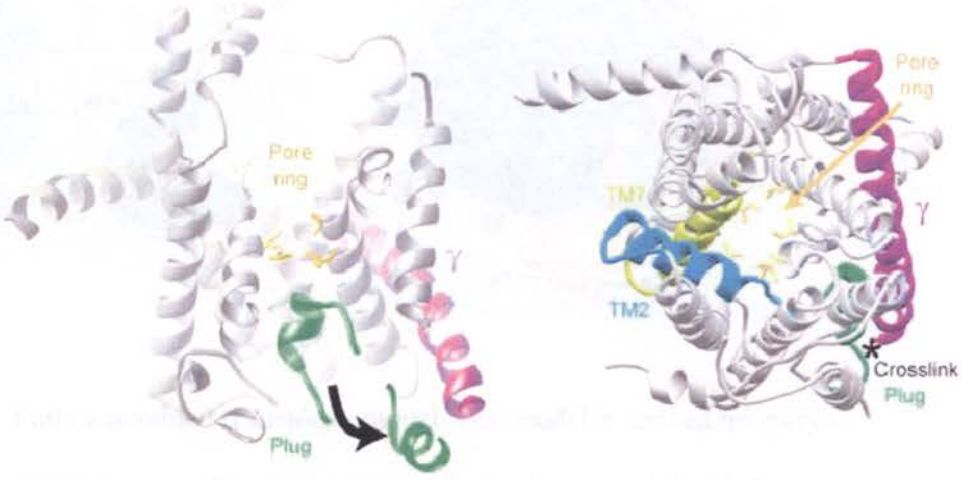

Figure Intro-3. 3.2Å x-ray crystal structure of M jannischii sec Y. X-ray crystallography of secY reveals a ~40 Å wide channel. A 5-8Å translocation pathway is defined by a pore ring of hydrophobic amino acid side chains (center, gold). In the closed state, secY is axially gated by a short helical plug (TM2a, green). The front of the molecule is comprised of TM7 (yellow) and TM2b (blue) forming a potential lateral passage for nascent TMs into the lipid bilayer. The back of the channel is clamped by secE (purple), the archael homolog of eukaryotic secγ. from van den Berg 2004.

Figure Intro-4

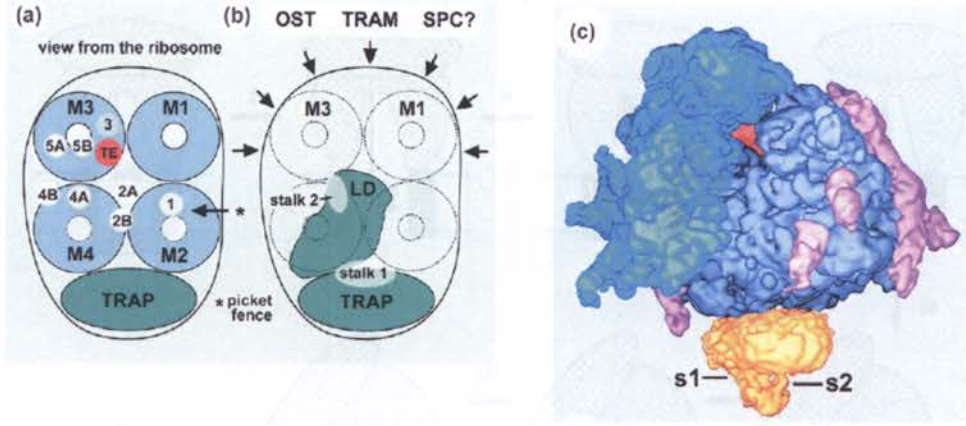

Figure Intro-4. Fully assembled translocon model. This model is derived from cryo-EM of ribosome translocon complexes from native ER membranes and the M. Jannischii secY x-ray crystal structure. a) Alignment of ribosome exit tunnel shown in red. Circles numbered 1, 2b, 3, 4A, 4B, 5A and 5B represent ribosomal connections. M1-4 are sec61 heterotrimers. Only the M1 sec61 is available for translocation due to steric hindrance from the ribosomal docking sites. The model leaves no room for other known translocon components (b) even though these were present as determined by western blot. The true architecture of actively translocating complexes is unknown c) ribosome translocon complex at 10Å resolution showing ribosome large and small subunits (light and dark blue) translocon (yellow) with stalk attachments for TRAP molecule (S1 and S2) and tRNA in ribosome E-site (red). from Menetret, 2005

Figure Intro-5

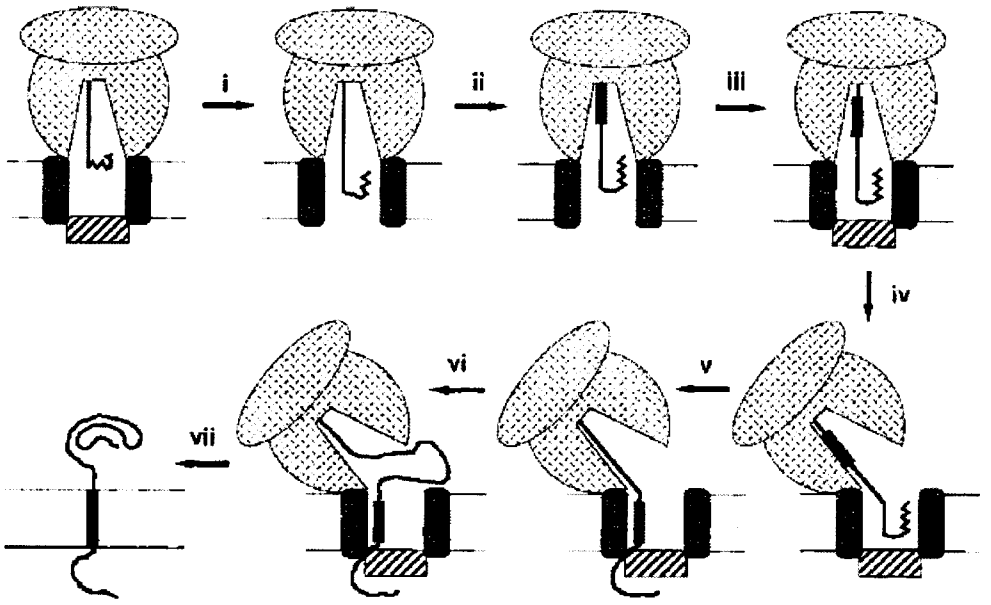

Figure Intro-5. Lumenal and Cytoplasmic Translocon Gating.

When the ribosome–nascent chain complex is first targeted to the translocon, the lumenal side of the translocon is closed. Once the nascent chain reaches 70 amino acids in length, the lumenal side opens (i). When the transmembrane segment is completely synthesized and located about four amino acids from the tRNA, the lumenal side closes (iii). After another five amino acids, the cytoplasmic side opens (iv). from Liao et al. (1997); Siegel, Cell, Vol. 90, 5–8, July 11, 1997,

Figure Intro-6

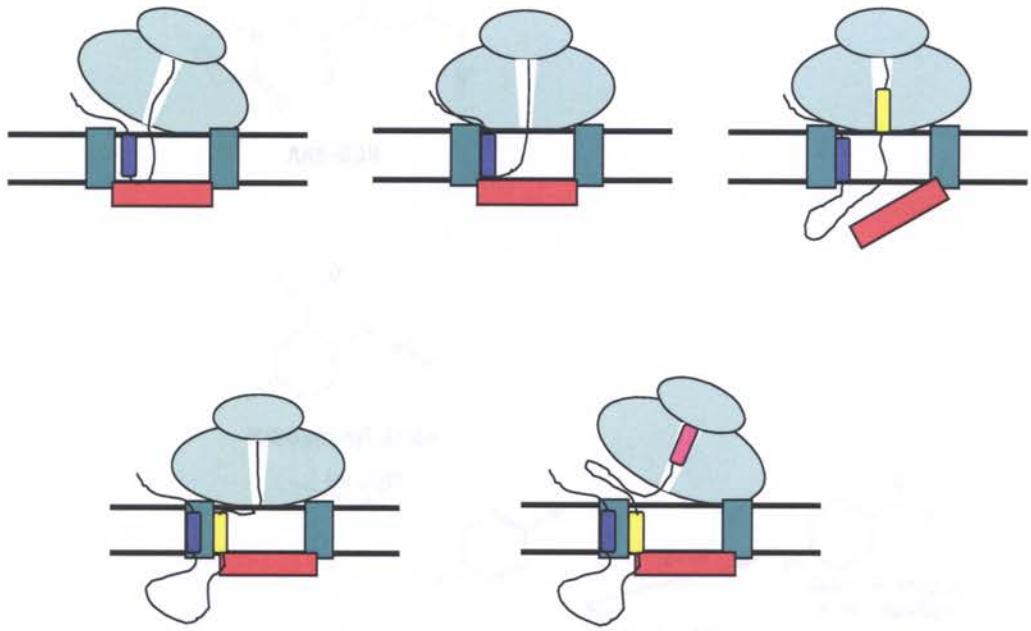

Figure Intro-6. Functional model of Sec61 axial gating – alternating cycles of ribosome/BiP binding. A type II signal anchor (blue) rotates to allow N-terminus of polypeptide into cytosol (top, left). Signal sequence character causes ribosomal sealing (top, center) followed by BiP release, opening axial gate (top, right). Stop transfer character of next TM (yellow) closes axial gate (bottom, left) followed by relaxation of ribosome translocon junction to allow downstream sequence cytosolic access.

Figure Intro-7

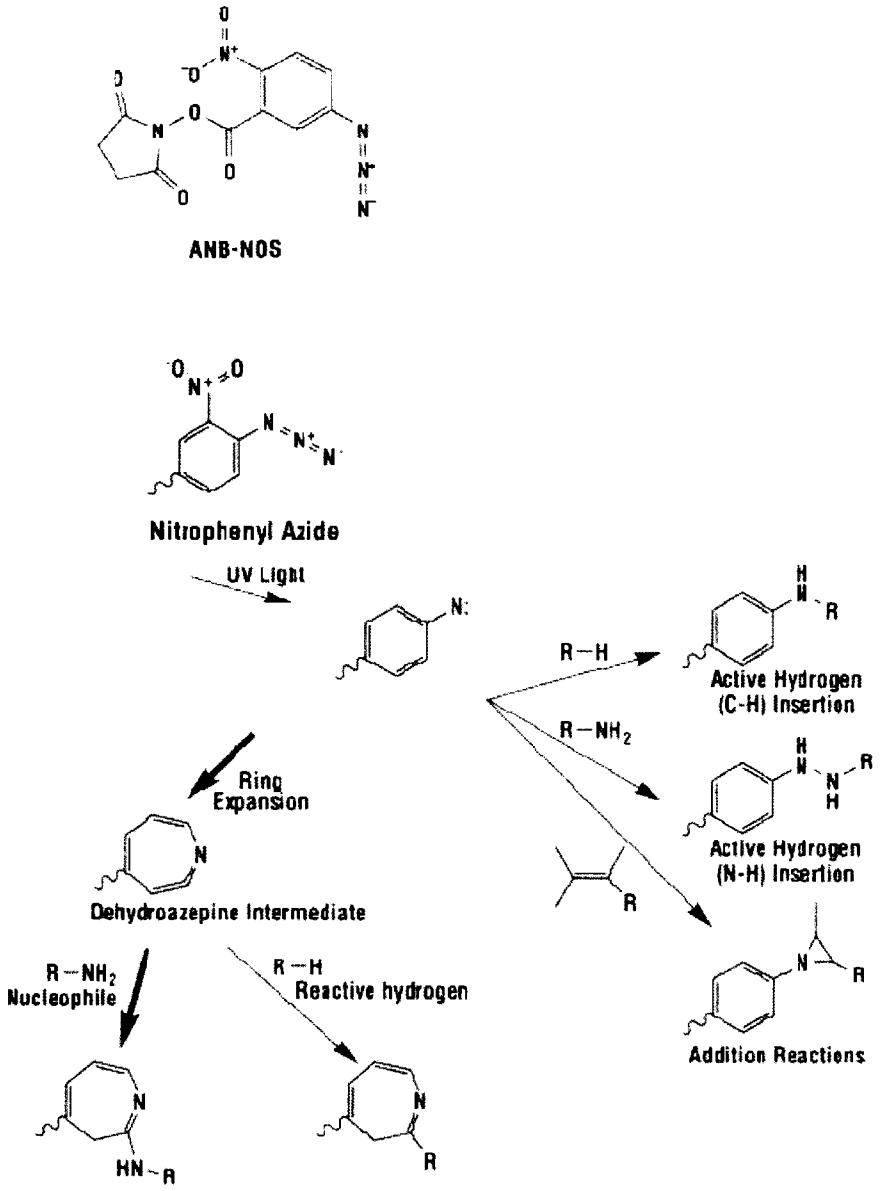

Figure Intro-7. ANB-NOS and nitrene chemistry: ANB-NOS with reactive N-oxysuccinimide ester group for linking to ε–carbon of lysine and nitrophenyl azide group

for crosslinking is shown at top. Conversion of nitrophenyl azide to nitrene with UV light is shown at center. Preferred reactions of nitrene singlet are shown at lower right. Triplet reactions are shown at lower left. Adapted from Pierce catalog.

Figure Intro-8

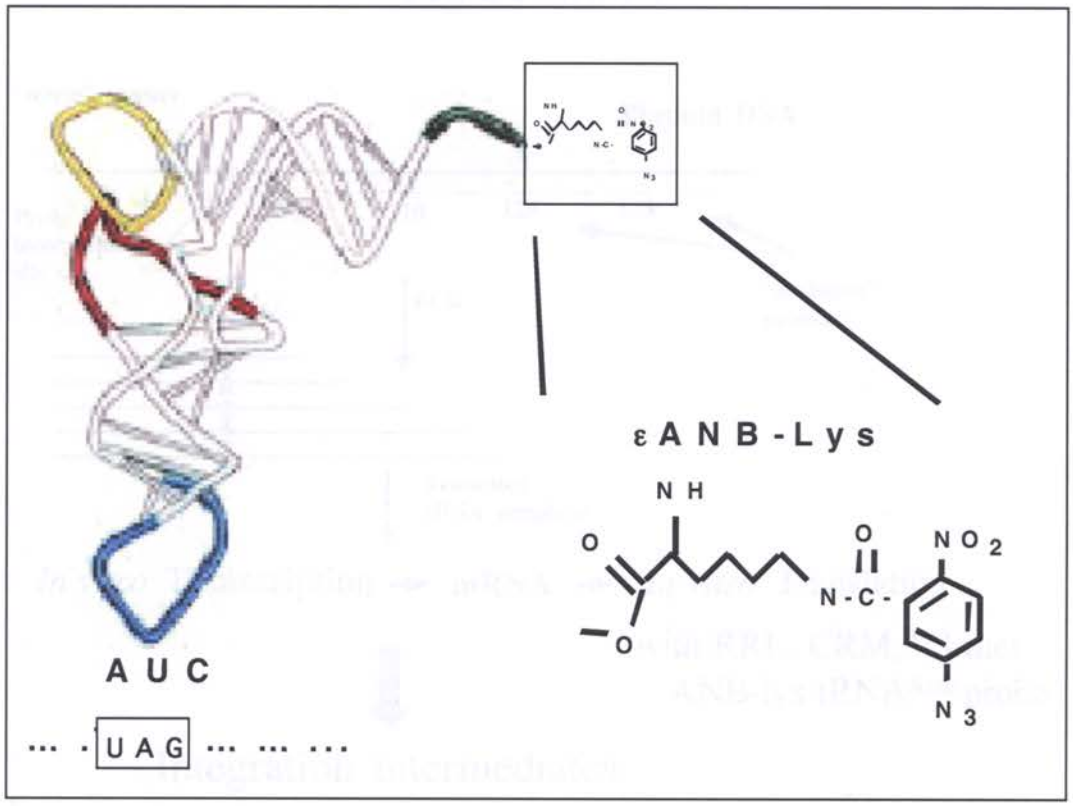

Figure Intro-8. The ε–ANB-lys-tRNA^{Amb} probe. Crosslinking probe generated from modified aminoacyl tRNA. Lysine anticodon AAG is modified to UAG. 14C-lysine alpha carbon is coupled to tRNA. ANB-NOS crosslinker is coupled to lysine epsilon carbon.

Figure Intro-9

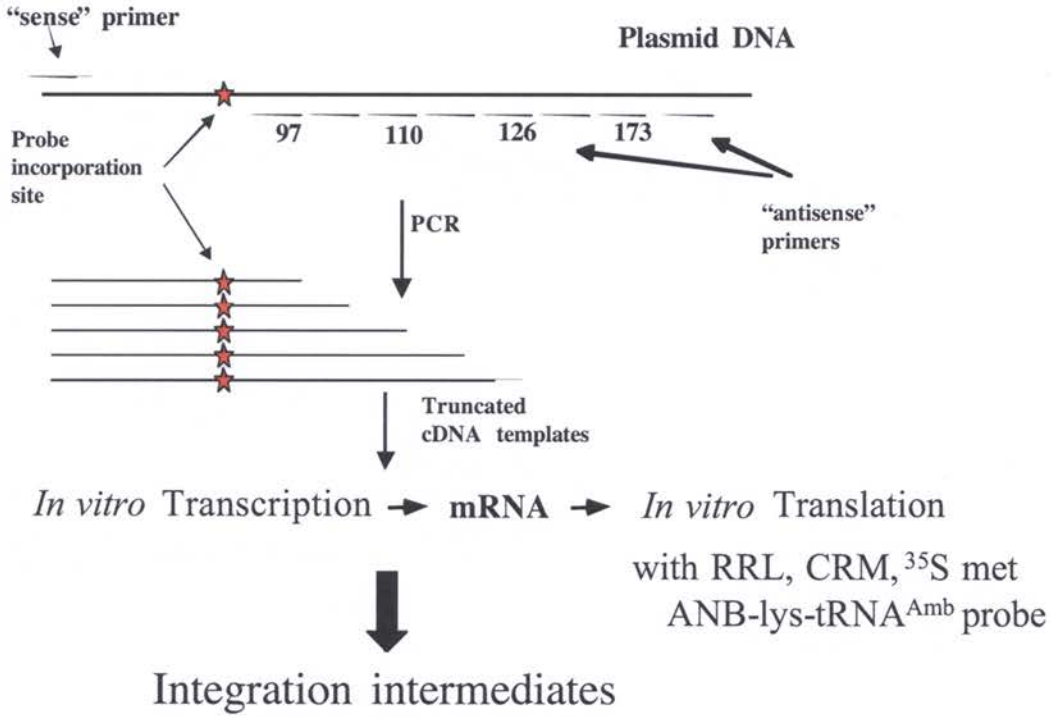

Figure Intro-9. Generation of integration intermediates. Shown is schematic for generating integration intermediates from cDNA templates. in which TAGs have been introduced at a specific residue by PCR overlap extension. Truncations are generated via PCR using a sense oligo and progressive C-terminal antisense oligos. PCR products are phenol extracted and ethanol precipititated and used in an in vitro SP6 driven transcription reaction. Transcripts are then phenol extracted, ethanol precipitated and used in an in vitro translation reaction with RRL, CRM, 35S methionine and the ANB-

tRNA probe. Because mRNAs have no terminal stop codon synthesis will end without release from the ribosome generating an integration intermediate (see fig. intro 4).

Figure Intro-10

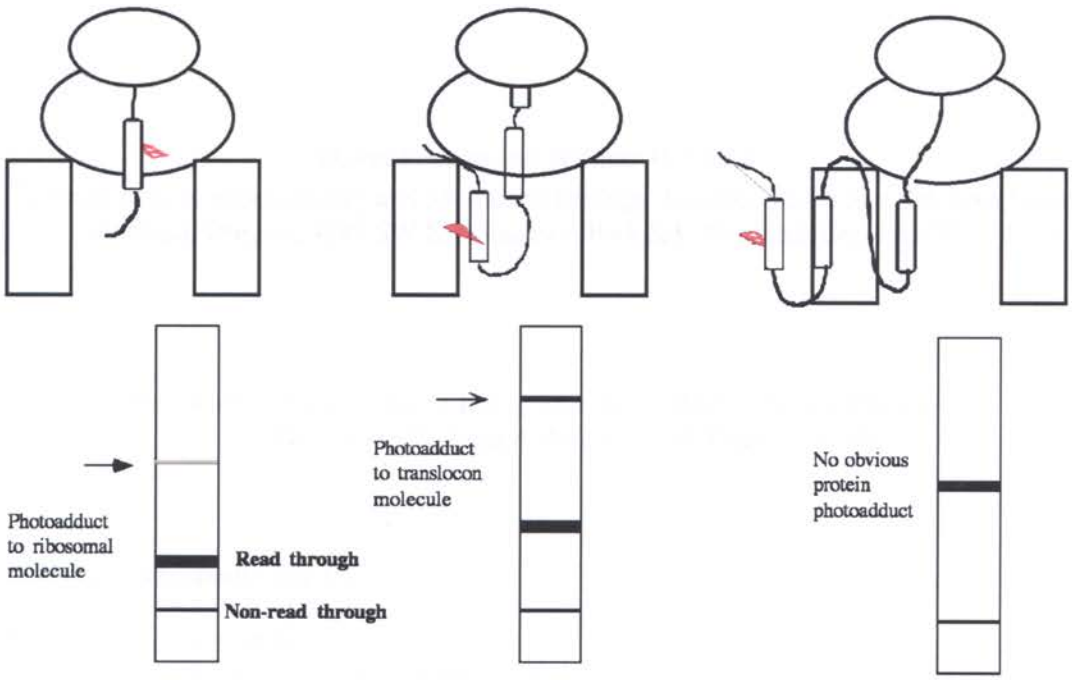

Figure Intro 10. Integration intermediates. Panels from left to right demonstrate that serial truncations of cDNAs with no terminal stop codons result in generation of polypeptides at progressive stages of synthesis. Probe is located at same sequence position for each construct. Position of probe is determined by length of tether to peptidyl transferase center of the ribosome. Non-read through bands all run with same electrophoretic mobility as demonstrated in cartoon gels at bottom. Constructs that incorporate probe will read-through the engineered UAG codon and electrophoretic mobility willl be determined by site of cDNA truncation. Protein photoadducts (arrows).

Introduction addendum: Manuscript 1

Molecular Mechanisms of Aquaporin Biogenesis by the Endoplasmic Reticulum Sec61 Translocon

David Pitonzo and William R. Skach
[1]Department of Biochemistry and Molecular Biology, Oregon Health and Sciences University
Portland, Oregon, 3181 SW Sam Jackson Park Rd. Portland, Oregon 97239, USA

Published in Biochimica et Biophysica Acta (BBA) - Biomembranes
Volume 1758, Issue 8, August 2006, Pages 976-988

Address correspondence to:

William R. Skach, M.D.
Department of Biochemistry and Molecular Biology
3181 SW Sam Jackson Park Rd, L-224
Oregon Health and Sciences University
Portland, OR 97239

TEL: 503 494-7322
FAX: 503 494-8393
E-mail: skachw@ohsu.edu

Key Words: Aquaporin, biogenesis, Sec61, endoplasmic reticulum, ER, translocon, polytopic protein

1)Abstract.

The past decade has witnessed remarkable advances in our understanding of aquaporin (AQP) structure and function. Much, however, remains to be learned regarding how these unique and vitally important molecules are generated in living cells. A major obstacle in this respect is that AQP biogenesis takes place in a highly specialized and relatively inaccessible environment formed by the ribosome, the Sec61 translocon and the ER membrane. This review will contrast the folding pathways of two AQP family members, AQP1 and AQP4, and attempt to explain how six TM helices can be oriented across and integrated into the ER membrane in the context of current (and somewhat contentious) translocon models. These studies indicate that AQP biogenesis is intimately linked to translocon function and that the ribosome and translocon form a highly dynamic molecular machine that both interprets and is controlled by specific information encoded within the nascent AQP polypeptide. AQP biogenesis thus has wide ranging implications for mechanisms of translocon function and general membrane protein folding pathways.

2. Introduction.

Recent advances in aquaporin structure and function have fundamentally changed our views of how water is transported across biological membranes. Cloning and characterization of the first definitive water channel [142, 143], CHIP28 (Aquaporin 1) confirmed early studies regarding the proteinaceous nature of the transporter [144-146] and initiated the birth of a rapidly expanding field that has touched broad aspects of biology. It is now clear that water channels are widely expressed throughout prokaryotic and eukaryotic kingdoms and that they play a major role in normal human physiology and disease [147-149]. Initial insight into the selective basis of water transport provided by Cryo-EM studies [150-152] has been refined by high resolution crystal structures to reveal the mechanism of water and glycerol selectivity at a molecular level [84, 85, 88, 153]. With the rapid maturation of this field, new challenges and questions have emerged. For example, much remains to be learned about the precise role of aquaporin expression, regulation, and intracellular trafficking in disease states. Details of AQP structure have also highlighted a particularly perplexing question. Namely, how are functional AQP molecules generated in living cells? This question has specific relevance because inherited mutations in AQP2 cause nephrogenic diabetes insipidus [154, 155] by disrupting early biogenesis events and thereby generating unstable structures that are recognized and degraded by cellular quality control machinery [156-158]. Currently, we have only a rudimentary understanding of normal AQP folding pathways and virtually no idea how these pathways are corrupted by disease-related mutations. This review will therefore attempt to summarize our current understanding of AQP biogenesis and provide insight into this particularly challenging aspect of aquaporin biology.

3. Role of the translocon in aquaporin biogenesis.

3.1 Aquaporin structure.

Aquaporins comprise a ubiquitous family of proteins that contain six transmembrane

segments (TMs) arranged in an inverse two-fold pseudo-symmetry around a central water-conducting pore [83, 87]. While AQPs generally exhibit a tetrameric quaternary structure [159], each monomer possesses an independent water-conducting channel. Early topologic studies demonstrated that AQP N- and C-termini reside in the cytosol [100, 160, 161] and TMs are connected by two relatively short intracellular loops (ICL1, 2) and three extracellular loops (ECL1, 2, 3, Figure 1A). ICL1 and ECL3 each contain a canonical NPA motif (β-turn) and a half-helix that partially cross the membrane and provide key residues for water and glycerol selectivity [83-85]. Thus the majority of mammalian aquaporin protein is deeply imbedded within the plane of the lipid bilayer, while the remainder is located in either cytosolic or extracytosolic environments (Figure 1B). The hydrophobic nature of AQPs and their elaborate transmembrane architecture therefore requires a precise mechanism for localizing peptide regions into multiple cellular compartments as well as efficient folding and packing of TMs within the membrane.

3.2 General models of translocon structure and function.

Like most eukaryotic polytopic proteins, AQP biogenesis is facilitated by highly specialized folding machinery in the endoplasmic reticulum (ER) [26, 162]. A central component of this machinery is the Sec61 translocon [163, 164], a large ovoid disc ~100 Å in diameter [49, 64] that spans the ER membrane and serves the principal function of translocating nascent polypeptide into the ER lumen and integrating TMs into the lipid bilayer. The translocation channel itself is comprised at least in part by the heterotrimeric protein Sec61αβγ [22, 48, 165]. Fully assembled translocons contain multiple copies of Sec61 [45], as well as numerous other associated proteins that include signal peptidase complex (SPC), oligosaccharyltransferase (OST), TRanslocation Associated Membrane protein (TRAM) and TRanslocation Associated Protein (TRAP) [26, 32, 34, 35, 166]. Ribosomes bearing secretory and membrane proteins are usually targeted to the ER very

early during synthesis as signal recognition particle (SRP) binds a signal sequence at the N-terminus of the nascent peptide, docks at its ER receptor, and transfers the entire ribosome nascent chain complex (RNC) to Sec61α [164, 167]. In the case of mammalian AQPs, the first TM facilitates membrane targeting upon emerging from the ribosome [98, 100] when less than 25% of the protein has been synthesized. Thus AQP translocation and membrane integration are temporally coupled to synthesis of the nascent chain by the ribosome-translocon complex (RTC). A major challenge currently facing biologists is to understand how these events are orchestrated within the context of this large and complex molecular machine (Figure 2).

Cryo-EM studies of detergent solubilized RTCs have indicated that the central axis of the translocon is directly aligned with the exit tunnel of the 60S ribosomal subunit [44, 46, 65]. This is consistent with crosslinking studies demonstrating that the nascent polypeptide encounters ER translocation machinery (Sec61, TRAM) as soon as it emerges from the ribosome [31, 168-171]. As the signal sequence contacts Sec61, it initiates translocation by opening a channel within the translocon to create a continuous gated aqueous translocation pathway that extends from the ribosome exit tunnel to the ER lumen [24, 25, 51]. Experiments with fusion proteins have demonstrated that TM1 from both AQP1 and AQP4 efficiently opens this channel to initiate translocation of the first extracellular loop [98, 100]. While it is generally agreed that the translocation pathway is lined at least in part by Sec61α and that Sec61α is one of the first proteins encountered by the newly synthesized nascent chain, the actual composition and dimensions of the translocation channel remain controversial. Crystal structures of a purified, solubilized Sec61 homolog (SecYEβ) derived from Methanococcus have suggested that translocation takes place through a relatively small pore (8-12 Å) formed by a single Sec61 heterotrimer (figure 2A) [48]. In contrast, fluorescence quenching experiments using assembled and functional translocons in native ER membranes have indicated that the

nascent polypeptide is located within a much larger pore (~40 Å) (Figure 2B) [51]. Thus further work is required to conclusively define the composition and physical environment of the translocation pathway in functional and intact translocons.

4. Mechanistic aspects of AQP topogenesis.

There are two central questions regarding early aspects of aquaporin biogenesis. How is AQP topology established across the ER membrane? And how are AQP TMs inserted, integrated and subsequently folded within the hydrophobic environment of the lipid bilayer? Several studies have begun to provide a mechanistic basis with which to view this process. Because AQP polypeptide encounters the translocon as it exits from the ribosome, the translocon must actively direct lumenal and cytoplasmic loops into their respective cellular compartments while at the same time ensuring that TMs are correctly inserted into the lipid bilayer. Moreover, this process must take place rapidly as the nascent chain is expelled from the ribosome exit tunnel at a rate of approximately 5 amino acid residues per second [172, 173]. In order for integration to occur in a co-translational manner (i.e. during synthesis), the translocation pathway must be highly dynamic, tightly controlled, and precisely coordinated with the synthesis of TM segments and peptide loops. Current evidence indicates that this process is orchestrated via reciprocal interactions whereby access of the nascent polypeptide to the ER lumen, cytosol and lipid bilayer is regulated by the RTC [26, 174]. In turn, the pathway through the RTC is controlled by specific topogenic information encoded within the nascent polypeptide [175, 176]. For example, topology of extracellular loops is established as they translocate into the ER lumen through the open gate of the translocon pore. However, after synthesis of an ECL, translocation must be terminated in order to direct the next peptide loop (ICL) into the cytosol. Similarly, after synthesis of an ICL, the translocation pathway must be re-opened to allow peptide movement into the ER lumen. Thus one would predict that during the cotranslational assembly of polytopic proteins,

specific signals within the nascent protein should open, close, and re-open the translocation pathway and thereby provide selective access of intracellular and extracellular loops to the cytosol and ER lumen, respectively [26].

4.1 AQP4 topogenesis.

Studies attempting to address how lumenal and cytosolic access is controlled during AQP biogenesis have examined the ability of TMs to change the direction of translocation as the nascent protein is synthesized within the RTC [98-100, 177, 178]. In the case of AQP4, TMs1, 3 and 5 function as signal (anchor) sequences to efficiently open the translocation pathway and direct movement of extracellular loops 1, 2, and 3 into the ER lumen [98, 99]. TMs2, 4, and 6 alternately terminate translocation, close the translocation pathway, and orient intracellular loops 1, 2 and the C-terminus into the cytosol [98]. Thus, as AQP4 TMs are synthesized, the translocation apparatus (RTC) is regulated such that at any given point of synthesis, the nascent polypeptide has only one pathway to follow, either into the ER lumen or into the cytosol (Figure 3A). In this manner the six-spanning topology is established efficiently and co-translationally as the polypeptide emerges from the ribosome. Surprisingly, not all AQPs achieve their topology via this mechanism.

4.2 AQP1 Topogenesis.

A detailed analysis of AQP1 revealed that some TMs were much "less efficient" at controlling the translocation pathway than their AQP4 counterparts [100]. Specifically, AQP1 TM2 does not efficiently terminate translocation either in its native context or in heterologous chimeric proteins [99, 100, 177]. As a result, TM2 passes through the translocon and ICL1 transiently enters the ER lumen in >50% of nascent polypeptides. Because TM2 does not close the translocation pathway, TM3 enters an open translocon. Rather than initiating translocation of ECL2, TM3 terminates translocation and initially

adopts a type I topology whereby the extracellular loop 2 is mislocalized to the cytosolic face of the ER membrane [100] (Figure 3B). This unorthodox behavior results in a mixture of nascent chain topologies in which most of the newly synthesized AQP1 molecules initially adopt a four-spanning topology, while only a minority of chains is cotranslationally directed into the six-spanning orientation [100, 177]. When first reported, these results caused significant confusion and consternation, as it was difficult to reconcile the initial cotranslationally established AQP1 topology in the ER membrane with the mature, six-spanning topology observed at the plasma membrane [161]. However, subsequent studies using C-terminal translocation reporters as well as inserted epitope tags have demonstrated that the four-spanning topology is actually a folding intermediate that subsequently matures into the six-spanning structure [179]. This is accomplished by an internal 180° rotation of TM3 that converts TM3 from a type I (N_{lum}/C_{cyto}) to a type II (N_{cyto}/C_{lum}) topology and brings TM2 and TM4 into the plane of the membrane (Figure 4).

Because of the vectoral nature of translation, the N-termini of internal signal anchor sequences (TM3 and TM5) in AQP1 and AQP4 first contact the cytosolic face of the translocon as they emerge from the ribosome (Figure 3). In the case of AQP4, TM3 cotranslationally acquires its type II (N_{cyto}/C_{lum}) topology such that its N-terminus remains on the cytosolic face of the membrane and its C-terminal flanking residues are directed into the ER lumen (Figure 3A). Thus, AQP4-TM3 also undergoes a 180° rotation (from downward- to upward-pointing, see Figure 3A) relative to the direction of polypeptide movement and its alignment within the ribosome/translocation pathway. A key difference between AQP1 and AQP4 biogenesis is therefore the timing and synthetic requirements of this inversion event. AQP4-TM3 functions efficiently as an independent type II signal anchor sequence such that orientation occurs cotranslationally and does not require synthesis of downstream TM segments [98, 99, 180]. In contrast, rotation of

AQP1-TM3 occurs at a much later stage of biogenesis and is highly dependent on the synthesis of TMs 4-6 [177, 179]. For most signal anchor sequences, TM orientation is rapidly established within the translocon [181] based on the distribution of flanking charged residues (positive-in-rule [57, 182, 183]), TM length and hydrophobicity [184], and the folding rate of flanking domains [185]. Analysis of AQP1 and AQP4 chimeras, however, have indicated that primary differences in TM3 translocation activity are caused by variations in C-terminal flanking residues (ECL2) that do not significantly affect these established parameters [99]. Instead, the data indicate that residues within the C-terminal half of AQP1 are primarily needed to properly orient N-terminal TM segments [179, 180].

Recent experiments have verified that initial AQP translocation events are similar in cell-free, Xenopus oocyte and mammalian cell expression systems, indicating that the unexpected AQP1 folding pathway is widely conserved [177]. There are, however, two caveats to these findings. AQP1 topological maturation in vitro (i.e. conversion from a 4- to a 6-spanning topology) is dependent upon the source of ER. AQP1 remains in its immature 4–spanning topology when translated in traditional canine rough ER microsomes, but acquires its mature topology when incorporated into Xenopus oocyte-derived ER membranes [179]. At present the specific ER factors required for AQP1 maturation remain unknown. Second, truncated AQP1 constructs (lacking TMs 4-6) become trapped in the immature topology and are relatively unstable. Thus immature topological isoforms generated from truncated proteins can only be observed in mammalian cells when examined at very short time intervals after synthesis [177, 178].

5. General implications of AQP topogenesis.

Studies of AQP topogenesis have several significant implications. First, they demonstrate that translocon gating is not necessarily absolute. Certain TMs that lack

strong topogenic properties can direct the translocon into alternate conformations whereby the nascent chain can gain access to either (or both) the cytosolic and lumenal compartments as it exits the ribosome. This contrasts with translocation of most secretory and simple membrane proteins in which signal sequences efficiently direct a uniform topology by establishing a continuous cytosolically inaccessible translocation pathway that extends from the ribosome exit tunnel through the translocon pore [24, 25]. It is currently unknown whether a given translocon can provide access to both compartments simultaneously, or whether access is provided in a stochastic manner by adoption of alternate conformations. We favor the latter explanation at this juncture because a translocon open to both ER and cytosol could result in significant mixing of lumenal and cytosolic contents. However, further work is needed to resolve this question.

Second, AQP1 biogenesis has revealed that a mechanism must exist for reorienting TMs and peptide loops that are initially directed into the wrong compartment (Figure 4). Such a mechanism must provide sufficient flexibility during early stages of biogenesis to allow for "topological editing" while downstream TMs are still being synthesized. Although the mechanism that drives TM3 reorientation remains unknown, it is interesting that this phenomenon is not restricted to AQP1 but has also been observed for other native and engineered eukaryotic polytopic proteins [13, 58, 186]. Particularly intriguing, in this respect, are findings that two bacterial transport proteins, lactose permease and phenylalanine permease, can exhibit different topologies depending upon membrane phospholipid composition [187, 188]. Both proteins require phosphatidylethanolamine (PE) for function and undergo a reversible topological reorientation of several TM segments and connecting loops, when PE is supplied after synthesis has been completed. Thus the unexpected folding pathway observed for AQP1 may be a relatively common feature of diverse membrane proteins that could be influenced by both the protein

machinery and lipid composition of the cell.

Third, a detailed analysis of AQP1 and AQP4 chimeras has demonstrated that the topogenic properties can be dramatically altered by a relatively small changes in primary sequence. For example, two residues at the N-terminus of TM2 (N49 and K51 in AQP1 versus M48 and L50 in AQP4) are responsible for the different topological behaviors and cotranslational topologies observed for AQP1 and AQP4 TM2. Interestingly, N49 and K51 also play a critical role in generating functional AQP1 water channels [99]. Understanding the role of these residues in AQP function may explain why two highly homologous proteins utilize such different folding pathways.

6. Molecular mechanism of membrane integration.

A second fundamental requirement for AQP biogenesis is that each TM segment must be integrated into the lipid bilayer. Because polypeptide translocation normally occurs through an aqueous pore, a natural question is whether TM segments actually translocate into the pore and if so, how and when are they transferred into lipid. This point has major implications since early interactions between nascent TM helices (i.e. packing and tertiary structure formation) are profoundly impacted by both general properties of the lipid bilayer as well as interactions with specific lipids [7, 153, 189, 190].

6.1 Competing models of lateral translocon gating.

Two current and somewhat competing models provide a mechanistic explanation as to how integration of a simple, single TM might occur. Both stipulate that in addition to controlling access into aqueous compartments (e.g. lumen and cytosol) the translocon also controls lateral access of the polypeptide into the bilayer. One model proposes that TM segments passively partition into the bilayer based on their affinity for the hydrophobic lipid environment [14] (Figure 5A). This is consistent with the recent

crystal structure of SecYEβ which revealed that the putative 8-12 Å translocation pore can potentially open laterally between the second and seventh TMs of Sec61α by a rearrangement of helices [48, 191]. Hydrophobic TM segments could therefore passively move through this lateral opening into the bilayer based on favorable thermodynamic interactions with membrane lipids [14, 190]. An alternate model proposes that TM segment integration occurs in a stepwise fashion that is mechanistically controlled and coordinated by the RTC [26, 33, 36]. In this latter model, TMs pass through and reside within distinct molecular environments within the fully assembled translocon for extended periods of time (Figure 5B). Release into the bilayer is triggered at specific stages of synthesis and/or at the termination of translation, presumably by conformational changes within the RTC that push out the previous TM [26]. While both models agree that TM segments enter the axial translocon pore and pass laterally into the membrane, the details and mechanism of this lateral movement remain to be reconciled.

7. Integration intermediates define the nascent chain environment.

Much current knowledge regarding membrane integration has been derived from biochemical studies of programmed translocation intermediates. When the ribosome reaches the end of a truncated mRNA that lacks an endogenous stop codon, translation ceases, but the polypeptide remains covalently attached to tRNA within the 80S ribosome. Thus by translating mRNAs truncated at different regions in the coding sequence, it is possible to create synchronized and stable cohorts of nascent chains that reflect the spatial relationships with respect to the RTC at precise stages of synthesis [26]. Early studies examining nascent chain-lipid interactions using alkaline, high salt and urea extraction confirmed that initial stages of translocation were protein mediated and could be temporally dissociated from membrane integration [54, 72, 100, 192-194]. In other words, some TM segments including those in AQP1 can achieve a transmembrane orientation without fully integrating into the bilayer. These early findings raise questions

as to whether TMs might remain within the translocon prior to integration and if so, where this might occur.

7.1 Crosslinking approaches.

Bifunctional chemical crosslinking agents and incorporated photoactive probes have begun to provide a more precise view of the timing and mechanism of integration by identifying proteins (and lipids) in the immediate vicinity of the nascent polypeptide. Bifunctional agents typically form covalent bonds between lysine or cysteine residues on adjacent proteins and exhibit relatively high crosslinking efficiencies. However, because they require the close proximity of specific reactive side chains they do not necessarily identify nearest neighbors if the reactive group is beyond the reach of the spacer arm. They also often generate unwanted secondary and tertiary crosslinks between multiple proteins in large complexes. Alternatively, photoactive probes such as 5-azido-2-nitrobenzoyl-lys (ANB-lys) and trifluoromethyl-diazirino-benzoyl-phe (TDB-phe) are introduced during translation at a unique codon that is recognized by a modified aminoacyl-tRNA [10, 168, 171, 195]. After translation, UV irradiation generates highly reactive radicals that form nonspecific covalent bonds to neighboring molecules. Because nascent chains contain a single photoactive probe, only one crosslink can be formed per polypeptide, and the efficiency of crosslinking directly reflects the proximity of the probe to the target protein. By varying the site of probe incorporation and mRNA truncation it is thus possible to assess the immediate environment of the polypeptide at virtually any location within the translocation pathway of a fully assembled and functional RTC. This technique provides a non-biased sampling of the nascent polypeptide environment with sufficient resolution to identify components adjacent to different regions (e.g. N- versus C-terminus) as well as different faces of TM helices. Because the reactive radical species have very short half-lives and are prone to solvent quenching, photo-crosslinking yields are generally lower than with bifunctional reagents.

Photo-crosslinking studies have confirmed that secretory proteins contact Sec61α as they pass through the pore, and that crosslinking to Sec61α is lost upon entry into the ER lumen [31, 171]. Crosslinking to TMs in bitopic proteins followed several different patterns [14, 33, 169]. Some TM segments containing TDB-phe were found to crosslink phospholipids almost immediately after contacting Sec61, and lipid crosslinking was stimulated by increasing TM segment hydrophobicity [10, 14]. This led to the proposal the TM rapidly passes through the lateral gate into the bilayer. In contrast, other studies have revealed that TMs can remain adjacent to Sec61α and other translocon components during the synthesis of relatively large cytosolic domains (Figure 5B) [33, 36]. These persistent TM interactions exhibit distinct asymmetry wherein residues on different faces of the helix reside in a stable and fixed orientation with respect to specific translocon components. It is difficult to generalize from these studies because few TMs have been examined in detail and because TDB and ANB may have different propensity for lipid crosslinking [36]. However, it would appear from the data that not all TMs proceed directly into the lipid bilayer by a simple partitioning mechanism and that the translocon may contain specific binding sites [196, 197] that may transiently accommodate TMs during relatively prolonged periods of polypeptide synthesis.

8. Integration of polytopic proteins.

To date few studies have examined how the translocon synchronizes the sequential integration of multiple TMs as they rapidly emerge from the ribosome during polytopic protein synthesis [56, 74, 198, 199]. This is particularly important for native proteins such as aquaporins because TMs from must not only integrate into the membrane, but must also acquire tertiary structure within the lipid bilayer. The early environment experienced by TMs will therefore play a major role in determining how and when helices begin to associate [190]. If TMs disengage from the translocon immediately as

they are synthesized, then helical packing would be driven primarily by the physical environment of the lipid bilayer as has been proposed by the two-step model of Popot and Engelman [8]. If, on the other hand, TMs exhibit prolonged interactions with translocon components, then the proteinaceous environment imposed by the translocon could significantly influence the rate and sequence of helical packing and hence the overall folding pathway. Thus understanding how the translocon controls the early environment of TMs is of more than academic interest, and has major implications for diseases in which folding is perturbed by inherited mutations.

8.1 Photocrosslinking to AQP4 integration intermediates.

To investigate this question, we recently performed a systematic analysis of interactions between all six AQP4 TMs and Sec61α during the entire process of synthesis and integration into the ER membrane [74]. The molecular environment of the nascent polypeptide was assessed by examining a comprehensive series of sequentially truncated AQP4 integration intermediates each of which contained a single photoactive crosslinking probe (ANB-lys) at one of three adjacent residues near the center of each TM. The position of probes within the translocation pathway (i.e. distance from the ribosome peptidyltransferase center) was controlled by varying the site of mRNA truncation, and three consecutive probe sites per TM were evaluated to determine the proximity of Sec61α to different faces of the helix. A key element of this analysis was that each truncation site represents a single point of synthesis and thus defines the spatial organization of the nascent polypeptide within the RTC at a single point in time. Crosslinking profiles of Sec61α photoadducts at 18 probe incorporation sites in a total of 204 synchronized integration intermediates thus enabled us to reconstruct dynamic changes experienced by AQP4 TM helices and to develop the first comprehensive description of how TMs enter, traverse and exit the translocon during synthesis of an entire native polytopic protein (Figure 6).

Several key findings emerge from this study that bear on both AQP integration and the general role of the translocon in the folding process. First, crosslinking patterns to Sec61α revealed a remarkable coordination of TM entry into, progression through, and exit from the translocon. Each TM moved through the translocon in a unique and highly ordered manner, exhibiting distinct transitions in its relationship to Sec61α that were tightly coupled to the stage of synthesis. As TMs contacted the translocon, they quickly acquired a fixed orientation relative to Sec61α and remained in this "binding" site only until the oriented entry of the next TM. This suggests that the translocon utilizes a specific primary entry site within Sec61α and that exit from this site is mechanistically coupled to entry of the next TM. Surprisingly, progression of TMs through the translocon was remarkably variable. Some TMs, such as TM2 and TM4, exhibited a single, well-defined period of crosslinking and then abruptly left the proximity of Sec61α. TM2 exhibited robust Sec61α crosslinking during synthesis of only 30 residues while the nascent chain size increased from 110-140 residues. Other TMs (e.g. TM1 and TM3) exhibited several distinct phases of crosslinking in which the helix moved sequentially into different molecular environments as demonstrated by changes in the relative efficiency of crosslinking to different residues around the helix. The most remarkable pattern was observed for TM1 which crosslinked to Sec61α at chain lengths of 80-100, 110-140 and again at a length of 210 residues (Figure 6).

8.2 Implication for translocon structure and function.

During AQP4 biogenesis, multiple TMs were found to reside within and/or adjacent to the translocon for relatively prolonged periods of time. Indeed, at chain lengths of 140 and 210 residues, crosslinking was simultaneously observed for TMs1-3, and TMs 1, 3, 4 and 5, respectively. While we do not yet know the precise location of each TM relative to all translocation components, these findings raise important questions regarding

translocon architecture and function during AQP biogenesis. If translocation takes place through the small pore formed by a single Sec61 heterotrimer, then secondary sites of contact must be located outside the pore. Moreover, if Sec61 molecules are arranged in a back-to-back configuration as has been proposed [47, 191], then TMs would exit laterally away from the translocon center and towards the lipid bilayer (Figure 7A). Given the short length of AQP4 connecting loops and the proposed ~80 Å distance between lateral Sec61 exit sites, this configuration would also require that only one Sec61 complex could be used for the entire synthesis and integration process [191]. Although lipid crosslinking was not detected in our study for technical reasons, this configuration would further suggest that secondary sites of AQP4 interaction take place at the translocon periphery. Alternatively, a recent structural model of two *E. coli* SecYEG complexes docked onto a translating ribosome has suggested a front-to-front arrangement [50]. Although an exit pathway was apparent from only one SecYEG pore, this configuration positions exit sites adjacent to one another such that TMs would initially exit from SecYEG into the space between the heterotrimers prior to reaching the lipid bilayer (Figure 7B). The proximity of exit sites could also potentially allow multiple heterotrimers to be used for translocation if sufficiently aligned with the ribosome exit tunnel.

Of course fully assembled eukaryotic translocons are more complex and have most recently been proposed to contain up to four Sec61 heterotrimers (as well as accessory proteins) arranged in a large ring-shaped structure [49]. Significant evidence has also indicated that fully assembled and functional translocons contain a large aqueous pore which, during polypeptide translocation, is continuous with the ribosome exit tunnel [24, 25, 27, 52, 200] (Figure 7C). If eukaryotic Sec61$\alpha\beta\gamma$ were arranged in a front-to-front organization, then Sec61 oligomers could potentially form a ring, and initial exit of AQP4 TM helices from the putative small translocation pore could take place towards the

center of the translocon complex (Figure 7D). Interestingly, this central region was initially visualized as a large open pore [44, 46, 201], but subsequent higher resolution structures detergent-solubilized translocons have revealed only a central depression that is been proposed to contain mainly lipid [49, 64, 65]. Because the functional status and subunit composition of purified translocons are unknown, much remains to be learned regarding the structure of fully assembled eukaryotic translocons. An intriguing possibility, although untested at this point, is that TMs might initially exit from Sec61 into a relatively hydrophobic, lipid-like environment that is physically and chemically distinct from the membrane bilayer and surrounded or partially surrounded by translocon proteins (Figure 7D).

8.3 Specific challenges for TM orientation and integration.

Regardless of the precise arrangement of Sec61 in the assembled eukaryotic translocon, the persistent, selective and asymmetric binding observed for AQP4 TMs provides strong evidence that helices do not always freely partition and equilibrate individually into the lipid bilayer. Rather, it would appear that some AQP4 helices accumulate at secondary and/or tertiary sites within an environment that is likely comprised of both protein and lipid components. Given that the rate of protein synthesis is remarkably slow when compared to secondary and tertiary structure formation, it is highly likely that early helix-helix interactions take place within this immediate environment. If so, then the translocon could impact early steps of membrane protein folding in unanticipated ways by influencing the composition and/or physical properties (i.e. strain energies) of adjacent lipids [190]. It is tempting to speculate that this might also provide a productive environment for formation and early maturation of folding intermediates such as those observed for AQP1. It will also be quite interesting to determine whether AQP half helices in ICL1 and ECL3 insert directly into membrane lipids or into a protein scaffold formed by other AQP TMs either within the translocon or after full release into the lipid

bilayer.

A second feature of AQP folding that must be considered is how TMs are properly oriented within the physical confines of the translocon apparatus. Since the nascent polypeptide exits the ribosome vectorally in an N-to C-terminal direction, TMs 1, 3, and 5 must rotate 180° in order to achieve their correct type II (N_{cyto}/C_{lum}) topology. For AQP4, this rotation occurs sequentially and does not require cooperative interactions between multiple TMs [98, 99]. Several lines of evidence have also suggested that TM helices can form very early within the translocation pathway and even within the ribosome exit tunnel [63, 202-204]. Our findings are consistent with this and raise the question as to when and where helix rotation takes place. Both the ribosome tunnel [205, 206] and putative Sec61α translocation pore [49] are clearly too small to accommodate rotation of a 30Å helix. Interestingly, crosslinking profiles revealed that TM3 initially contacts the translocon in a relatively random orientation and then (~10 residues later) enters into a fixed binding site within Sec61α where it remains during synthesis of nearly 80 additional residues. Thus TM3 rotation occurs either before entry into Sec61 or remarkably late as it transitions into its site of secondary interaction.

Early rotation could conceivably take place at the base of the ribosome, particularly if the ribosome-membrane junction were relaxed as TM2 terminated translocation and initiated movement of ICL 1 into the cytosol [27]. TM3 rotation could be facilitated by electrostatic interactions between basic residues near its N-terminus and residues within Sec61α [57, 181]. Alternatively, rotation could conceivable take place in the context of a larger translocon pore or central location within the fully assembled translocon (Figure 7C, D) as has been demonstrated by fluorescence quenching experiments [24, 25, 51]. In this case, TM3 would reinitiate translocation upon entry into Sec61α by reestablishing the ribosome-translocon junction and opening the translocation pathway [27, 29, 52]. A

third possibility is that TM3 could enter the translocon in a type I topology as has been suggested for other signal anchor sequences and then rotate after its exit into its secondary site of interaction [181, 207].

A similar constraint arises with the sequential arrival of TMs4 and 5, which are separated by a very short connecting loop (~9 residues). Both helices exhibit peak crosslinking at the same stage of synthesis, i.e. at a nascent chain length of 216 residues. However, they do not insert in a loop-wise fashion because TM5 must rotate 180° about its axis to initiate translocation of ECL3. It is difficult to conceive how a single Sec61 heterotrimer could simultaneously accommodate TM4, TM5, TM5 rotation, and a strand of ECL3 given the small confines of a single hourglass shaped pore. Thus the observation that TMs 4&5 simultaneously crosslink Sec61 support the presence of a larger structure (possibly a large pore) that can accommodate and provide conformational flexibility to relatively large peptide regions. Important questions therefore remain as to where closely spaced helices reside during the orientation and integration process.

9. Conclusions.

Advances in our understanding of translocon structure and function, as well as the biogenesis mechanisms of translocon "substrates" have led to various models that attempt to explain translocation across and integration into the ER membrane. At the same time, studies of secretory, transmembrane and polytopic protein biogenesis have provided key information that must be incorporated into these models. Studies of AQP biogenesis have revealed novel and unexpected folding pathways that begin to explain how its characteristic transmembrane structure is formed. These studies also have general implications for both membrane protein folding and mechanisms of translocon function. For example, the sequential entry and exit of AQP4 TMs into a primary binding site is consistent with a relatively small translocation pore that accommodates one helix at a

time. In contrast, simultaneous association of multiple helices, the location and timing of helix rotation, and physical constraints imposed by short connecting loops require that a cohesive model of translocon structure and function incorporate the biogenesis needs of protein substrates.

It is now clear that the translocon is integrally involved in directing early events of AQP biogenesis. Evidence also suggests that its role is not solely limited to translocation of extracellular domains and orientation and integration of TM helices. Rather, the early stages of secondary and possibly tertiary folding are likely initiated within the immediate environment of the translocon and prior to release of the entire polypeptide into the lipid bilayer. A full understanding of how these folding events are orchestrated is currently far from our grasp and will undoubtedly require a more precise knowledge of the structural organization of assembled and functional translocons and their specific interactions with the nascent chain. Solving this complex and perplexing problem will require a variety of perspectives and the concerted efforts of numerous individuals using complementary techniques. Ultimately, both complementary and conflicting results must be developed into a unified model that will describe and enable predictions of membrane protein folding pathways with accuracy similar to or greater than that now available for soluble proteins. This information will then facilitate the formidable task of rational therapeutic intervention in situations where the folding pathway has been corrupted by disease related mutations.

Fig. 1-1

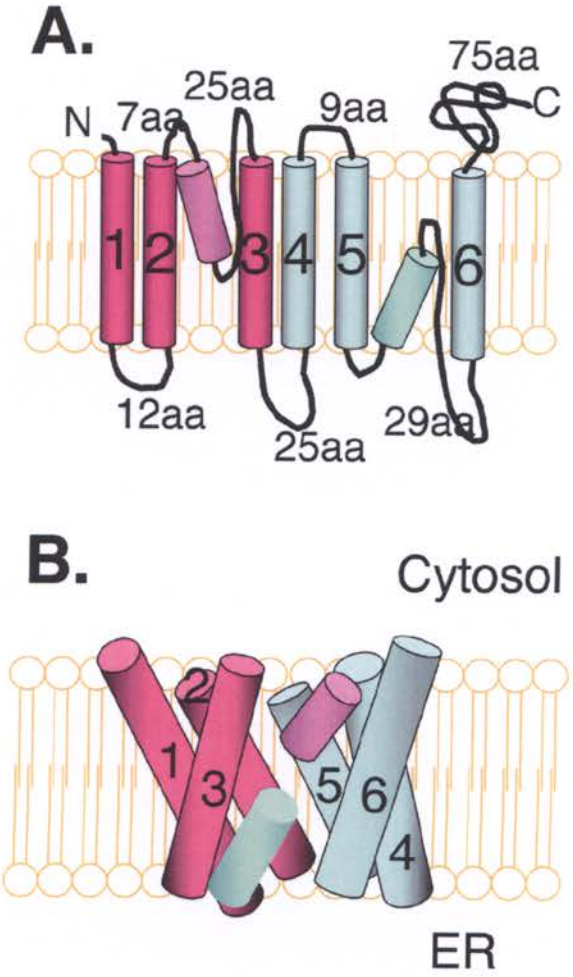

Figure 1-1. Aquaporin structure. **A)** Transmembrane topology of AQP1 showing relative orientation of N- and C-termini , TM segments and half helices. Two "half helices" dip partially into the membrane, and their C-termini comprise the canonical NPA motifs which are necessary for water permeation. Both N- and C-termini of native

AQPs reside in the cytosol. **B)** 3-D arrangement of TMs based on crystal structure of Sui et al. [85]. Note that N-and C-terminal half helices are partially aligned along their major axis and together form an integral part of the outer ring of the water-conducting pore.

Fig. 1-2

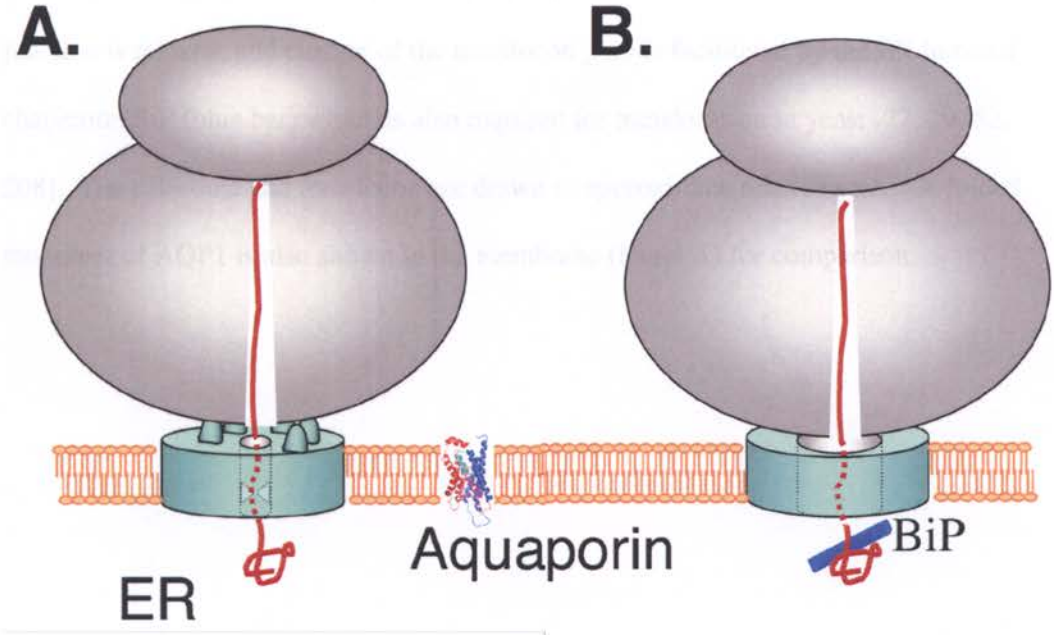

Figure 1-2. General architecture of the ribosome-translocon complex. **A)** Structural model based on cryo-EM studies of detergent solubilized complexes showing ribosome (gray) bound to the translocon (blue) at numerous points of contact (translocon projections). A gap of ~12 Å is apparent between the complexes. The ~10 Å putative translocon pore (internal dotted cylinder) is proposed to be gated by a helical plug (not shown) and a central ring of hydrophobic residues (hydrophobic gasket, gray triangles). **B)** Alternate model of the RTC derived from fluorescence quenching experiments performed on fully assembled and functionally engaged RTC in native ER membranes. The ribosome is shown docked onto a translocon containing a large central pore that is permeable to iodide ions and other aqueous agents. The ribosome exit tunnel and translocon pore forms a continuous aqueous pathway that is inaccessible to the cytosol.

This seal is proposed to be maintained by tight binding of the ribosome to the translocon [24, 25]. During synthesis of cytosolic polypeptide domains the ribosome-translocon junction is relaxed, and closure of the translocon pore is facilitated by the ER lumenal chaperone BiP (blue bar) which is also required for translocation in yeast [27, 29, 52, 208]. The ribosome and translocon are drawn to approximate relative scale. A folded monomer of AQP1 is also shown in the membrane (Panel A) for comparison.

Fig. 1-3

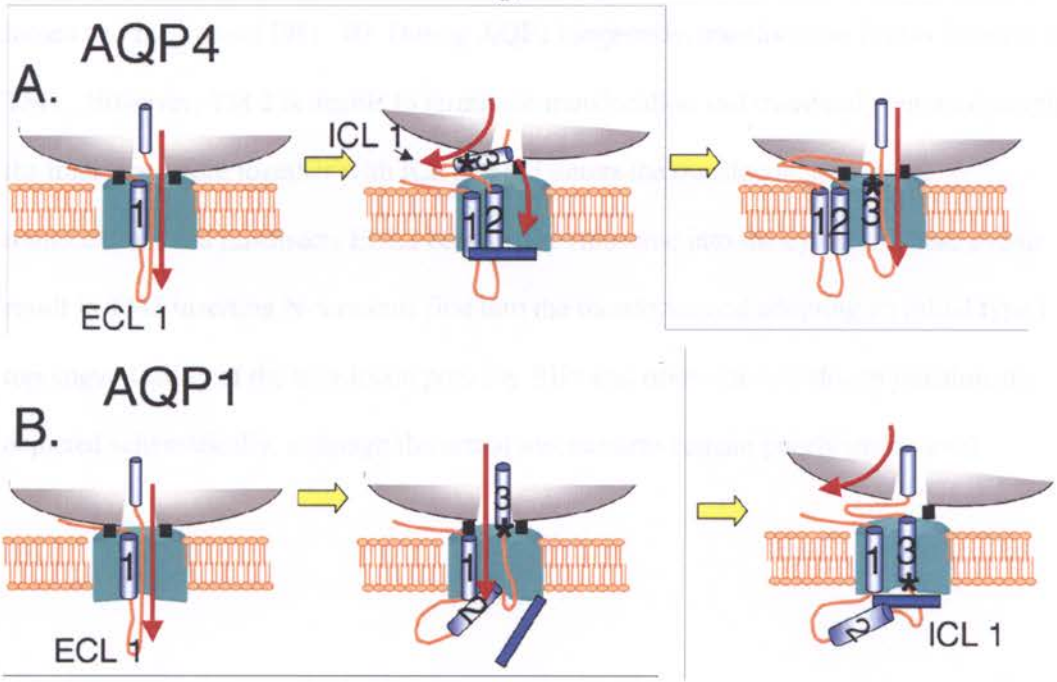

Figure 1- 3. Different mechanisms of AQP1 and AQP4 topogenesis. A) AQP4 topogenesis begins as TM1 (blue cylinder) opens the translocon (teal) at the base of the ribosome (gray disc) and initiates translocation of ECL1 through the translocon pore (left panel). Direction of polypeptide movement is shown by maroon arrow. As TM2 enters the translocon (middle panel) it terminates translocation and presumably closes the translocon gate via BiP (dark blue bar). Polypeptide movement is then redirected beneath the base of the ribosome and into the cytosol to establish topology of ICL 1. TM3 exits the ribosome N-terminus first and resets the RTC by opening the translocation pathway into the lumen thus preventing movement of ECL 2 into the cytosol. During this process, TM3 must rotate 180° such that its N-terminus (designated by *) remains facing the base of the ribosome and its C-terminus flanking residues are translocated. In this manner, AQP4 TMs

are co-translationally oriented via the alternating movement of peptide loops into the ER lumen and the cytosol [98]. **B)** During AQP1 biogenesis, translocation is also initiated by TM1. However, TM 2 is unable to terminate translocation and transiently passes through the translocon pore together with ICL1. TM3 enters the translocon, terminates translocation, and misdirects ECL2 beneath the ribosome into the cytosol. These events result in TM3 inserting N-terminus first into the translocon and adopting an initial type I topology. Gating of the translocon pore (by BiP) and ribosome-translocon junction are depicted schematically, although the actual mechanisms remain poorly understood.

Fig. 1-4

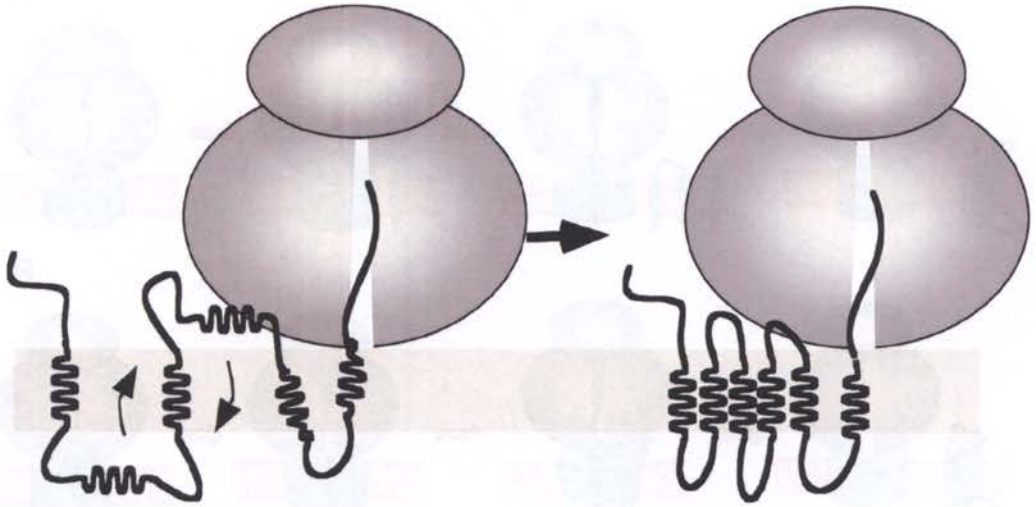

Figure 1- 4. Mechanism of AQP1 topological maturation. To acquire its mature six-spanning topology TMs 2, 3 and 4 must be reoriented during and/or following later stages of synthesis. This involves a late 180° rotation of TM3 that converts it from a type I (N_{lum}/C_{cyto}) to a type II (N_{cyto}/C_{lum}) topology and simultaneously positions TM2 and TM4 across plane of the membrane. The efficiency of TM3 rotation is increased as TMs 4, 5 and 6 are synthesized. Thus C-terminal folding information is required for reorienting N-terminal segments. It is currently unknown whether this unexpected folding step takes place within or adjacent to the RTC or after complete integration of the polypeptide into the lipid bilayer.

Fig 1-5

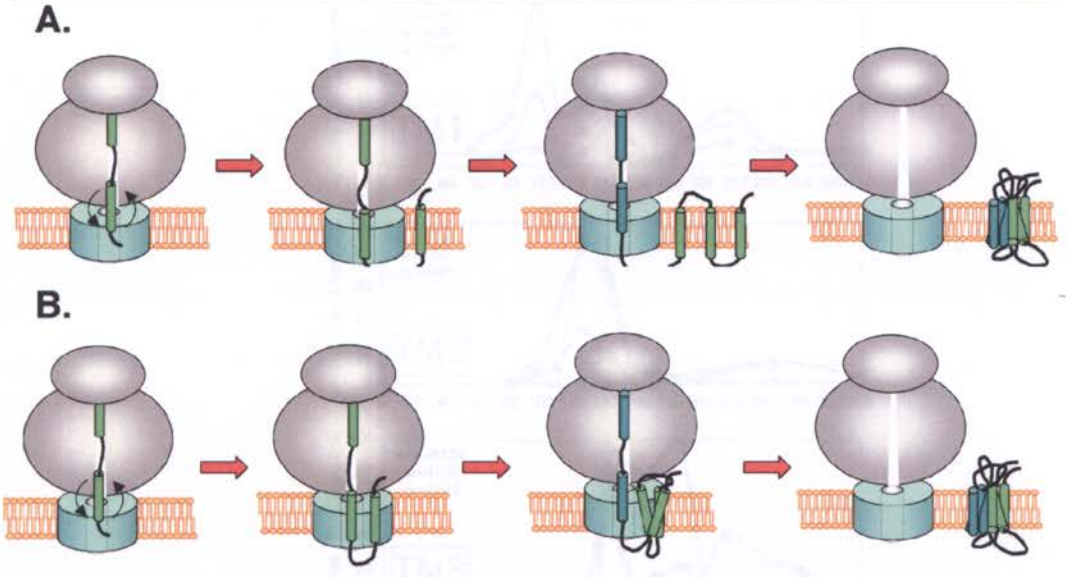

Figure 1-5. Alternate models of TM segment integration. A) In the sequential integration model, TMs (colored cylinders) enter the translocon (blue disc) and rapidly and independently pass through a lateral gate where they equilibrate with the lipid bilayer. Packing of helices and tertiary structure formation would thus take place entirely within the ER membrane. **B)** An alternate model is based on evidence that TMs reside within the translocon for prolonged periods of time prior to integration. This model has significant implications for polytopic proteins because early TM interactions and folding events could be impacted by the physical properties of translocon proteins and associated lipids. This latter model predicts that the translocon may provide a unique and more permissive folding environment that enables nascent TMs to sample alternate conformation prior to adapting their final transmembrane structure.

Fig. 1-6

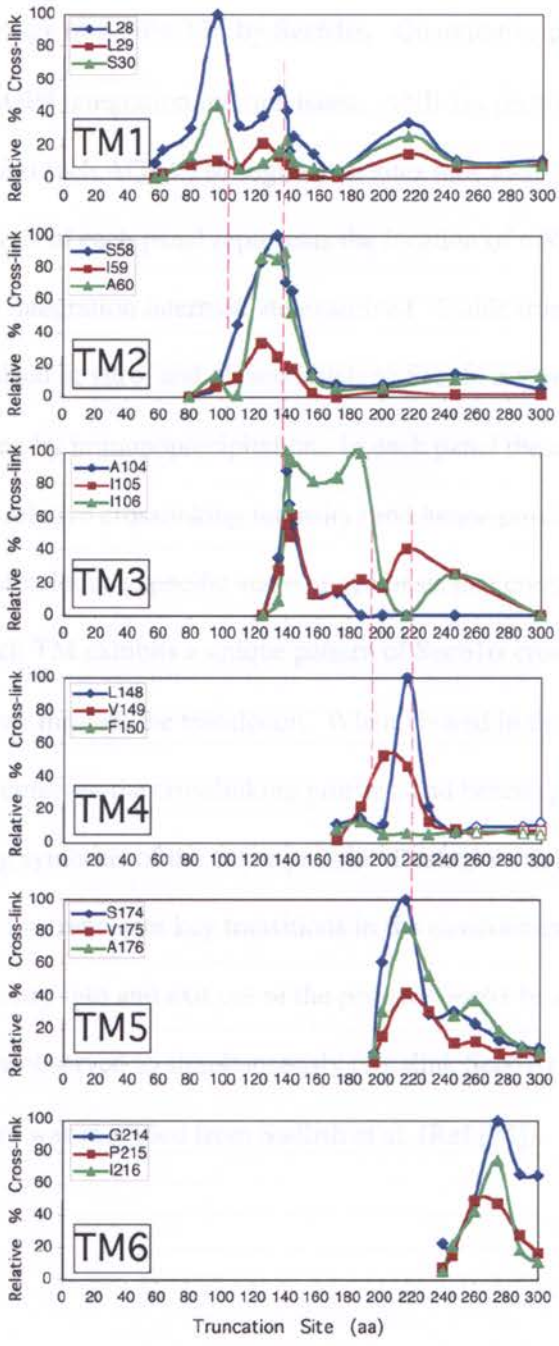
Relative % Cross-link
L28
L29
S30
TM1
S58
I59
A60
TM2
A104
I105
I106
TM3
L148
V149
F150
TM4
S174
V175
A176
TM5
G214
P215
I216
TM6
0 20 40 60 80 100 120 140 160 180 200 220 240 260 280 300
Truncation Site (aa)

Figure 1-6. Sequential triage of AQP4 TM by Sec61α. Quantitative profile of Sec61α crosslinking to truncated AQP4 integration intermediates. ANB-lys photocrosslinking probes were incorporated into each AQP4 TM segment at sites indicated (inset) at the upper left of each panel. The X-axis of each panel represents the location of mRNA truncation and hence the length of the integration intermediate examined. Stable truncated integration intermediates were synthesized in vitro, and photoadducts to Secc61α were identified and quantitated after crosslinking by immunoprecipitation. In each panel the amplitude of the curves therefore shows the relative crosslinking intensity (and hence proximity) of residues on different faces of the TM helix at a specific stage of synthesis that corresponds to the site of truncation. Note that each TM exhibits a unique pattern of Sec61α crosslinking that reflects its particular pathway through the translocon. When viewed in this manner, it is possible to simultaneously compare the crosslinking profiles, and hence spatial relationship of all six AQP4 TMs during synthesis of the entire protein. Dashed vertical lines show specific stages of synthesis that represent key transitions in the environment of TMs and the coordinated timing of TM entry into and exit out of the primary Sec61 binding site. Note also that multiple TMs were observed to simultaneously crosslink Sec61α at the same nascent chain length. Figure was modified from Sadlish et al. (Ref [74]).

Fig. 1-7

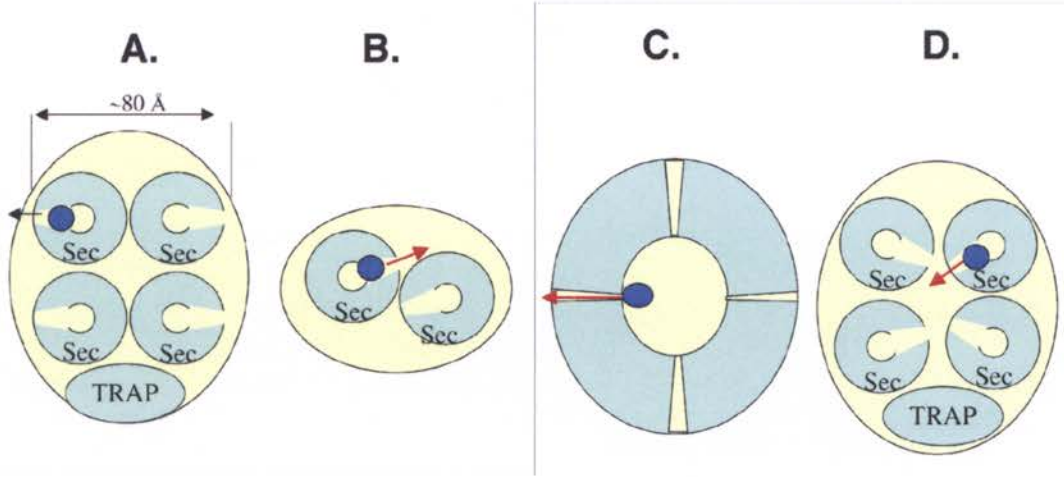

Figure 1-7. Models of the Sec61 lateral exit gate. A) Back-to-back configuration. Possible arrangement of Sec61αβγ heterotrimers (Sec) based on Cryo-EM structure of solubilized ER translocons, 2-D crystals of E. coli SecYEG, and high resolution of the Methanococcus SecYEβ [47-49]. The lateral gate is Shown in yellow and is proposed to reside between TM2 and TM7 of SecY. The size of individual heterotrimers would place exit sites ~80 Å from one another [191]. Blue circle represents nascent TM. Approximate size of the translocon (oval) and proposed location of TRAP is indicated. **B)** Schematic representation of front-to-front arrangement of SecYEG dimers bound to a translating ribosome [50]. **C)** Model of translocon derived from fluorescence quenching experiments showing a large central pore surrounded by oligomeric ring of Sec61 and other translocon proteins [24-26, 51]. Lateral exit sites are shown between putative translocon subunits. **(D)** Hypothetical arrangement of four Sec61 heterotrimers arranged in a front-to-front configuration showing the lateral exit sites of Sec61 heterotrimers

oriented towards the center of the complex where helices could potentially reside prior to passage between subunits into the lipid bilayer.

III. Results - Manuscript 2

Sequential Triage of Transmembrane Segments by Sec61α During Biogenesis of a Native Multispanning Membrane Protein

Heather Sadlish[1*], David Pitonzo[1*], Arthur E. Johnson[2,3], William R. Skach[1]

[1]Division of Molecular Medicine, Oregon Health & Sciences University, Portland, OR 97239

[2]Department of Medical Biochemistry and Genetics, Texas A & M University System Health Science Center, College Station, TX 77843-1114

[3]Departments of Biochemistry and Biophysics and of Chemistry, Texas A&M University, College Station, TX 77843-1114

Published in Nature Structural and Molecular Biology Vol. 12, No. 10 Ict. 2005 pp 870-877

Address correspondence to:

William R. Skach, M.D.
Department of Biochemistry and Molecular Biology
3181 SW Sam Jackson Park Rd, NRC-3
Oregon Health and Sciences University
Portland, OR 97239

Key Words: Protein biogenesis, polytopic protein, membrane integration, translocon, membrane protein, aquaporin, Sec61α.

Author's Contributions. These authors contributed equally to this work.

Abbreviations: AQP, aquaporin; ER, endoplasmic reticulum; PTC, peptidyltransferase center; RRL, rabbit reticulocyte lysate; RNC, ribosome-nascent chain complex; RTC, ribosome-translocon complex; TM(s), transmembrane segment(s).

1. Abstract

During polytopic protein biogenesis, the Sec61 translocon must rapidly orient and integrate multiple transmembrane segments (TMs) into the endoplasmic reticulum membrane. To understand this process, interactions between Sec61α and all six TMs of the aquaporin-4 water channel were examined at defined stages of biogenesis. We now show that each TM interacts with and moves through the translocon in a highly ordered and sequential fashion. Strong asymmetric Sec61α crosslinking was observed for only one helix at a time, suggesting the presence of a single primary binding site. However, up to four TMs could simultaneously contact Sec61α from different molecular environments. Thus, aquaporin-4 integration by Sec61α involves sequential triage of TMs from their initial portal of entry into multiple secondary and tertiary sites within the translocon. This mechanism provides a means to facilitate early membrane protein folding events prior to release into the lipid bilayer.

2. Introduction

The Sec61 translocon is responsible for directing translocation and integration of secretory and membrane proteins in the endoplasmic reticulum[26, 209]. The structural core of the translocon is comprised of the heterotrimeric complex, Sec61α, β and γ, which functions in association with a variety of proteins including oligosaccharyltransferase, signal peptidase, TRAM, and TRAP[26, 49, 210]. Sec61α is thought to form the central aqueous pore through which the nascent polypeptide translocates[22, 25, 48] and is one of the first translocon components to interact with proteins as they emerge from the ribosome[31, 36, 171, 211]. Thus it plays a major role in dictating the immediate environment and the early fate of nascent secretory and transmembrane polypeptides.

During membrane protein biogenesis, hydrophobic transmembrane segments do not normally pass axially through the translocon but rather must be transferred laterally into the lipid bilayer in order to acquire their proper topology. TMs also play a critical role in regulating the ribosome-translocon complex (RTC) by functioning to close the lumenal gate of the translocon pore, relax the ribosome-translocon junction, and expose the growing nascent polypeptide to the cytosol[27, 52, 63]. Crosslinking studies have revealed that as TMs exit the ribosome they enter the translocon at a site adjacent to Sec61α[9, 10, 14, 33, 170, 211]. One important question and still controversial issue in protein biogenesis is at what stage of synthesis and by what mechanism is membrane integration carried out. One view is that TMs passively partition into the bilayer solely or largely by hydrophobic interactions with membrane lipids[10, 14]. Another view is based on the observation that some TMs are held in a fixed orientation adjacent to translocon components for extended periods of time[33, 36] and are released into the bilayer at specific points of synthesis and/or at the termination of translation[33, 36, 56, 198, 211]. These latter studies suggest that the translocon contains relatively specific

binding sites for TMs and that entry into and exit from these sites is regulated by protein-protein interactions within the RTC[33, 36].

In the case of polytopic proteins, relatively little is known regarding how the translocon synchronizes translocation and integration of multiple TMs as they emerge from the ribosome in rapid succession. The translocon must properly orient lumenal and cytosolic loops, maintain the ER permeability barrier and provide a lateral passage for each TM into the lipid bilayer[74, 174, 207]. As with bitopic proteins, polytopic proteins contact Sec61α as they enter the translocon[36, 56, 198]. However, membrane extraction studies have indicated that these TMs may integrate into the bilayer independently, in pairs, or even in groups depending upon the specific substrate and/or folding pathway[54, 55, 100, 194]. Based on its large size (~95 Å diameter) and oligomeric structure[46, 49, 64, 65, 201], it has been proposed that the translocon could potentially accommodate multiple nascent TMs[212, 213]. Such a model, however, raises questions as to how a particular site might be chosen and how the lateral exit of TMs would be coordinated.

To define how the translocon triages TMs during polytopic protein biogenesis, we examined the integration process for the native Aquaporin-4 (AQP4) water channel. Aquaporins comprise a highly conserved protein family that forms water-selective pores in biological membranes[87, 148, 149]. They share a common topology in which six TMs are arranged in an inverse two-fold symmetry around a single monomeric pore[84, 85]. Although folding pathways of different aquaporins vary[98, 100], AQP4 utilizes a strict co-translational mode of topogenesis both *in vitro* and *in vivo*, whereby the topology of each TM is established independently and sequentially as it emerges from the ribosome[98, 99]. AQP4 therefore provides an ideal substrate to define how early translocon interactions mediate co-translational translocation and integration events. In the current study, the molecular environment of each AQP4 TM was examined using

photoactive crosslinking probes incorporated into synchronized integration intermediates. Crosslinking profiles to Sec61α revealed that all six TM helices enter and progress through the translocon in an ordered and sequential fashion. This progression was remarkably variable, related to TM orientation and topogenic properties, and could be quite prolonged. In each case, the initial Sec61α interactions observed for a given TM were disrupted upon entry of the next TM. However, multiple TMs (up to 4) were observed to simultaneously contact Sec61α after displacement from their initial site of interaction. These results suggest that the translocon utilizes a single primary site for TM entry while providing a scaffold, or protected environment that facilitates early folding of polytopic proteins prior to their release into the lipid bilayer.

3. Results

Experimental Strategy.

Programmed translocation intermediates have been widely used to investigate interactions between nascent polypeptides and ER translocon components. In this technique, translation of truncated mRNAs (i.e. lacking a terminal stop codon) yields stable ribosome-translocon complexes (RTCs) that contain a uniform cohort of nascent chains arrested at a pre-defined stage of synthesis. Here we used a modified tRNA, N^{ε}-(5-azido-2-nitrobenzoyl)-Lysine-$tRNA^{amb}$ (εANB-Lys-$tRNA^{amb}$), to introduce a photoactive crosslinking probe at isolated engineered amber (TAG) codons placed near the center of each AQP4 TM. Upon encountering the amber codon, the ribosome either terminates translation and releases the nascent chain, or inserts the εANB-Lys moiety and continues translation until the end of the mRNA is reached. This precisely positions the probe at a unique location in the polypeptide which remains tethered to the ribosome via its covalent peptidyl-tRNA bond. UV-irradiation then converts ANB into a highly reactive nitrene radical that forms non-specific covalent crosslinks to adjacent molecules. The short lifetime of the nitrene group and the 12 Å Lys spacer arm limits crosslinking to

the immediate vicinity of the probe. Importantly, each nascent polypeptide can form only one crosslink because it contains a single ANB moiety. Crosslinking patterns therefore provide specific spatial information regarding proximity of the probe to neighboring molecule(s). Our strategy was to use sequentially truncated mRNAs of different lengths to generate a series of synchronized 'static' integration intermediates, each of which represents a defined step along a dynamic assembly pathway. Transient nascent-chain interactions with Sec61α at each stage of synthesis were then captured by photocrosslinking and used to reconstruct changes in the molecular environment experienced by all six AQP4 TMs as they enter, traverse and exit the ER translocon.

Photoactive probe incorporation does not alter AQP4 biogenesis.

Although the εANB-Lys probe is uncharged and has previously been shown to have minimal effects on protein topology[31, 33], we first confirmed that it did not affect AQP4 biogenesis. For these studies amber codons were placed near the center of the last TM in a series of previously described fusion proteins[98] that contained a passive C-terminal translocation reporter (**Fig. 1a**). When translated *in vitro*, addition of εANB-Lys-$tRNA^{amb}$ resulted in read-through of the TAG codon and generation of full length fusion proteins (**Fig. 1b**). Extra bands (bracketed) were observed for V140-I105TAG (read-through) and T164-V149TAG (truncated) constructs because removal of TM4-6 results in N-linked glycosylation of a consensus site at residue Asn132 as described previously[98]. Protease protection revealed that ANB-containing constructs exhibited very similar topology to WT proteins (**Fig. 1c & d**). The reporter domain was protected from protease in the absence but not the presence of detergent when it was fused C-terminal to TMs 1, 3 and 5, whereas the reporter was uniformly protease accessible (cytosolic) when it was fused downstream of TMs 2, 4 and 6. This is consistent with previous studies and demonstrates that TMs 1, 3 and 5 initiate polypeptide translocation

into the ER lumen, while TMs 2, 4 and 6 terminate translocation and orient downstream peptide loops towards the cytosol. Thus the presence of an ANB probe does not significantly influence the topogenic behavior of AQP4 TMs.

Nascent chain crosslinking in intact RTCs.

Amber stop codons were next introduced individually at three adjacent sites within each TM of full length AQP4 (**Fig. 2a**), and truncated mRNAs were generated from PCR-amplified DNA templates using antisense oligonucleotides as described in Methods. When translated in the presence of ER microsomes, these mRNAs generate RTCs that contain nascent AQP4 polypeptides with a single ANB probe precisely positioned relative to the ribosome peptidyltransferase center (PTC) and translocon. To examine the environment of probes incorporated into TM1, TAG codons were engineered at residues 28, 29 or 30, and AQP4 mRNA was truncated at codon 96. This length is sufficient to target the ribosome-nascent-chain complex to the ER membrane (data not shown), initiate translocation, and position the εANB-Lys moiety ~66 residues from the PTC. Incorporation of εANB-Lys was confirmed by TAG codon read-through and generation of polypeptides that co-migrated with the 11 kDa WT protein fragment (**Fig 2b**). UV irradiation of ANB-containing polypeptides resulted in the appearance of a major photoadduct that slowed migration by ~35-40 kDa (**Fig. 2b,** downward arrowheads). Both read-through and photoadduct formation were dependent upon the presence of εANB-Lys-$tRNA^{amb}$ and were not observed after puromycin release of nascent chains from the ribosome. Thus the interactions captured by photocrosslinking are specific for intact physiological translocation intermediates. Immunoprecipitation identified Sec61α as the major photoadduct to TM1 (**Fig 2b,** lanes 17-20). Similar experiments performed using polypeptides truncated at residues 123, 144, 216 and 260 also confirmed site-specific Sec61α photocrosslinking to each of the remaining five AQP4 TMs (**Fig. 2c**). Peak crosslinking efficiency was ~5-15% for most TMs examined which is consistent

with previous studies[36, 56]. Crosslinking also varied significantly for different probe incorporation sites even within the same TM, indicating that adjacent residues can exhibit different relative proximities to translocon components.

TM proximity to Sec61α is coupled to the stage of translation.

If the translocon integrated each TM into the lipid bilayer independently, then crosslinking should reflect a relatively rapid movement away from Sec61α as the nascent polypeptide elongates. On the other hand, if the translocon accommodated multiple TMs simultaneously, then interactions should persist and overlap with one another. To distinguish between these possibilities, AQP4 mRNAs were truncated at sequential sites in the coding sequence and used to generate integration intermediates containing εANB-Lys. Because each integration intermediate reflects the spatial organization of the RTC at a defined stage of AQP4 synthesis, collective crosslinking profiles at multiple nascent chain lengths provide a series of snapshots of the molecular environment experienced by a given TM during its passage through the translocon. This approach is illustrated in **Fig.3** where polypeptides were truncated at residues 96, 125, 135, 140, 157, 201, 246 and 300, and ANB probes were incorporated near the center of TM2 at codons 58, 59 or 60. Nascent chains that terminated at the TAG codon migrated as ~7 kDa polypeptides, whereas εANB-Lys incorporation resulted in translational read-through and progressively larger sized proteins. Appearance of a UV-dependent photoadduct to TM2 was faintly observed following truncation at codon 96 when the ANB probe had reached a distance of ~37 residues from the PTC (**Fig. 3, first panel**). The efficiency of crosslinking increased as translation proceeded to residues 125, 135 and 140 and decreased after synthesis of residue 157. Thus TM2-translocon interactions are very transient and dependent upon the specific stage of polypeptide synthesis.

AQP4 TMs exhibit distinct profiles of Sec61α interactions.

Genetic, biochemical and functional studies have identified Sec61α as the major translocon component involved in facilitating translocation, orientation and integration of membrane proteins[26, 209]. We therefore focused attention on interactions with Sec61α as a primary measure of entry into and movement through the translocon. Integration intermediates were generated from AQP4 mRNAs truncated at ~15 residue intervals (closer where indicated), and crosslinking was performed in parallel for WT and probe-containing constructs. To compare crosslinking efficiencies at different sites and different chain lengths it was necessary to compensate for wide variations in translation and read-through efficiency among a large number of samples. This was accomplished by a rigorous quantitation of translation products as described in Methods. Translation reactions for all truncations and probe incorporation sites within a single TM were simultaneously analyzed in duplicate or triplicate by SDS-PAGE and imaged on a single phosphorimaging screen to determine the intensity of WT and read-through bands. Equal amounts of radiolabeled products were then reevaluated by SDS-PAGE/phosphorimaging to confirm the accuracy of normalization. Representative raw data used for quantitation and normalization of a series of TM1 constructs are shown in **Supplementary Fig. 1**.

Equal amounts of UV-irradiated translation products were then immunoprecipitated (in duplicate) under denaturing conditions with excess Sec61α antisera. All samples obtained for a given TM were processed and imaged together. **Fig. 4** shows a representative set of immunoprecipitations obtained for each group of TAG codons and truncations for all six AQP4 TMs. Because the input was normalized prior to immunoprecipitation, bands intensities directly reflect the relative crosslinking efficiency at each probe incorporation site within a given TM. In each case, Sec61α photoadducts were compared to WT controls which were translated and immunoprecipitated in parallel. As expected WT signal was negligible in most cases although low levels of non-specific

background were detected in some experiments (i.e. **Fig. 4c**). This was not due to misincorporation of probe in WT protein but rather resulted from a very low level of crosslinking due UV irradiation of endogenous residues (data not shown). By correcting for WT background in each experiment we were able to determine the net signal attributable to crosslinking at the engineered probe incorporation site. Specific ANB-mediated crosslinking was readily observed for each TM examined, and each TM exhibited a characteristic crosslinking profile. For example, Sec61α crosslinking to TM2 and TM4 revealed a sharply defined, transient interaction (**Fig. 4b & 4d**). In contrast, TM1, TM3 and TM5 crosslinked Sec61α during relatively prolonged periods of polypeptide synthesis (**Fig. 4a, 4c, 4e**). Crosslinking profiles also differed for probe incorporation sites located at adjacent residues within the same TM. For most samples, Sec61α photoadducts were isolated as well-defined species, although some longer truncations (e.g. TM6-G214) exhibited a more diffuse appearance (**Fig. 4f**). This may reflect aberrant migration due to their increased hydrophobicity of photoadducts or possibly crosslinking to different TM regions within Sec61α as previously described[196].

TM1 passes through multiple environments within the Sec61 translocon.

To compare the profile translocon interactions for different TMs, the average relative intensity of Sec61α photoadducts (obtained from at least two independent experiments) was plotted as a function of nascent chain length (**Fig. 5**). This analysis provided a useful means to visualize the unique spatial relationship between Sec61α and each TM during synthesis of the entire AQP4 protein. Sec61α crosslinking was first observed for TM1 at a polypeptide length of 60 residues, and maximal crosslinking occurred at a length of 96 residues (**Fig. 5a**). Residues within TM1 yielded marked differences in crosslinking efficiency (L28>S30>>L29), suggesting that probes located on different faces of the helix exhibited different proximities to Sec61α. This is consistent with

previous studies[36, 198] and suggests that when TM1 is optimally located within the translocon, it is not oriented randomly but is held in a fixed position relative to Sec61α. It is unlikely that the asymmetry of these interactions is due to steric constraints imposed by the helix because relative crosslinking was more dependent on the stage of synthesis than on the location of a particular residue. At truncation 110, TM1 crosslinking decreased significantly, presumably because TM1 was at least partially displaced from Sec61α. Crosslinking was again observed at a nascent chain length of 120-160 residues, although the intensity of Sec61α photoadducts was reduced. The profile of these secondary interactions suggests that TM1 moved into a different molecular environment than it had previously occupied at a chain length of 96 residues. TM1 exited this secondary site after synthesis of residue 172, but exhibited yet a third phase of weak crosslinking at a nascent chain length of 216 residues. Thus, as TM1 progressed through the translocon, it encountered at least three distinct molecular environments. Each phase of crosslinking occurred during a specific stage of synthesis, and was separated by periods of reduced or absent Sec61α contact.

AQP4 TMs are sequentially triaged from their initial binding site and follow different paths through the translocon.

The profile of TM2 crosslinking differed significantly from that of TM1. TM2 initially contacted Sec61α at a nascent chain length of ~96 residues (**Fig. 5b**). It then entered a site characterized by strong crosslinking to residues 58 and 60 but weak crosslinking to residue 59 and remained in this environment during synthesis of ~40 residues. Within the resolution of our measurements, TM2 entry into Sec61α (i.e. at synthesis of residue 110) coincided remarkably well with the exit of TM1 from its initial site of interaction. However, TM2 crosslinking occurred during the same interval observed for secondary TM1 crosslinking. Thus both TMs were simultaneously adjacent to Sec61α at a chain length of 120-160 residues. In contrast to TM1, TM2 exhibited only a single, sharply

delineated phase of crosslinking, and no significant interactions were observed after synthesis of residue 157. The timing of these events suggests that TM2 entry into Sec61α is mechanistically coordinated with TM1 exit and reentry into a secondary site of interaction. Alternatively, changes in TM1 crosslinking patterns might also be caused by direct interactions between TM1 and TM2. In either case, however, TM1 is displaced into a new molecular environment as TM2 enters Sec61α at a chain length of 110 aa.

TM3 entered into the translocon abruptly at a nascent chain length of 135-140 residues as evidenced by simultaneous crosslinking to Sec61α at all three probe incorporation sites (**Fig. 5c**). This was rapidly followed by a dramatic decrease in crosslinking to residues 104 and 105 but persistent crosslinking to residue 106. Because TM3 exits the ribosome N-terminus first and because it functions as a type II signal anchor sequence, TM3 must rotate 180° about the plane of the membrane in order to acquire its N_{cyt}/C_{exo} topology. The brief concurrent crosslinking to probes at residues 104, 105 and 106 , together with topogenesis data (**Fig. 1**), suggests that TM3 initially encounters Sec61α in a relatively unrestricted environment that might accommodate this rotation and that TM3 movement is subsequently restricted once its proper topology is established. During synthesis of residues 135-144, TM1, TM2 and TM3 all simultaneously crosslinked to Sec61α. This pattern was consistently and repeatedly observed for multiple closely spaced truncations in this region of AQP4 (**Figs. 4&5, panels a-c**). Remarkably, the stage at which TM3 acquired its fixed orientation within the translocon (truncations 144-157) coincided with the loss of TM2 crosslinking. These results demonstrate that highly coordinated transitions take place during remarkably brief intervals of translation as sequential TMs enter the translocon. Specifically, TM2 appears to be displaced from Sec61α not at the initial contact of TM3 (truncation 135), but rather 10-20 residues later as TM3 enters into its specific (fixed) binding site. TM3 entry also coincided with release of TM1, which

indicates that TM1 and TM2 depart from Sec61α together at a chain length of ~157 residues.

TM4 crosslinking was first detected during synthesis of residues 172-187 (**Fig. 5d**). Once again, the timing of TM4 entry into Sec61α coincided with abrupt disruption of TM3 interactions. Like TM1, however, TM3 was displaced into a different environment adjacent to Sec61α in which the relative crosslinking efficiency to residues 105 and 106 was reversed (**Fig. 5c**). Two other events occurred at this stage of synthesis (i.e. at a length of 216 aa). TM1 crosslinking to Sec61α was again detected, and TM5 entered the translocon. Thus, for a brief interval, four different TMs were in simultaneous contact with Sec61α. Crosslinking to both TM4 and TM5 peaked during synthesis of residue 216. This is likely due to the very short connecting peptide loop (~9 residues) and the fact that TM5 must rotate 180° in order to acquire its proper N_{cyt}/C_{exo} topology while at the same time remaining in close proximity to TM4. It is interesting that the pattern of TM4 crosslinking changed significantly during this time. As TM4 initially entered the translocon, residue 149 crosslinked more strongly than residue 148, whereas this pattern was reversed (residue 148>149) upon TM5 entry. Taken together, these data suggest a scenario whereby TM4 displaces TM3 and is then rapidly influenced by TM5. At this stage (synthesis of residue 230-240), only TM5 and TM3 remained adjacent to Sec61α.

TM6 entered the translocon and crosslinked to Sec61α at truncation 275. Consistent with other TMs, TM6 entry corresponded with exit of TM5. Sec61α-TM6 crosslinking was also observed at truncation 300, which is only three residues upstream of the native termination codon. Thus, TM6 remains adjacent to Sec61α during synthesis of the entire cytosolic C-terminal domain, and AQP4 is ultimately released from the translocon only after the last remaining residues are synthesized and translation is terminated.

Crosslinking profiles obtained for individual TMs revealed that at nascent chain lengths of 140 aa and 216 aa, , TMs1, 2, 3 and TMs 1, 3, 4, 5, respectively, are in simultaneous contact with Sec61α (**Fig. 5**). These results of indicate that the translocon can interact with multiple TMs at different stages of synthesis. To test this finding in a more direct manner, we examined crosslinking to multiple TMs in AQP4 constructs that were all truncated at the same length. Experiments were also carried out to identify AQP4 interactions with TRAM, which has been shown to crosslink a subset of signal sequences and TMs [33, 36, 198]. Despite clear photoadducts to Sec61α, TRAM photocrosslinks were could not be reproducibly detected and quantitated when probes were incorporated into TMs1 -2 (12-15 truncations sites, **Supplementary Fig. 2**) or TMs 3-4 (8-9 truncations examined, data not shown). This was not a result of crosslinker specificity or immunoprecipitation conditions, because TRAM photoadducts were easily identified when εANB-lys was incorporated into the signal sequence of a known TRAM-interacting protein, bovine preprolactin, (**Supp. Fig. 2**). Consistent with previous studies [31], the N-terminus of this cleavable signal sequence (codons #4&9) predominantly crosslinked TRAM whereas nearby residues within the hydrophobic core (codon 18) crosslinked only Sec61α. Thus while our findings indicate that the center of AQP4 TMs preferentially contact Sec61α, it remains possible that TRAM might interact with other regions of AQP4 not examined here.

4. Discussion.

This study provides the first comprehensive description of how multiple TMs enter, traverse and exit the Sec61 ER translocon during the complete biogenesis and integration of a native polytopic membrane protein. A key element of our analysis is that each AQP4 truncation site represents a single point of synthesis and thus defines a specific spatial arrangement of helices relative to the translocon at a single point in time. Crosslinking profiles of multiple TMs at different points of synthesis and at multiple

probe sites per TM thus provide a sense of the dynamic changes experienced by each individual AQP4 helix within translocon environment. Although crosslinking patterns cannot be extrapolated to define the full nature of TM interactions, our results indicate that TM helices undergo specific transitions from one environment to another and that these transitions are tightly coupled to specific stages of synthesis. From these analyses we have developed a model to describe how the system triages multiple TMs in a spatial and time-dependent manner during translation of the nascent polypeptide (**Fig. 7**). While this model does not attempt to provide precise conclusions about structural changes or kinetics associated with protein folding, it does provide a relatively complete view of the proximity of a native polytopic protein to Sec61α as it is synthesized, oriented and integrated in native ER membranes. Specifically, we show that each TM helix interacts with and moves through the translocon in an ordered and sequential fashion. The progression of different TMs through the translocon is remarkably variable, is related to their orientation and topogenic properties, and can be quite prolonged. This model now provides a framework upon which to compare proteins with different properties and folding pathways.

A principal finding of our studies is that upon emerging from the ribosome, each TM rapidly enters a specific environment within or adjacent to Sec61α that is characterized by asymmetric crosslinking to different faces of the helix. In most cases, a given TM occupied this initial fixed binding site only until the oriented entry of the next TM. This consistent, precise and sequential movement suggests that the translocon contains (or at least utilizes) a single primary site of entry. However, further studies are required to determine whether TMs are actively displaced from this site by the entering TM and how their environment might be affected during synthesis of a large extramembranous domain. As TMs exit from this site, they either lost their associations with Sec61α completely or were transferred to secondary (or tertiary) sites with distinctly different

molecular environments. For example TMs 2 and 4 exhibited a single period of Sec61α crosslinking that persisted during synthesis of ~40-55 residues, whereas TM1, 3 and 5 underwent prolonged and/or multiple distinct phases of Sec61α crosslinking. The result of this process was that up to four AQP4 TMs could be simultaneously adjacent to Sec61α during a single stage of integration. Moreover, both entry into and release of TMs from primary and secondary sites were precisely coordinated. This behavior strongly suggests that membrane integration of polytopic proteins does not involve rapid spontaneous movement of TMs into the lipid bilayer, but rather a regulated progression through successive sites of interaction with translocon components. Progression of TMs into and through these secondary sites varied markedly, further indicating that such interactions are likely governed by individual TM properties and/or specific features of the particular folding pathway. Taken together, our results suggest that the translocon may function as a highly complex scaffold whereby TMs enter through a common pathway and are then sorted to intermediate locations where they reside for various times during sequential stages of synthesis, folding and assembly.

An important and poorly understood aspect of translocon function is how Sec61 and its associated components are organized beneath actively translating ribosomes and facilitate membrane protein translocation and integration. The mammalian translocon is a dynamic ovoid disc ~95 Å (diameter) by 50 Å that contains multiple copies of the heterotrimeric protein Sec61αβγ [45, 201] and a putative aqueous translocation pore closely aligned with the ribosome exit tunnel at the base of the 60 S subunit[25, 44, 46, 64, 65]. Based on the crystal structure of an archaebacterial Sec61 homolog, SecYEβ, it has been proposed that Sec61 heterotrimers form channel-like translocation pores 8-12 Å in size with a single lateral opening into the lipid bilayer[48]. Cryo-EM studies of *E. coli* SecYEG 2-D crystals have also indicated a rigid back-to-back configuration that places the lateral exit sites ~80 Å apart [47, 48]. If this were the case for actively engaged

mammalian translocons, then the short length of AQP4 connecting loops (9-25 residues) would significantly constrain sequential TMs from exiting different pores, and force AQP4 to use only one of the translocon channels potentially available [49]. Our data partially support such a model in that the translocon appears to utilize a single portal of entry that accommodates only one primary helix at a time. However, in the case of TM4 and TM5, the translocon must accommodate both TMs simultaneously while providing adequate space for the signal anchor (TM5) to rotate and initiate translocation of its C-terminal flanking residues. The precise mechanism by which this takes place is unknown but would likely require significant expansion of the proposed pore beyond its predicted size. Thus productive phases of translocation and integration, possibly induced by ribosome and or substrate binding, might create an expanded entry site or multiple entry sites governed by allosteric interactions and/or specific substrate requirements. Consistent with this possibility, significant Sec61 reorganization has been reported following translocon binding to ribosomes and SecA in eukaryotic and prokaryotic systems, respectively [201, 214].

This study provides further insight into previous reports that the translocon can simultaneously accommodate multiple TM helices[54, 55, 194]. Based on current low resolution structures of functionally engaged ER translocons it is difficult to predict where secondary and tertiary interactions might take place. However, the dynamic nature of Sec61α crosslinking indicates that TMs do not accumulate at the initial entry site used for translocation. Rather, secondary sites are likely located away the translocation pathway itself, perhaps along the lateral passage(s) into the lipid bilayer or near the translocon periphery [33, 36]. Our results are also compatible with models in which Sec61 heterotrimers, together with other components, might collectively surround a larger translocon "pore", perhaps partially filled with lipid as suggested by recent cryo-EM studies, that could accommodate and facilitate release of TMs through one or more

lateral exit sites [44, 46, 51, 64, 65, 201]. One appealing although speculative hypothesis is that upon exiting Sec61, TMs might be transiently retained in the lipid-rich environment near the center of the translocon complex which could provide a unique protected environment to facilitate early membrane polytopic protein folding. Importantly, functional models must now account for the ability of Sec61 to simultaneously accommodate TMs with very short connecting loops (i.e. TMs 4,5), allow for simultaneous TM binding and reorientation of signal anchor sequences (i.e. TM2 and 3), and provide a means to accumulate multiple TMs adjacent to one or more Sec61 heterotrimers.

Secondary Sec61α interactions might also be influenced by tethering of TMs to the nascent polypeptide. While we can not rule out this possibility, we think this unlikely to fully explain our findings. First, different faces of tethered helices would not be expected to exhibit the specific and asymmetric crosslinking observed. Second, crosslinking to several TMs (e.g. TMs 1 and 3) decreased significantly before secondary Sec61α interactions occurred. This implies a distinct exit and reentry into a different site similar to that observed for the bacterial protein Lep[56]. Third, release of several TMs from secondary sites of interaction occurred over a relatively short duration of synthesis, which would have relatively minor effects on the "tether" length. Fourth, TM2 and TM4 did not exhibit secondary Sec61α interactions even though they should remain in close proximity to the translocon. Thus these helices were either completely released from Sec61α, transferred into secondary sites formed by other translocon components or masked by intramolecular interactions with other AQP4 TMs.

The primary focus of this study was to define the principle events by which native TMs are triaged from the translocon pore by Sec61α. However, other translocon-associated proteins (i.e. Sec61β, TRAM, TRAP, PAT10, STT3, and ribophorin I) can interact in a

selective manner with a subset of nascent polypeptides and their TMs[33, 36, 37, 56, 75, 141, 198]. Thus it seems likely that translocon components in addition to Sec61α will interact with AQP4 during different stages of synthesis and integration. We were unable to demonstrate such interactions for TRAM using probe incorporation sites near the center of TMs 1-3. However, it is possible that different residues within TMs (cytosolic or lumenal ends) might be more favorably positioned relative to TRAM[31]. Similarly, certain interactions might be more apparent at different nascent chain lengths. Further detailed studies are therefore needed to delineate the complete complement of proteins (and lipids) that facilitate AQP4 integration. Identification of such components, their duration of interaction, and ultimate function in the integration process represent important areas of future investigation.

AQP4 utilizes a well defined, co-translational mechanism of biogenesis in which each TM acquires its topology in a sequential and vectorial manner as it emerges from the ribosome[98]. Thus in one sense, AQP4 biogenesis represents the simplest mechanism because each TM acts as an independent topogenic determinant. Yet even in this case, the translocon exhibits remarkable flexibility in handling TMs with different topogenic and structural properties. Given that the short AQP4 connecting loops require TMs to remain in relatively close proximity to one another, it seems likely that patterns of Sec61a interactions may also reflect intermediate stages of folding. High resolution structures of two aquaporins, AQP1 and GlpF, have revealed a common two-fold symmetry in which TMs1-3 and TMs4-6 form inverted but structurally similar units[84, 85]. Thus it is tempting to speculate that recruitment of TM1 back to Sec61a, and simultaneous release of TMs 1 and 3 at a chain length of 230-240 residues may reflect early folding events (i.e. early helical packing) of the first half of AQP4 while synthesis and orientation of the C-terminal half is being completed. If this were the case, then the translocon might provide a permissive environment that allows formation of partially folded intermediates prior to

stable integration of the entire protein into the membrane. While TM association might be predicted to result in intramolecular crosslinks, detecting such events using incorporated photocrosslinkers is difficult and relies on subtle changes in protein migration during SDS-PAGE which we were unable to detect in the current study. Additional, more sensitive approaches are therefore required to define precisely when and where AQP4 TM helices begin to form tertiary structure.

Finally, recent studies have indicated that polytopic proteins also utilize a number of variations on the cotranslational biogenesis pathway examined here. Such variations involve cooperative interactions between topogenic determinants [54, 215], delayed membrane integration[55, 194], and even reorientation of initial topology of internal TMs[58, 179]. The next challenge is to compare how basic mechanisms of translocon function facilitate the diverse array of folding pathways utilized by native polytopic proteins and to determine how specific steps in these pathways are disrupted in protein folding disorders.

5.Methods

Plasmid Construction

Plasmid pSP64T-MIWC[216] was used as a template to insert amber TAG stop codons into the rat AQP4 cDNA at residues L28, L29, S30, S58, I59, A60, A104, I105, I106, L148, V149, F150, S174, V175, A176, G214, P215, and I216. Site directed mutagenesis was performed using PCR overlap extension (Vent DNA polymerase (New England Biolabs, Beverly, MA)) as described previously[215]. In some constructs, silent mutations were introduced adjacent to the TAG codon for screening purposes. Final PCR fragments were digested with either HindIII (5' polylinker) and BstX I (in AQP4) or BstX

I and Xba I (3' polylinker) depending on location of the TAG codon, and re-ligated into a similarly digested pSP64T-MIWC plasmid. Truncated WT AQP4 fusion proteins are described elsewhere[98] and encode the AQP4 coding sequence (residue 1 to V46, K92, V140, T164, W209, and V297) fused upstream of a C-terminal translocation reporter containing the C-terminal 142 residues of bovine prolactin. Fusion proteins containing engineered TAG codons were prepared in the same manner using AQP4 templates that contained a single TAG codon at indicated residues. Templates were chosen such that the TAG codon was located within the TM just prior to the fusion site. PCR fragments were digested with NheI (in pSP64 vector) and BstEII and ligated into a reporter-containing NheI/BstEII-digested vector previously described[98]. All regions of PCR-amplified DNA were verified by sequencing.

In vitro transcription, translation

AQP4 cDNA was amplified by 20 cycles of PCR. The 5' oligonucleotide was complementary to pSP64 bp 2757 (AGGATCTGGCTAGCGATCACC). 3' oligonucleotides were complementary to the AQP4 coding sequence and contained an additional two codons (TCA GGT in sense direction) such that all truncated nascent chains ended in Ser Gly to standardize for spontaneous peptidyl-tRNA hydrolysis of translocation intermediates. The lengths of amplified AQP4 including the Ser Gly addition were: 57, 63, 80, 96, 110, 125, 135, 140, 142, 144, 157, 172, 187, 196, 201, 208, 216, 230, 240, 246, 260, 275, 289 and 300 residues. PCR products were transcribed *in vitro* at 40°C for 1 hour using SP6 RNA polymerase (Epicentre, Madison, WI) as described in detail elsewhere[99]. Transcripts were extracted with phenol/chloroformed precipitated in ethanol, dissolved in an equal volume of water and stored at –80° C.

In vitro translations were performed as described elsewhere[99] in reactions containing [^{35}S]methionine (Tran[^{35}S]label, ICN, Costa Mesa, CA), 40% hemin-supplemented and

nucleased rabbit reticulocyte lysate, and canine pancreas microsomal membranes (OD_{280}=6.0-10.0) with the following modifications. Reactions contained 40 μM each of 18 amino acids (not methionine or lysine). DTT was replaced with 2 mM reduced glutathione, and εANB-Lys-$tRNA^{amb}$ and/or puromycin were added to a final concentration of 0.9 pmol/μl (Lys moiety) and 1 mM, respectively, where indicated. All reactions containing crosslinker probe were assembled and carried out in a photographic darkroom under safe-light conditions. Translation times were determined empirically to minimize peptidyl-tRNA hydrolysis and ranged from 25 to 60 min.

Protease protection

Translation samples were incubated on ice for 1 h in the presence of proteinase K (0.2 mg/ml final concentration) and Triton X-100 (1% w/v) as indicated. Protease was inactivated by addition of PMSF (10 mM) and rapid mixing with 10 volumes of 1% (w/v) SDS, 0.1 M Tris-HCl (pH 8.0) preheated to 100°C. Equal samples from each reaction were immunoprecipitated as described below with 1 μl of anti-prolactin antisera (ICN Biomedicals, Costa Mesa, CA) prior to SDS-PAGE. Gels were quantitated by phosphorimaging, and reporter translocation (% protection) was determined by the fraction of prolactin reactive peptides protected from protease compared to starting material after correcting for methionine content of fragments and efficiency of the assay based on a control secretory protein (typically 80%).

Photocrosslinking nascent chain intermediates

εANB-Lys-$tRNA^{amb}$ was prepared as described previously[36]. Briefly, tRNA was synthesized by cell free transcription (T7 RNA polymerase) from a plasmid containing an E. coli lysine-accepting tRNA in which the anticodon was mutated to recognize an amber codon, thereby yielding $tRNA^{amb}$. tRNA was purified by FPLC and enzymatically aminoacylated with [^{14}C]Lys (Amersham, Piscataway, NJ). Lys-$tRNA^{amb}$ was

precipitated, dialyzed and coupled to ANB-NOS (Pierce), re-precipitated, dialyzed and stored at -80°C. Coupling efficiency to the ε-amino group of Lys was >85%.

Crosslinker was activated by irradiation on ice for 10 min with collimated 280-350 nM UV light from a 500W mercury arc lamp (Oriel, Strafford, CT) dichroic mirror (300-400 nm) and 350 nm long pass cut off filter. Microsomal membranes were then pelleted for 10 min at 180,000 x g through 0.5 M sucrose, 50 mM HEPES (pH 7.5), 0.1 M KOAc, 5 mM $MgOAc_2$, and 100 mM DTT. The membrane pellet containing targeted RNCs was solubilized in 1% (w/v) SDS, 10 mM Tris-HCl (pH 8.0). All samples were incubated in 0.02-0.05 mg/ml RNase A for 15 min at 24°C to remove peptidyl-tRNA immediately prior to SDS-PAGE.

Quantitation and normalization of photoadduct yields

To compensate for differences in translational read-through at different TAG codons, duplicate aliquots of translation products (prior to UV) were analyzed by SDS-PAGE. All truncations and all three incorporation sites (plus WT) for each TM were analyzed simultaneously. All gels were fixed, dried, and exposed en mass on a single Kodak Phosphor Storage Screen. Bands corresponding to read-through polypeptides were quantitated using a Bio-Rad Personal Molecular Phosphoimager FX (Quantity One software). Background signal was subtracted, and results of duplicate samples were averaged to determine efficiency of translational read-through. Samples volumes were corrected to yield equivalent signal in the read-through polypeptide, and normalization was verified by repeat SDS-PAGE and phosphorimaging. Experiments in which the variation of normalized sample intensities was less than +/-10% SEM were used for subsequent immunoprecipitation.

Immunoprecipitation and crosslinking efficiency

Immunoprecipitations were performed simultaneously on all truncated samples containing amber codons within a given TM. Normalized amounts of read-through translation products were denatured at 37°C for 45 min in 1% (w/v) SDS, 0.1 M Tris-HCl (pH 8.0). Samples were then diluted with 10 vol of Buffer A [0.1 M NaCl, 1% (w/v) Triton X-100, 2 mM EDTA, 0.1 mM PMSF and 0.1 M Tris-HCl (pH 8.0)] and mixed on ice with 2 μl of peptide-specific Sec61α antisera (raised against peptide AIKFLEVIKPGCC, generously provided by Dr. Kent Matlack) and 5 μl of Protein A Affi-gel (Bio-Rad, Hercules, CA). Samples were rotated overnight at 4°C, washed twice with 0.5 ml of ice cold Buffer A, and twice with 0.5 ml of 0.1 M NaCl, 0.1 M Tris-HCl (pH 8.0) prior to SDS-PAGE. Gels were fixed, dried, and quantitated by phosphorimaging as above. All immunoprecipitations were performed in duplicate and averaged for each experiment. Background signal of WT samples (lacking TAG codons) was subtracted to determine crosslinking efficiency to each probe at each truncation site. The signal obtained for each sample was then converted to a percentage of the total signal in the experiment. Independent crosslinking experiments for each TM were repeated at least twice. Results from at least two independent experiments (four immunoprecipitations) were averaged and the relative crosslinking efficiency was plotted as a function of polypeptide length.

Acknowledgments.

The authors thank Dr. Kent Matlack for the generous gift of Sec61α antisera, Colin Daniel and Jamie Knowles for their excellent technical assistance, and Dr. Peter McCormick for advice and suggestions. This work was supported by NIH DK51818 and GM53457 (W.R.S.), GM26494 (A.E.J), the American Heart Association (H.S and W.R.S.), and the Robert A. Welch Foundation (A.E.J.).

Fig. 2-1

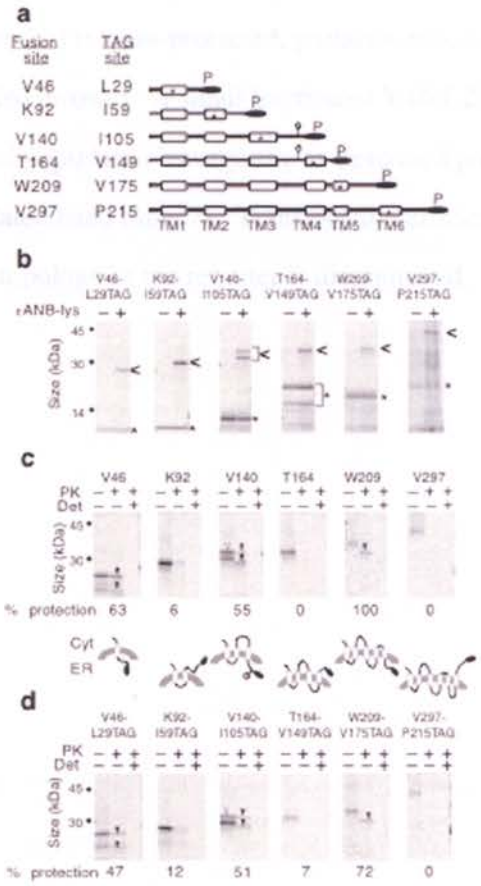

Figure 2-1: AQP4 biogenesis is unaffected by εANB-Lys incorporation. **(a)** Diagram of AQP4 fusion proteins showing location of fusion sites and amber codons. Rectangles represent AQP4 TMs, black oval represents the C-terminal prolactin-derived reporter. Open circle shows an N-linked glycosylation consensus site between TM3 and TM4. **(b)** Fusion proteins containing TAG codons were translated in the presence or absence of ε-ANB-Lys-tRNA^{amb} (ANB-Lys). Polypeptides terminated at the amber codon (*) and read-through products (<) are indicated. Glycosylated species of V140-I105TAG (read-through) and T164-V149TAG (truncated) are bracketed. WT **(c)** and TAG-containing

(**d**) fusion proteins were digested with proteinase K (protease) in the presence or absence of Triton X-100 (detergent). Protease-protected, prolactin-reactive polypeptides are indicated (downward filled arrows). A small fraction of V46-L29TAG polypeptides were cleaved at a cryptic signal peptidase cleavage site as described previously [98]. Hollow arrow indicates glycosylated band (*lane 7*). Translocation efficiency (% protection; mean, n=3) and relative topology of the reporter is diagrammed.

Fig 2-2

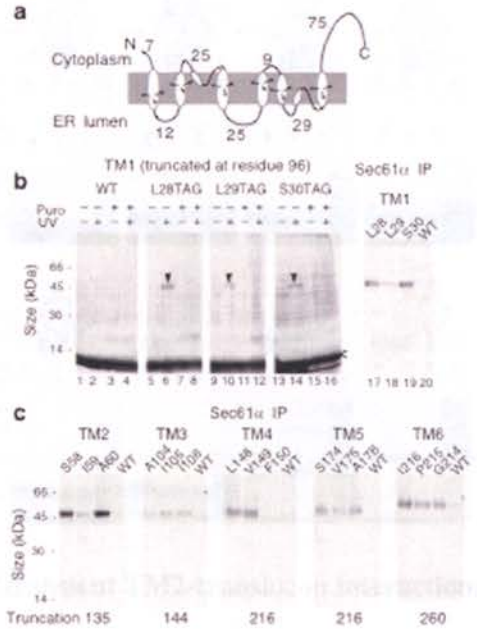

Figure 2-2: Crosslinking to AQP4 translocation intermediates. **(a)** Diagram of predicted AQP4 topology showing relative location of probes (asterisk) within helices (white ovals) and length of connecting loops (based on ref [85]). **(b)** Autoradiograms of AQP4 polypeptides truncated at residue 96, showing read-through of indicated TAG codons (<) translated in the presence of εANB-Lys-tRNA^{amb}. Photoadducts (downward arrowheads) were observed in ANB-containing polypeptides (*lanes* 6, 10, 14), but not in WT constructs (*lanes* 1-4) or when puromycin (puro) was added prior to UV exposure (*lanes* 4, 8, 12, and 16). UV-irradiated photoadducts were isolated by immunoprecipitation with Sec61α antisera (*lanes* 17-20). **(c)** εANB-Lys photoadducts to AQP4 TMs 2-6 were generated as in panel **b** and isolated by immunoprecipitation with Sec61a antisera following UV irradiation. Location of TAG codon in each TM and site of AQP4 truncation are indicated.

Fig. 2-3

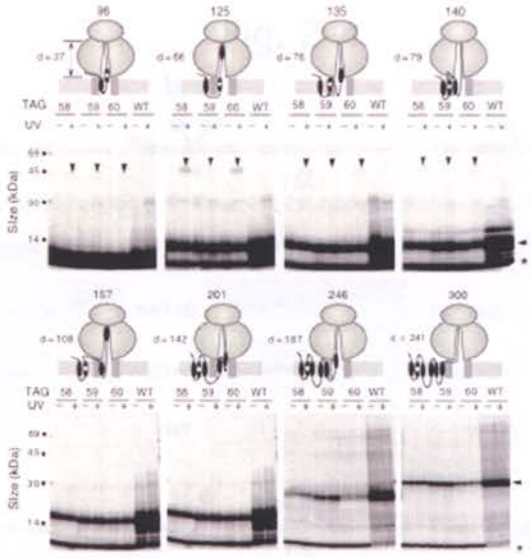

Figure. 2-3: Capture of transient TM2-translocon interactions. AQP4 transcripts containing TAG codons at positions 58, 59, 60 were truncated at sites indicated. Early terminated (asterisk) and read-through polypeptides(<) are shown. UV-dependent crosslinked bands are indicated by downward arrowheads. No crosslinking was observed for WT. Diagrams show translocation intermediates with predicted location of TMs (black ovals) and probe (white circle) relative to Sec61 (gray rectangles). Distance in aa residues (d) from the probe to ribosomal PTC is indicated for each sample.

Fig. 2-4

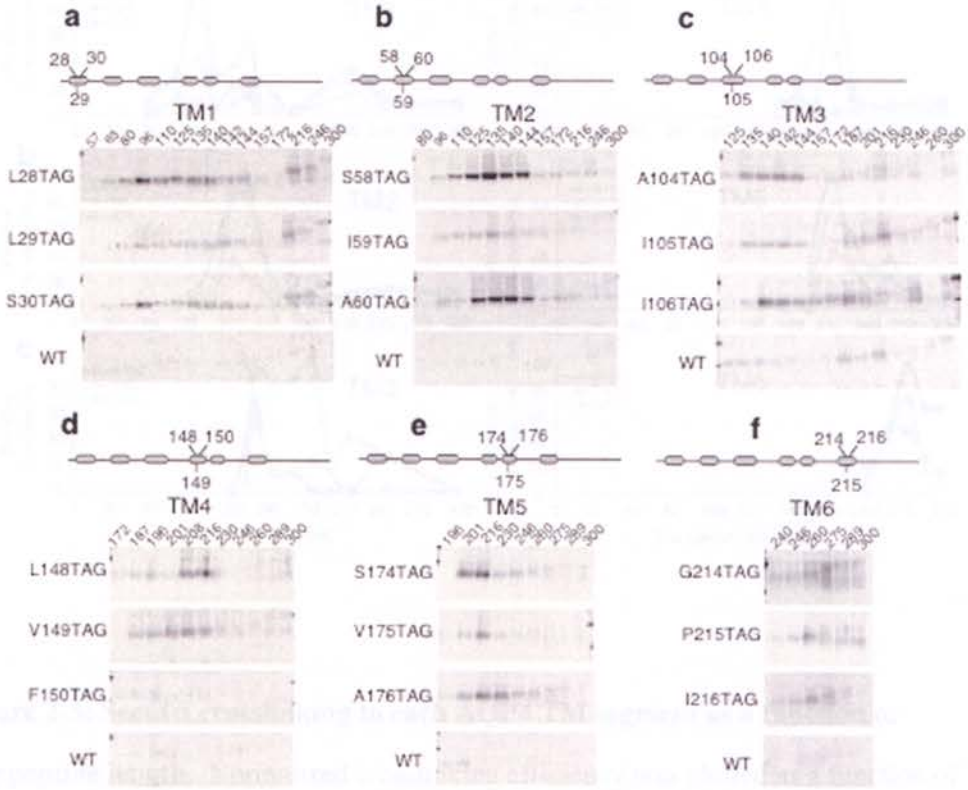

Figure 2-4: Quantitation of Sec61α-AQP4 crosslinking. Normalized amounts of εANB-Lys-containing read-through translation products were immunoprecipitated with excess Sec61α antisera as described. Position of εANB-Lys probe within the TM is indicated at the left of each autoradiogram. AQP4 truncation sites are shown above each lane, and the TM examined is indicated at the top of each panel.

Fig. 2-5

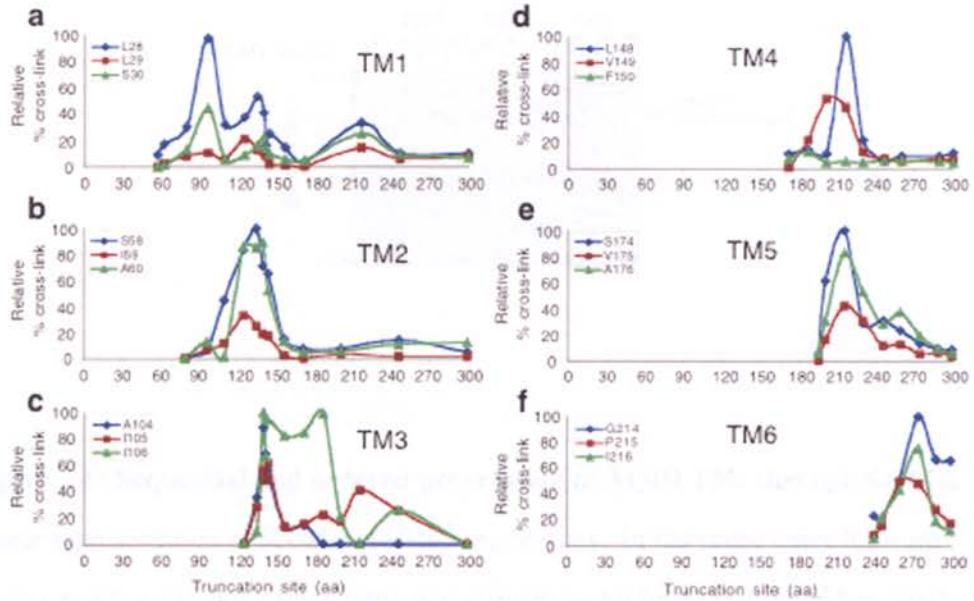

Figure 2-5: Sec61α crosslinking to each AQP4 TM segment as a function of polypeptide length. Normalized crosslinking efficiency was plotted as a function of polypeptide length. The resulting profiles show unique crosslinking pattern for the three probe incorporation sites and reveal that each TM quickly acquires a specific, non-random orientation adjacent to Sec61α. Moreover, the entry of each TM into the translocon, detected by Sec61α crosslinking, coincides with the exit of the prior TM, suggesting a mechanism of sequential displacement from the initial site of translocon entry. Recovery of photocrosslinking at longer nascent chain lengths for TMs 1, 3 and 5 also demonstrates the presence of secondary Sec61α interactions, consistent with movement of these TMs into different molecular environments within the translocon. Averaged data from at least 2 independent crosslinking experiments are shown.

Fig. 2-6

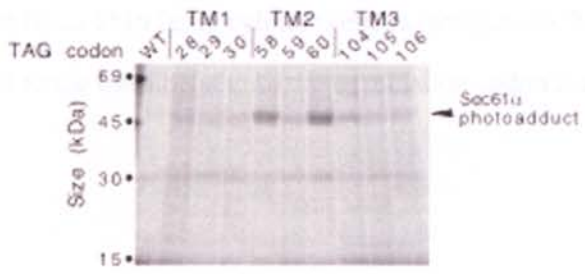

Figure 2-6: Sequential and ordered progression of AQP4 TMs through Sec61α. (a) Linear representation of Sec61α crosslinking profiles. Initial probe entry (upward arrow), peak crosslinking (diamond), and primary (solid lines) and secondary (dashed lines) crosslinking to Sec61α are shown relative to length of AQP4 polypeptide synthesized. **(b)** Relative location of polypeptide (black line) and TM segments (colored cylinders) within the ribosome (blue) and Sec61α (green) translocation pathway is shown schematically based on structural studies of the RTC and crosslinking patterns shown in Figure 5. Truncation site for each integration intermediate is indicated above the diagrams. Certain nascent chain lengths elicit major transitions in TM environment. Initial contact of TM1 (red cylinder) with Sec61α occurs at a chain length of ~60 residue, and maximal crosslinking is observed at truncation 96. TM2 (orange cylinder) enters the translocon (truncations 96-100) and disrupts TM1 crosslinking at truncation 110. TM1 then moves to a different site but is still in close proximity to Sec61. TM3 (yellow cylinder) initially contacts Sec61 in a random orientation that allows helical rotation (truncation 135), displaces TM2 (truncation 140-150), and acquires a fixed orientation adjacent to Sec61α that persists until TM4 (purple cylinder) enters the translocon (truncation 180-200). TM4 is rapidly displaced by TM5 (blue cylinder) and TM4 completely exits Sec61α at truncation 230. Note that at a nascent chain length of 216

residues, four different TMs (1, 3, 4 and 5) are simultaneously contacting Sec61α. TM5 is displaced from Sec61α as TM6 (gray cylinder) enters (truncations 240-260), and only TM6 remains adjacent to the translocon until the termination codon is reached.

Fig. 2-7

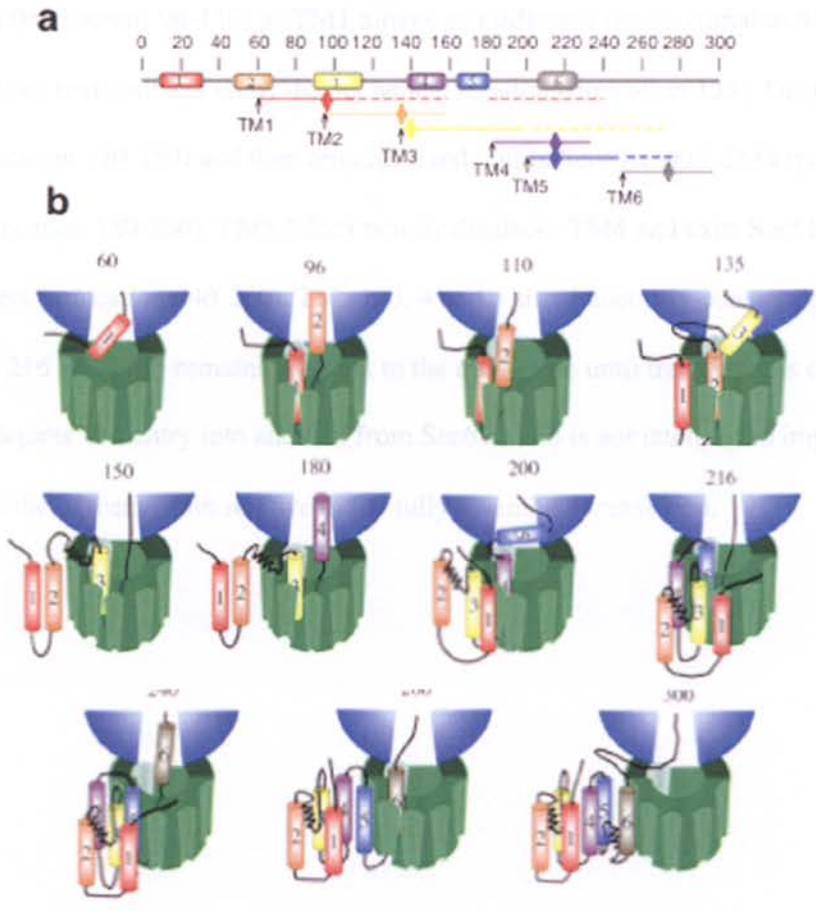

Fig. 2-7 Model of AQP4 progression through Sec61α. (a) Linear representaion of Sec61α crosslinking. Arrow, initial probe entry; diamond, peak crosslinking; solid and dashed lines, primary and secondary interactions, respectively. (b) Structural transitions proposed on the basis of crosslinking profiles shown in Fig. 5.. Black line, polypeptide; blue, ribosome; green, Sec61α. The relative sizes of th naascent chain and Sec61α are expanded. Other translocon components are omitted for clarity. Truncation site is indicated above each diagram. TM1 (red) initially initially contacts sec61 at truncation 60

and maximal crosslinking is observed at truncation 96. TM2 (orange) enters the translocon (truncations 96-110) as TM1 moves to a different site proximal to Sec61α. TM3 (yellow) first contacts sec61 during helical rotation (truncation 135), Displaces TM2 (truncation 140-150) and then remains fixed within Sec61α until TM4 (purple) enters (truncation 180-200). TM5 (blue) rapidly displaces TM4 and exits Sec61α as TM6 (gray) enters (truncation 240-260). TMs 1, 3, 4 and 5 simultaneously contact Sec61α at truncation 216 and TM6 remains adjacent to the translocon until translation is completed. Diagram depicts TM entry into and exit from Sec61α and is not intended to imply location of the nascent chain relative to the fully assembled translocon.

Fig. Supp. 2-1

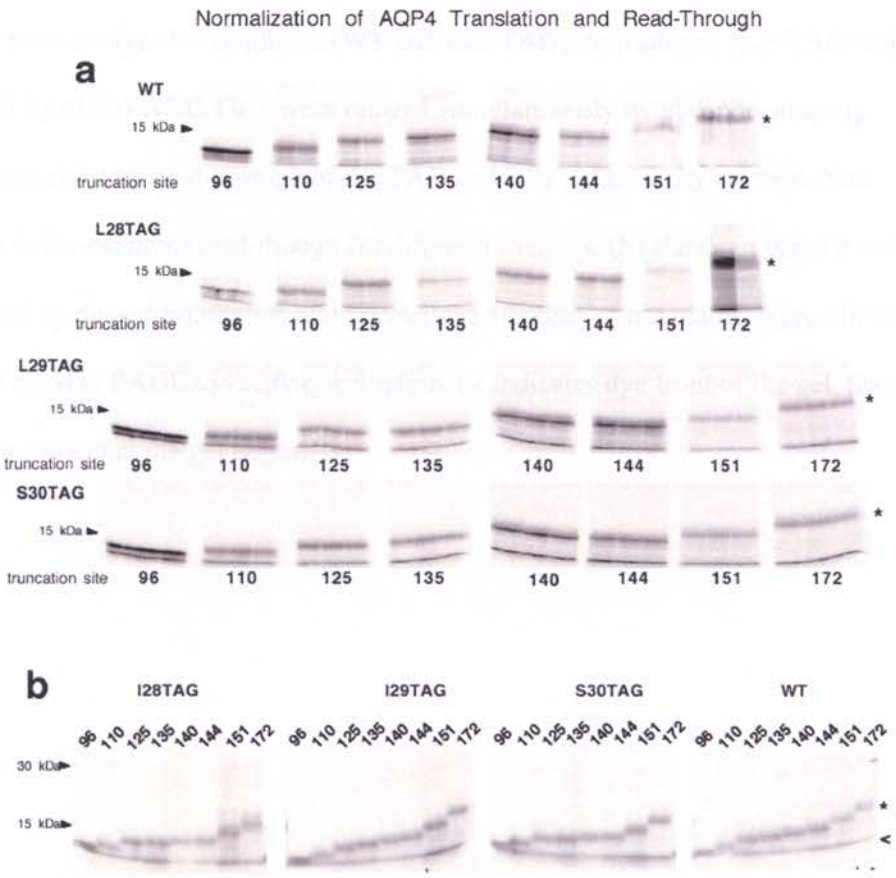

Supplementary Figure 1. Quantitation and normalization of read-through translation products. To compare crosslinking for constructs of different lengths containing TAG codons, translation and readthrough efficiency for all truncations of a given TM were quantitated and normalized simultaneously on a single large format phosphorimaging screen. Screens were thoroughly erased (>1h), handled under a hood to

eliminate stray light and multiple exposures were obtained with gels in different positions to correct for variations in the screen. Shown are examples of normalization protocols for probes incorporated into TM1. **(a)** Plasmids containing TAG at codons 28, 29, 30 were truncated as indicated and translated in RRL in the presence of £`ANB-Lys-tRNAamb. Samples were analyzed in duplicate (WT and L28 TAG), or triplicate (L29TAG and S30TAG) by SDS-PAGE. Gels were imaged simultaneously by phosphorimaging. Protein generated by read-through of the TAG codon is indicated by asterisk. Note variation in the extent of read-though for different samples. **(b)** Bands in panel **a** were quantitated by phosphorimaging, and normalized amounts of radiolabeled protein was re-analyzed by SDS PAGE to verify quantitation. (**<** indicates dye front of the gel. Some smiling is evident at the gel edges).

Fig. Supp. 2-2

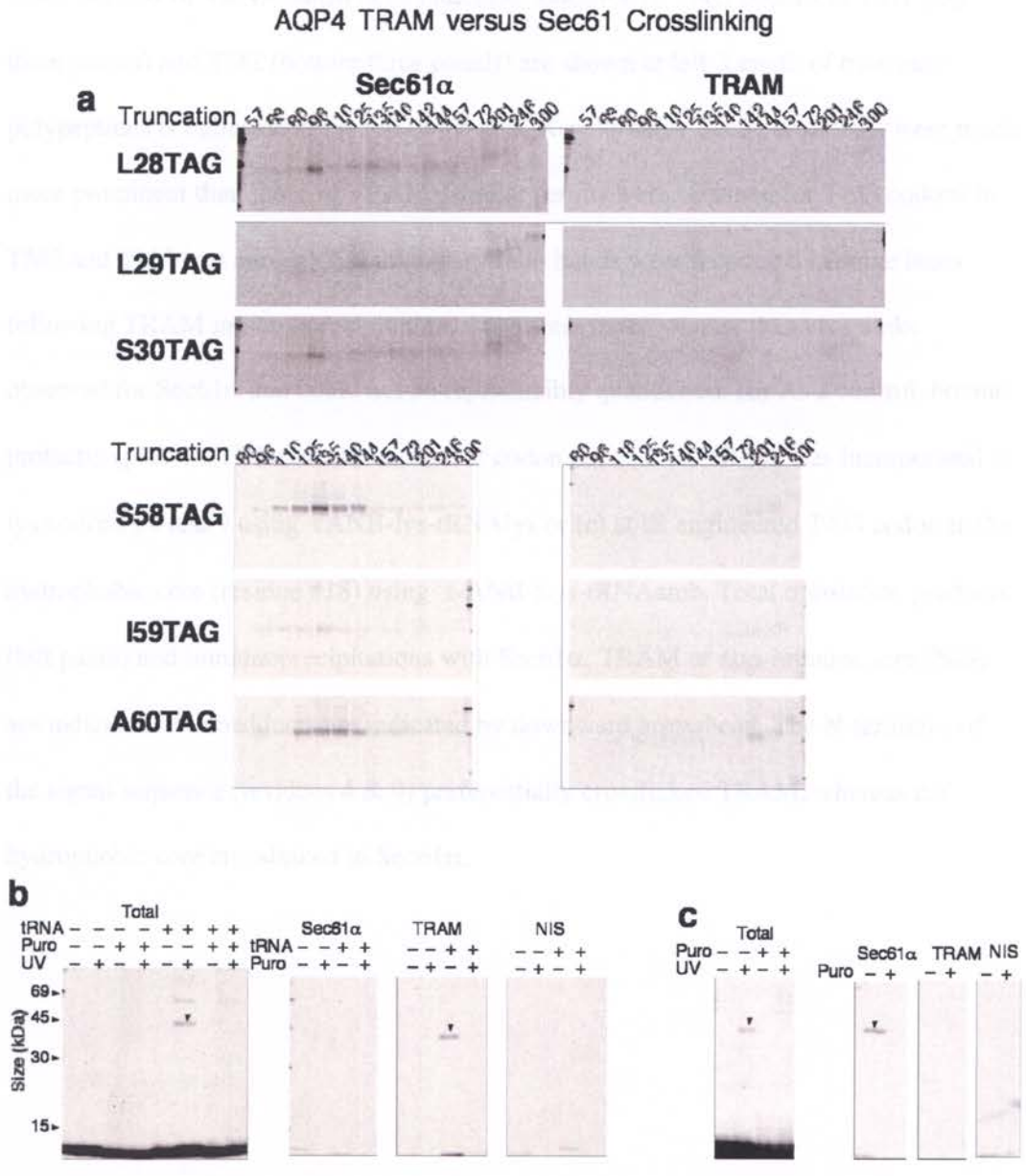
AQP4 TRAM versus Sec61 Crosslinking
a
Sec61α
TRAM
Truncation
L28TAG
L29TAG
S30TAG
S58TAG
I59TAG
A60TAG
b
Total
tRNA
Puro
UV
Sec61α
TRAM
NIS
Size (kDa)
69
45
30
15
c
Total
Puro
UV
Sec61α
TRAM
NIS

Supplementary Figure 2. TRAM crosslinking to AQP4. (**a**) Normalized amounts of UV irradiated translation products were divided, denatured, and immunoprecipitated with either Sec61α or TRAM antisera as indicated. Location of TAG codons in TM1 (top three panels) and TM2 (bottom three panels) are shown at left. Length of truncated polypeptides is indicated at the top of the gels. Results show Sec61 crosslinks were much more prominent than those of TRAM. Similar results were obtained for TAG codons in TM3 and TM4 (not shown) Although very faint bands were recovered in some lanes following TRAM immunoprecipitation, these were much weaker than crosslinks observed for Sec61α and could not be reproducibly quantitated. (**b**) As a control, bovine prolactin (pPL 86) cDNA was truncated at codon 86, and εANB-lys was incorporated at lys codons #4 and 9 using εANB-lys-tRNAlys or (**c**) at an engineered TAG codon in the hydrophobic core (residue #18) using ε-ANB-Lys-tRNAamb. Total translation products (left panel) and immunoprecipitations with Sec61α, TRAM or non-immune sera (NIS) are indicated. Photoadducts are indicated by downward arrowhead. The N-terminus of the signal sequence (residues 4 & 9) preferentially crosslinked TRAM, whereas the hydrophobic core crosslinked to Sec61α.

Manuscript 3

Site-Specific Retention of a Nascent Translocating Polypeptide in the ER Sec61 Translocon

David Pitonzo[1,2], Zhongying Yang[1], Karl Rusterholtz[1], Arthur Johnson[3,4], William R. Skach[1]

[1]Department of Biochemistry & Molecular Biology, Oregon Health & Sciences University, Portland, OR 97239
[2]Dept. of Physiology and Pharmacology, Oregon Health and Sciences University, Portland, OR, 97239
[3]Department of Molecular and Cellular Medicine. Texas A&M University System Health Science Center, College Station, TX 77843-1114
[4]Departments of Chemistry and of Biochemistry and Biophysics, Texas A&M University, College Station, TX 77843

Running Head: Discontinuous translocation through Sec61α

Manuscript in preparation

Address Correspondence to:
William R. Skach, MD,
3181 SW Sam Jackson Park Rd, L-224,
Portland, OR 97239.
FAX: 503 494-7368;
E-mail: skachw@ohsu.edu

Abstract:

The Sec61 translocon mediates polytopic protein membrane integration by facilitating lateral transfer of transmembrane segments (TMs) into the lipid bilayer. Transient interaction with Sec61 has heretofore only been observed in nascent chains that remain attached to the ribosome. Here, we use a photocrosslinking approach to define translocon entry and exit of an unusual TM derived from the cystic fibrosis transmembrane conductance regulator (CFTR), a multi-domain membrane protein that contains two 6-spanning TM domains. Engineered amber (TAG) stop codons were used to incorporate a photoactive Nε-5-azido-2-nitrobenzoyl-lysine (ANB-Lys) into CFTR-TM8 using a modified amber suppressor aminoacyl-t-RNA. mRNAs encoding the second membrane spanning domain (starting at CFTR residue 837) were truncated and expressed in reticulocyte lysate to generate uniform cohorts of intact integration intermediates. Photoadducts to CFTR residues #912, 913 and 914 revealed that TM8 enters the translocon upon exiting the ribosome and remains adjacent to Sec61 until the nascent peptide extends another 70 aa. For nascent chains truncated between CFTR residues 957-967, puromycin treatment resulted in lateral release of TM8 into the bilayer as evidenced by loss of Sec61α crosslinking. However, nascent chains truncated between residues 971-1017 continued to crosslink Sec61 alpha after cleavage of the peptidyl-tRNA bond. Sec61 crosslinking to untethered nascent chains was disrupted by removal of an acidic residue (D924V) near the putative center of TM8 and was restored by glutamate substitution (D924E). Persistent crosslinking was also stabilized by ATP depletion and destabilized by disruption of the ribosome translocon complex with EDTA or 1M NaCl. These results indicate that the translocon does not necessarily function as a passive conduit for TM movement but can form relatively stable interactions, presumably with polar residues, that persist even after the nascent protein is released from the ribosome.

Introduction

Eukaryotic transmembrane protein biogenesis is facilitated by a large multi-protein complex in the endoplasmic reticulum membrane that is comprised of the translating ribosome and a protein conducting channel termed the Sec61 translocon [26, 210]. A principal function of the ribosome-translocon complex (RTC) is to cotranslationally orient lumenal, cytosolic and transmembrane domains as the nascent polypeptide elongates within the ribosome exit tunnel while maintaining compartmental integrity. Because 20-30% of proteins in the typical genome have at least one membrane spanning domain and enter the secretory pathway via the RTC [1] and because correct protein folding is critical for human health and disease [2], understanding the mechanics of membrane protein translocation and integration is of fundamental importance to biology and medicine.

The efficiency with which membrane protein domains fold is critically dependent upon the chaperone content and physical properties (hydrophobicity, redox conditions, etc) of specific cellular environments. The RTC therefore performs a fundamental role by ensuring that, during protein synthesis, the nascent polypeptide domains are delivered into the proper compartment at the proper time as they pass through exit tunnel of the 60S ribosomal subunit [212, 217, 218]. This is accomplished through a series of highly coordinated interactions between ribosome and translocon that simultaneously control the axial pathway for hydrophilic peptide movement into the ER lumen and a lateral pathway for TM movement into the hydrophobic core of the ER membrane. Remarkably, the RTC is in turn controlled by topogenic determinants encoded within the nascent

polypeptide itself (signal and stop transfer sequences) [219] that function to open and close the lumenal pore of the translocon and provide access to the cytosolic compartment [29].

How then, does the translocon facilitate movement of hydrophobic TMs from an aqueous environment to hydrophobic core of the lipid bilayer? Functional translocons contain multiple copies of the sec61αβγ heterotrimer as well as a several associated proteins and protein complexes that include the TRanslocation Associated Protein (TRAPαβγδ), TRanslocation Associated Membrane protein (TRAM), oligosaccharyltransferase (OST), and signal peptidase complex (SPC) [22, 37, 41, 45, 49]. Sec61α is a ten-spanning protein that lines the protein conducting channel and provides an aqueous pathway for nascent secretory proteins to enter the ER lumen as they exit from ER-docked ribosomes [31, 74, 195, 198, 199]. Sec61 also provides a lateral pathway through which hydrophobic TM segments gain access to the apolar enviromnent of the ER membrane. While it is possible that TMs could passively partition into the lipid bilayer through a simple lateral translocon gate [10, 14, 48, 220], growing evidence suggests that TM integration is mechanistically triggered by functional transitions in the RTC at specific stages of synthesis [27, 33, 221]. Crosslinking studies have also indicated that TMs frequently pass through a series of molecular environments characterized by differential proximity to Sec61 and/or other translocon components prior to frank integration [33, 36, 75]. Most remarkably, some TMs appear to integrate in pairs or groups [54, 56, 72, 74, 194] depending on their physical characeristics [56, 100] which suggests that intramolecular interactions between TMs may be initiated on ribosome-attached

polypeptides in the context of translocation machinery and may be needed for stable entry into the bilayer.

Until now, the close proximity of TMs to Sec61 has been entirely dependent on the presence of an intact covalent peptidyl-tRNA bond that connects the nascent polypeptide to the ribosome. When this bond is severed either physiologically (at the end of translation) or prematurely (by addition of puromycin), chemical and photocrosslinks to Sec61 are disrupted, although some TMs may remain adjacent to other translocon components such as TRAM [33] and Ribophorin I [75]. This has suggested that TMs reside within or adjacent to Sec61 only while they remain attached to the ribosome and that once released, Sec61 does not remain actively engaged or participate in subsequent folding events. This is consistent with the behavior of secretory protein intermediates, which spontaneously fall into the ER lumen upon puromycin treatment [222-224]. In other words, Sec61 provides a relatively non-specific conduit that is permissive for both axial and lateral protein movement. Indeed, specific Sec61 interactions with nascent polypeptides would have significant implications given the magnitude and diversity of proteins that pass through the secretory pathway.

The cystic fibrosis transmembrane conductance regulator (CFTR) is a PKA- and ATP-dependent chloride channel expressed in the apical membrane of selected epithelial tissues. It exhibits the typical domain architecture of ATP Binding Cassette (ABC) transporters comprising two 6-spanning transmembrane domains (TMDs), two nucleotide-binding domains (NBDs) and a unique regulatory domain (R). Inherited

mutations in CFTR cause cystic fibrosis, most commonly by disrupting a critical, but as yet uncharacterized, folding step in the ER. Previous studies have demonstrated that CFTR domains fold via both co- and post-translational mechanisms [105, 110, 225]. Despite their similar topology , CFTR TMDs contain topogenic determinants that exhibit different functional properties and direct different translocation events [15. ***]. Here we show that TM8 in CFTR TMD2, can remain stably associated with Sec61α after cleavage of the peptidyl-tRNA bond. These persistent interactions were disrupted by removal of a single acidic residue, D924V, within TM8; restored by glutamate substitution, D924E; stabilized by ATP depletion and disrupted by ribosome stripping from the ER membrane with EDTA or high salt. These findings indicate that the translocon can interact with nascent TMs in a sequence specific and regulated manner and further implies that sec61 does not always act simply as a passive conduit but can actively influence the timing of TM integration in a manner that has implications for protein folding. Lateral exit of TMs from Sec61α is not always a spontaneous process (i.e. is not necessarily a passive conduit). Rather, sec61, can play an active role in integration depending on 1° sequence and, potentially, through specific interactions with residues in the nascent polypeptide.

Results

Experimental Strategy:

CFTR contains two 6-spanning transmembrane domains (TMDs) that are separated by a large cytosolic nucleotide binding domain (NBD1) and an intrinsically unstructured regulatory (R) region (Fig. 1A). To examine the mechanism of TMD2 biogenesis, we removed TMD1, NBD1 and the R-domain, and used met 837 as the translation start

codon. cDNAs of different lengths were then generated by PCR and transcribed to generate truncated mRNAs that encode TM7, TM8 and variable lengths of downstream CFTR sequence (Fig 1B). When translated in vitro in the presence of canine rough microsomes, these truncated mRNAs, generate integration intermediates that retain an intact peptidyl -tRNA bond and thus are trapped in a normally transient state of biogenesis within the intact ribosome-translocon complex. To characterize the molecular environment of the nascent chain at each stage of biogenesis, we introduced a photocrosslinking probe at engineered amber (UAG) stop codons near the N-terminus of TM8 (Fig. 1C) using a modified suppressor tRNA, N^{ε}-(5-azido-2-nitrobenzoyl) lys-$tRNA^{Amb}$ (ε-ANB lys-$tRNA^{Amb}$). Upon encountering the stop codon, the ribosome either terminates translation and releases the nascent chain, or incorporates the ANB-Lys photocrosslinking probe and continues translating to the end of the mRNA. In our system, ε-ANB lys-$tRNA^{Amb}$ results in efficient read-through of stop codons and generates a series of nascent chains with increasing length (Fig. 1D). Note that both the prematurely terminated and read-through peptides undergo glycosylation at the two known N-linked consensus sites in ECL4, Asn 894 and Asn 900 (Fig. 1D and Supplemental Figure 1). In this manner it is possible to position the photocrosslinking probe at precise locations within the ribosome and translocon by varying nascent chain length and hence the distance between the probe and the ribosome peptidyltransfersase center (PTC). Assembled integration intermediates are then irradiated to convert the ANB moiety to an electrophilic nitrene that forms a single non-specific crosslink to any reactive atom within range of the 12Å spacer arm. By examining a series of such static intermediates, each differing in length and probe environment, it is possible to reconstruct

the dynamic changes that take place as a nascent TM enters, traverses and leaves sec61α during the integration process.

To determine how and when TM8 enters and leaves the translocon, we incorporated a single ε-ANB-Lys probe at one of three consecutive residues (Ser912, Tyr913, Tyr914) in TMD2 nascent chains that were serially truncated between CFTR residues 935 and 1027. For clarity, glycosylation was suppressed by addition of acceptor peptide. At truncation 935, when the probe was 22 residues from the PTC (measured to the middle residue Tyr 913) several photoadducts (~28kDa, 43kDa and 75 kDa) were observed upon UV irradiation of ANB-Lys-containing peptides prior to peptidyl-tRNA release by puromycin (Fig. 2). These crosslinks are consistent with previously described ribosomal proteins [27, 36] as would be expected because 23 extended residues are generally insufficient to extend the probe beyond the ribosome exit tunnel. After synthesis of an additional 22 residues (truncation 957) a different pattern of photocrosslinking was observed. All three residues yielded a predominant photoadduct of ~55 kDa which corresponded to a ~38-40 kDa.shift in size (Fig. 2). Additional crosslinks to a smaller (8 kDa) protein were also observed. These photoadducts were observed until truncation 977, at which point photocrosslinking to residue 914 was lost. Residues 913 and 912 continued to generate photoadducts until truncation 1027 at which point photocrosslining to all three sites was lost. Thus TM8 appears to reside in a proteinaceous environment until probe sites were more than 100 aa from the PTC (truncation 1027) when TM9 would be expected to be exiting the ribosome and synthesis of TM10 was nearly completed. Similar results, performed for truncations 935-987, were also obtained in the absence of acceptor peptide (Supplementary Fig. 2). Surprisingly, for a significant

translation interval, truncations 967-1007, photoadducts to residue 913 and to a lesser extent 912, were observed both before and after addition of puromycin and was most obvious for truncation 977. This suggested that releasing the nascent polypeptide from the ribosome PTC did not correspond to release of the polypeptide freely into the lipid bilayer. Rather the nascent chain remained adjacent to a ~38-40 kDa protein.

Photoadducts are identified as sec61α.

To determine the identify of the photoadduct observed in Figure 2, equal amounts of crosslinked translation products were immunoprecipitated with antisera raised against Sec61α, TRAM and TRAPα, each of which migrates with similar mobility on SDS-PAGE [22, 37]. The 913 TAG construct was initially chosen for this purpose because of its relatively strong crosslinking efficiency. As shown in Figure 3A (lanes 1-4), the photoadduct was recovered only with Sec61α antisera, indicating that Sec61α is the major translocon protein adjacent to this region of TM8 at this stage of synthesis. Moreover, crosslinking efficiency was only modestly affected by puromycin treatment. Upon much longer exposure, however, weak crosslinking to TRAM was detected that was also relatively unaffected by puromycin treatment (supplemental Figure 3).

These results suggest either that TM8 exhibits novel behavior and remains associated with the translocon in the immediate proximity of Sec61α after cleavage of the peptidyl-tRNA bond, or alternatively, that puromycin was unable to effect release of the nascent polypeptide. To distinguish these possibilities, integration intermediates were examined directly by SDS-PAGE prior to RNase digestion. Under these conditions, the majority of

read-through polypeptides migrated as larger peptidyl-tRNA precursors (Fig. 4 lane 1). However, nascent chain release was observed as soon as 30 seconds after puromycin addition (Fig. 4B, lane 2). Parallel samples irradiated at each time point after puromycin addition revealed little change in photocrosslinking efficiency during the 10 minute incubation period. Additional experiments showed that the peptidyl-tRNA bond was preserved in assembled integration intermediates for over 1 h in the RRL translation reaction (data not shown – see dissertation appendix fig A2-3). We conclude from these experiments that TM8-Sec61α photoadducts observed after puromycin treatment result from persistent association of the nascent chain within or adjacent to the translocon after peptidyl-tRNA cleavage.

Persistent TM8-Sec61α interaction requires an intact ribosome translocon complex. While puromycin results in efficient peptidyl-tRNA cleavage, it does not necessarily disrupt ribosome binding to Sec61α [226]. We therefore wished to test whether persistent association of free CFTR nascent chains was dependent upon an intact ribosome translocon complex. As shown in Figure 5, while puromycin alone had little effect on the TM8 photoadduct, ribosome stripping with EDTA prior to or following puromycin treatment completely abolished photocrosslinking (compare lanes 2, 3 and 7, 8). TM8-Sec61 photocrosslinking was also abolished by 1M but not 300 mM NaCl (Fig 5, compare lanes 4, 5 and 9,10) which also disrupts the ribosome translocon junction [226]. Thus persistent interaction of the nascent chain with Sec61α, both before and after peptidyl-tRNA cleavage requires the presence of an intact ribosome-translocon complex.

ATP dependence of nascent chain-translocon interactions.

Previously we showed that full-length CFTR also remained associated with ER biosynthetic machinery after peptidyl-tRNA cleavage [227] and that release was stimulated by the presence of ATP and cytosol. Because none of the major translocon components exhibit a known requirement for ATP it seemed most likely that CFTR release might require a higher-order folding event. We therefore quantitated the efficiency of photoadduct formation at various time intervals after peptidyl-tRNA bond cleavage to determine whether persistent TM8-Sec61α association might also be influenced by ATP. In the absence of puromycin, persistent crosslinks were observed for more than two hours, consistent with a very stable peptidyl-tRNA bond (Figure 6A, lanes 3-6). Puromycin again efficiently cleaved the peptidyl-tRNA bond (Figure 6A, lanes 1, 2) which resulted in a slow decline of photocrosslinking within 30-60 minutes (Fig. 6A Lanes 7-10 and panel B). In contrast, when ATP was first depleted by addition of apyrase, puromycin treatment had no effect on photocrosslinking for up to two hours (Lanes 11-14). To ensure that depletion of ATP did not affect puromycin release, cleavage of the peptidyl-tRNA bond was documented (Fig. supp. 4). These results, therefore, suggest that release of CFTR TM8 from Sec61 is an active and energy dependent, rather than passive process.

The presence of two proximal N-linked glycosylation sites is not responsible for persistent translocon interaction.

It has been previously shown that amyloid precursor protein C99' can persistently crosslink to ribophorin I, a subunit of translocon component OST, after peptidyl-tRNA bond cleavage [75]. This raised the possibility that N-linked consensus sites might result in persistent association of one or more regions of peptide with other translocon components. Because CFTR contains two closely-spaced glycosylation consensus sites in ECL4 (N894, N900), we tested whether these sites might contribute to translocon retention of TM8. Glycosylation, per se, did not affect TM8 retention because nascent chain crosslinking (to residue 913) was unaffected by addition of the NYT acceptor peptide (Figure 7A). We then systematically removed one or both consensus sites by replacing Asn with Ala (N894A, N900A and N894A-N900A) which resulted in the expected effect on glycosylation (Fig. 7B). Importantly, elimination of glycosylation sites did not change the crosslinking pattern either before or after puromycin treatment (Fig. 7C). We therefore conclude that the two proximal N-linked glycosylation sites in ECL4 do not contribute to the persistent TM8-Sec61 interactions.

A polar residue in TM8, Asp924, contributes to persistent Sec61α photocrosslinking.

Our lab previously showed that Asp924, near the center of TM8, affects the ability of TM8 to terminate translocation and cotranslationally span the membrane [15]. It is also well established that Asp and Glu residues strongly stimulate helix-helix interactions in apolar environments [76, 78, 80]. These findings raise the possibility that as TM8 enters the Sec61 translocon pore, Asp924 might form transient polar interactions with a

translocon component that could persist independently of ribosome attachment and thereby delay TM8 integration into the membrane. If this were the case then the translocon could potentially modulate the integration process via specific interactions with different substrates.

To test this possibility, Asp924 was mutated to Val and crosslinking to residue 913 was directly compared to WT TM8. Consistent with our hypothesis, the D924 mutant not only eliminated the persistent crosslinking following peptidyl-tRNA cleavage, but also fundamentally changed the TM8 crosslinking profile. When examined in the 977 truncation, D924V reduced sec61 photoadducts both before and after puromycin treatment demonstrating that residue 913 was no longer adjacent to Sec61 at this stage of synthesis (Fig. 8A). Photocrosslinking to nascent chains truncated at 10aa intervals identified Sec61 crosslinks at truncations 957 and 967, that disappeared at truncation 977 after the probe had passed more than 64aa from the PTC (Fig. 8B). This suggested that the D924V mutant leaves Sec61 at an earlier stage of synthesis than its wild-type counterpart. Moreover, no crosslinks were observed after puromycin treatment indicating that the presence of a polar Asp residue can directly impact interactions between Sec61 and a nascent TM.

Next we tested whether other polar residues at position 924 would similarly alter TM8 crosslinking. Substitution of a Glu residue resulted in slightly reduced crosslinking efficiency at the 977 truncation both before and after puromycin treatment (Fig. 8 Panel C, compare lanes 5, 6 and 9,10 black arrows). Despite this reduction, however, Glu924-

TM8 also resulted in persistent (after puromycin) Sec61α crosslinking which was not observed for the Val924 construct (Figure 8, panel D, compare lanes 7, 8 and 11, 12). Substitution with Arg resulted in very weak crosslinks (fig 8 panel C lanes 7, 11, white arrows). These data suggest that persistent crosslinking is dependent upon an acidic residue at position 924.

Discussion

In this study, we show that CFTR TM8 remains in association with sec61α following peptidyl-tRNA cleavage. Further, we show that release from sec61 after peptidyl-tRNA cleavage is significantly delayed, and energy dependent. We then demonstrate that persistent TM8 residence proximal to sec61 is dependent upon an intact ribosome-translocon complex and a polar aspartate residue within the TM8 hydrophobic core. Persistent crosslinking of TM8 is lost upon mutation of D924 to valine but restored with glutamate. Further, TM8-D924V leaves sec61 more rapidly and does not show a persistent interaction after peptidyl-tRNA cleavage, suggesting that it may partition into lipid more quickly. Interestingly, previous studies in our laboratory have demonstrated that full length CFTR also remains in association with the ribosome-translocon complex following the completion of synthesis [227] and release of full length CFTR into a smaller protein complex that does not contain the RTC is both ATP and cytosol dependent.

Mechanisms of TM segment integration into the lipid bilayer are critical to understanding early events in membrane protein folding. The two-step model of Popot and Engelman

[7, 8] proposes that TMs are individually integrated, then assemble and coalesce into tertiary structure. Studies have provided evidence, however, that some TMs may integrate in pairs [13, 14, 54] or groups [72, 74]. This is interesting in light of evidence that TMs encounter lipid soon after entering sec61 [9, 10] and that some substrates remain in proximity to translocon components such as TRAM [33] and ribophorin I [75] after traversing sec61 and following peptidyl-tRNA cleavage. Interpretation of the above studies has therefore fostered an interesting debate as to whether TMs integrate by passive thermodynamic equilibration and partitioning into lipid or by a multi-step, translocon-regulated process.

Understanding membrane protein folding is inextricably tied to understanding translocon function. While a recent structural study of archael secY [48] has provided great insight, it also suggests certain functional limitations that are inconsistent with biogenesis requirements of polytopic membrane proteins, especially if integration is mediated by a single sec61 heterotrimer. For example, our prior photocrosslinking study of AQP4 [74] demonstrates that TMs 4 and 5 enter the translocon simultaneously, suggesting that, somewhere, there must be room for 2 TMs, a lumenal loop, plus the rotation of a type II signal anchor (TM5). Clearly, AQP4-TM5 rotation must occur prior to the productive engagement of TM5 with sec61 because correct topology is established co-translationally [98]. CFTR also contains TM pairs which likely enter sec61 simultaneously as helical hairpins due to short interconnecting loops (see Fig1a, e.g. TMs 3-4, 5-6, 9-10, and 11-12). Additionally, CFTR TM7 is a type II signal anchor that must rotate prior to entering sec61 and almost simultaneously open the axial translocon gate to the ER lumen to

permit translocation of ECL4 (Fig.1a). Consistent with early TM7 rotation, the N-linked glycosylation site at residue 894 is accessible to ER lumenal OST at truncation 967. Just four residues later, at truncation 971, both sites are accessible (fig 1c left panel). Not all current structural eukaryotic translocon models can explain where multiple substrate TMs and loops might accumulate prior to integration. Central to this question is whether the sec61α lateral gates of a multimeric assembly face away from [48, 49] or towards [50, 228] each other. Clearly, a greater understanding of the active translocon's architecture and stoichiometry is needed. Although a recent study using prokaryotic secY shows that a single secY heterotrimer of an oligomeric complex is used to translocate OmpA [60], its targeting signal sequence is the only alpha helical domain so this is essentially a secretory substrate. Further, although secY and sec61 may be structural homologs, they possess <50% sequence homology; this could be critical if specific sec61α. residues play a role in membrane protein folding, as has recently been demonstrated [229]. Additionally, the proteomes of the prokaryotic (secA, YidC, secDEF) and higher eukaryotic (BiP, TRAM, TRAP) translocons are quite different suggesting significant functional evolutionary divergence.

The ability of polar residues to contribute to helix-helix interactions has been well documented [76, 77, 80, 230]. Aspartate has a particular propensity to hydrogen bond with certain residues in membrane proteins, specifically lysine, tyrosine, asparagine and arginine [76]. Interestingly, polar residues are well represented within the putative TM boundaries of canine sec61α. Sec61α-TM7, which constitutes part of the putative lateral TM exit gate [48], contains two asparagines, two tyrosines a lysine and a glutamine.

Further, an asparagine and a glutamine are located within the hydrophobic core of sec61α.-TM7. Hydrogen bonds are also more likely to form in a lower dielectric lipid-containing environment consistent with studies that demonstrate early nascent chain-lipid interactions [9, 10]. Interestingly, CFTR TM7 contains a polar glutamate residue (E873) near the center of its putative boundaries. Indeed, preliminary work in our laboratory suggests that CFTR-TM7 has a crosslinking pattern initially similar to that of TM8 in that release from sec61 after peptidyl-tRNA cleavage is delayed. CFTR-TM7 then remains in proximity to sec61 up to truncation 977 but loses its persistent crosslink just when TM8 begins to demonstrate persistent interaction (data not shown – see dissertation appendix, Fig. A2-2). While we have not yet elucidated a precise molecular mechanism for stop-transfer cooperativity, it is conceivable that serial permutations of TM7-TM8 -sec61α hydrogen bonding are involved. Studies performed in prokaryotic secY [229] suggest that specific residues, some of which are polar, play an active role in protein folding, implying a residue-specific chaperone-like activity to the translocon. Additionally, yeast sec61p charged residues have been shown to play a critical role in topogenesis [57]. We propose that the persistent interaction of CFTR-TM8 with sec61α after release from the ribosome is caused by a hydrogen bond-mediated, chaperone-like activity of the translocon. Charged residue D924 is essentially sequestered by the translocon until another residue within the nascent chain, possibly E873, displaces sec61α. Alternatively, chaperoning may persist until a salt bridge is formed with R347 in TMD2-TM6 [231] necessitating H-bonding with a sec61α polar residue in a location outside the primary binding site in the lateral gate. This hypothesis is consistent with changes seen in the TM8 molecular environment (Fig. 2) and would reasonably protect the protein from off-

pathway (helix-helix) interactions, consistent with the primary function of a chaperone protein.

The Sadlish study [74] demonstrates that, during at least one point in biogenesis, as many as 4 AQP4 TMs are simultaneously in proximity to sec61. Additionally, some TMs (e.g. AQP4 -TM1) experience multiple environments within the vicinity of sec61α, until late in synthesis and while downstream TMs are also in the translocon. Other TMs pass through sec61α quickly (e.g AQP4 TM2) and display a single, limited set of interactions. The study presented here demonstrates a prolonged (during synthesis of >70 aa) and persistent (after peptidyl-tRNA cleavage) interaction of CFTR-TM8 with sec61α. This suggests that the substrate remains bound to sec61α after release of the polypeptide chain from the ribosome. Some TMs might not, therefore, spontaneously integrate upon release from the ribosome and, in fact, may continue to require an intact ribosome translocon complex (Fig. 5). This is wholly consistent with evidence that ribosomes remain bound to sec61 upon completion of protein synthesis [66-68]. Hence, the simple two-step folding model of Popot and Engelman [7, 8] may not be used by all polytopic proteins. Rather, sec61 can retain multiple TMs until after the completion of synthesis and provide a protein/lipid environment that permits sampling of helical packing landscapes and possibly preliminary tertiary folds through chaperoning, as well as thermodynamic partitioning mechanisms.

Materials and Methods:

Plasmid Construction: Plasmids for CFTR TM7-12 were generated from pSp64CFTR [232] as previously described [15]. A methionine codon at CFTR residue 837 was utilized to initiate translation. CFTR TM7-8 truncations were generated by PCR amplification with sense oligo TAGAGGATCTGGCTAGCGAT ~258 BP upstream of the initiator methionine within the pSp64 plasmid generating an Nhe1 restriction site. Antisense oligos were $CACACCTCTGAAGAATCCCAT_{(935)}$, $CACAACAGAATGTAACATTTTGTG_{(957)}$, $CACCGTGTTGAGGGTTGACAT_{(967)}$, $CACACTAGTTTTCAACGTGTTGAG_{(971)}$, $CACGAATCTATTAAGAATCCC_{(977)}$, $CACAAGGTCATCCAAAATTGC_{(987)}$, $CACCTGGATGAAGTCAAATATGG_{(997)}$, $AACTGCTATAGCTCCAATCACAAT_{(1007)}$, $AACAAAGATGTAGGGTTGTAAAACTGC_{(1017)}$, $CACAAAAGCCACTATCACTGGCACTGT_{(1027)}$, $CACCAGTTGTTTGAGTTGCTGTGAGG_{(1044)}$, $CACTTTGGTCACCAGAGTTTCAAAGTAAGG_{(1076)}$. All truncations ended with Val codons to minimize and standardize for spontaneous peptidyl-tRNA hydrolysis. The D924V mutation was engineered into pSp64CFTRTM7-12 as previously described [15]. Glycosylation site knockout constructs were generated by PCR overlap extension with sense oligos $GGGGCTAGCACTCATAGTAGAAATAACAG_{(N894A)}$, $CATTCTAGAGCGAACAGCTATGCAGTGATTAT_{(N900A)}$, $GACAAAGGGGCTAGCACTCATTCTAGAGCGAAC_{(N894A/N900A)}$ and antisense oligos $GTTATTTCTACTATGAGTGCTAGCCCCTTTGTCTTGAAGAGG_{(N894A)}$, $TGCATAGCTGTTCGCTCTAGAATGAGTACTATTCCCTTT_{(N900A)}$,

AGAATGAGTGCTAGCCCCTTTGTCTTGAAGAGG$_{(N894A/N900A)}$. All PCR amplified cDNA was verified by direct sequencing.

In vitro transcription and translation: CFTR PCR products were transcribed in vitro at 40°C for one hour as previously described [99]. mRNA was extracted with phenol chloroform, ethanol precipitated and dissolved in volumes of molecular biology grade water equal to the original transcription reaction. Transcripts were flash frozen and stored at -80°C. In vitro translations were performed as previously described [99]. Translation reactions were supplemented with canine rough microsomes (OD_{280} =2) stripped of endogenous ribosomes by incubating in 25mMEDTA, 250mM sucrose, 50mM triethanolamine (TEA) pH7.5, and 1mM dithiotreitol (DTT) for 15 minutes on ice, pelletting through 0.5M sucrose, 50mM Hepes pH7.5, 100 mM KoAc and 5mM MgoAc (buffer A) at 180,000g x 10 minutes and resuspending in 250 mM sucrose 50mM TEA pH7.5 and 1mM DTT equal to the starting volume. Translation reactions contained 4μM each of 18 essential amino acids minus lysine and methionine. DTT was replaced with 2mM reduced glutathione. ε-ANB-lys-$tRNA^{Amb}$ was added to a final concentration of 1μM. All reactions were carried out in the dark for 30-45 minutes. Where indicated, reactions were split for treatment with and without 1μM puromycin.

Photocrosslinking: $tRNA^{Amb}$ and ε-ANB-lys-$tRNA^{Amb}$ were synthesized as previously described [36, 74]. Translation products were irradiated on ice with collimated 300-350 nM UV light from an Oriel 500W mercury arc lamp. Membranes were collected by pelleting through 100mM DTT in buffer A at 180,000g x 10 minutes. The membrane

pellet containing targeted ribosome-nascent chain complexes was solubilized in 0.5% (w/v)sodium dodecyl-sulfate (SDS) and 10 mM Tris-HCl pH8. Except where indicated, all samples were digested in 0.05mg/ml RNaseA for 15 minutes at room temperature prior to SDS-PAGE.

Autoradiography, quantitation, and immunoprecipitation: Samples were analyzed on 12-17% gradient gels by SDS-PAGE, destained and treated with EN^{3}HANCE (Perkin-Elmer) and subjected to autoradiography . Representative gels were scanned with a UMax III scanner and Adobe Photoshop. Gels for quantitation were placed onto Kodak phosphor screens for 12-48 hours and bands corresponding to read-through polypeptides were analyzed with a Bio-Rad Personal FX phosphoimager and Quantity-One software. Sample volumes for immunoprecipitation were normalized to yield equivalent signal in the read-through band and reanalysed by SDS-PAGE to confirm the accuracy of quantitation. Further adjustments in sample volumes for immunoprecipitation were made as appropriate.

Normalized amounts of read-through translation products were denatured in 1% SDS and 100mM Tris-Cl pH8, diluted in 1 ml of 1% (w/v) Triton X-100, 100mM NaCl, 2 mM EDTA and 100mM Tris -Cl pH8 (buffer B) and incubated on a rotator overnight with 1 μL of sec61α, TRAM or TRAPα antiserum and 5 μL protein A affigel (Bio-Rad). Beads were washed twice with 0.5 ml of ice cold buffer B and 0.5 ml of ice cold 100 mM NaCl/100 mM Tris-Cl pH8. Samples were then analysed by autoradiography as above.

Fig. 3-1

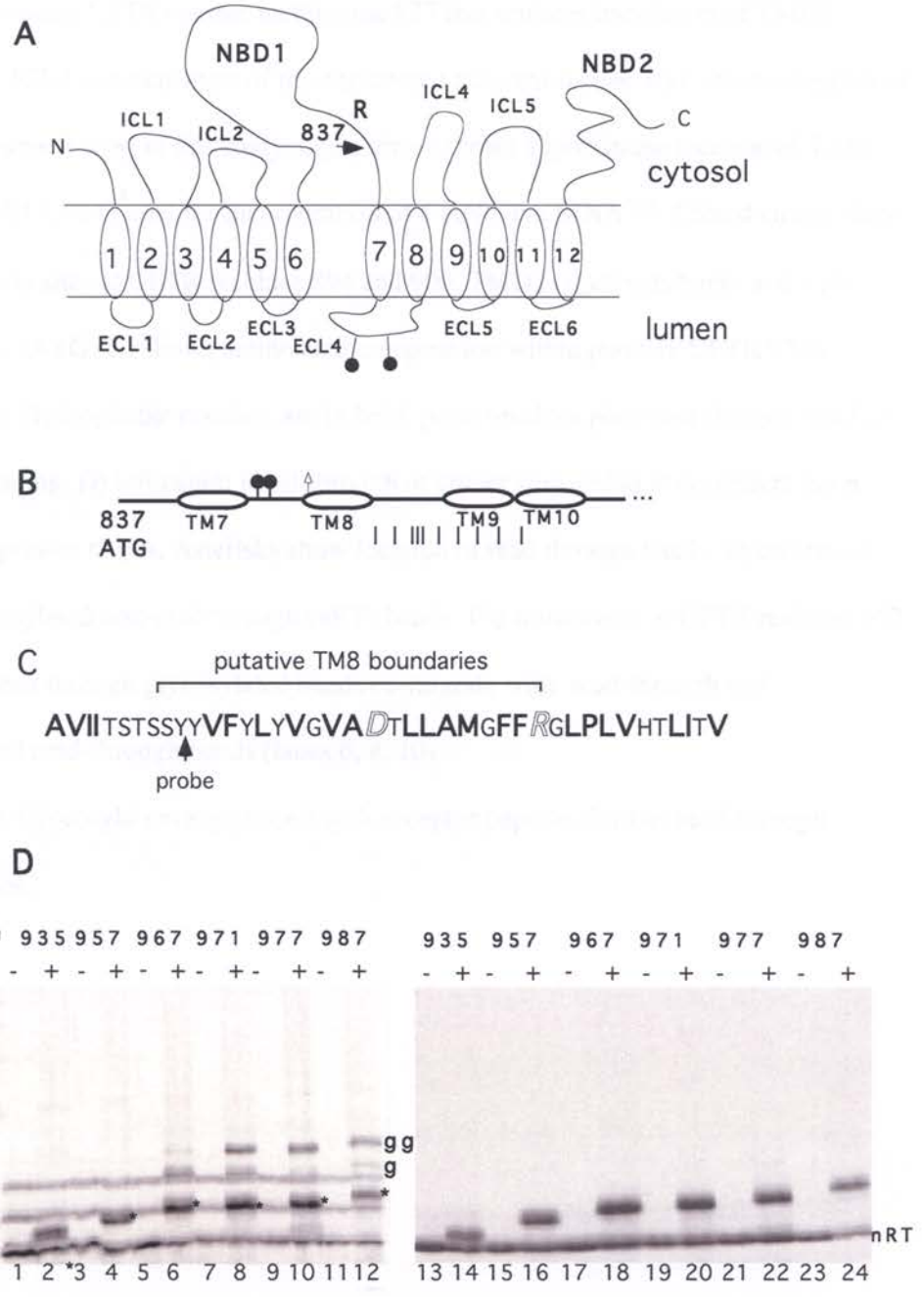
A
NBD1
NBD2
ICL1
ICL2
ICL4
ICL5
R
837
N
C
cytosol
1 2 3 4 5 6 7 8 9 10 11 12
ECL1
ECL2
ECL3
ECL4
ECL5
ECL6
lumen
B
837
ATG
TM7
TM8
TM9
TM10
C
putative TM8 boundaries
AVIITSTSSYYVFYLYVGVADTLLAMGFFRGLPLVHTLITV
probe
D
truncation 935 957 967 971 977 987 935 957 967 971 977 987
tRNAAmb - + - + - + - + - + - + - + - + - + - + - +
67
45
30
14
gg
g
*
nRT
1 2 *3 4 5 6 7 8 9 10 11 12 13 14 15 16 17 18 19 20 21 22 23 24

Figure 3-1 Characterization of CFTR TM8 read-through polypeptides A) Diagram of putative structure and topology of CFTR showing intra- (ICL) and extra-cellular (ECL) loops. Closed circles show location of two N-linked glycosylation sites in ECL4. Arrow represents CFTR residue methionine 837 that initiates translation of TMD2 constructs. ICL4 contains most of the engineered truncation sites. B) Cartoon diagram of CFTR constructs used in this study. Open arrow shows approximate location of TAG sites (912, 913, 914) used for incorporation of ε-ANB-lys-$tRNA^{Amb}$. Closed circles show glycosylation sites at CFTR residues 894 and 900. TMD2 constructs begin at CFTR residue 837 (ATG) C) shows amino acid composition within putative CFTR TM8 boundaries. Hydrophobic residues are in bold, polar residues plain and charged residues hollow lettering. D) left panel: Read-through of amber stop codon is dependent upon amber suppressor tRNA. Asterisks show location of read through bands. Open arrows show glycosylated non-read through (nRT) bands. For truncations at CFTR residues 967-977, non-read through glycosylated bands co-migrate with read-through and glycosylated read-through bands (lanes 6, 8, 10)

right panel: Glycosylation suppressed with acceptor peptide clarifies read-through polypeptides.

Fig. 3-2

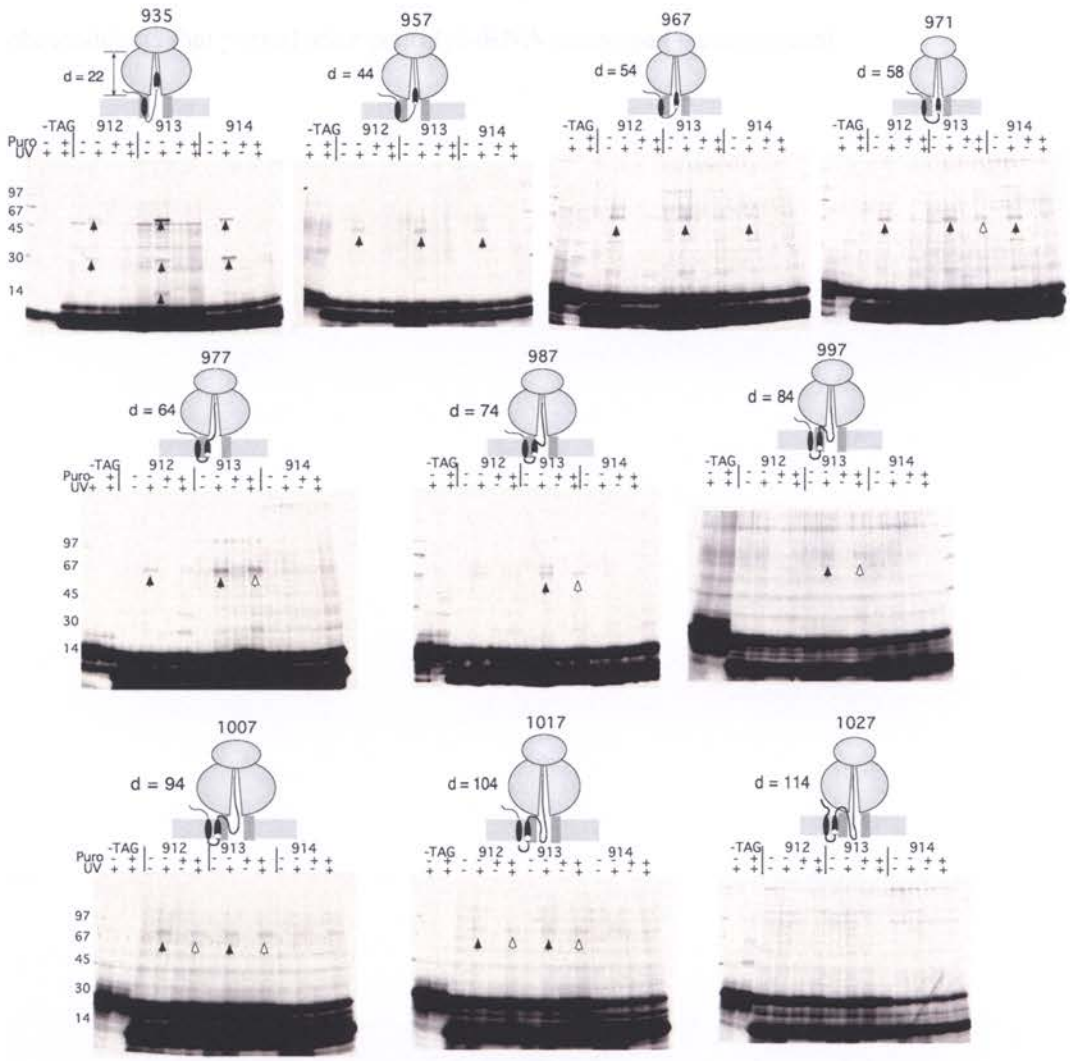

Fig 3-2 Progression of CFTR TM8 through sec61 alpha. Crosslinking pattern with probe at residues 912, 913 or 914 for CFTR truncations 935 to 1027 (amino acid residues refer to location within full-length CFTR). Translations performed in the presence of acceptor peptide. Cartoon RTCs shows location of probe (white circle at N-terminus of TM8) with respect to sec61α. d= distance from probe to the ribosome peptidyl-

transferase center. Black arrows represent likely photoadducts. White arrows are possible photoadducts that persist after peptidyl-tRNA cleavage (+ puromycin).

Fig 3-3

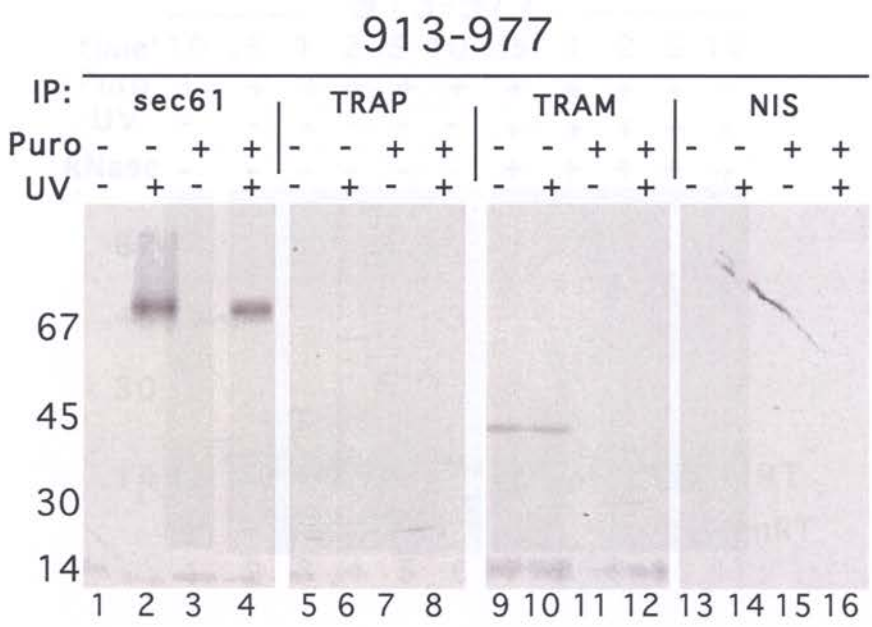

Fig 3-3 CFTR TM8 remains in proximity to sec61 alpha after peptidyl-tRNA cleavage. IPs with sec 61α antiserum of Y913TAG, truncation 977 (lanes 1-4) shows that photoadducts both before and after puro treatment are to sec 61α. No obvious reactivity with antiserum to TRAP α (lanes 5-8) or to TRAM lanes 9-12) is seen. Equal amounts of translation products used in each lane.

Fig. 3-4

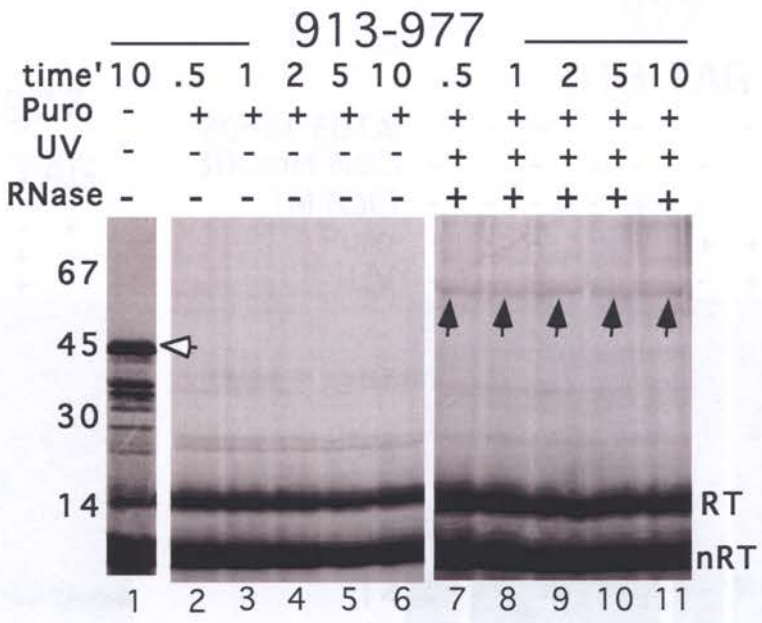

Fig. 3-4. Puromycin effectively cleaves peptidyl-tRNA bond. Open arrow shows peptidyl-tRNA band of read-through product at truncation 977. Peptidyl-tRNA bond rapidly and efficiently cleaved (lanes 2-6) as evidenced by lack of peptidyl-tRNA band. Persistent crosslinks in presence of UV are stable out to 10 minutes incubation at room temperature post-puromycin (lanes 7-11 black arrows) Experiment performed in presence of acceptor peptide.

Fig. 3-5

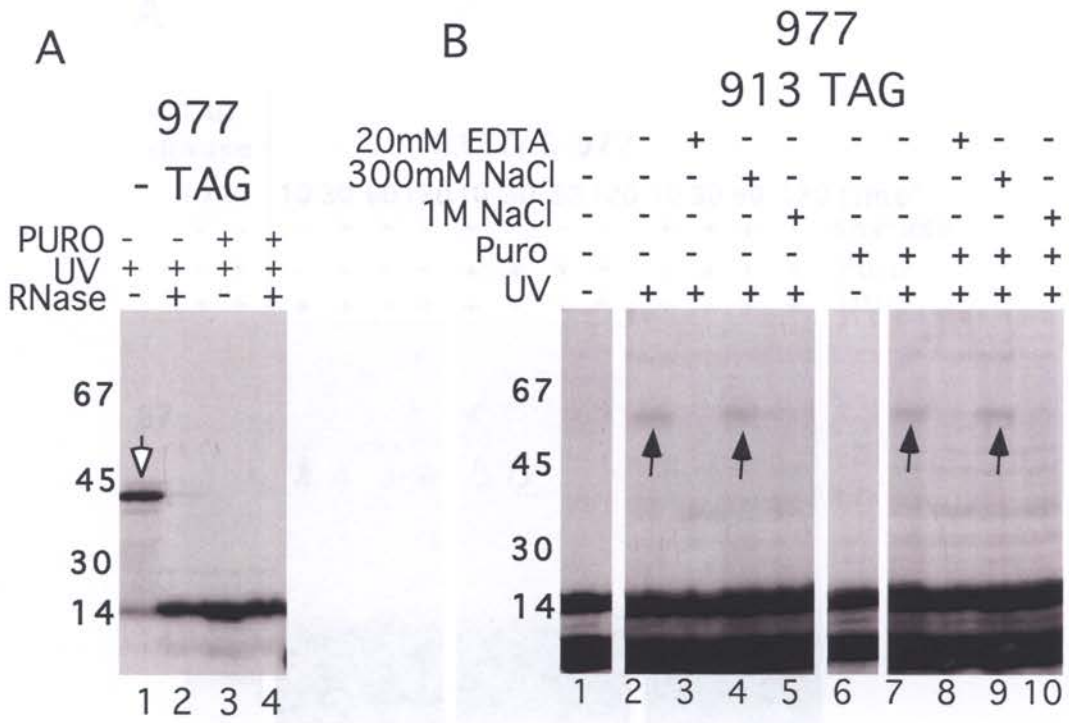

Fig 3-5 Persistent CFTR TM8-sec61α crosslinking requires an intact ribosome translocon complex. A. Efficiency of puromycin release. White downward arrow: peptidyl tRNA band. Puromycin releases ~100% of chains (lane 3). RNase effectively digests peptidyl-tRNA of integration intermediate (lane 2). B. Comparison of photoadducts (black upward arrows) minus (lanes 1-5) and plus (lanes 6-10) puromycin. After 10 min incubation with 1mM puro, nascent chains remain in association with sec61 alpha (compare lanes 2 (-puro) and 7 (+puro). Minus UV samples do not cross-link (lanes 1, 6) Treatment with 20 mM EDTA abolishes crosslinking -/+ puro (lanes 3, 8). 300mM salt has little effect on stability of TM8-sec61 interaction (lanes 4 and 9). 1M salt disrupts interaction (lanes 5, 10).

Fig. 3-6

A

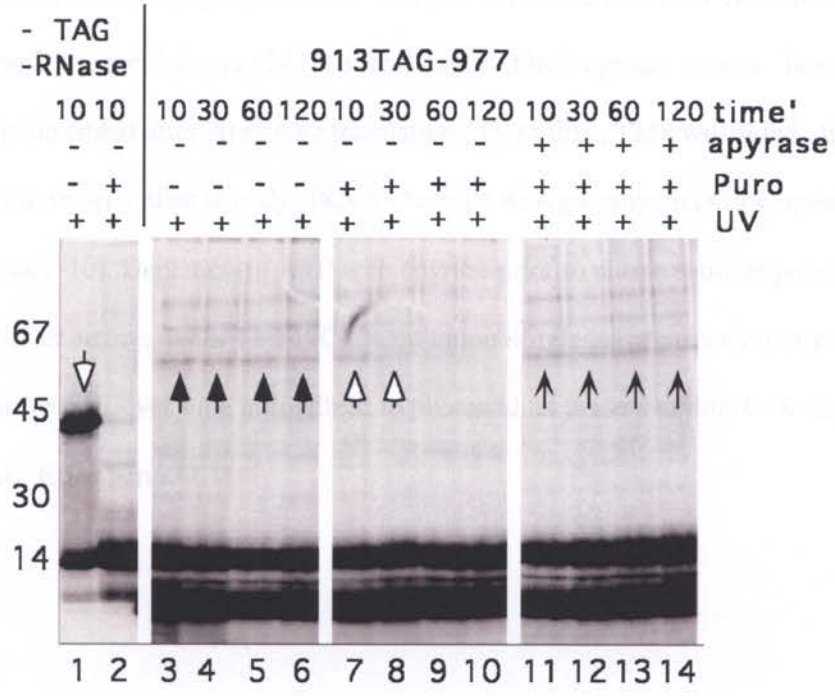
- TAG
-RNase
913TAG-977
10 10 10 30 60 120 10 30 60 120 10 30 60 120 time'
- - - - - - - - - + + + + apyrase
- + - - - - + + + + + + + + Puro
+ + + + + + + + + + + + + UV
67
45
30
14
1 2 3 4 5 6 7 8 9 10 11 12 13 14

B

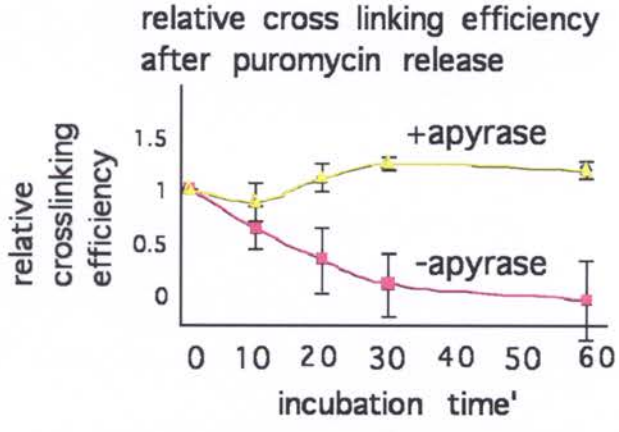
relative cross linking efficiency
after puromycin release
relative crosslinking efficiency
1.5
1
0.5
0
+apyrase
-apyrase
0 10 20 30 40 50 60
incubation time'

Fig. 3-6 Release of CFTR-TM8 from sec61 after peptidyl-tRNA cleavage is time and energy dependent. A) Puromycin released >>90% of chains in this experiment (lane 1-white downward arrow=peptidyl-tRNA – compare with lane 2). Sec61 crosslinks are stable out to 2 hrs. incubation at 24° post-translation (black upward arrows - lanes 3-6, cyclohexamide added after 30 minute translation). Over time, TM8 will slowly be released from sec61α after peptidyl-tRNA cleavage with puromycin (white upward arrows, lanes 7-10). Depletion of ATP with apyrase prior to puro treatment prevents release (slender arrows, lanes 11-14) C) quantitation of release of puromycin treated chains from sec61α over time normalized to photoadduct present at time 0. Average of 4 experiments. Error bars=SEM

Fig 3-7

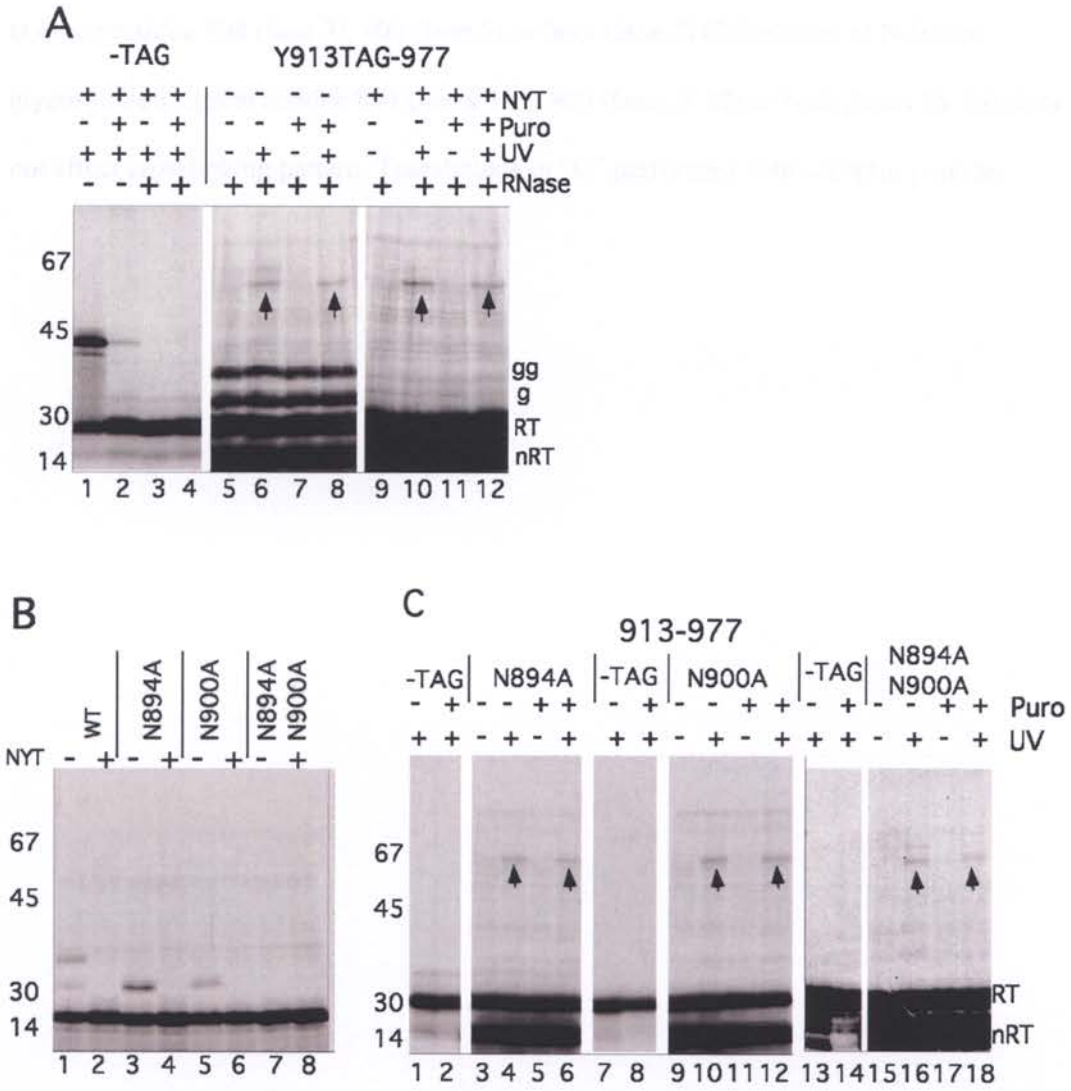

Fig. 3-7. Two proximal N-linked glycosylation sites in ECL4 do not cause persistent sec61 interaction.

A) Demonstrates similar crosslinking pattern (black upward arrows) of Y913TAG-977 in absence (lanes 6, 8) or presence (lanes 10, 12) of acceptor peptide. Acceptor peptide efficiently disrupts glycosylation (compare singly (g) and doubly (gg) glycosylated bands

in lanes 5-8 vs 9-12). B) Replacement of asparagine with alanine eliminates glycosylation at either residue 894 (lane 3), 900 (lane 5) or both (lane 7) C) Deletion of N-linked glycosylation sites at residue 894 (lanes 3-6), 900 (lanes 9-12) or both (lanes 15-18) does not affect crosslinking pattern. Translations in "C" performed with acceptor peptide.

Fig 3-8

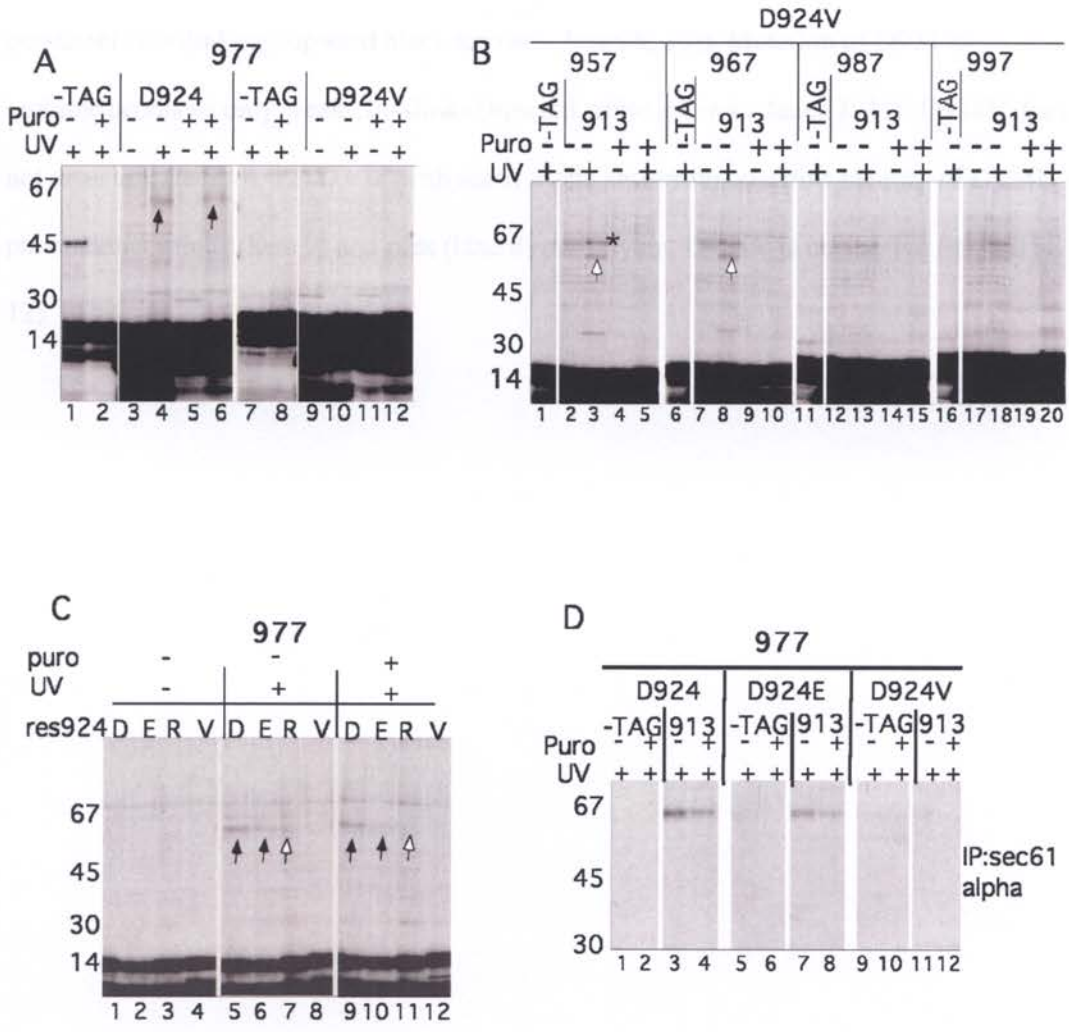

Fig 3-8. Polar residue in center of TM8 causes persistent crosslinking.

A) Sec61α crosslinks present -/+ puro in TM8 D924 (Y913TAG truncation 977 -lanes 4, 6, black upward arrows)) are no longer present in D924V mutation (lanes 10, 12) B) D924V only crosslinks at earlier amino acid truncations 957 and 967 and only in the integration intermediates (white upward arrows). Asterisked band present in all truncations is an unidentified background band that is present to a lesser extent in the

absence of UV. C) In Y913TAG-977, mutation of aspartate to glutamate preserves the persistent crosslinking (upward black arrows – lanes 6, 10)). Mutation of D924 to arginine produces only weak crosslinks (upward white arrows – lanes 7, 11). D924V does not crosslink (lanes 8, 12) D). IP with sec61 alpha antiserum confirms identity of D924E photoadduct minus (lane 7) and plus (lane 8) puromycin. D924V is unreactive (lanes 11-12).

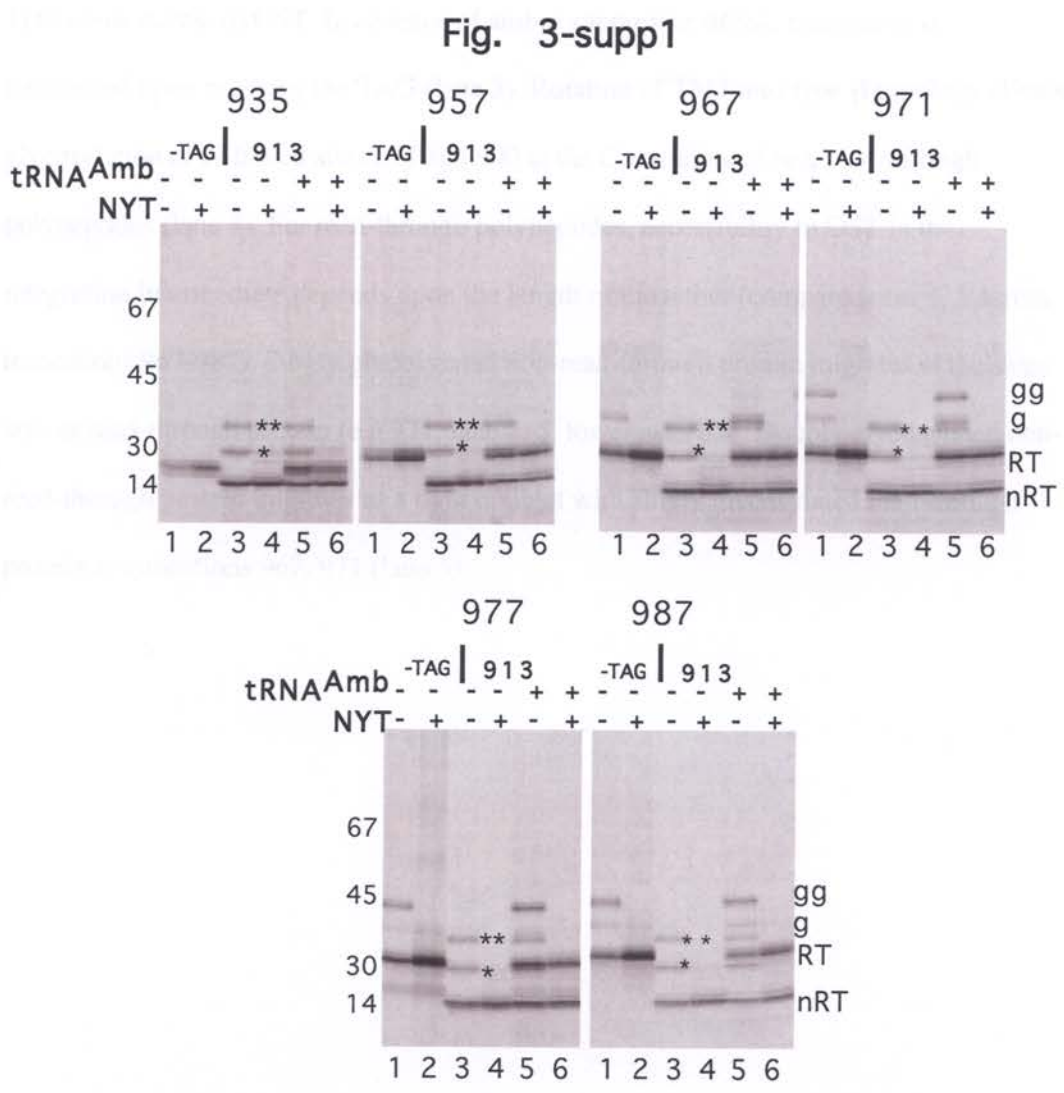

Fig. Supplement 3-1: Detailed analysis of glycosylation patterns of TMD2 polypeptides. Shown are glycosylation patterns of 935-987 truncations -/+ amber suppressor tRNA and -/+ acceptor peptide. -TAG protein demonstrates that acceptor peptide efficiently suppresses glycosylation (lanes 1-2, truncations 957-987) Nascent chain tether in integration intermediate is not long enough for 935 –957 truncations (lane

1) to allow access to OST. In absence of amber suppressor tRNA, translation is terminated upon reaching the TAG (lane 3). Rotation of TM7 into type II topology allows glycosylation of N-linked sites 894 and 900 at the C-terminus of non-read-through polypeptides (lane 3). For read-through polypeptides, accessibility to OST in the integration intermediate depends upon the length of the tether (compare lanes 1, 5 across truncations 967-987). Singly glycosylated non-read-through protein migrates at the same size as read-through protein (e.g 971, lane 3, 5, lower asterisk). Doubly glycosylated non-read-through protein migrates as a tight doublet with singly glycosylated read-through protein at truncations 967, 971 (lane 5)

Fig 3-Supp 2

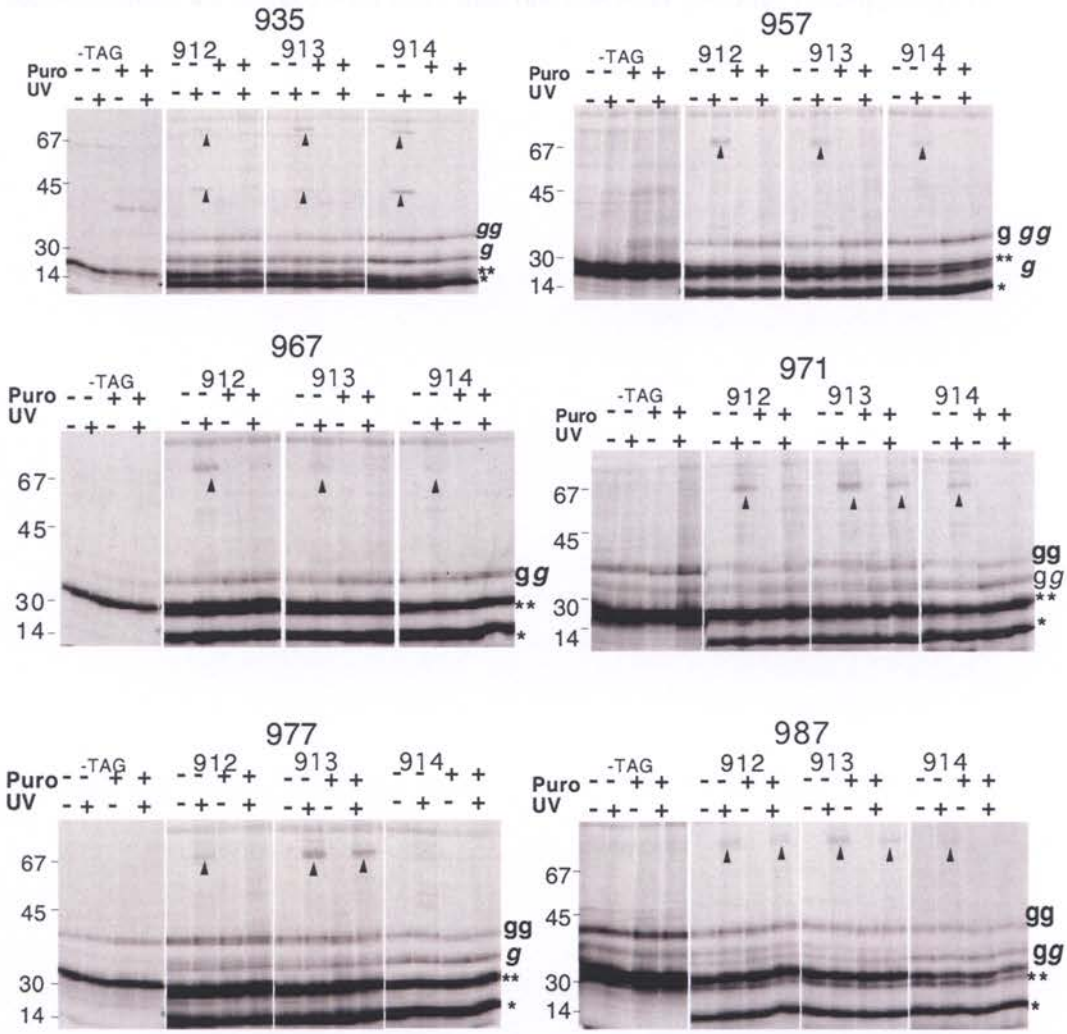

Fig. Supplement 3-2. Crosslinking at TM8 N-terminus in normally glycosylated polypeptides is similar to acceptor peptide treated translations

Photoadducts (upward arrows) are similar in glycosylated polypeptides. Compare to figure 2 for truncations 935-987. * - non read through band; ** - read-through band, g singly glycosylated read-through band. gg – doubly glycosylated read-through band, *g/gg*

–singly and doubly glycosylated non-read-through bands, respectively. Overlapping bands/doublets are marked with more than one character (see Fig. 1d, Supp. Fig. 1)

Fig. Supp. 3-3

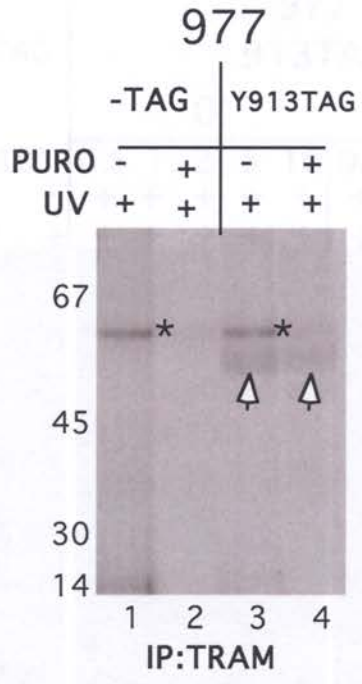

Fig. Supplement. 3-3. Long exposure IP demonstrates weak TRAM crosslink. Lanes 3-4, white arrows, persistent but weak TRAM crosslink of probe incorporated at residue 913. Construct that does not contain probe does not show this crosslink (lanes 1-2). Non-probe specific TRAM crosslink denoted by asterisk is only present in integration intermediate (lanes 1, 3).

Fig. Supp. 3-4

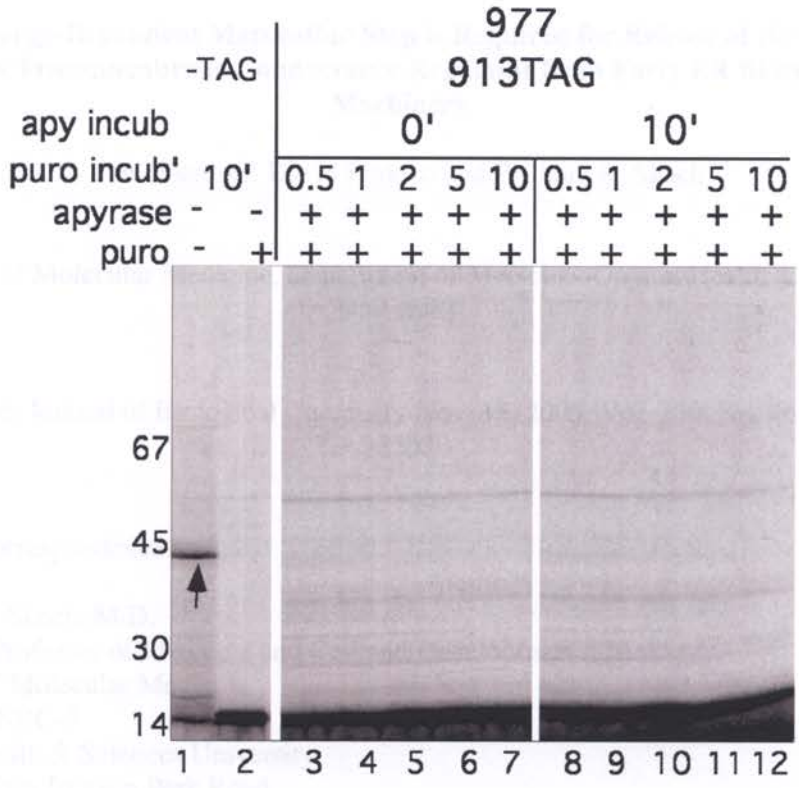

Fig. Supplement 3-4. Apyrase does not affect puromycin release. Untreated sample demonstrates peptidyl –tRNA band (black arrow, lane 1) 10' incubation with puromycin in absence of apyrase fully releases nascent chain (lane 2). Lanes 3-7, apyrase and puromycin added simultaneously and incubated for 0.5-10min. Nascent chain fully released as evidenced by lack of persistent peptidyl-tRNA band. Lanes 8-10, pre-incubation for 10' with apyrase prior to addition of puromycin. Release of nascent chain remains unaffected.

Manuscript 4

An Energy-Dependent Maturation Step is Required for Release of the Cystic Fibrosis Transmembrane Conductance Regulator from Early ER Biosynthetic Machinery

Jon Oberdorf, David Pitonzo and William R. Skach

Division of Molecular Medicine, Department of Medicine, Oregon Health & Sciences University

Published in Journal of Biological Chemistry Nov. 18, 2005, Vol. 280, No. 46 pp 38193-38202

Address Correspondence to:

William R. Skach, M.D.
Associate Professor of Medicine and Cell and Developmental Biology
Division of Molecular Medicine
Mail code NRC-3
Oregon Health & Sciences University
3181 SW Sam Jackson Park Road
Portland, Oregon 97239

Abbreviations: CFTR, cystic fibrosis transmembrane conductance regulator; DTSSP, 3,3-dithiobis[sulfosuccinimidylproprionate]; DTT, Dithiothreitol; ER, endoplasmic reticulum; ERAD, ER-associated degradation; MSD, membrane spanning domain; NBD, nucleotide binding domain, TM, transmembrane; RRL, rabbit reticulocyte lysate; RTC, ribosome-translocon complex. Triton , Triton X-100.

1. Abstract.

Polytopic proteins are synthesized in the endoplasmic reticulum (ER) by ribosomes docked at the Sec61 translocation channel. It is generally assumed that upon termination of translation, polypeptides are spontaneously released into the ER membrane where final stages of folding and assembly are completed. Here we investigate early interactions between the ribosome-translocon complex and CFTR, a multi-domain ABC transporter, and demonstrate that this is not always the case. Using *in vitro* and Xenopus oocyte expression systems we show that during and immediately following synthesis, nascent CFTR polypeptides associate with large, heterogeneous and dynamic protein complexes. Partial-length precursors were quantitatively isolated in a non-covalent, puromycin-sensitive complex (>3,500 kDa) that contained the Sec61 ER translocation machinery and the cytosolic chaperone Hsc70. Following the completion of synthesis, CFTR was gradually released into a smaller (600-800 kDa) ATP-sensitive complex. Surprisingly, release of full-length CFTR from the ribosome and translocon was significantly delayed after translation was completed. Moreover, this step required both nucleotide triphosphates and cytosol. Release of control proteins varied depending on their size and domain complexity. These studies thus identify a novel energy-dependent step early in the CFTR maturation pathway that is required to disengage nascent CFTR from ER biosynthetic machinery. We propose that contrary to current models, the final stage of membrane integration is a regulated process that can be influenced by the state of nascent chain folding, and we speculate that this step is influenced by the complex multi-domain structure of CFTR.

2. Introduction.

The Cystic Fibrosis Transmembrane Conductance Regulator (CFTR) is a polytopic membrane protein that is synthesized in the endoplasmic reticulum (ER) and expressed in the apical membrane of selected epithelial tissues [103]. Inherited mutations that disrupt CFTR expression, trafficking, stability or chloride channel activity cause clinical manifestations of cystic fibrosis (CF) [233]. In >90% of CF patients the fundamental defect is failure of mutant CFTR to fold properly [118]. Both wild type and mutant proteins are initially synthesized in an immature, unstable conformation, and both can achieve functional activity in the ER [234]. However, CFTR requires an ATP-dependent conformational change in order to complete its intracellular processing and delivery to the plasma membrane [139, 235]. In most heterologous systems, approximately 70% of wild type and nearly 100% of common mutant variants (e.g. ΔF508) fail to complete this maturation step and are recognized and degraded via the ubiquitin-proteasome ER associated degradation (ERAD) pathway [120, 129, 236]. Recent studies have further indicated that maturation is dependent on cell type and that wild type protein is efficiently trafficked in native epithelial cells under physiologic growth conditions [130].

CFTR exhibits a modular, multi-domain structure characteristic of the ABC transporter superfamily [103]. It is comprised of two membrane spanning domains (MSDs) with six transmembrane (TM) segments each, two cytosolic nucleotide binding domains (NBDs), and a unique cytosolic regulatory (R) domain. A poorly understood, but important aspect of CFTR biogenesis is how folding and assembly of different domains are coordinated by cellular machinery in different cellular compartments. Topology of MSDs is established during synthesis as the ribosome and nascent chain target to the ER membrane and bind a large protein conducting channel (translocon) comprised of Sec61α and its associated proteins [15, 26, 105, 209]. As translation proceeds, internal sequences within the

nascent CFTR polypeptide interact with the ribosome and translocon where they initiate polypeptide translocation into the ER lumen, properly orient cytosolic loops, and direct transmembrane segment integration into the lipid bilayer [15, 176, 237, 238].

CFTR folding is facilitated by cytosolic and ER chaperones (Hsc70, Hsp90, calnexin) [119, 127, 239] and co-chaperones (Hsp40 homologs and CHIP) [240, 241]. Hsc70 and Hsp40 decrease NBD aggregation and improve productive folding *in vitro* [242, 243]. Similarly, Hsc70 and Hsp40 homologs bind cytosolic domains *in vivo,* and chaperone release correlates with acquisition of a stable structure in the ER membrane [140, 242]. In contrast, unstable conformations of CFTR remain bound to Hsc70 which, together with the co-chaperone/E3 ligase CHIP, can result in polyubiquitination [244, 245]. The dynamic complement of chaperone interactions therefore links CFTR biosynthetic and degradation pathways by facilitating both the acquisition of a trafficking-competent conformation [127, 242, 243, 246, 247] as well as the ubiquitination and degradation of misfolded conformers [125, 244, 245, 248]. While few steps of the *in vivo* CFTR folding pathway have been well characterized, these studies predict that the early fate of CFTR is tightly regulated by protein-protein interactions that begin during translation and culminate as the mature protein is packaged for ER export [249].

Several lines of evidence indicate that proper formation of domain-domain contacts is the rate limiting step for trafficking-defective CFTR mutants [104, 108, 110, 111, 140]. Thus, to understand how defects in CFTR biogenesis cause disease, it is necessary to determine how cellular folding machinery coordinates secondary and tertiary structure formation as the protein is synthesized and folded at the ER membrane. In this regard, some substrates are able to fold cotranslationally such that N-terminal domains acquire functional activity even while C-terminal domains remain tethered to the translating

ribosome [172, 173]. Other membrane proteins complete their folding posttranslationally only after the polypeptide has been fully synthesized and released from the ribosome-translocon complex (RTC) [250-252]. In the case of CFTR, it is likely that ribosome binding to the cytosolic face of the ER membrane constrains folding and association of the MSDs, NBDs and R domain. Thus, release from early biosynthetic machinery represents an important biosynthetic step towards conformational maturation. While it has generally been assumed that polypeptides are spontaneously released from the RTC when translation is terminated, the precise mechanism by which membrane integration is coordinated for complex multi-domain proteins such as CFTR remains unknown.

The above considerations predict that dynamic interactions of cellular proteins with nascent CFTR play a critical role in early folding events. Because of their transient nature, it has been difficult to capture protein-protein interactions before polypeptide synthesis is completed. In the current study, we have overcome this limitation using cell free and whole cell expression systems that enable us to visualize and manipulate actively translating CFTR biogenesis intermediates. Our results confirm that even at the earliest stages of translation, CFTR interacts with highly dynamic protein complexes. Partially synthesized precursors were initially isolated with functional RTCs and cytosolic chaperones. CFTR was then gradually released into a smaller ATP-dependent 600-800 kD complex after the completion of synthesis. Surprisingly, full-length CFTR exhibited prolonged interactions with early ER biosynthetic machinery, and release from the RTC was not spontaneous but required both NTPs and cytosolic factors. Thus, contrary to current models, the final step of CFTR integration into the membrane is an active rather

than passive process that is regulated in a substrate-specific manner and likely reflects unique requirements of the CFTR folding pathway.

3. Materials and Methods.

In vitro transcription/translation. WT and ΔF508 CFTR (plasmid pSPCFTR [232] and an identical plasmid missing Phe508), myc-tagged human P-glycoprotein (plasmid pSPMDR1 [232] containing LEQKLSSEEDLQ inserted after codon Lys681), bovine prolactin [54] or myc-tagged AQP2 [253] were transcribed *in vitro* at 40°C for 1 hr in reactions containing 0.2-0.4 mg/ml plasmid DNA, 40 mM Tris, pH 7.5, 6.0 mM $MgOAc_2$, 2 mM spermidine, 0.5 mM each of ATP, CTP, UTP, 0.1 mM GTP, 0.5 mM GpppG (Amersham Pharmacia, Piscataway, NJ), 10 mM DTT, 0.2 mg/ml bovine calf tRNA, 0.75 U/ml RNAse inhibitor (Promega, Madison, WI), and 0.4 U/ml SP6 RNA polymerase (Epicentre, Madison, WI). RRL was prepared from New Zealand White Rabbits as described [254, 255]. Translation was performed at 25°C for 1-2 hrs in reactions containing 20% transcript mixture, 40% nucleased rabbit reticulocyte lysate [254] plus 1 mM ATP, 1 mM GTP, 12 mM creatine phosphate, 40 μM each of 19 essential amino acids except methionine, 1 μCi/μl of Tran[^{35}S]-label (ICN Pharmaceuticals, Irvine, CA), 40 μg/ml creatine kinase, 0.1 mg/ml tRNA, 0.2 U/μl RNAse inhibitor (Promega, Madison WI), 10 mM Tris, pH 7.5, 100 mM KOAc, and 2 mM $MgCl_2$. Canine pancreas microsomal membranes, prepared as described [256], were added at the start of translation (final concentration, 7.0 OD_{280}). 50-100 μM aurin tricarboxylic acid was added after 12-15 min to synchronize translation. Prior to solubilization, ER microsomes were isolated by pelleting through 0.5 M sucrose in Buffer A (20 mM Tris-HCl (pH 7.5), 50 mM KCl, 5 mM MgCl2, and 2 mM DTT) at 180,000 X g for 10 min as described [254, 257].

Chemical crosslinking was performed by pelleting CFTR containing-microsomes through 0.5 M sucrose, 50 mM N-2-hydroxyethylpiperazine-N'-2-ethanesulfonate (HEPES)-KOH, (pH 7.5), 100 mM KOAc and 5 mM $Mg(OAc)_2$. Pellets were solubilized in 0.2% SDS, 1% Triton X-100 (Triton) or 2% digitonin in 20 mM HEPES-KOH (pH 7.5), 50 mM KCl (NaCl for SDS), 5 mM $MgCl_2$, and 5% glycerol. Samples were incubated in 1 mM 3,3-dithiobis[sulfosuccinimidylproprionate] (DTSSP) for 30 min at 24°C and quenched in 100 mM Tris-HCl, pH 7.5 for 10 minutes. Samples were then denatured in 1% SDS, 10 mM EDTA and 100 mM Tris-HCl (pH 8.0) at 37°C for 30 min prior to immunoprecipitation.

Xenopus oocyte expression: Oocytes were surgically removed from anesthetized Xenopus laevis and digested for 3 hrs at room temperature in ~4 vol. of calcium free MBSH, (88 mM NaCl, 1 mM KCl, 2.4 mM $NaHCO_3$, 0.82 mM Mg SO_4, 0.33 mM $Ca(NO_3)_2$, 0.41 mM $CaCl_2$, 10 mM sodium- HEPES, pH 7.4) containing 0.2U/ml of Blendzyme III (Roche Applied Sciences). Stage VI oocytes were collected and stored at 17° C in MBSH containing 100U/ml penicillin, 100 mM/ml streptomycin and 50μg/ml gentamicin. Oocytes were injected on an ice cold stage with 50 nl of a 1:5 mixture (transcript:10X concentrated Tran[^{35}S]-label) as described [15, 258]. Incubations were carried out at 17°C. Incubation times were determined empirically to capture both partial- and full-length CFTR protein at the time of initial homogenization. This ensured that active translation of radiolabeled CFTR was still ongoing and enabled us to distinguish different behaviors of these different populations of polypeptides. For gradient analysis, oocytes were homogenized in 5 volumes of 0.25M sucrose in buffer A supplemented with 1 X protease inhibitor I or protease inhibitor III (CalBiochem, La Jolla, CA). Homogenate was centrifuged at 800 x g for 10 min. Supernatant was layered onto 0.1 ml of 1.8M sucrose in buffer A and 0.4 ml of 0.5M sucrose in buffer A and

centrifuged at 250,000 x g for 10 min. Oocyte membranes were collected at the 0.5/1.8M sucrose interface, diluted 1:5 with buffer A and pelleted at 250,000 x g for 10 min. Except where indicated, homogenates and extracts were kept at 4°C. For *ex vivo* release assays, membranes were resuspended in buffer A or freshly prepared oocytoplasm (supplemented with protease inhibitors) and ATP/GTP, puromycin and cyclohexamide as indicated. When comparing different release conditions and sequential time points, samples were taken from the same batch of injected oocytes and processed and analyzed together. All experiments were repeated (two or more times) to verify reproducibility.

Glycerol gradient centrifugation: Microsomal membranes from *in vitro* translations or Xenopus oocytes were solubilized for 30 min in either 2% digitonin (CalBiochem), 1% Triton or 0.2% SDS in Buffer B, (50 mM KCl (or NaCl), 5 mM $MgCl_2$, 20mM Tris-HCl, pH 7.5), and 0.5% protease inhibitor cocktail III (CalBiochem, Hercules, CA). Samples were clarified by centrifugation at 16,000 x g for 10 min and layered onto an 8% to 35% glycerol step gradient (8 x 110μl steps 8.5, 12.5, 16.3, 20, 23.8, 27,5, 31.3, 35%), in buffer B containing 0.1-0.2% of the same detergent used for solubilization. For SDS gradients, NaCl was substituted for KCl with no observable effect on the gradient profile. Gradients were centrifuged at 180,000 x g (max.) for 2 hr (Beckman TLS55 rotor). 12 X 75μl aliquots were collected. For crosslinking experiments, the solubilization and gradient buffers contained HEPES instead of Tris. The positions of chromatography standards bovine serum albumin (67 kDa), alcohol dehydrogenase (140 kDa), apoferritin (440 kDa) and thyroglobulin (670 kDa) were determined on parallel gradients.

Preparation of oocytoplasm: 100-200 injected (or uninjected) oocytes were rinsed several times in MBSH and centrifuged at 500 x g for 1 min to compress the oocytes and remove excess buffer. Oocytes were then lysed (in the presence of 50 μg/ml cytochalasin) by centrifugation at 19,000 x g (max.) for 15 min (Beckman TLS55 rotor).

The resulting grayish supernatant (middle layer) containing cytosol and cellular membranes was collected (oocytoplasm) and supplemented where indicated with an ATP generation system (10 mM creatine phosphate, 0.1 mg/ml creatine kinase), 50 mM KCl, 1 mM $MgAc_2$, 2 mM glutathione (GSH), protease inhibitors, and 7.5 units/ml RNAse inhibitor. Translation inhibitors were added as indicated. Extracts were incubated at 17°C after which samples were diluted in 0.4 ml of 0.25M sucrose in Buffer A, layered over 0.5 ml of 0.5M sucrose in Buffer A and sedimented at 250,000 x g (max.) for 10 min. The membrane pellet was then extracted in buffer B containing 2% digitonin and prepared for glycerol gradient centrifugation as described above. In some experiments membranes containing radiolabeled CFTR were resuspended in a small volume of buffer B, 1mM DTT and translation inhibitors as indicated. They were then combined with fresh oocytoplasm (oocytoplasm: microsome ratio of 2:1), incubated at 17°C, and prepared for glycerol gradient fractionation as described above.

Immunoprecipitation and SDS-PAGE: Gradient fractions from *in vitro* translations were either analyzed directly by SDS PAGE or immunoprecipitated in Buffer C (0.1 M NaCl, 2 mM EDTA, 0.1M Tris-HCl (pH 8.0), and 0.5 mM PMSF) containing 0.2% detergent. Samples from oocyte gradients were immunoprecipitated by denaturation in 100 μl 1.0 % SDS, 100 mM Tris HCl, pH 8.0, 10 mM EDTA, and 1 X protease inhibitor cocktail III. Extracts were incubated at 37°C for 20-30 min, diluted with 1.0 ml 1% Triton in Buffer C, incubated on ice for an additional 20 min and clarified by centrifuging at 16,000 x g for 10 min. 1 μl of antisera and 5μl of Protein A agarose (BioRad, Hercules, CA) were added. The CFTR antibody is a polyclonal rabbit antisera raised against CFTR residues 45-65 [140]. The anti-Hsc/Hsp70 polyclonal rabbit antisera was a generous gift of Dr. W. Welch. Samples were mixed overnight and washed 3 X 1ml of 1% Triton in buffer C and 2 X with 1ml of 100 mM Tris-HCl (pH 8.0), 100mM NaCl and subjected to SDS-PAGE. Gels were analyzed by autoradiography with or without

En^{3}Hance (NEN Life Science Products, Boston, MA) fluorography and digitized with an UMax Powerlook III scanner and Adobe Photoshop software. Band signals were quantitated using a BioRad Molecular PhosphorImager Fx (Kodak screens, Quantity-1 software).

4. Results.

In vitro formation of CFTR complexes. Identification of cellular proteins that participate in cotranslational CFTR folding requires expression conditions where both full-length and partial-length polypeptides can be visualized. *In vitro* translation systems are well suited for such analysis and have been used to define mechanisms of CFTR topogenesis [15, 105, 237], identify early CFTR chaperone interactions [259] and characterize CFTR degradation pathways [121, 257]. We previously showed that rabbit reticulocyte lysate (RRL) supplemented with ER derived microsomal membranes faithfully reconstitutes CFTR synthesis, core glycosylation and membrane integration [121, 254]. In addition, because RRL lacks other cellular organelles, it provides a source of nascent polypeptide in which processing is limited to early events that occur within the ER compartment.

To capture interactions with nascent CFTR polypeptides, ER microsomal membranes containing *in vitro*-synthesized CFTR were solubilized in denaturing or non-denaturing detergents and analyzed by glycerol gradient centrifugation. In SDS, full-length CFTR sedimented with an apparent size of a 160 kDa monomer (Figure 1, top panel). In contrast, non-denaturing detergents generated two distinct CFTR populations. The first was a very large and stable complex that pelleted through the gradient (Figure 1 middle and bottom panels, lane 12). The second was a smaller heterogeneous complex that migrated with an apparent molecular mass of 300-400 kDa in Triton and 400-800 kDa in digitonin. This profile suggested that non-covalent CFTR-protein interactions are

preserved in non-denaturing detergents. Differences in migration patterns for Triton and digitonin are consistent with milder properties of digitonin and its ability to better preserve membrane protein interactions [41, 66, 260]. However, it is also possible these detergents bind with different stoichiometry to CFTR hydrophobic domains and/or associated membrane phospholipids. In contrast to full-length CFTR, partial-length translation intermediates were found in the lighter fractions in SDS, whereas they were almost exclusively recovered in the gradient pellet under non-denaturing conditions. This is consistent with their expected persistent binding to the RTC (>4,000 kDa).

Immature forms of CFTR bind Hsc70 *in vivo* [119]. *In vitro*-synthesized CFTR also co-immunoprecipitated with Hsc70 (Figure 2A, lanes 1-3), and binding was disrupted when microsomes were pelleted in the presence of ATP (Figure 2A, lanes 4-6). Thus Hsc70 undergoes physiological cycles of CFTR binding and release during *in vitro* ADP-ATP exchange. We therefore examined the effect of ATP on CFTR sedimentation. When microsomes were solubilized in the presence of ATP, CFTR that was released from the gradient pellet sedimented primarily in fractions 2-5 similar to the pattern observed for SDS (Figure 2B&D). In contrast, ATP depletion prior to solubilization resulted in a shift in sedimentation towards denser fractions (fractions 4-7) indicating stabilization of protein-protein interactions. While ATP depletion yielded relatively small changes in CFTR migration, the shift in peak migration, representing an average mass difference of ~200 kDa, was highly reproducible (figure 2D). Immunoprecipitation of gradient fractions with Hsp70 antisera further revealed that Hsc70-bound CFTR was recovered predominantly fractions 6-9 and in the gradient pellet (fraction 12) (Figure 2C&E). Thus *in vitro* synthesized CFTR exhibits ATP-dependent protein interactions that include Hsc70 and influence its sedimentation through glycerol gradients.

Sec61α is a major translocon component that transiently interacts with nascent membrane proteins during translocation and integration [9, 33, 36, 261]. We therefore wished to identify the population of CFTR complexes (if any) that remained associated with the translocon. For these studies we used the bifunctional chemical crosslinking agent 3,3-dithiobis[sulfosuccinimidylproprionate] (DTSSP) that covalently reacts with free amino groups and contains a cleavable disulfide bond within its 12 Å spacer arm. Following Triton and digitonin solubilization, DTSSP converted CFTR into a large covalent complex that was readily detected by SDS-PAGE at the top of the gel. This material decreased and full length CFTR (155 kDa) was again visualized, when the crosslinker was cleaved by DTT (Figure 3A, compare lanes 3-4 and 6-7). Although *in vitro*-synthesized CFTR exhibited relatively diffuse migration under non-reducing conditions, significant full-length protein was visualized in the absence of crosslinker and when solubilized in SDS prior to crosslinking (Figure 3A lanes 1-2). Some CFTR smearing was also observed after cleavage with DTT, presumably due to persistent modification of CFTR lysine residues and/or non-specific aggregation. These findings provide independent evidence that *in vitro*-synthesized CFTR is bound to large non-covalent complexes that can be stabilized by chemical crosslinking. To determine which population of CFTR interacted with Sec61α, gradient fractions prepared with non-denaturing detergents were similarly crosslinked with DTSSP and immunoprecipitated with Sec61α antisera. Co-immunoprecipitated CFTR was then analyzed by SDS-PAGE and autoradiography after crosslinker cleavage (Figure 3B). These experiments confirmed that CFTR associates with Sec61α during early stages of its biogenesis and that complexes containing translocation machinery are recovered primarily at the bottom of the gradient.

CFTR complexes represent distinct steps of a maturation pathway. The RRL system faithfully reconstitutes early aspects of biogenesis. However, most CFTR is unable to

reach a mature conformation *in vitro* and remains sensitive to ER-associated degradation [121, 257]. We therefore used Xenopus oocytes to determine whether CFTR complexes observed *in vitro* were also formed *in vivo*. Oocytes have been widely used for CFTR synthesis and functional studies [123, 262]. In addition, we previously demonstrated that they efficiently process wild type CFTR (~90% efficiency) similar to that observed for native airway epithelia [130]. However, they recognize and degrade CFTR trafficking mutants [140] and therefore also maintain an intact ER quality control system.

Synthesis was initiated by coinjecting mRNA and [^{35}S] methionine to induce a rapid pulse of radiolabeled CFTR. Under standard conditions, incorporation of radiolabel into full length CFTR requires ~45-90 minutes, and little CFTR is trafficked out of the ER for 5-8 hours [140]. Solubilized oocyte membranes were analyzed on glycerol gradients, and CFTR was recovered by immunoprecipitation with N-terminus specific antisera. SDS solubilization again resulted in uniform sedimentation of ~160 kDa CFTR monomers (Figure 4, top panel), whereas non-denaturing detergents generated two distinct CFTR populations, a small heterogeneous complex that sedimented with an apparent mass of ~350 -800 kDa and a larger complex that pelleted through the gradient. The migration of these complexes was very similar to those observed *in vitro*.

To ensure that the cohort of CFTR recovered in the gradient pellet did not represent an off-pathway aggregate or degradation intermediate, *in vivo* pulse-chase metabolic labeling studies were carried out. These and subsequent experiments were performed using digitonin solubilization to better preserve CFTR interactions. At early time points after microinjection, greater than 95% of immunoreactive CFTR sedimented through the gradient (Figure 5A). Some of this material migrated as full-length protein (160 kDa) but most consisted of a mixture of polypeptides (60-150 kDa) representing partial-length nascent chains that were captured during intermediate stages of synthesis (Figure 5A,

lane 12). When oocytes were chased in unlabeled media prior to homogenization, these partial-length polypeptides were converted into full-length CFTR protein that was gradually released from the gradient pellet and recovered in fractions 4-8 (Figure 5A&B). Thus the large CFTR complex (in fraction 12) represents a true physiological intermediate in the CFTR maturation pathway. However, there appeared to be a significant delay in the release of full-length CFTR into the lighter gradient fractions, suggesting that this transition was temporally uncoupled from the completion of protein synthesis (discussed further below).

Similar gradient profiles were observed for both WT and ΔF508 CFTR (Figure 5D-F). Translational precursors of ΔF508 were recovered solely in the gradient pellet at early time points, and full-length protein was gradually released from this complex into fractions 4-8 during the three hour chase. At later time points than those examined here, less ΔF508 CFTR was recovered because the mutant protein is degraded via the ERAD pathway (Ref. [121] and data not shown). Since both proteins were able to undergo this release step with similar efficiency, subsequent experiments focused on WT protein.

Reconstitution of CFTR complex maturation ex vivo. Requirements for CFTR maturation were further examined using a hybrid *in vivo/ex vivo* expression system that allowed us to manipulate final conditions of CFTR synthesis. Following co-injection of mRNA and [^{35}S]methionine, oocytes were gently crushed by centrifugation, and translation of pre-programmed ribosomes was completed *ex vivo* in the collected oocytoplasm. By carefully controlling the time of homogenization, most immuno-reactive CFTR could be initially captured as partial-length translation intermediates (faint 80-150 kDa bands, better visualized in Figure 6B). These intermediates efficiently chased into full-length protein in both intact oocytes and isolated oocytoplasm (Figure 6A). Full-length CFTR generated in oocytoplasm did not result from de novo translation because it appeared

very quickly and because oocytoplasm was unable to efficiently initiate translation [263, and our unpublished observations]. To determine whether maturation of CFTR complexes was also completed *ex vivo*, membranes were collected at each time point (from oocytoplasm shown in panel A), solubilized and independently analyzed on glycerol gradients (Figure 6B). For each gradient, CFTR recovered in fractions 5-8 was pooled and compared to fractions 11-12. As we observed for intact oocytes, CFTR precursors (translation intermediates) were recovered exclusively in fractions 11-12 (Figure 6B, lanes 1&5). Full-length CFTR also initially appeared in these fractions and was then slowly and selectively released into fractions 5-8. At the end of the chase period, greater than 90% of CFTR precursors had completed synthesis, and nearly 70% of CFTR had been released into the smaller, more mature protein complex.

CFTR complexes recovered in gradient fractions 5-8 are too small to contain the ribosome-translocon machinery. This suggests that time dependent changes in migration reflect abrupt changes in protein-protein interactions that involve the release of nascent chains from early ER biosynthetic machinery. We therefore tested whether the transition of CFTR into the smaller complex would be mimicked by the aminoacyl-tRNA analog puromycin, which results in premature chain termination and cleavage of the peptidyl-tRNA bond. When oocytoplasm was incubated in the absence of puromycin, translation continued to generate full-length polypeptides that were selectively released into gradient fractions 5-8 (Figure 6C&D). Consistent with our hypothesis, puromycin inhibited protein synthesis and facilitated the premature release of both full-length and CFTR precursors out of the gradient pellet (Figure 6D).

CFTR complex maturation requires NTPs and cytosolic components. Nascent membrane proteins remain attached to the RTC during synthesis and are usually spontaneously released as the terminal peptidyl-tRNA bond is cleaved upon translation termination [9,

33, 36]. However, a significant proportion of full-length CFTR was consistently recovered at the bottom of the gradient (fractions 11-12), suggesting that the final stage of integration into the lipid bilayer did not occur immediately after translation was completed. Indeed, when oocyte membranes were resuspended in buffer containing puromycin, cyclohexamide and/or supplemental ATP/GTP, neither full-length nor partial-length CFTR polypeptides were released into the lighter gradient fractions (Figure 7A). However, when membranes were resuspended in oocytoplasm collected from uninjected oocytes, puromycin released the majority of CFTR-reactive polypeptides into the smaller complex (Figure 7B). While puromycin might have failed to catalyze peptidyl-tRNA cleavage due to conformational-specific ribosomal stalling, this seems unlikely because similar effects were observed for a relatively broad range of CFTR polypeptides (~100-160 kDa) in which the ribosome would be positioned on different portions of the mRNA. In addition, we and others have shown that puromycin efficiently cleaves peptidyl-tRNA bonds and releases polypeptides from ribosomes under the buffer conditions tested [41, 260].

It remained possible, however, that delayed release of so called "full-length" CFTR might be caused by translational stalling at or near the very end of the coding sequence. If so, then polypeptides near the end of synthesis would appear to migrate as full-length by SDS-PAGE but could remain tethered to the ribosome if the stop codon had not yet been reached. To rule out this possibility, oocyte membranes were isolated and incubated with cyclohexamide together with exogenous oocytoplasm and NTPs. Under these conditions, partial-length CFTR precursors remained in gradient fractions 11-12 (Figure 8A). Thus CFTR release cannot occur if the peptidyl-tRNA bond remains intact. When CFTR was homogenized at a slightly later time point to allow full-length CFTR to accumulate, only full-length polypeptides were selectively released into fractions 5-8 in the presence of ATP supplemented oocytoplasm but not in ATP-depleted oocytoplasm

(Figure 8B). Because protein synthesis was inhibited throughout the incubation, CFTR must have completed translation prior to homogenization. Yet these full-length polypeptides remained associated with ER biosynthetic machinery during membrane isolation and were released only upon further incubation. These results demonstrate that disassociation of CFTR from early ER biosynthetic machinery involves a novel maturation step that requires both energy and cytosolic components.

Conditions of RTC release are substrate specific. To determine whether requirements for RTC release were unique to CFTR, we examined several control proteins including a secretory protein (preprolactin, 26 kDa) and a small polytopic protein with six transmembrane segments (aquaporin-2, 29 kDa) and a related ABC transporter human P-glycoprotein (P-gp). Prolactin has been widely used as a model substrate to investigate nascent chain-translocon interactions *in vitro* and has been shown by crosslinking studies to spontaneously release from the translocon upon cleavage of the peptidyl-tRNA bond [26, 31, 195]. Consistent with this, greater than 95% of newly synthesized prolactin was released from the RTC at the earliest time points that gradient fractions could be visualized (30 min after injection) (Figure 9B). Similarly, ~90% of the transmembrane protein aquaporin-2 was also released from the RTC coincident with the completion of synthesis (Figure 9D). Because radiolabeled prolactin and aquaporin are only first detected 15-20 min after microinjection (Figure 9A,C, respectively), these newly synthesized proteins must be release from the RTC almost immediately after the completion of translation. Thus RTC interactions with simple secretory and transmembrane proteins differ substantially from those of CFTR.

P-gp is similar in size to CFTR (140 kDa) and like CFTR contains two six-spanning MSDs and two large cytosolic nucleotide binding domains [264]. It also contains three N-linked glycosylation sites that undergo carbohydrate processing and is efficiently

trafficked in oocytes with somewhat faster kinetics than CFTR (data not shown). We therefore expressed a myc-tagged P-gp construct in pulse-chase labeled oocytes to analyze RTC release. At early time points following injection, partial-length P-gp fragments were quantitatively recovered in fraction 12 as expected (Figure 10A, top panel). Full-length P-gp was also initially recovered in fraction 12 and fractions 4-8. After 90 min of chase, nearly all P-gp (full length and larger glycosylated species) were released from the RTC (Figure 10A middle panel). Therefore P-gp maturation resembles that of CFTR, although there appeared to be subtle differences. In contrast to CFTR most full-length P-gp was already released from the RTC when partial-length intermediates were still plainly visible (compare Figure 5A,B with Figure 10A). Consistent with this, we were unable to capture sufficient P-gp associated with the RTC for ex-vivo release assays, because the majority full-length protein was consistently released into the lighter fractions at early time points examined (Figure 10B). Taken together, these findings suggest that the rate of RTC release depends upon both the complexity of domain structure and unique properties of the substrate protein.

5. Discussion.

In this study, cell free and Xenopus expression systems were used to capture partial-length nascent CFTR polypeptides and examine the dynamic behavior of early protein complexes in the ER membrane. CFTR solubilization in non-denaturing detergents revealed that both partial- and full-length polypeptides are initially bound to a very large protein complex containing ER biosynthetic machinery. Following the completion of synthesis, CFTR was gradually released into a smaller (~600 kDa), ATP-dependent complex and continued to bind cellular chaperones. This transition represented a distinct step in the maturation pathway, occurred in a time dependent manner in Xenopus oocytes and isolated oocytoplasm, and required either the completion of protein synthesis or

premature cleavage of the peptidyl-tRNA bond. While we do not know the complete composition of the large protein complex, its size, sensitivity to puromycin and quantitative binding to partial-length translation intermediates strongly indicate that it contains the ribosome and ER translocon complex. Consistent with this, CFTR recovered in gradient pellets crosslinked and co-immunoprecipitated with Sec61α, the major component of the translocation channel. Surprisingly, release of full-length CFTR from the RTC both *in vivo* and *in vitro* did not occur spontaneously upon the completion of protein synthesis. Rather, this critical step required both NTPs and cytosolic components. Our results therefore identify a novel, energy-dependent step in the early CFTR maturation pathway that is required for newly synthesized polypeptide to be released from ER biosynthetic machinery.

CFTR folding begins cotranslationally, while the nascent polypeptide is bound to the RTC [15, 105, 238, 265]. The ribosome and Sec61 translocon play a critical role in these early stages of folding by translocating polypeptide into the ER lumen, orienting peptide loops into the cytosol, and integrating TM segments into the lipid bilayer (reviewed in, [26, 176, 261]). During this process, cytosolic domains must be localized near the interface between the translocon and the membrane-bound 60S ribosomal subunit [26, 66, 266, 267]. Given the limited space available, it is unlikely that final steps of CFTR folding and domain-domain association could be completed until TM segments are released laterally from the translocon into the ER membrane. In this regard, TM segments from some bitopic proteins passively partition into the ER membrane during translation [10, 14], whereas others can remain within the translocon for significant periods of time [33, 36, 268]. In the latter case, integration is proposed to be triggered upon translation termination and/or cleavage of the peptidyl-tRNA bond as evidenced by

rapid loss of contact with translocon components, [9, 33, 36, 42, 195]. For polytopic proteins, integration patterns are more complex, and TM segments can integrate into the membrane individually [269], in pairs [54, 194] or in groups [55, 100]. However, it has generally been assumed that nascent polypeptides are spontaneously released from the RTC into the lipid bilayer once the peptidyl-tRNA bond is severed [26].

We now show that for CFTR, RTC release is temporally dissociated from the completion of protein synthesis and is subject to regulatory (energy dependent) influences. Thus our results raise new questions regarding how and where such polypeptides might persistently interact with RTC components. Recent crosslinking studies have indicated that TM segments, including those from polytopic proteins, occupy and move through specific environments within the translocon during membrane integration [36, 56, 74, 198]. Detailed analysis of AQP4 integration has further shown that the translocon can accommodate multiple TMs simultaneously, suggesting that early tertiary folding of transmembrane domains could begin place in the immediate vicinity of Sec61α [74]. It is therefore plausible that final integration of polytopic proteins might require formation of a stable structure within the membrane. In this regard, CFTR contains an unusual number of charged residues in its TM segments (4 Arg, 2 Lys, 3 Glu, 1 Asp, and 1 His) that play important functional roles and might influence the stability of isolated TM segments within the lipid bilayer [231, 270, 271]. Indeed, preliminary studies from our group have demonstrated that certain individual TM segments continue to crosslink Sec61α even after puromycin release (D. Pitonzo and W. Skach, unpublished

observations). Alternatively, regions of CFTR might also remain associated with peripheral translocon components such as ribophorin I as was recently demonstrated for fragments of the amyloid precursor protein and opsin [75].

It is difficult to explain a direct role for NTPs in TM segment integration because no core translocon components have been demonstrated to bind or hydrolyze nucleotides. On the other hand, ATP plays a key role in the function of several chaperones implicated in CFTR folding [119, 127, 242, 245]. The ATP dependence observed here raises the possibility that RTC release might be coordinated or perhaps influenced by the folding of cytosolic domains or perhaps initiation of domain-domain interactions. Limited proteolysis experiments have revealed that ATP is required to convert CFTR into a mature structure prior to exit from the ER [119, 235]. Our data demonstrate that Hsc70 is cotranslationally recruited to CFTR while the nascent chain is still attached to the RTC and continues to bind after RTC release. Thus maturation that occurs within the RTC likely represents early stages of folding that take place before a mature, trafficking-competent structure is acquired. This is supported by our results that ΔF508 CFTR is released from the RTC to nearly the same extent as WT protein even though it fails to mature and is ultimately subject to ERAD [140]. Similar results have been reported in mammalian cells in which solubilized WT and ΔF508 CFTR are both found in a heterogeneous smaller complex similar to that observed here, but only WT is able to complete the maturation process [239]. Taken together, the maturation step required for RTC release appears to occur before the structural change required for CFTR intracellular trafficking [235]. CFTR therefore undergoes at least 2 separate energy-dependent steps

as it matures in the ER compartment. Understanding how these two processes are related represents an important area for CF and other disorders of membrane protein folding.

It has been particularly difficult to examine RTC-nascent chain interactions in mammalian cells because they are transient and highly dependent on the rate of protein synthesis, stability of interactions, and rate of RTC release. Xenopus oocytes provide a distinct advantage in this regard. They have been widely used for heterologous expression studies [123, 262, 272] and efficiently process CFTR at levels similar to those observed in native epithelial cells [130]. Moreover, their reduced rate of protein synthesis at physiological temperatures allowed us to identify transient populations of full- and partial-length nascent CFTR polypeptides prior to RTC release. Importantly, oocyte RTCs do not indiscriminately exhibit prolonged interactions with substrates. Simple secretory and transmembrane control proteins were released at a rate too fast to be detected. In contrast, partial- and full-length intermediates of human P-glycoprotein (P-gp) were released only slightly faster than CFTR. Unfortunately, we were unable to determine whether P-gp release from the RTC also required ATP and cytosol [264] because insufficient full-length protein remained associated with RTCs during the post-homogenization studies. Because P-gp and CFTR exhibit a similar size, domain architecture and topological profile, it is likely that RTC interactions are influenced by both the complexity of domain organization as well as key features of the CFTR folding pathway. Given the diversity of native membrane proteins and the high degree of conservation in biosynthetic machinery, it is likely that the biogenesis requirements observed here for CFTR will also apply to other substrates and expression systems.

Acknowledgments.

The Authors thank Dr. W. Welch and K. Matlack for providing Hsc/Hsp70 and Sec61α antisera, respectively, and J. Eledge for excellent technical assistance. This work was supported by the Cystic Fibrosis Foundation Therapeutics Inc. and by the National Institutes of Health, DK51818 and GM53457 (W.R.S.) and T32 DK07674 (J.O.).

Fig. 4-1

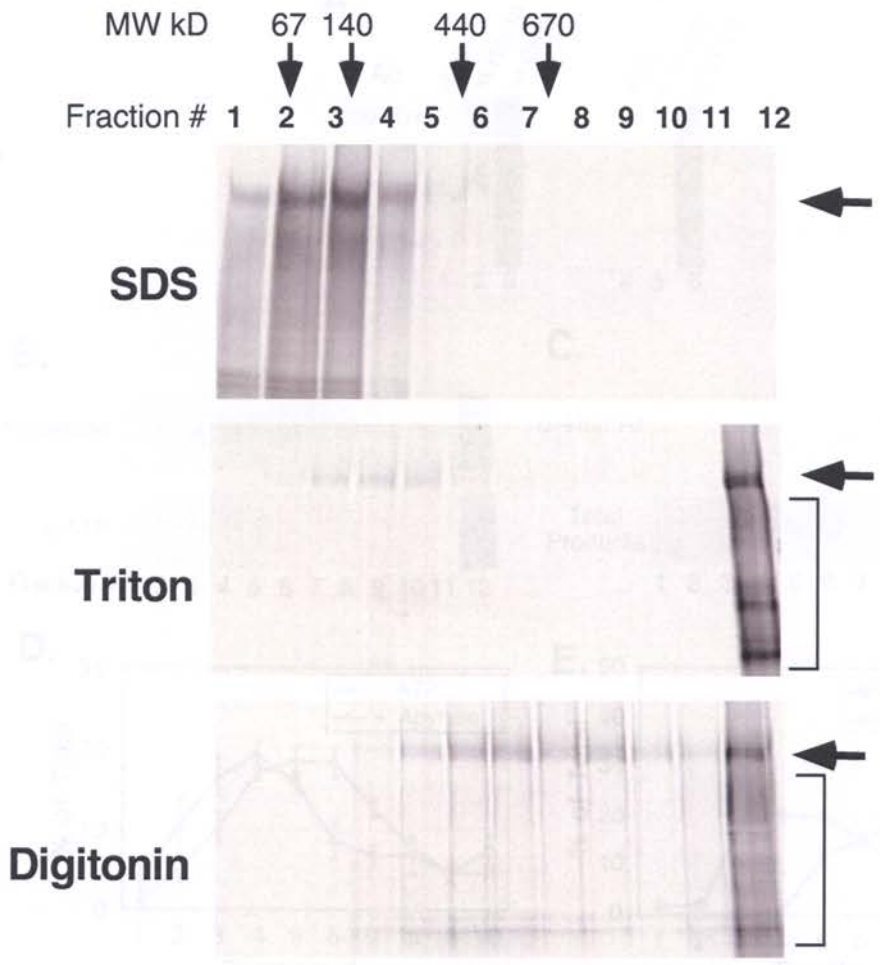

Figure 4-1: *Nascent CFTR binds to large protein complexes in vitro.* Microsomal membranes containing *in vitro* translated CFTR were solubilized in SDS (**A**), Triton (**B**) or digitonin (**C**) and centrifuged through a glycerol gradient as described in Methods. Gradient fractions top-to-bottom were collected and analyzed by SDS PAGE. Migration of MW standards are indicated above autoradiograms (downward arrows). Location of full-length CFTR (horizontal arrow) and partial-length translation products (brackets) are indicated on the right.

Fig. 4-2

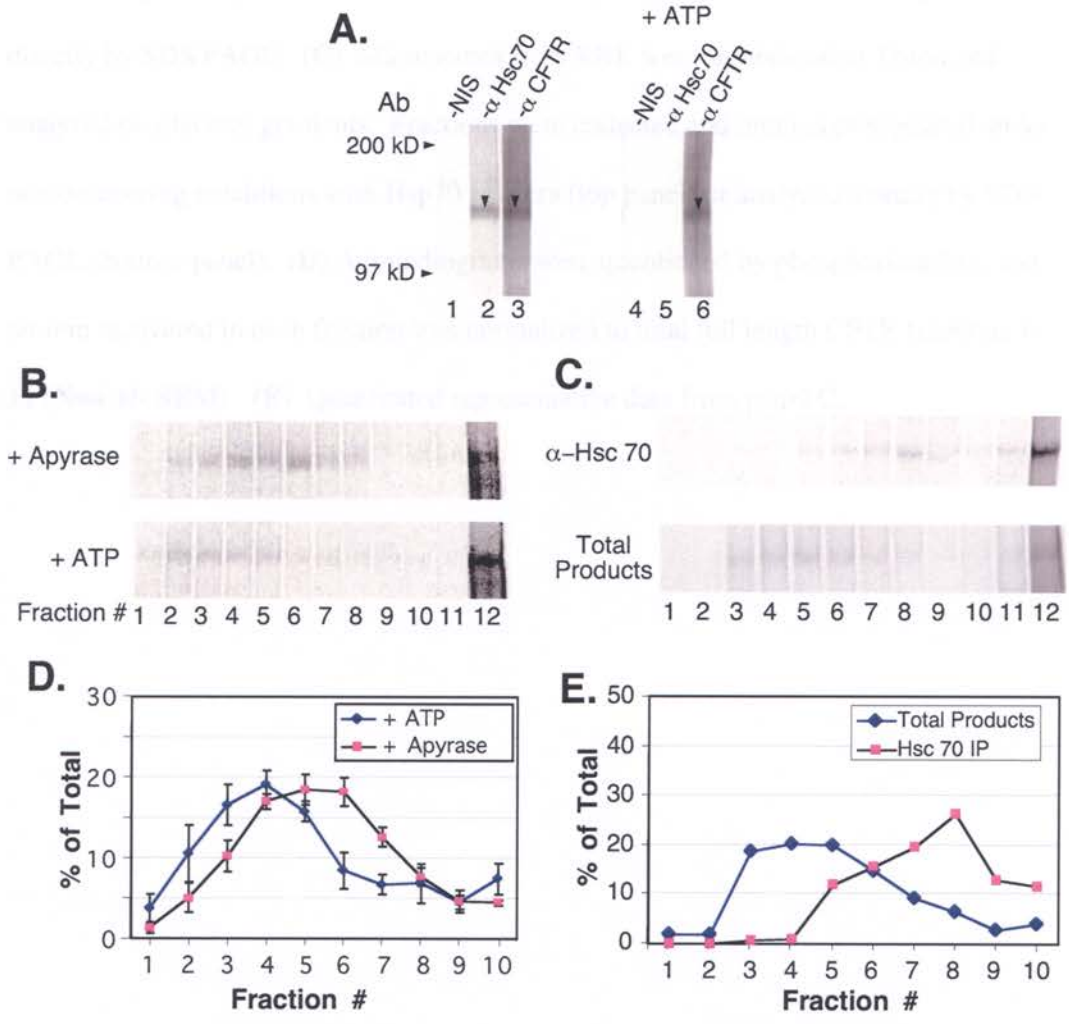

Figure 4-2. *CFTR complexes are ATP sensitive and contain Hsc70.* **(A)** Microsomes containing *in vitro* translated CFTR were pelleted through a sucrose cushion in the presence or absence of ATP as indicated. Membranes were solubilized in Triton and immunoprecipitated with non-immune sera (NIS), Hsc70 antisera, or CFTR antisera [121] and analyzed by SDS PAGE and autoradiography. **(B)** RRL translation mixtures were incubated with apyrase (0.1 u/μl) or ATP (3 mM) for 10 min prior to microsome

pelleting, Triton solubilization and glycerol gradient centrifugation. Where indicated, buffers for pelleting also contained added ATP. Gradient fractions were analyzed directly by SDS PAGE. **(C)** Microsomes from RRL were solubilized in Triton and analyzed on glycerol gradients. Fractions were collected and immunoprecipitated under non-denaturing conditions with Hsp70 antisera (top panel) or analyzed directly by SDS-PAGE (bottom panel). **(D)** Autoradiograms were quantitated by phosphorimaging, and protein recovered in each fraction was normalized to total full length CFTR fractions 1-11 **(N=4 +/- SEM)**. **(E)** Quantitated representative data from panel C.

Fig. 4-3

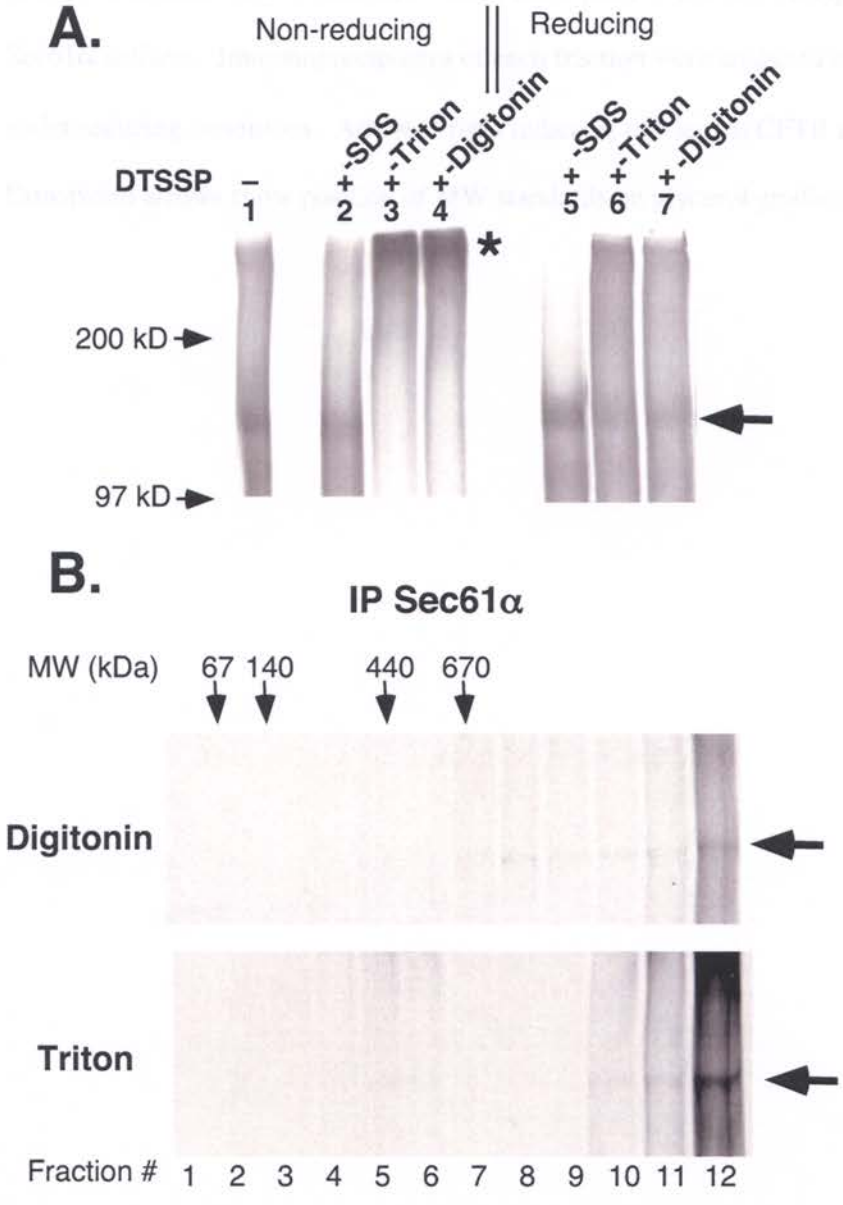

Figure 4-3. *CFTR crosslinking to Sec61α.* **(A)** *In vitro*-translated CFTR was subjected to DTSSP crosslinking after solubilization in the indicated detergent and analyzed under

non-reducing (lanes 1-4) or reducing (lanes 5-7) conditions. (*) indicates DTSSP-dependent CFTR complexes. **(B)** CFTR gradients were prepared as in Figure 1 and gradient fractions were crosslinked with DTSSP prior to immunoprecipitation with Sec61α antisera. Immunoprecipitates of each fraction were analyzed by SDS-PAGE under reducing conditions. Arrow at right indicates full-length CFTR translation product. Downward arrows show position of MW standards on glycerol gradients.

Fig. 4-4

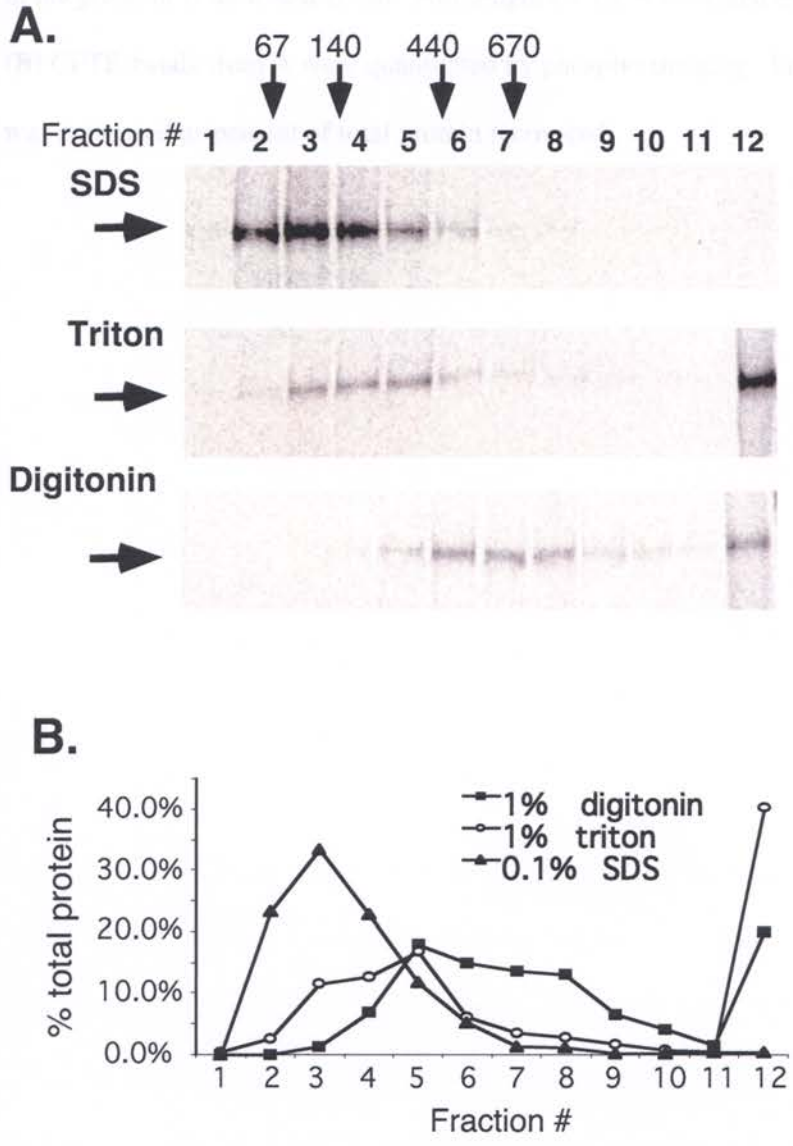

Figure 4-4. *Formation of CFTR-protein complexes in vivo.* **(A)** CFTR mRNA and [^{35}S] methionine were coinjected into in *Xenopus laevis* oocytes. Membranes were collected, solubilized in the detergent indicated and analyzed by glycerol gradient centrifugation as

in Figure 1. Each fraction was denatured in SDS, immunoprecipitated with CFTR antisera and analyzed by SDS-PAGE and autoradiography. Migration of MW standards in the gradient is indicated at top. Full-length CFTR is indicated by horizontal arrows. **(B)** CFTR bands from A were quantitated by phosphorimaging. Protein in each fraction was expressed as percent of total protein recovered.

Fig. 4-5

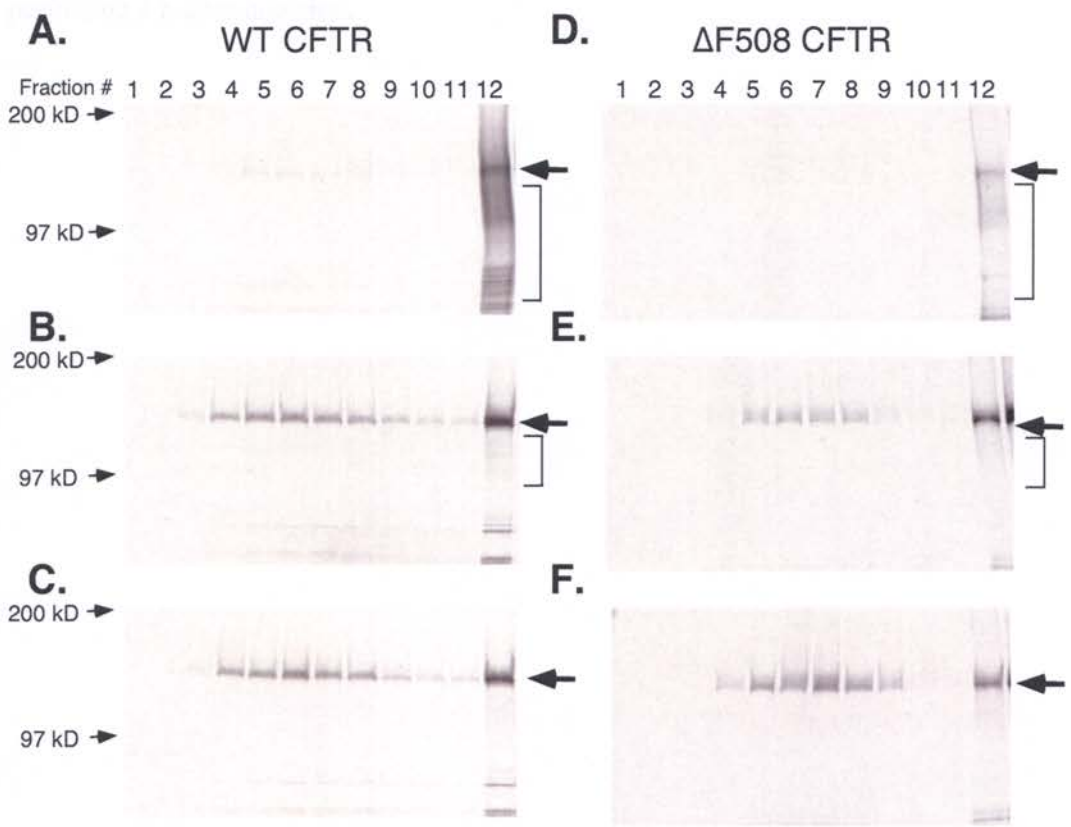

Figure 4-5. *CFTR complexes are dynamic.* **(A-C)** Oocytes expressing WT CFTR were incubated at 17°C for 1.5 hours and chased in media containing 1 mM unlabeled methionine. Membranes were collected **(A)** 1.5 h, **(B)** 3 h and **(C)** 4.5 h after injection, solubilized in digitonin and subjected to glycerol gradient centrifugation as in Figure 4. Migration of full-length CFTR (horizontal arrow) and partial-length CFTR intermediates (bracket) are indicated on the right. During the incubation period, translation intermediates chase into full-length protein, and full-length protein is released from fraction 12 into fractions 4-8. **(D-F)** Oocytes expressing ΔF508 CFTR were injected and

processed as in panels A-C except that the initial homogenization (panel D) was performed 1 h after injection.

Fig. 4-6

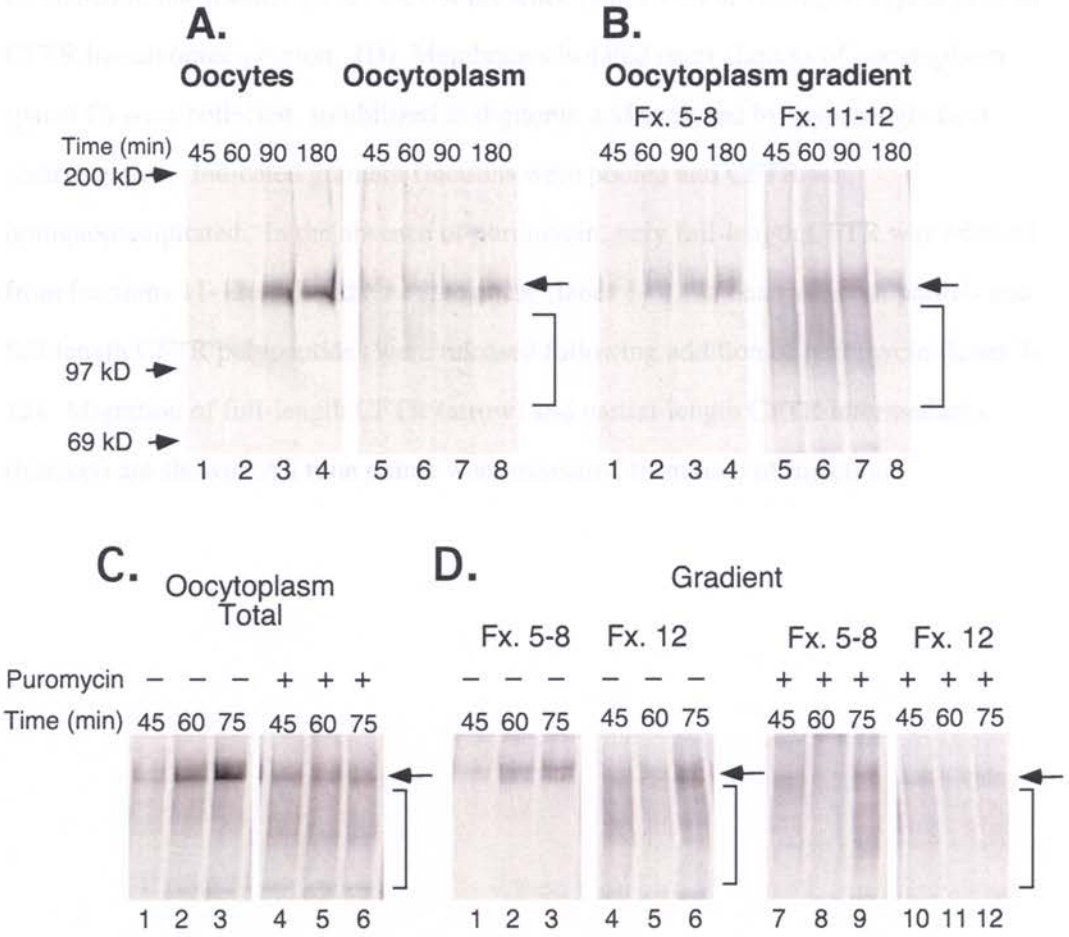

Figure 4-6. *Ex vivo CFTR complex maturation.* **(A)** Microinjected oocytes were incubated for 45 min and chased in unlabeled methionine (lanes 1-4), or crushed by centrifugation to generate oocytoplasm (lanes 5-8). At times indicated (after injection) homogenates were immunoprecipitated with CFTR antisera and analyzed by SDS-PAGE and autoradiography. **(B)** Pelleted membranes from oocytoplasm (obtained from panel A) were solubilized in digitonin and subjected to glycerol gradient centrifugation as in

Figure 5. Fractions 5-8 and 11-12 were pooled prior to immunoprecipitation. (**C**) Oocytoplasm was prepared from crushed oocytes 45 min after microinjection and incubated in the absence (lanes 1-3) or presence (lanes 4-6) of 1mM puromycin prior to CFTR immunoprecipitation. (**D**) Membranes isolated from aliquots of oocytoplasm (panel C) were collected, solubilized in digitonin and analyzed by glycerol gradient centrifugation. Indicated gradient fractions were pooled and CFTR was immunoprecipitated. In the absence of puromycin, only full-length CFTR was released from fractions 11-12 during the *ex vivo* chase (lanes 1-6). In contrast, both partial- and full-length CFTR polypeptides were released following addition of puromycin (lanes 7-12). Migration of full-length CFTR (arrow) and partial-length CFTR intermediates (bracket) are shown. All time points were measured from time of injection.

Fig. 4-7

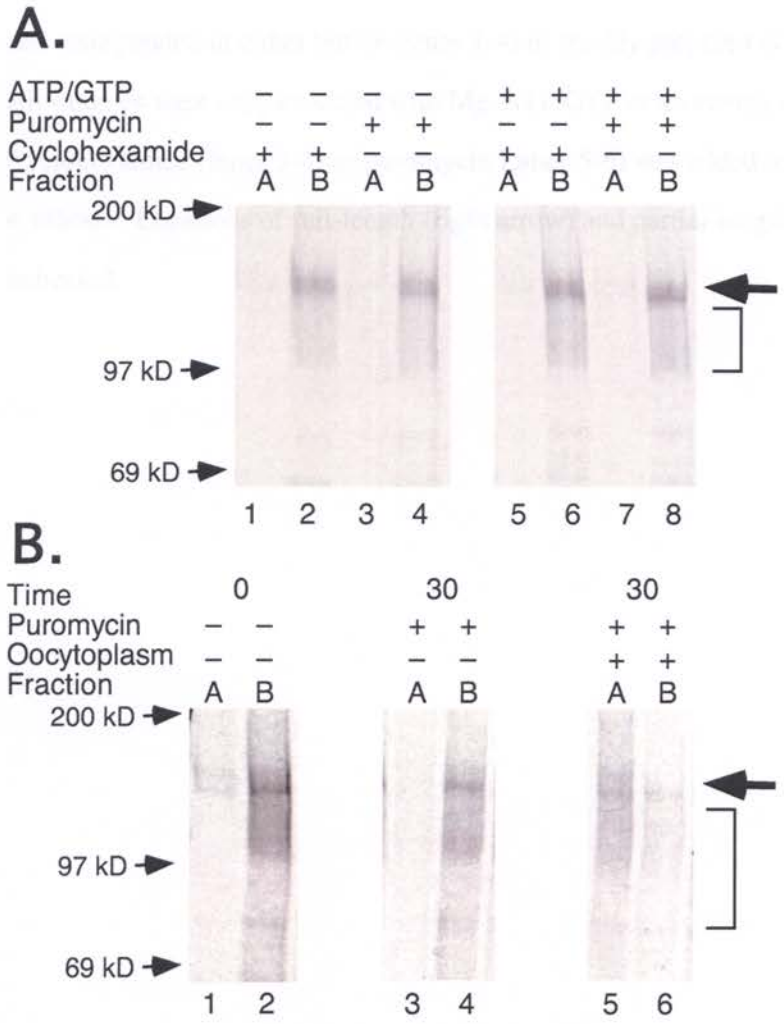

Figure 4-7. *CFTR release from the RTC is cytosol dependent.* **(A)** Oocytes were homogenized 1 hour after RNA injection, and membranes were pelleted, resuspended in buffer and supplemented with cyclohexamide (lanes 1-2, 5-6), puromycin (lanes 3-4, 7-8) and MgATP/GTP (lanes 5-8). Incubation was carried out at 17° C for an additional 30 min, and membranes were repelleted, solubilized in digitonin and subjected to glycerol

gradient centrifugation. Fractions 5-8 (A) and 11-12 (B) were pooled and immunoprecipitated as in Figure 6. (**B**) Oocyte membranes were collected as in panel A and resuspended in either buffer (lanes 1-4) or freshly prepared oocytoplasm (lanes 5-6). All samples were supplemented with Mg-ATP/GTP or an energy regenerating system. Cyclohexamide (lanes 3-4) or puromycin Lanes 5-6) was added to block protein synthesis. Locations of full-length (right arrow) and partial-length (bracket) CFTR are indicated.

Fig. 4-8

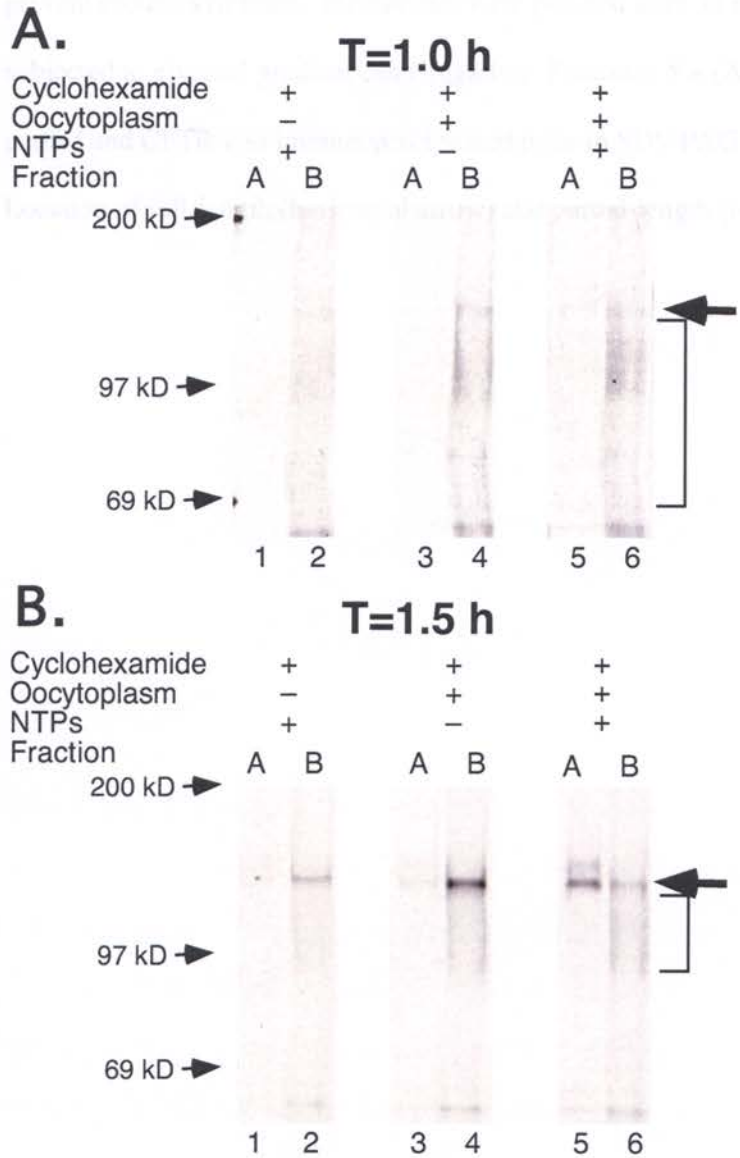

Figure 4-8. *CFTR release from the RTC requires cytosol and NTPs but not protein synthesis*. Oocytes were homogenized 1 h (**A**) or 1.5 h (**B**) after RNA microinjection. Membranes were collected and incubated in buffer supplemented with 1 mM ATP/GTP

(lanes 1-2), in freshly prepared oocytoplasm treated with apyrase (lanes 3-4) or with an ATP regeneration system (lanes 5-6). Cyclohexamide was present in all samples to prevent protein synthesis. Membranes were pelleted after 30 min, solubilized and subjected to glycerol gradient centrifugation. Fractions 5-8 (A) and 11-12 (B) were pooled and CFTR was immunoprecipitated prior to SDS-PAGE and autoradiography. Location of full-length (horizontal arrow) and partial-length (bracket) CFTR is shown

Fig. 4-9

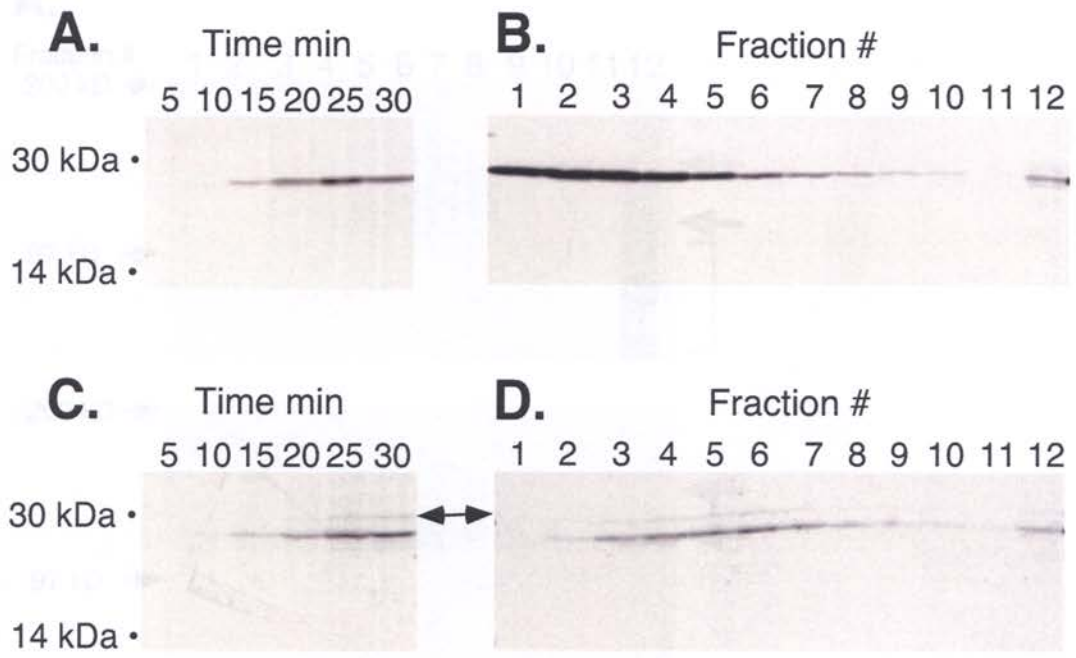

Figure 4-9. *RTC release of secretory and TM control proteins.* **(A)** Oocytes were co-injected with preprolactin mRNA and [^{35}S] Methionine and homogenized at times indicated. Radiolabeled prolactin was recovered by immunoprecipitation and analyzed by SDS-PAGE and autoradiography. **(B)** Oocytes were injected as in panel A, and membranes were collected after 30 minutes and analyzed on glycerol gradients as in Figure 5. Gradient fractions were immunoprecipitated with prolactin antisera. **(C)** Myc-tagged AQP2 mRNA was expressed in oocytes as in panel A and AQP-2 was recovered at times indicated myc monoclonal antibody (9E10). **(D)** Oocytes expressing myc-AQP2 were processed and analyzed on glycerol gradients 30 min after injection as in panel B. Minor band of glycosylated AQP2 is indicated (arrow).

Fig. 4-10

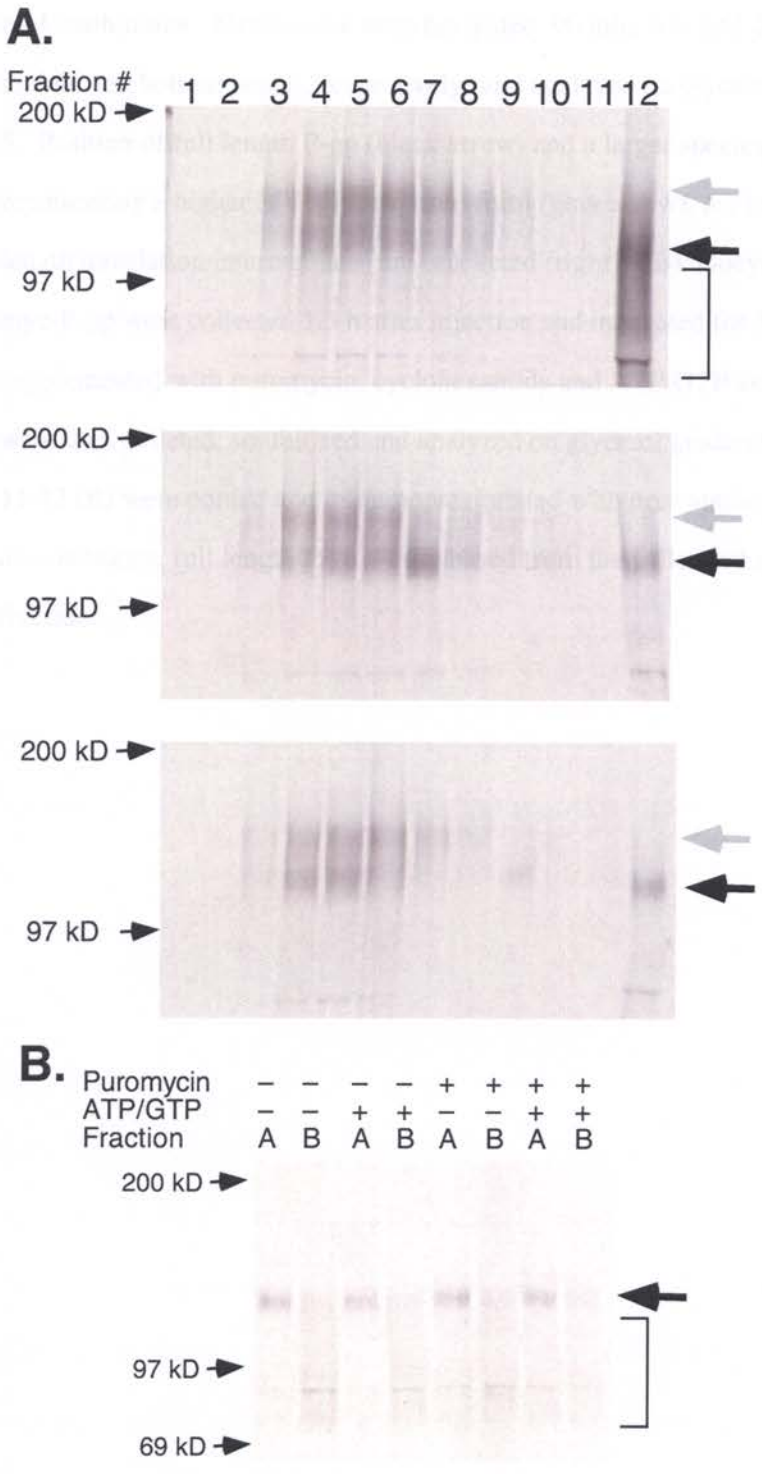
A.
Fraction #
1 2 3 4 5 6 7 8 9 10 11 12
200 kD
97 kD
200 kD
97 kD
200 kD
97 kD
B.
Puromycin – – – – + + + +
ATP/GTP – – + + – – + +
Fraction A B A B A B A B
200 kD
97 kD
69 kD

Figure 4-10. *P-glycoprotein release from the RTC.* (**A**) Oocytes expressing myc-tagged human P-glycoprotein were labeled for 1.5 hour and then chased in media containing 1 mM methionine. Membranes were harvested 90 min, 3 h, and 4.5 h after injection (top, middle and bottom panels, respectively) and analyzed on glycerol gradients as in Figure 5. Position of full length P-gp (black arrow) and a larger species, presumably representing a higher MW glycosylated form (gray arrow), are indicated on right. Partial length translation intermediates are bracketed (right). (**B**) Oocyte membranes containing myc-P-gp were collected 1.5 h after injection and incubated for 30 min in buffer supplemented with puromycin, cyclohexamide and ATP/GTP as indicated. Membranes were then pelleted, solubilized and analyzed on glycerol gradients. Fractions 5-8 (A) and 11-12 (B) were pooled and immunoprecipitated with myc antibody as in Figure 7. Under all conditions, full length P-gp was released from the pellet and recovered in lighter fractions.

IV) Summary and Future Directions

A) Summary

The studies presented in this dissertation focus on interactions of nascent membrane proteins with sec61α. The role of sec61 in the integration process has been debated as either a passive conduit or active regulator. This has fundamental consequences in determining the basic mechanisms of membrane protein folding. The most widely cited, extant hypothesis is the 2 step folding model of Popot and Engelmann [7, 8] which states that individual TMs are first stably integrated into lipid and then pack to acquire tertiary structure. Such a model would require that TMs are released from the translocon in an orderly and sequential manner, as has been suggested in simple models of co-translational integration. Alternatively, accumulating evidence now suggests that TM segments do not always possess properties that permit independent partitioning into lipid, thus necessitating interaction with other more stable TMs [14, 15, 33, 54, 74, 273]. This suggests that a simple sequential model of integration is not adequate to explain the variety of integration mechanisms used by native polytopic proteins.

Manuscript 2

To better define parameters that specify integration mechanisms, we initially chose a native substrate that was not only integrated co-translationally but possessed TMs that had previously been shown to independently direct topology [98]. Manuscript 2 resulted in several important findings:1) TMs enter a primary sec61 binding site upon exiting the ribosome and are displaced from this site by the arrival of the next TM. This is consistent with entry into a lateral "gate" [48]. Another study performed on a 3-TM truncation of

bovine opsin, however, suggested that TM3 can depart sec61 independently [274]. The specific behavior of TMs therefore is structure and context dependent. 2) TMs can occupy more than one molecular environment proximal to sec61 at progressive stages of synthesis. This implies that TMs do not always passively partition into lipid as has been suggested [14] but that integration is facilitated by higher order translocon interactions. Interestingly, in the case of AQP4 this multi-modal interaction pattern is limited to signal anchor sequences (see manuscript 2, figure 5 – TMs 1, 3, 5). 3) Several AQP4 TMs (TMs 1,3,4 and 5) accumulate within or closely adjacent to sec61 prior to integration. This implies that, even for co-translationally integrated polytopic proteins, mechanisms of integration are more complex than previously proposed. 4) Accumulated TMs can exit the translocon *en bloc* (i.e. crosslinking to TMs 1,3,4 and 5, manuscript 2, figure 5, truncation 216). One possibility is that these TMs may acquire preliminary tertiary structure while still in a translocon-proximal environment and integrate as a unit. While studies have shown that TMs can contact lipids when still near sec61 [9, 10, 36] TMs that span the bilayer can still be extracted at alkaline pH [54] or by urea [72] showing that, prior to leaving sec61, stable integration has not yet occurred. Taken together, these results indicate that the two-step folding model may not apply to all proteins and that TM-TM helical interactions, helical packing and formation of tertiary structure can be initiated in a proteinaceous rather than a strictly lipid environment. Such a finding has major implications for forces that drive early protein folding.

An interesting question that arises from our study concerns the location of secondary and tertiary interaction sites. The M. jannischii crystal structure of secYEβ (sec61αβγ

homolog) suggests that a putative lateral "gate" could accommodate perhaps one TM. If this structure represents a complete, functional translocation channel, as has been proposed, then TM-sec61 interactions likely occur outside of the pore itself but within the larger confines of the fully assembled translocon. The location of TM-sec61 interaction sites within the oligomeric translocon assembly remains an unknown but critically important question. A number of models have been put forth to explain how oligomeric sec61 assemblies are constructed [49, 50]. Our model (manuscript 1, figure 7) requires that lateral TM exit gates in adjacent sec61 heterotrimers face each other to create a single, much larger translocation/integration pathway.

Manuscript 3

CFTR is a complex polytopic protein that contains 11 potentially charged residues within the confines of its putative TM boundaries. Many of these residues are essential for function and/or tertiary stability. One of these residues, aspartate 924 near the putative center of CFTR TM8 causes an independent TM8 sequence to be translocated rather than integrated [15]. In a native context, TM8 requires the presence of TM7 to effect stop transfer. I asked if this polar residue resulted in an alternate mechanism of integration vis à vis its sec61 interactions.

The aspartate residue caused a unique pattern of sec61 interactions, as determined by photocrosslinking, the hallmark of which was continued sec61 proximity after puromycin cleavage of the peptidyl-tRNA bond. Puromycin treatment presumptively results in release of the nascent chain from the ribosome. Persistent interaction of a transmembrane

segment with sec61 after nascent chain release from the ribosome has never before been demonstrated. I therefore embarked upon a detailed examination of this phenomenon, the results of which are described in manuscript 3. Briefly, after ensuring that persistent crosslinking was not due to inadequate peptidyl-tRNA cleavage or to engagement by OST, I determined that the post-release interaction was dependent upon an intact RTC and the polar aspartate residue. Replacement of the aspartate with valine eliminated the interaction while replacement with glutamate restored it. Interestingly, persistent crosslinking after peptidyl t-RNA cleavage was time and energy dependent; most of the nascent chain was released into the bilayer over 30-60 minutes and release was delayed by the depletion of ATP with apyrase.

CFTR TM8 retains proximity to sec61 over at least 70 amino acids of synthesis and, like AQP4 TMs 1, 3 and 5, appears to reside in multiple environments. Surprisingly, persistent crosslinking after peptidyl-tRNA cleavage also manifests in at least two independent environments (truncations 967-997 and 1007-1017 – Fig. 3-2).

I conclude from this study that certain TM interactions with the translocon can be prolonged, persistent and dependent upon specific residues in the nascent chain sequence. A further implication is that membrane proteins can be retained by the translocon after the completion of synthesis. It is unclear, however, how translocon retention contributes to the cooperative stop transfer function of CFTR TM7-8 [15]. This should be a subject for future study. The inability of native TM8 to spontaneously integrate upon peptidyl tRNA cleavage, as well as the energy dependence of nascent chain release from sec61

suggest an active role for sec61 in the integration of certain polytopic proteins. It should be noted that in the final CFTR folded structure, D924 forms a stabilizing salt bridge with R347 in TMD1-TM6. Inherited mutations of residue 924, while rare, cause a clinical CF phenotype. Interestingly, the novel biogenesis step required by the presence of CFTR-D924 is reminiscent of polar residues in AQP1 that necessitate a unique post-translational rotation of TM3 [Daniel, et al, 2008, manuscript submitted]. Mutation of those residues can restore co-translational topology acquisition but will adversely affect water permeation [102]. As protein-family isoforms obtain new functions through evolutionary mutation of specific residues, the biogenesis machinery must co-evolve to acquire the flexibility to facilitate integration.

Manuscript 4

My last set of in vitro studies was as second author of manuscript 4. I performed all in vitro experiments for this study. We asked whether full length CFTR was released into the membrane following the completion of synthesis. Briefly, we found, using velocity centrifugation gradients, that release from the RTC was significantly delayed, but was facilitated by energy and cytosolic factors. Additionally, we found that nascent full length CFTR associated with large molecular weight complexes that included both sec61 and the cytosolic chaperone Hsc70. Solubilization in SDS, Triton X-100 and digitonin demonstrated that complex stability was sensitive to detergent conditions. Non-ionic detergents allowed the preservation of larger molecular weight complexes including the persistent CFTR-RTC association.

Addition of ATP to solubilized translation products prior to gradient centrifugation demonstrated a reproduceable ~200kD decrease in complex size when compared to incubation with apyrase. Co-immunoprecipitation of CFTR-containing complexes with Hsc70 antibody revealed that higher molecular weight complexes, including the gradient pellet, contained Hsc70. We concluded that Hsc70 bound to CFTR cytosolic domains prior to release from the RTC and that Hsc70 remained bound to a subset of CFTR molecules following release from the RTC.

Identification of sec61 containing complexes was performed by chemically crosslinking gradient fractions with the reducible, homobifunctional agent 3,3 dithio-bis(sulfosuccimidylpropionate) (DTSSP) subsequent to native solubilization but prior to gradient fractionation. Fractions were then immunprecipitated with sec61α antibody. Full length CFTR-sec61 complexes were found primarily in the RTC-containing pellet following immunopurification. I concluded that full length CFTR molecules remained bound to RTCs following the completion of synthesis.

Conclusion

My studies of early biogenesis of two polytopic substrates demonstrate that each uses distinctly different integration strategies, implying that sec61α can mechanistically control release of TMs from the translocon. Further, the release strategy for a given TM is strikingly sequence specific. TM segments can accumulate within a translocon-proximal environment even in relatively simple, co-translationally integrated proteins.

Therefore, the two-stage membrane protein folding model of Popot and Engelmann likely needs revision for many substrates.

Further, integration can be delayed until after the completion of synthesis suggesting a role for sec61 beyond that of passive conduit. Binding of nascent chains to both the RTC and Hsc70 simultaneously suggests multi-domain chaperoning; Hsc70 in the cytosol and sec61α in the membrane. It has also previously been shown that the ER chaperone calnexin interacts with CFTR lumenal domains [275]. Unfortunately, detailed lipid-containing architectural models of the translocon are unavailable which makes it difficult to determine exactly where TMs reside prior to integration. We suggest that nascent chains may interact within the center of a tetrameric sec61 translocon complex to facilitate early protein-lipid contacts and to allow the nascent protein to sample multiple folding states. This implies a front-to-front lateral gate arrangement of sec61 molecules (manucript 1 figure 7d).

B.) Future Directions

Will AQP4 TMs depart the primary sec61 interaction site on their own when not followed by the next TM? We showed that initial AQP4-sec61α interactions were disrupted by the arrival of the next TM. Other studies have suggested that, perhaps, TMs can leave sec61α prior to the arrival of the next TM [274]. This could be examined by doubling or tripling the loop between TMs 1 and 2 to see if TM1 will leave on its own or whether departure from sec61α is delayed. It is important that sequence variations not be introduced

because the role of flanking TM sequence in disengagement from the primary sec61 binding site is unknown.

Will TM6 leave the translocon prior to the termination of synthesis? Doubling the C-terminal cytosolic domain (75 aa) Should determine whether residue G214 can depart the translocon prior to the end of synthesis or if termination of synthesis is required.

Does AQP4 interact with more than one sec61 heterotrimer during synthesis? This is arguably one of the most important questions in the biology of translocon architecture/function. Numerous studies have shown evidence for oligomeric assembly of sec61 heterotrimers in the translocon [44, 45, 47, 49, 50, 64, 214] although a study in prokaryotic secY suggests that only one secY of the oligomeric assembly forms the active translocating pore [60]. This question might best be addressed by simultaneously using AQP4 probe sites at L148 (TM4) and S174 (TM5) at a truncation of 216 aa residues (see manuscript 2, Fig. 4). Our study suggests that both TMs enter sec61 simultaneously yet the X-ray crystal structure of secY suggests a lateral passageway that could accomodate only one TM. At truncation 216, both of the above residues crosslink with reasonable efficiency; perhaps enough that a mobility shift suggesting a double crosslink could be seen. These photoadducts would need to be immunoprecipitated with antibodies to sec61α, TRAM and TRAPα since all run with similar electrophoretic mobility. A double sec61α crosslink would constitute a remarkable finding, as concomitant engagement of two sec61 channels by the same nascent chain has not yet been demonstrated. One potential question is whether the length of nascent chain (9aa -

~30Å) between TM4-5 is long enough to span two sec61 molecules. Another option is to use probes at either L28 (TM1) or I105 (TM3) and at L148 (TM4) which all are in proximity to a sec61α molecule at the 216 aa truncation.

When and where do TM3 and TM5 rotate to acquire native topology? TM3 and TM5 are type II signal anchors which must rotate to translocate their C-termini. In the case of AQP1 this is a relatively late event in topogenesis, as discussed in the introduction and in manuscript 1 [98, 100]. In AQP4, topology is acquired co-translationally as determined by N-linked glycosylation assays and by proteinase protection (manuscript 1 Fig. 1 b, d). Further, when AQP4 is truncated at residue 144 before complete synthesis of TM4, and released with puromycin, an N-linked glycosylation site in ICL2 is utilized by OST, indicating early TM3 rotation (see data not shown). TM4 enters sec61 just prior to TM5, and both TMs exhibit maximal crosslinking at the same truncation. Due to the short 9 amino acid loop between the two TMs they likely form a helical hairpin, implying early rotation for TM5 as well. This is confirmed by proteinase protection of a TM5-C-terminal reporter domain (manuscript 2, Fig.1d).

If type II signal anchor rotation occurs between the ribosome and sec61, a significant gap must be present immediately before the TM C-terminus is translocated, leading to potential mixing of cytosolic and lumenal compartments. A gap between the ribosome and translocon is seen in many structural studies using detergent solubilized membranes (see Introduction). A narrow translocon aqueous pore [48] could be occluded by the translocating chain preserving compartmental integrity. Alternatively, a tight ribosome

translocon seal would imply that rotation occurs within sec61, consistent with a large pore diameter as determined by fluorescence quenching studies [51]. This could be studied by placing quenchable probes within the flanking sequences N- or C-terminal to TM3 (or TM5). If a RTC gap is present, an N-terminal probe should be quenchable from the cytosol. If rotation occurs in the cytosol, probes at either end should be quenchable. If a tight ribosome junction forms early, neither probe should be quenchable. If a tight junction forms as TM3 enters, a C-terminal probe should only be quenchable from the lumen. An N-terminal probe may or may not be quenchable depending upon the diameter of the translocon pore.

Do all stop transfer sequences have a limited interaction with sec61? In our AQP4 study (manuscript 2), only signal anchors showed secondary and tertiary crosslinks to sec61α. Crosslinking studies should be done on other substrates to see if this pattern is consistent. Aprevious study of bovine opsin demonstrated that some TMs possess both signal sequence and stop transfer character [193]. Additionally a study of the asialoglycoprotein receptor showed that the same TM could function as signal sequence or stop transfer depending on order of presentation to sec61 [276]. Rearranging the TMs of AQP4 would be interesting to see if the order of presentation modifies the crosslinking interaction and whether stop transfer per se limits residence time near sec61.

Does CFTR TM8 return to sec61 alpha at a later point in synthesis? My study (manuscript 3) showed that the initial pattern of TM8-sec61 interactions lasted over at least 70 residues of synthesis. Probe sites at residues 912, 913 and 914 at truncations after

synthesis of TMs 9, 10 and 11 could show if TM8 returns to the vicinity of sec61 during later points in synthesis.

Is TM7 in the translocon simultaneously with TM8? Preliminary studies suggest that TM7 has a crosslinking pattern similar to that of TM8. At a truncation at CFTR residue 925, TM7 remains proximal to sec61 following puromycin release. This may be due to a glutamate residue at position 873, in the center of the putative TM7 boundaries. Further, TM7 remains near sec61 at truncation 977, when TM8 is also present (see data not shown) but the TM7 interaction at 977 does not persist following peptidyl-tRNA cleavage. A thorough crosslinking study of TM7 at multiple truncations could elucidate the details of TM7 interactions.

What is the molecular mechanism of TM7-8 stop-transfer cooperativity? My CFTR crosslinking study (manuscript 3) primarily evaluated TM8 -translocon interactions. The next logical step after the evaluation of TM7-translocon interactions is to study the mechanism for stop transfer cooperativity. Stop transfer must be mediated early enough to direct ICL4 into the cytosol which suggests it should occur no later than the time of TM8 entry into sec61. Further, a direct interaction between the two TMs should result in crosslinking between the two TMs resulting in faster electrophoretic mobility. At truncations from 957-977 there is no evidence of any change in electrophoretic mobility other than that expected from the truncation size. It may be, however, that this interaction occurs at some fleeting point between the studied nascent chain lengths. A very closely spaced series of truncations should be studied to evaluate this possibility.

Alternatively, the cooperativity mechanism may be indirect, via a conformational change in sec61 caused by TM7-translocon interactions, for example. TM8 has previously been studied in an isolated context [15] and was found to be translocated in the absence of TM7. It would be interesting to perform photocrosslinking and protease protection assays on TM8 chimeric proteins in which TM7 is replaced by other signal anchor sequences. The effect of replacing the E873 residue should also be examined. Does elimination of the polar residue in TM7 eliminate TM8 stop transfer activity and/or alter the TM7 or TM8 crosslinking pattern?

Is the D924 residue responsible for persistent full length CFTR association with the RTC? This could be examined by running native velocity centrifugation gradients of full length CFTR with the D924V mutation. Does the D924V mutation in CFTR TM8 affect release of full length CFTR from the gradient pellet (manuscript 4, Fig. 1)? Native solubilized translation products of CFTR D924V can be chemically crosslinked prior to running gradients and immunoprecipitated with anti-sec61α antibody to test whether the persistent sec61 association is lost (manuscript 4, Fig. 3b).

Are specific residues in sec61 responsible for retaining CFTR TM8 following peptidyl-tRNA cleavage? This question would be best evaluated in a yeast system where sec61p knockout strains are available [57]. Specific mutations in recombinant sec61p can be engineered by PCR and introduced into yeast cells via plasmid shuffling. After testing whether WT sec61p can recapitulate the TM8 results from canine rough microsomes,

mutations in specific residues in sec61p (e.g. secY TMs 2b and TM7 homologs) can be evaluated for their effect on crosslinking by immunoprecipitating any CFTR TM8-sec61p photoadducts before and after treatment with puromycin.

Is persistent crosslinking an artefact of incomplete release of the C-terminus of the polypeptide from the ribosome tunnel? While I find this scenario unlikely because the D924V construct does not exhibit persistent crosslinking, it can be easily tested by replacing the TM8 C-terminal flanking region with a reporter sequence from bovine prolactin which has been previously shown to be released from the ribosome [222-224].

Preface to Appendix A:

This appended manuscript is a study on the role of the AAA-ATPase p97 in the degradation of the ERAD substrate CFTR. My role in this study was the characterization of p97 interactions with the membrane, ostensibly to elucidate a potential membrane receptor. I discovered that a 100-fold dilution of membranes in "Buffer B" (see methods) resulted in depletion of p97 beyond the limit of detection by western blot in several membrane preps studied. (Fig. 2d and Fig. Intro-A1). Once depleted, p97 could be rebound with either recombinant his-tagged protein or the rabbit reticulocyte lysate endogenous pool (Fig. A-2e).

Depletion of p97 followed by incubation with increasing concentrations of recombinant his-tagged p97 and quantitated via West Pico chemoluminescence resulted in a saturation binding curve with a suggested K_D of ~75nM (Fig. Intro-A-2A). These results were somewhat suspicious, however because additional quantitation with the Odyssey system suggested that the chemoluminence assay was not sensitive enough at the higher p97 concentrations and that binding was mostly non-specific (Fig IntroA-2B). The study was repeated with p97 concentrations to 2μM without evidence of saturable binding (Fig. Intro-A-2c) This implies that p97 does not bind to a specific membrane receptor but may, alternatively, bind directly to membrane substrates.

Fig Intro-A1

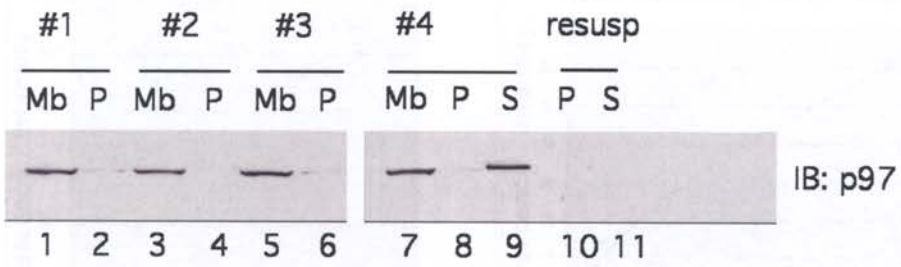

Fig. Intro-A-1. Endogenous p97 can be depleted from canine rough microsomes. In four separate membrane preps (lanes 1-2, 3-4, 5-6, 7-8) a 100-fold dilution of membranes in buffer B (see manuscript A-1 Materials and Methods) at 24 ° results in nearly complete dissociation of endogenous p97 (pellets lanes 2, 4, 6). For prep 4 (lanes 7-11) all p97 is present in supernatant after dilution (lane 9). Resuspension and pelleting of material in lane 8 confirms that p97 has been thoroughly depleted (lanes 10-11)

Fig. IntroA-2

A

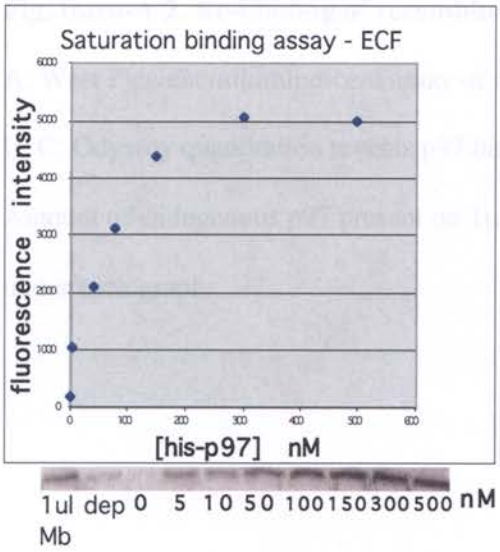

B

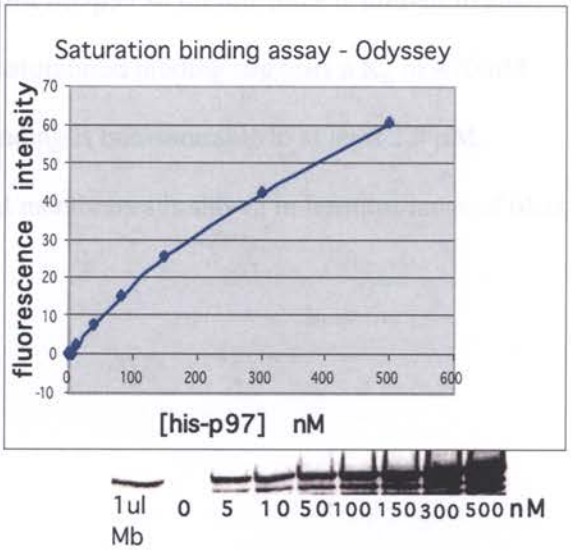

C

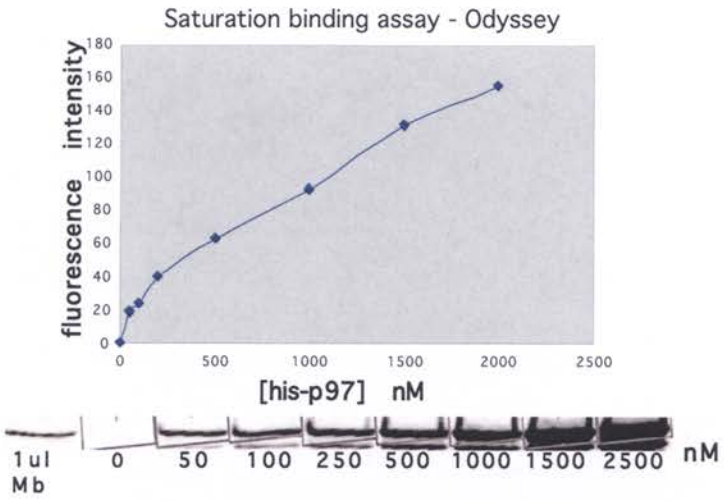

Fig. Intro-A-2. Re-binding of recombinant his-p97 to membranes is non-saturable.

A: West Pico chemiluminescent assay of saturatuion binding suggests a K_D of ~70 nM.

B, C: Odyssey quantitation reveals p97 binding is non-saturable to at least 2.5 μM.

Amount of endogenous p97 present on 1μl membranes is shown in leftmost lanes of blots under each graph.

Appendix 1

p97 Functions as a Non-Essential Auxiliary Factor for TM Domain Extraction during CFTR ER-Associated Degradation

Eric J. Carlson[1], David Pitonzo[2], and William R. Skach[3*]

[1]Department of Cell and Developmental Biology, [2]Department of Physiology and Pharmacology, and [3]Department of Biochemistry and Molecular Biology, Oregon Health & Science University, Portland, Oregon 97239

Published in EMBO Journal Vol. 25, No. 19, pp 4557-4566

*Corresponding author:
Dept. of Biochemistry and Molecular Biology
Mail Code: L224
Oregon Health & Science University
3181 SW Sam Jackson Park Road
Portland, OR 97239
Phone: 503-494-7322
Fax: 503-494-8393
Email: skachw@ohsu.edu

Key Words: ERAD/polytopic protein/CFTR/p97/ER-Associated Degradation

Subject Category: proteins/membranes and transport

1. Abstract

The AAA-ATPase p97 has been implicated in the degradation of misfolded and unassembled proteins in the endoplasmic reticulum (ERAD). To better understand its role in this process, we used a reconstituted cell-free system to define the precise contribution of p97 in degrading immature forms of the polytopic, multi-domain protein CFTR. Although p97 augmented both the rate and the extent of CFTR degradation, it was not obligatorily required for ERAD. Only a 50% decrease in degradation was observed in the complete absence of p97. Moreover, p97 specifically stimulated the degradation of CFTR transmembrane (TM) domains but had no effect on isolated cytosolic domains. Consistent with this, p97-mediated extraction of intact TM domains was independent of proteolytic cleavage and influenced by TM segment hydrophobicity, indicating that the relative contribution of p97 is partially determined by substrate stability. Thus we propose that p97 functions in ERAD as a nonessential but important ancillary component to the proteasome where it facilitates substrate presentation and increases the degradation rate and efficiency of stable (TM) domains.

2. Introduction

A fundamental obstacle in membrane protein degradation is the presentation of substrate to cytosolic and/or extracytosolic proteases. In this regard, two AAA-ATPases (ATPases Associated with various cellular Activities) [277] have been proposed to facilitate retrotranslocation and membrane extraction of misfolded and unassembled proteins in the endoplasmic reticulum (ER) [278-282]. One ATPase is comprised of a ring of six subunits located at the base of the 19S proteasome regulatory complex (RC) [283]. The second is the homohexameric protein p97 (VCP/cdc48) that functions together with cofactors Ufd1 and Npl4 [284]. Both ATPases associate with the 20S proteasome, bind directly to polyubiquitinated proteins and facilitate degradation of both ER and cytosolic substrates [282, 284, 285]. The base of the 19S RC has been reported to interact directly with the Sec61 translocation machinery [286]. In contrast, p97 binds the ER via one or more large complexes that include several ubiquitin ligases (gp78, Doa10 and/or Hrd1), VIMP1, the tetraspan protein Derlin-1, and Ubx2 [287-291].

Despite genetic, biochemical and functional evidence implicating the 19S RC and p97 in ER-associated degradation (ERAD), their precise role remains unknown and somewhat controversial. Of the 18 proteins in the 19S RC, few have known functions. However, AAA-ATPases (Rpt1-6) collectively open the gate into the 20S core [292], exhibit chaperone-like activity [293, 294] and facilitate assembly and disassembly of the 26S proteasome during the degradation cycle [295]. Based on structural and functional homology to archaebacterial ATP-dependent proteases PAN [296] and ClpX [297], the eukaryotic 19S RC is thought to unfold and actively translocate substrates into the 20S

catalytic chamber. Thus an appealing, although largely untested possibility is that 19S unfolding activity might play a direct role in dislocating ERAD substrates from the ER lumen and/or bilayer. Consistent with this notion, functional proteasomes are required for the tight coupling of membrane extraction and proteolytic cleavage during degradation of ER membrane proteins [121, 278]. In addition, purified 19S RC is sufficient for ATP-dependent dislocation of the luminal substrate, pro-alpha factor [298].

On the other hand, accumulating evidence has suggested that p97 rather than the 19S regulatory subunit is primarily responsible for ER dislocation. Like the 19S RC, p97 together with its cofactors, Ufd1 and Npl4, exhibits unfolding/segregating activity and plays an important role in presenting substrates to the proteasome [299, 300]. Indeed, inactivation of p97, ufd1, or npl4 blocks the degradation of ubiquitinated membrane and luminal ERAD substrates including the ABC transporters PDR5, Ste6 and CFTR [301, 302], HmgCoA reductase [303, 304], ER-localized transcription factors, Spt23 and Mga2 [305, 306], and CPY* [307, 308]. p97 inhibition or addition of dominant negative p97 also decreases accumulation of cytosolic intermediates generated in the presence of proteasome inhibitors, reduces US11-dependent retrotranslocation and degradation of MHC I [280] and stabilizes a mutant form of CFTR (ΔF508) [309]. Thus, understanding the precise role of p97 has broad and significant implications for the function and regulation of cellular degradation pathways

Despite the growing perception that p97 is an essential component of the ERAD machinery, interference with p97 function typically decreases but does not completely

abolish degradation of ERAD substrates. This has been a particularly challenging issue to address in vivo because p97/cdc48 null mutants are lethal in yeast [310], and conditional mutants arrest during cell division [311]. Likewise, p97 (VCP) siRNA blocks cell cycle progression in HELA cells with arrest in prometaphase/metaphase and induces apoptosis [312]. To define the precise role of p97, we therefore used an *in vitro* system that efficiently reconstitutes the ERAD pathway [313, 314] and examined the stability of a prototype substrate, the cystic fibrosis transmembrane conductance regulator (CFTR). CFTR is an epithelial, ATP-gated chloride channel that exhibits a typical eukaryotic domain architecture of the ATP Binding Cassette (ABC) transporter superfamily (Figure 1). It contains 2 transmembrane (TM) domains with six TM segments each, two large cytosolic nucleotide binding domains (NBDs) and a cytosolic regulatory (R) domain [103]. In most cell types studied to date, approximately 60-80% of wild type CFTR and nearly 100% of common mutant variants are rapidly degraded via ERAD [118, 120, 236, 245]. Importantly, this phenotype is recapitulated *in vitro*, where newly synthesized, membrane integrated CFTR is efficiently degraded into TCA soluble fragments in an ATP- and proteasome-dependent manner [121, 257, 315].

In the current study, we show that while p97 specifically augments CFTR degradation, it is not obligatorily required for ERAD. Rather, both the rate and efficiency of CFTR degradation were decreased by only 50% in the absence of p97. Interestingly, p97 had no stimulatory effect on the degradation of isolated CFTR cytosolic domains but specifically increased both the extraction efficiency and degradation rate of CFTR TM domains. Moreover, p97-mediated domain extraction occurred independently of proteolytic

cleavage and was specifically influenced by TM segment hydrophobicity, suggesting that the requirement for p97 is determined at least in part by substrate domain stability. Together, these data demonstrate that p97 plays a non-essential but important ancillary role in ERAD by increasing the degradation rate (and efficiency) of selected and possibly more thermodynamically stable protein domains.

3. Results

Reconstitution of *in vitro* CFTR degradation

CFTR was expressed *in vitro* in the presence of [^{35}S]methionine and ER microsomal membranes to generate a ~150-160 kDa core-glycosylated protein that was cotranslationally integrated into the ER membrane (Figure 1B,C). Microsomes were then collected and added to fresh rabbit reticulocyte lysate (RRL) lacking exogenous hemin, and degradation was monitored by substrate conversion into trichloroacetic acid (TCA) soluble peptides (Figure 1D). After a brief five minute lag, the rate of TCA-soluble fragment production was linear for 30-60 min (Figure 1D, inset). Thus there is little delay in degradation due to substrate ubiquitination, a finding consistent with transient accumulation of polyubiquitinated CFTR observed in earlier studies [121]. Under these conditions, ~65-70% of CFTR was completely converted into TCA-soluble fragments (Figure 1D). Moreover, degradation is entirely ATP-dependent and sensitive to a variety of proteasome inhibitors [121, 257]. At later time points a gradual decrease in degradation was observed, primarily due to run-down of RRL degradation activity (Figure 1E). Because proteasome-mediated CFTR degradation is a multi-step process, the overall degradation rate depends on ubiquitination, dislocation, translocation into the

catalytic core, and lastly, peptide cleavage. We have previously shown that for fully functional proteasomes, the capacity for peptide cleavage exceeds the rate of CFTR unfolding and extraction [315]. Thus, the initial rate of TCA-soluble fragment production (expressed as the percent of CFTR converted into TCA-soluble fragments per minute, Figure 1E) provides an approximate measure of the rate limiting steps of CFTR degradation that include membrane extraction, unfolding and delivery of substrate to the 20S catalytic core.

p97 facilitates CFTR degradation *in vitro*

To determine the precise contribution of p97 to CFTR degradation, RRL was depleted of p97 and its cofactors by affinity chromatography using two Ni-immobilized recombinant His-tagged proteins (Figure 2A). The first was a nonhydrolyzable ubiquitin fusion protein that contained the E2 enzyme ubcH5a fused to the C-terminus of ubiquitin^{G76V} (referred to as uu5). The second protein was p47, an independent p97 binding protein implicated in membrane fusion [316]. Adsorption of RRL to uu5 coated beads removed ~50% of p97 as determined by immunoblotting (Figure 2B, lane 1-4), and no further reduction was observed upon serial adsorption (data not shown). Quantitation was based on standard curves of purified, recombinant p97 (Supplemental Figure 1). Interestingly, uu5 adsorption depleted ufd1 to below the limits of detection (Figure 2B, lane 4), consistent with reports that ubiquitin fusion proteins bind p97 via the specific adapters ufd1/npl4 [317]. In contrast, a single adsorption step using p47 coated beads depleted ~ 99% of p97 from RRL but had no effect on ufd1 levels (Figure 2B, lane 6), whereas sequential adsorption with uu5 followed by p47 depleted both ufd1 and p97 (Figure 2B, lane 5).

We next carried out CFTR synthesis and degradation in a p97-depleted system. CFTR was translated in p97-depleted RRL, which was supplemented with p97-stripped microsomal membranes (Figure 2B). Although adsorption by Ni-NTA beads slightly decreased the initial degradation rate (0.53% +/- 0.02/min vs. 0.64% +/- 0.03/min) due to dilution of RRL (Figure 1E versus 2D), p97 depletion had no specific effect on CFTR translation, glycosylation, or membrane integration (data not shown). In contrast, p97 depletion resulted in a ~50% reduction in both the initial rate and overall extent of CFTR degradation that was partially restored by the addition of purified recombinant His-p97 (Figure 2C&D). Depletion of both p97 and ufd1 resulted in a similar (50%) decrease in the rate of CFTR degradation, but in this case degradation activity was not restored upon addition of wild type p97 (Figure 2E&F). These results provide biochemical evidence that p97 directly contributes to the degradation of membrane-bound CFTR and that its function in ERAD requires the adaptor protein ufd1. However, CFTR continues to be degraded albeit at a reduced rate even after highly effective p97 (and ufd1) depletion. This indicates either that CFTR degradation can occur independently of p97 or that small amounts of residual p97 might account for the remaining degradation activity.

p97 is not an essential ERAD component

To rule out the possibility that trace amounts of p97 might be sufficient for CFTR degradation, RRL was incubated with increasing amounts of p47-saturated Ni beads, and the inhibition of degradation was examined as a function of p97 depletion (Figure 3A). These results revealed that only ~20% of endogenous p97 was needed to sustain near

normal CFTR degradation activity (Figure 3A). This was not surprising given that the *in vitro*-translated CFTR present in microsomal membranes is several orders of magnitude less than endogenous RRL p97 (data not shown). We then subjected RRL to two serial depletions with p47, which together with microsomal stripping, removed > 99% of total p97 from the reaction. Consistent with results of Figure 2, this decreased the rate of CFTR degradation by only 48 +/-2.3% (Figure 3B). Small amounts of undepleted RRL (0.25%, 1%, 2%, and 4% of total volume) were then added back to titrate the effects of very low p97 levels. When the amount of residual p97 was titrated between 1% and 5%, a roughly linear relationship was obtained between the initial degradation rate and the p97 concentration. Linear regression analysis (R^2=0.91) indicated that at 100% p97 depletion the rate of CFTR degradation would be decreased by only 51% (Figure 3B). These results provide strong evidence that CFTR degradation can be carried in the complete absence of p97, and that the major effect of p97 is to increase the degradation rate by approximately 2-fold.

p97 selectively stimulates degradation of CFTR TM domains.

p97 exhibits the unique ability to discriminate among polyubiquitinated substrates and selectively present individual components of multi-protein complexes to the proteasome [285, 305, 306]. However, it is unknown whether p97 exerts different effects on different domains within the same protein. CFTR provides an ideal ERAD substrate to examine this question because it contains multiple well-defined domains that reside either in the cytosol or within the ER membrane (Figure 1). We therefore examined the requirement for p97 on the degradation of isolated CFTR cytosolic and TM domains. His-tagged

constructs encoding cytosolic NBD1 (residues V358-S588) or NBD1-R (residues V358-D835) domains were translated in p97-depleted RRL, isolated by Ni-affinity purification, and added directly to degradation reactions. As shown in Figure 4, both constructs were rapidly converted into TCA soluble fragments in an ATP-dependent manner. The degradation rate of NBD1 was ~4 fold faster than that of full length CFTR, and nearly 90% of the polypeptide was converted into TCA-soluble fragments within two hours (Figure 4A, B). Remarkably, p97 depletion had no effect on NBD1 degradation and only a minor effect on NBD1-R turnover (15% decrease in initial rate). Thus, degradation of CFTR cytosolic domains was nearly entirely independent of p97. Similar results were also observed for two other soluble proteasome substrates, lysozyme and casein (data not shown).

We next examined degradation requirements for CFTR TMD1 (residues M1-V393), which contains the first 6 TM segments and connecting loops that vary in length from 2-66 residues (Figure 5A). *In vitro* translated TMD1 was quantitatively resistant to carbonate extraction, indicating that the protein was fully integrated into the ER membrane (Figure 5A). Because twelve of the thirteen TMD1 methionines (92%) are located within 30 residues of the membrane, and the linear distance from the 19S ATPase ring to proteolytic sites in the 20S core is ~11nm [318], only the N-terminal methionine should be accessible to proteolytic cleavage in the intact domain [319]. TMD1 was also subject to ERAD as demonstrated by ATP-dependent conversion into TCA soluble fragments and MG132 sensitivity (Figure 5B). Approximately 45% of TMD1 methionines were converted into TCA soluble fragments, confirming that TMD1 was

also extracted from the ER membrane during degradation. The initial rate of degradation (0.44+/-0.04%/min) was somewhat slower than for full-length CFTR (Figure 5C). In addition, p97 depletion resulted in a ~50% reduction in both the rate and extent of TMD1 degradation which was almost entirely restored by addition of recombinant p97 (Figure 5B&C). These data indicate that CFTR TMD1 is degraded 2-5 fold slower than isolated cytosolic NBD1 and NBD1-R domains in intact RRL and 3-9 fold slower in p97-depleted RRL. Thus p97 selectively enhances the rate of TMD1 degradation over that of CFTR cytosolic domains.

p97 contribution is dependent on TM domain hydrophobicity

The inverse correlation between degradation rate and p97 dependence suggested that p97 might selectively facilitate the unfolding of more thermodynamically stable (and hence more slowly degraded) peptide regions. If this were true, then TMs that were less stable in the lipid bilayer might also show less p97 dependence. We therefore examined a shorter construct containing the CFTR N-terminus and first two TM segments (Figure 6A). This construct (TM1-2) efficiently acquires its correct two-spanning topology *in vitro* and contains 5 methionines, 4 of which are located within 18 residues of the membrane. Like TMD1, *in vitro* synthesized TM1-2 was membrane-integrated (Figure 6B) and was degraded by the proteasome only slightly faster (0.73+/-0.08%/min) than full length CFTR (Figure 6C,D). In contrast to TMD1, however, the rate of TM1-2 degradation was only modestly affected (~20% reduction) by p97 depletion.

CFTR is somewhat unusual in that both TM1 and TM2 contain potentially charged residues [103], namely E92 and K95 reside near the center of TM1 (Figure 6A), and R134 resides near the C-terminus of TM2. E92 and K95 were therefore replaced with alanine residues to generate a more stable transmembrane structure (predicted free energy of transfer (ΔG) for TM1 decreases from -5.1 kcal/mol to -10.1 kcal/mol (octanol-water partitioning, whole residue hydrophobicity scale [320]). The TM1-2 E92A/K95A mutations had a striking effect, decreasing the initial degradation rate by ~2.5-fold (0.28%+/-.03/min) in the presence of p97 (Figure 6E&F), and further decreasing the degradation rate by an additional 2.3-fold following p97 depletion (0.12% +/- 0.01/min). Degradation was substantially restored by the addition of recombinant p97.

p97 specifically augments TM domain extraction independently of proteolytic cleavage.

Finally, to determine whether p97 facilitates extraction of CFTR TM domains directly and independently of proteasome-mediated peptide cleavage, TMD1 degradation products were separated into membrane-bound and cytosolic fractions prior to analysis. Consistent with previous studies [315], all cytosolic fragments were TCA soluble under control conditions (Figure 7A). In the presence of MG132, however, very few TCA-soluble fragments were generated, but CFTR continued to be released into the cytosol as large TCA insoluble polypeptides (Figure 7A, vertical arrow). These cytosolic fragments were predominantly comprised of full length TMD1, which had been integrated into the ER membrane during translation (Figure 5A), but then extracted en block during the degradation reaction (Figure 7C, lanes1-5). p97 depletion decreased the rate of fragment

release as expected but had no effect on the TCA solubility of cytosolic fragments (Figure 7B). When degradation was inhibited by MG132, p97 depletion again decreased the rate of TMD1 release from the ER membrane by ~3 fold (Figure 7D,E). Under these conditions, release of TCA-insoluble cytosolic fragments was also decreased (Figure 7B) as was the cytosolic accumulation of full-length TMD1 (Figure 7C, lanes 1-5 versus lanes 6-10). No cytosolic fragments were visualized in ATP-depleted RRL or in the absence of MG132 (Figure 7C, lanes 11-20). These results demonstrate that p97 can facilitate extraction of intact CFTR TMs, and that the stimulatory effect of p97 on CFTR degradation occurs independently and upstream of proteolytic cleavage.

4. Discussion

Two AAA-ATPase complexes, p97-ufd1-Npl4 and the proteasome 19S RC, are currently implicated in the dislocation and degradation of misfolded proteins from ER membrane. Using an *in vitro* system that reconstitutes the ERAD pathway, we now quantitate the relative contribution of p97 in facilitating degradation of a prototypical ERAD substrate, CFTR. In the complete absence of p97, the rate of CFTR degradation was decreased by only ~50% as determined by proteasome-dependent conversion of substrate into TCA soluble fragments. Detailed depletion and add-back experiments confirmed that residual traces of p97 did not account for the substantial degradation activity observed after depletion. Thus while p97 clearly facilitates the degradation of ERAD substrates, it is not obligatorily required for either extraction, unfolding or proteolysis of a large, membrane integrated polytopic membrane protein.

Remarkably, the stimulatory effect of p97 on CFTR degradation was restricted to TM domains, whereas degradation of cytosolic domains was nearly entirely p97 independent. The relative contribution of p97 was also markedly influenced by changes in the hydrophobicity of individual TM segments. These findings raise the possibility that p97 primarily increases the degradation efficiency of specific domains that are more stable and/or slowly degraded. Indeed, we found a strong inverse correlation between the baseline degradation rate of different CFTR domains and the stimulatory contribution of p97 (Figure 8). Although additional studies are clearly needed before this effect can be generalized, our analysis suggests p97 does not exert stimulatory effects until the degradation rate falls below a critical threshold (<0.5%/min in our study). p97 also directly stimulated the extraction and membrane release of intact TM domains independently of proteolytic cleavage. Thus, p97 functions as a non-essential, yet important ancillary component of the ERAD pathway that stimulates presentation of thermodynamically stable substrates or domains to the 26S proteasome.

Cryo EM studies have suggested that unfolding by AAA-ATPases occurs via conformational changes caused by ATP binding/hydrolysis [277]. For example, unfolding by the prokaryotic PAN AAA-ATPase takes place on the surface of the hexameric ring and leads directly to peptide translocation through the central pore [296]. In the case of the 26S proteasome, substrate must also be translocated through both 19S AAA-ATPase and the axial pore of the 20S cylinder. Although it is unlikely that translocation occurs through the pore of p97 [321], there may be an analagous unfolding on the surface of the hexamer. However, our findings clearly demonstrate that such an

interaction with p97 is not necessarily obligatory even for substrates where p97 can and normally does facilitate degradation. This raises a significant mechanistic question. How and when is p97 recruited to substrate? Two scenarios seem to be most likely. One possibility is that the proteasome provides a baseline unfolding activity that (processively) degrades substrate until it encounters a stable region that it is unable to unfold [319]. This stalled complex could then recruit p97 to assist in extraction/unfolding and thus stimulate the degradation rate. In a second, and perhaps more plausible model, both the 26S proteasome and p97 could processively scan and unfold substrates together. However, p97 would not contribute substantially to the rate of unfolding until a specific region of protein was encountered in which its ATPase activity would increase the basal rate provided by the proteasome. In support of the former possibility, purified 26S proteasomes are clearly capable of degrading substrates *in vitro* in the absence of p97 [298]. However, the proteasome and p97 can also interact directly during substrate presentation [285].

A third plausible explanation for our findings is that substrate presentation to the proteasome occurs via multiple pathways [299]. These involve a growing repertoire of proteasome interacting proteins (PIPs) that include p97, rad23, and hPLIC/dsk2 as well as co-chaperones such as BAG-1 [322]. Thus it is possible that CFTR could use parallel means for recruitment, ubiquitination and presentation to the 19S RC. Consistent with this we recently reported that during proteasome-mediated degradation, CFTR N-terminal, C-terminal and R-domain epitopes were lost at similar rates, suggesting degradation could be initiated at multiple sites within the polypeptide [315]. Moreover, CFTR ubiquitination and degradation can be initiated by a cytosolic complex involving

the U-box protein CHIP, Hsc70 and ubcH5 [245] as well as membrane bound E2/E3 proteins Hrd1/Hrd3, Doa10 and Ubc6 [301]. Thus different recognition machinery may operate on different CFTR domains depending on their cellular compartment and the nature of the folding defect. This model is further supported by recent studies indicating that a large protein complex at the ER membrane involving Der1, Rma1 and Ubc6 is specifically involved in recognizing destabilizing mutations within TMD1 (D. Cyr, Personal Communication) whereas the CHIP-Hsc70-UbcH5 complex primarily recognizes cytosolic (NBD) folding defects [244]. Intriguingly, the Hrd1/3 and Doa10 pathways in yeast, and the Rma1 pathway in mammalian cells, all converge at p97/cdc48. If p97 functions to present substrates to the proteasome as predicted, this may also explain why CFTR TMDs preferentially display augmented degradation in the presence of p97. Recently, it was reported that the yeast tetraspan protein ubx2 is a central component of this complex and through its UBA and UBL domains links substrates with E3 ligases, Der-1 and p97 [287, 288]. It will therefore be most interesting to determine whether Ubx2 and additional components are also required for p97 augmentation of TMD degradation.

To our knowledge this is the first study demonstrating that p97 contributes differentially to the degradation of different domains derived from the same protein. While recruitment of degradation machinery likely plays a role in this process, it is also important to consider that the inefficient maturation of CFTR observed in most cell types is caused by failure to acquire proper tertiary and/or quaternary structure. Although the timing of NBD folding during synthesis is somewhat controversial [225, 323], NBDs are thought to fold

particularly inefficiently, and this kinetic defect is amplified by deletion of a phenylalanine at residue 508 in NBD1, a commonly inherited mutation found in nearly 90% of CF patients [111, 323, 324]. Thus the relatively unfolded state of isolated NBD1 (and NBD-R) in RRL likely contributes to the rapid baseline degradation rate observed and the lack of requirement for p97. By contrast, CFTR TM helices buried in the lipid bilayer are degraded much more slowly and demonstrate a clear augmentation by p97. These findings parallel observations for the cytosolic substrate, titin, which can also exhibit two degradation rates, a slow rate that requires domain unfolding and fast rate when the substrate is presented in a pre-denatured state [325]. Each pathway is characterized by marked differences in energy consumption, four ATP/aa for the folded substrate versus 1 ATP/aa for denatured substrate. This difference results from the inefficient, iterative engagement of folded substrates with the AAA-ATPase ClpXP, which is cooperatively promoted during denaturation at the surface of the ring [325]. Moreover, this process provides a mechanism for partitioning stable from misfolded or denatured substrates based on their affinity for the AAA-ATPase [326]. By analogy the eukaryotic 19S RC is predicted to have a similar cooperative unfolding behavior such that unfolded or partially unfolded substrates would energetically less costly and more efficiently degraded.

Importantly, the unfolding process is highly cooperative and influenced by local structure (helices and surface loops) at the site of initial unfolding [319]. In the case of membrane proteins, extraction of TMDs likely represents a significant energy barrier, particularly where short lumenal loops (e.g. CFTR TM3-4, TM5-6) necessitate pair-wise extraction of

TM segments. Indeed, TMD1-6 was degraded at a much slower rate than cytosolic domains, suggesting that membrane extraction may be generally a rate-limiting step in polytopic protein degradation. In the TM1-2 construct, polar/charged residues likely provide a locally unstable environment in the lipid bilayer for which the 19S ATPases provide sufficient force for extraction. Interestingly, replacing TM1 charged residues with alanine resulted in the most stable of the constructs examined and slowed degradation by nearly 5 fold (in the absence of p97) when compared to wild type TM1-2 and nearly 20 fold when compared to the isolated NBD1. p97 likely plays a key role in stimulating TM1-2 E92A/K95A degradation by providing a second step for substrate partitioning, thus generating a locally unfolded domain which preferentially engages the AAA-ATPase ring of the 19S RC. The net result of two serial partitioning steps would be to dramatically increase the efficiency of engagement by both AAA-ATPases and the ultimate delivery of substrate into the proteasome catalytic core

5. Materials and methods

Constructs: Plasmid cloning details are described in Supplemental Online-information.

Recombinant proteins: Recombinant protein expression was induced in transformed BL21(DE3) cultures using 0.4mM isopropyl β-D-1-thiogalactopyranoside (IPTG; Fisher Scientific, Pittsburgh, PA) as previously described [327]. Cell lysates were loaded onto a 5 ml Ni-NTA column (Qiagen, Inc., Valencia, CA), washed with 50 ml 300mM NaCl, 1mM βME, 5% glycerol, 0.4mM PMSF, 25mM imidazole, and 50mM Tris-HCl, pH 7.5, and eluted with a 25mM-500mM linear gradient of imidazole. Fractions were pooled, dialyzed against 100mM NaCl, 1mM βME, and 25mM Tris-HCl, pH 7.5 (Buffer A), then

concentrated, and stored at –80°C. Aliquots were thawed once and discarded.

Affinity Depletion of RRL and CRM: Rabbit reticulocyte lysate (RRL) and canine pancreatic rough microsomes (CRMs) were affinity depleted as described [327]. Briefly, Ni-NTA beads containing near saturating amounts His-tagged recombinant proteins were added to RRL at a ratio of 5:1 (RRL:Ni-NTA) and incubated at least 4 hr at 4°C with continuous mixing. Supernatants were removed and frozen in liquid nitrogen. Mock depletions were performed using equal volumes of uncoupled Ni-NTA beads. CRMs were depleted of p97 by 50-fold dilution in 0.25M sucrose in Buffer B (1mM DTT, and 50 mM triethanolamine-acetate, pH 7.5) at 24°C for 15 min. Membranes were pelleted at 180,000 x g for 20 min, and resuspended in their original volume of Buffer B. Following depletion, RRL or CRMs were separated by SDS-PAGE, transferred to nitrocellulose or PVDF, and blotted with mouse α–p97 (1:500; BD Transduction Laboratories, San Jose, CA) or mouse α-ufd1 (1:1,000; BD Transduction Laboratories) followed by α-mouse-HRP secondary Ab (1:20,000. Biorad, Hercules, CA). The blots were imaged on Kodak film using Pierce west pico supersignal substrate according to the manufacturer's directions (Pierce Biotechnology, Inc., Rockford, IL). For quantitation (see supplemental Figure1) α-mouse-AP secondary antibody (1:2,500; Promega, Madison, WI) was used in conjunction with ECF substrate (Amersham Biosciences, Piscataway, NJ), and blots were imaged using a Biorad FX phosphoimager (Biorad, Hercules, CA) followed by analysis with QuantityOne software.

In vitro transcription/translation: mRNA was transcribed with SP6 RNA polymerase for 1 hour at 40°C and translated in a transcription-linked reaction for 1-2 hr at 24°C as described in detail elsewhere [327]. RNAse-free H_2O was substituted for DNA in mock transcription reactions. Endogenous RRL and CRM mRNAs were digested prior to translation [327]. Canine pancreatic rough microsomal membranes (A_{280}= 4) were added at the start of all translations, except the cytosolic NBD and NBD-R constructs. Aurin tricarboxylic acid (25 - 50μM) was added after 15-20 minutes to synchronize translation. Following translation, CRM containing *in vitro*-synthesized protein were isolated by centrifugation, 180,000 x g for 10 min, through a cushion containing 0.5M sucrose in Buffer C (100mM KCl, 5mM $MgCl_2$, 1mM DTT, 50mM HEPES, pH 7.5) and resuspended in 1/2 original volume in 0.1M sucrose in Buffer C. Prior to pelleting, TM1-2 E92A/K95A was released from ribosomes by addition of 1mM puromycin. Soluble NBD and NBD-R proteins were isolated by diluting translation reactions with 3 volumes of Buffer A and mixing with 10 μl Ni-NTA at 4°C for 30 minutes. Beads were then washed in 10 x 1ml 10mM imidazole in Buffer A, and proteins were eluted with 250mM imidazole in Buffer A.

Degradation Assay: Isolated CRMs from translation reactions were added to RRL supplemented with 1mM ATP, 12mM creatine phosphate, 5mM $MgCl_2$, 3mM DTT, 10mM Tris-Cl, pH 7.5 and 4μg creatine kinase/50μl reaction [327]and incubated at 37°C. 100μM MG132 or 20mM 2-deoxyglucose and 20U hexokinase was added to the reaction mixture as indicated to inhibit proteasomes or deplete ATP, respectively. Recombinant p97 (200ng/μl RRL) [315] was also added to p97-depleted RRL where indicated.

Samples were removed at indicated times (T_n), precipitated in 20% TCA and centrifuged at 16,000 x g for 10 min. TCA supernatants (TCA Sol) were then counted in ScintiSafe (Fisher Chemicals) using a Beckmann LS6500 scintillation counter. Total [^{35}S] present in each sample was determined by directly counting an aliquot of the degradation reaction. Mock reactions were used as a control to correct for small amounts of nonspecific, ATP-independent association of [^{35}S] with the membranes [327]. The percent of protein degraded at each time point was determined using the following formula:

$$\% \text{ of total counts} = \{(CFTR(T_n\text{-}T_0) - Mock(T_n\text{-}T_0))/(CFTR(total - TCA\ sol\ T_0) - Mock(total - TCA\ sol\ T_0))\}*100$$

Where T_n = TCA soluble counts at T=n and T_0 = TCA soluble sounts at T=0 for indicated CFTR and Mock translation reactions. All values are reported as mean of 3 or more experiments+/- SEM.

Membrane Release Assay: The release assay is similar to the degradation assay except that at each time point microsomes from degradation reactions were first pelleted at 180,000 x g for 10 min through 0.5M sucrose in Buffer B. The cytosolic supernatant was then either counted directly to measure total CFTR released from the membrane, precipitated in 20% TCA to determine TCA soluble counts released, or analyzed by SDS-PAGE and autoradiography. The percent membrane-bound CFTR substrate released into the supernatant and %TCA soluble counts released at each time point were calculated by the same formula as used for the degradation assay.

Carbonate extraction: CRMs containing translation products were added to 1 ml 0.25M

sucrose, 1μg BSA, and 0.1M Tris-Cl, pH 7.5 or 1 ml 0.1M Na_2CO_3, pH 11.5, 1μg BSA and incubated on ice for 30 min, followed by centrifugation at 180,000 x g for 30 min. Pellets were solubilized in 30 μl SDS-PAGE loading buffer. Supernatants were precipitated in 20% TCA, and the resulting pellets were solubilized in 30 μl SDS-PAGE loading buffer. Samples were analyzed by SDS-PAGE and EN^{3}HANCE (Perkin Elmer, Boston, MA) fluorography and imaged on Kodak film.

Acknowledgements

We thank Dr. H. Meyer for the gifts of p47 and p97 cDNAs, Dr. M. Hochstrasser for human ubiquitin cDNA, and Dr. P. Howley for ubcH5a cDNA. Also, we thank Drs.C. Enns, K.Frueh, L. Musil, and S. Lutsenko for helpful comments on the manuscript.

Supplemental Information.

Plasmid Constructs. Plasmids pSPCFTR, pSPTM1-6, and pSPTM1-2, and are described elsewhere (Xiong. et al., 1997. J. Clin. Invest. 100: 1079-1088). PTrc-p47, and pQE-p97 were generously provided by Dr. Hemmo Meyer. Coding sequences for p97 and p47 were subcloned into Nco1 and BamH1 sites in frame to the His-6 tag of pET15b (EMD Biosciences, San Diego, CA) for heterologous expression.

Plasmids encoding His6-tagged CFTR NBD1 and NBD1-R domains were constructed as follows. CFTR residues V358-S589 were amplified by PCR using sense

(TTTCCCTCCATGGTACAAACATGGTATGAC) and antisense (AGTTTCTGCAGCTAGCTTTCAAATATTTCTT) primers and ligated into NcoI/BamHI sites of a modified pSP64 plasmid described elsewhere (Skach, et al., Cancer Research, 54:3202-3209, 1994). Primers introduced an in-frame ATG translational start codon (NcoI site) immediately before CFTR codon V358 and a TAG stop codon at CFTR residue C590. Plasmid pSPNBD1 thus contains the coding sequence of NBD1 downstream of the SP6 promoter of pSP64. This construct pSPNBD1was then used as the template for a second PCR amplification using the same sense primer and an antisense primer (GAAGGATCCTCAGTGATGATGATGGTGGTGGCTTTCAAATATTTCTTT) encoding six in-frame His codons immediately upstream of a TGA stop codon. The PCR product was digested with BamHI and the resulting 414 BP BamHI fragment was ligated into BamHI-digested pSPNBD1 plasmid to generate pSPNBD1His6.

Plasmid pSPNBD1-R was generated by ligating a BamHI/PvuII fragment (PvuII site is in pSP64 vector) from pSPCFTR836X, which encodes a TAG stop codon at residue D836 (Xiong, et al., J. Clin. Invest. 100:1079-1088, 1997), into BamHI/PvuII digested pSPNBD1. The resulting plasmid, encoding CFTR residues V358 to D835, was then used as a PCR template with sense (TTTCCCTCCATGGTACAAACATGGTATGAC) and antisense (AGACAGCTGTTAATGATGGTGGTGATGATGATCAAAAAGGCACTCCTT) primers. The antisense primer encodes (His)6Val, immediately upstream of the stop codon followed by an engineered PvuII site. This fragment was digested with BamHI

and PvuII and inserted into BamHI/PvuII digested pSPNBD-R, yielding NBD-R with a C-terminal His6-tag.

Plasmid pETUbG76V was made by amplifying the human ubiquitin cDNA coding sequence (gift of Dr. M. Hochstrasser) with sense primer (AAGACTTCATGATGCAGATCTTCGTCAAC) and antisense primer (AACCAGCCATGGCCACACCTCTTAGTCTTAAGAC), digesting with NcoI and BspHI, and ligating into an NcoI digested pET15b vector. The antisense primer also introduced a G to V mutation at Ubiquitin codon 76. Plasmid pETUb-ubcH5a was then made by amplifying ubcH5a (gift of Dr. Peter Howley) with sense primer (TGACCCATGGCGCTGAAGAGGATT) and antisense primer (TCCGGCGGATCCTTAGTGATGATGATGATGATGCATTGCATATTTCTGAGT), digesting with NcoI and BamHI and ligating between the NcoI and BamHI sites of pET15ubG76V. The resulting in pET15Ub-ubcH5a ecodes a non-cleavable ubiqutin fusion protein with a C-terminal His6 tag.

TM1-2 (E92A/K95A) was amplified from plasmid pSPCFTR E92A/K95A (Lu et al., J. Biol. Chem. 273:658-576,1998) with sense primer (AGGATCTGGCTAGCGATCACC) and antisense primer (GTTCAGGTTTCACGTCACCTTGTTGGAAAGGAGACT), and the resulting DNA fragment was used directly in transcription reactions.

Recombinant protein production. Recombinant protein expression was induced in transformed BL21(DE3) cultures using 0.4mM isopropyl b-D-1-thiogalactopyranoside

(IPTG; Fisher Scientific, Pittsburgh, PA) as previously described (Carlson et al., 2005). Cell lysates were loaded onto a 5 ml Ni-NTA column (Qiagen, Inc., Valencia, CA), washed with 50 ml 300mM NaCl, 1mM bME, 5% glycerol, 0.4mM PMSF, 25mM imidazole, and 50mM Tris-HCl, pH 7.5, and eluted with a 25mM-500mM linear gradient of imidazole. Fractions were pooled, dialyzed against 100mM NaCl, 1mM bME, and 25mM Tris-HCl, pH 7.5 (Buffer A), then concentrated and stored at -80OC. Aliquots were thawed once and discarded.

Immunoblots. Following depletion, RRL or CRMs were separated by SDS-PAGE, transferred to nitrocellulose or PVDF, and blotted with mouse a-p97 (1:500; BD Transduction Laboratories, San Jose, CA), mouse a-Rpt5 (1:2,500 BioRad), a-c9 antisera (1:2,500; [315]) or mouse a-ufd1 (1:1,000; BD Transduction Laboratories) followed by a-mouse- or a-rabbit HRP secondary Ab (1:20,000. Biorad, Hercules, CA). The blots were imaged on Kodak film using Pierce west pico supersignal substrate according to the manufacturer's directions (Pierce Biotechnology, Inc., Rockford, IL). For quantitation (see Supplemental Figure 2) a-mouse-AP secondary antibody (1:2,500; Promega, Madison, WI) was used in conjunction with ECF substrate (Amersham Biosciences, Piscataway, NJ), and blots were imaged using a Biorad FX phosphoimager (Biorad, Hercules, CA) followed by analysis with QuantityOne software.

Fig. A-1

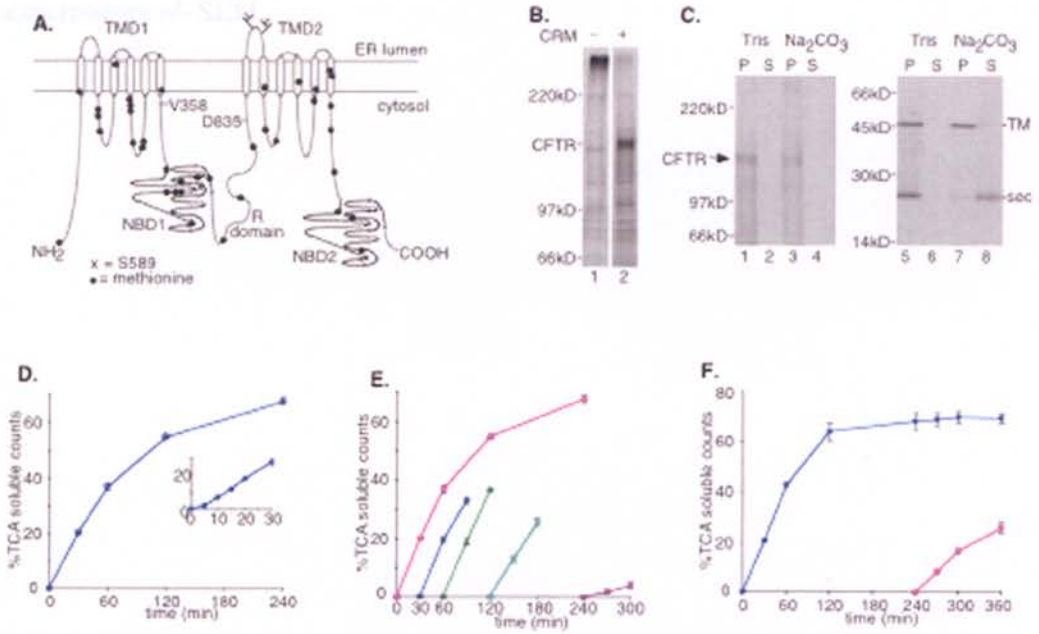

Figure A-1. CFTR is degraded into TCA soluble peptides. Schematic representation of CFTR showing relative location of methionine residues and topology of transmembrane domains (TMDs), nucleotide binding domains (NBDs), and regulatory (R) domain. Approximate location of residues V358, S589 and D835 are also indicated. (B) CFTR translated in the presence (lane 2) of CRMs yields the expected full length ~150-160 kD glycosylated protein. (C) Carbonate extraction of CFTR (lanes 1-4) and control transmembrane TM and secretory (sec) proteins (lanes 5-8) [54]. (D) *In vitro* CFTR degradation showing the % of intact, [^{35}S] methionine-labeled protein that is converted into radiolabeled TCA soluble fragments at each time point. Inset shows brief delay and then linear degradation during the first 30 min. (E) RRL was preincubated at 37 °C for indicated times prior to addition of CRM containing radiolabeled CFTR. Values indicate the rate of CFTR degradation (% CFTR converted to TCA soluble

fragments/min) during the first 30 min. All values are reported as mean of 3 or more experiments +/- SEM.

Fig. A-2

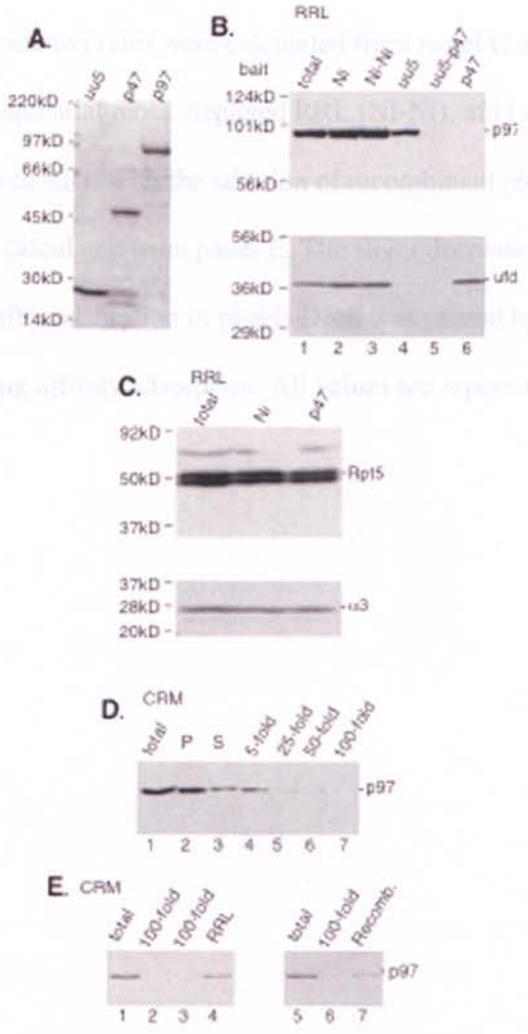

Figure A-2. RRL depletion of p97 and p97 complexes. (A) Coomassie stained gel of recombinant His-tagged proteins used as bait for RRL affinity depletion. **(B)** Immunoblots for either p97 (top) or ufd1 (bottom) of intact RRL (lane 1), RRL following a single adsorption with Ni-NTA beads (lane 2), uu5 coated beads (lane 4) or p47 coated beads (lane 6), and two sequential adsorptions with Ni-NTA beads (lane 3) or uu5

followed by p47 (lane 5). (**C**) CFTR degradation using mock depleted RRL (Ni RRL), RRL depleted of p97 using p47 (depl. RRL), or p97-depleted RRL plus recombinant p97 (depl.+p97). (**D**) Initial degradation rates were calculated from panel C as in Figure 1A. (**E**) CFTR degradation in sequential mock-depleted RRL (Ni-Ni), ufd1 and p97-depleted RRL (depl. RRL) and depleted RRL with the addition of recombinant p97 (depl.+p97). (**F**) Initial degradation rates calculated from panel E. The slight decrease in the initial rates of CFTR degradation after adsorption in panels D&E was caused by dilution of RRL by the beads used during affinity adsorption. All values are reported as mean of 3 or more experiments +/- SEM.

Fig. A-3

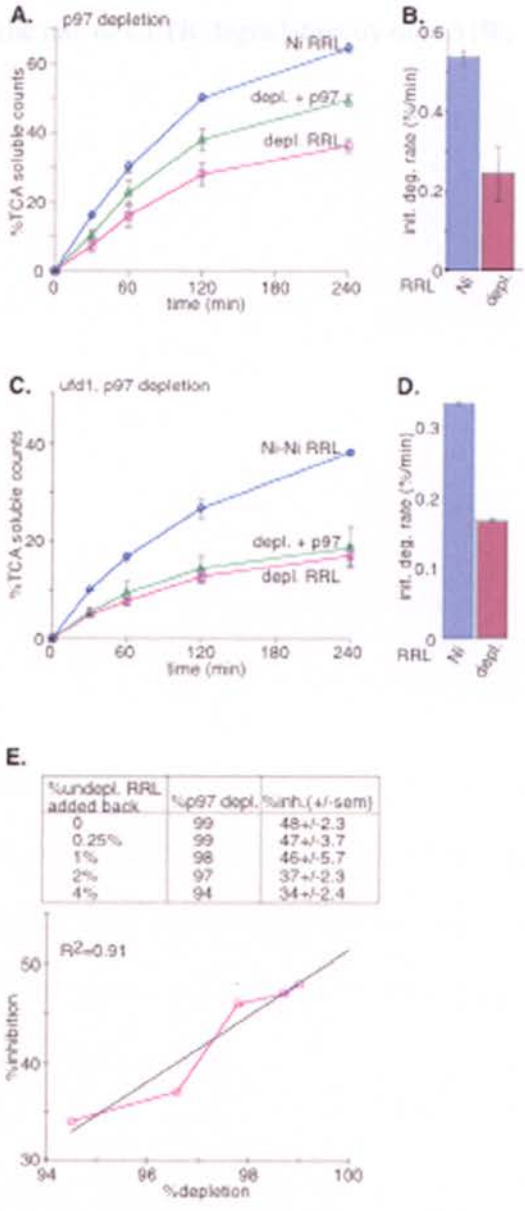

Figure A-3. p97 is effectively depleted from RRL. (A) RRL p97 was depleted by varying the amount of p47-saturated Ni-NTRA coated beads. % inhibition of the CFTR degradation rate is plotted as a function of the % p97 depletion and shown in the inset. **(B)** RRL was serially depleted (x2) with p47 Ni-NTA beads and supplemented with the

indicated amounts of undepleted RRL (inset) to quantitate the % inhibition of CFTR degradation at very low p97 concentrations. The linear regression predicts that 100% p97 depletion would inhibit the rate of CFTR degradation by only 51%.

Fig. A-4

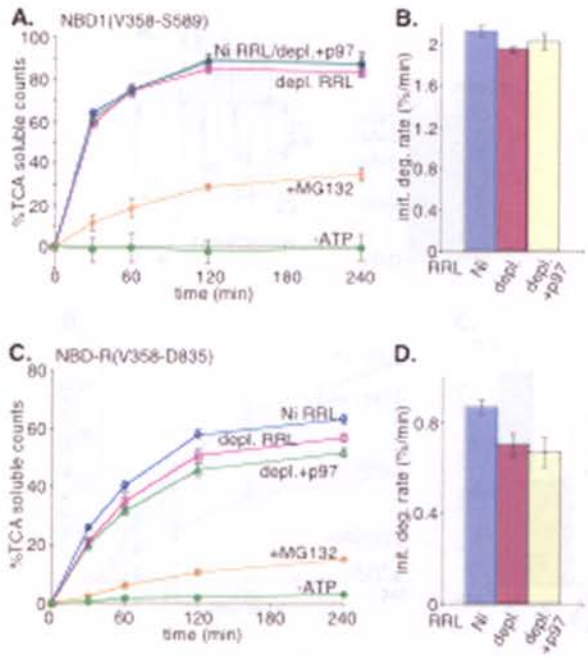

Figure A-4. Degradation of CFTR cytosolic domains is unaffected by p97. Purified NBD1 (**A**) or NBD-R (**C**) was added directly to degradation reactions containing mock-depleted RRL, or p97-depleted RRL with or without added recombinant p97. **(B&D)** Initial degradation rates were calculated from panels A and C. Location of residues in CFTR polypeptide is indicated in Figure 1A.

Fig. A-5

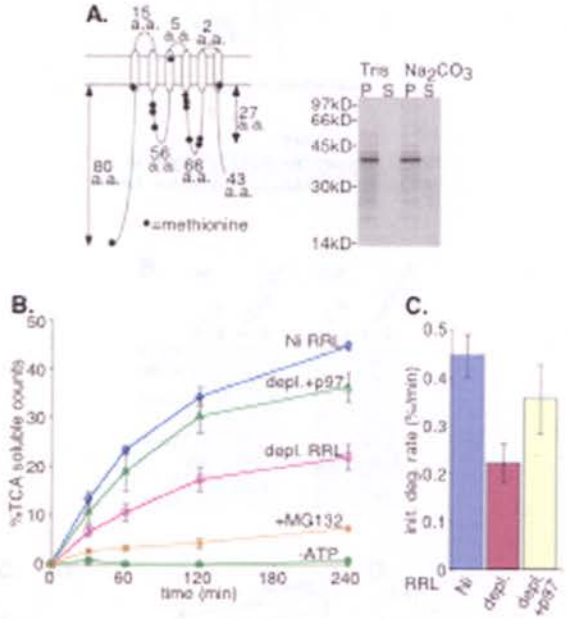

Figure A-5. P97 augmented degradation of a CFTR TM domain. **(A)** Schematic of the TMD1 construct, indicating location methionines and the number of amino acid residues in cytosolic or lumenal loops. Carbonate extraction of *in vitro*-expressed TMD1. **(B)** TMD1 degradation was assayed in the presence and absence of p97. Also shown are effects of MG132 and ATP depletion **(C)** Initial rates of TM1-6 degradation in mock RRL, p97-depleted RRL and after p97 supplementation.

Fig. A-6

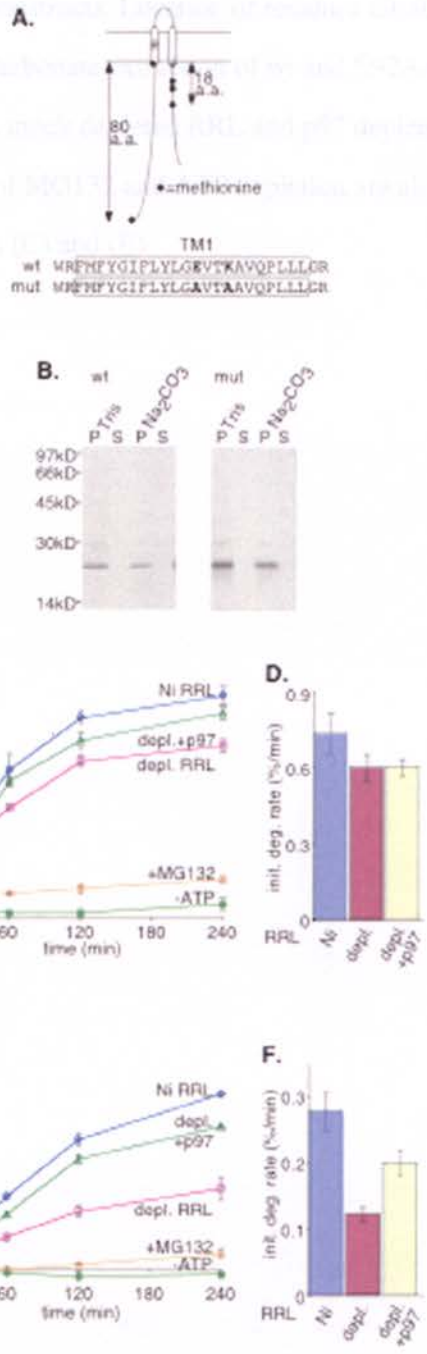
A.
18 a.a.
80 a.a.
•=methionine
TM1
wt MRFMFYGIPLYLGAVTAAVQPLLLCR
mut MRFMFYGIPLYLGAVTAAVQPLLLCR
B.
wt
mut
P Tris S P Na2CO3 S
97kD
66kD
45kD
30kD
14kD
C.
WT
Ni RRL
depl.+p97
depl. RRL
+MG132
-ATP
%TCA soluble counts
time (min)
D.
init. deg. rate (%/min)
RRL
Ni
depl.
depl. +p97
E.
Mut
Ni RRL
depl. +p97
depl. RRL
+MG132
-ATP
%TCA soluble counts
time (min)
F.
init. deg. rate (%/min)
RRL
Ni
depl.
depl. +p97

Figure A-6. p97 effects are influenced byTM segment hydrophobicity. (A) Topology and methionine distribution TM1-2 constructs. Location of residues Glu92 and Lys95 are shown within the TM1 sequence. (B) Carbonate extraction of wt and E92A/K95A polypeptides. (C&E) Degradation assays performed in mock depleted RRL and p97 depleted RRL with or without added recombinant p97. Effects of MG132 and ATP depletion are also shown. (D&F) Initial degradation rates calculated from (C) and (E).

Fig. A-7

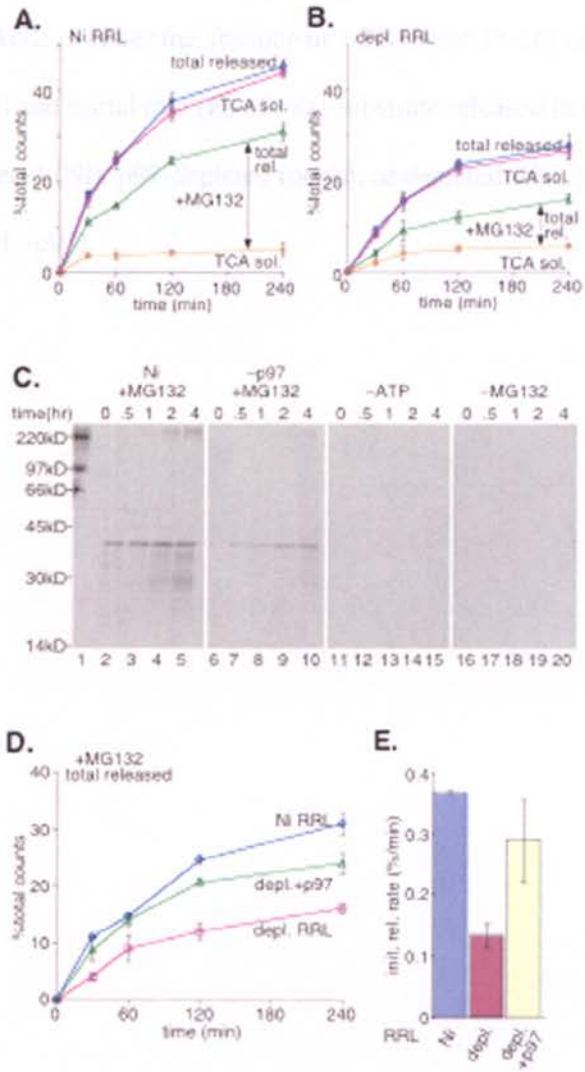

Figure A-7. p97 directly facilitates membrane extraction of TMs. TMD1 degradation reactions were carried out in **(A)** mock- or **(B)** p97-depleted depleted RRL and supernatants were analyzed for CFTR fragments prior to (total released) or after (TCA sol) TCA precipitation. Vertical arrow indicates TCA insoluble peptide fragments that accumulate in the supernatant. **(C)** Autoradiograms showing dislocated full length

TMD1 degradation products generated in the presence of MG132 (lanes 1-10), in Mock-depleted (Ni lanes 1-5) or p97-depleted (–p97, lanes 6-10) RRL. No fragments were visualized by SDS-PAGE in either the absence of ATP (lanes 11-16) or MG132 (lanes 16-20). The extent (**D**) and initial rate (**E**) of total substrate released in the presence of MG132 in mock depleted (Ni), p97-depleted (depl.), or depleted RRL supplemented with recombinant p97 (depl.+p97).

Fig. A-8

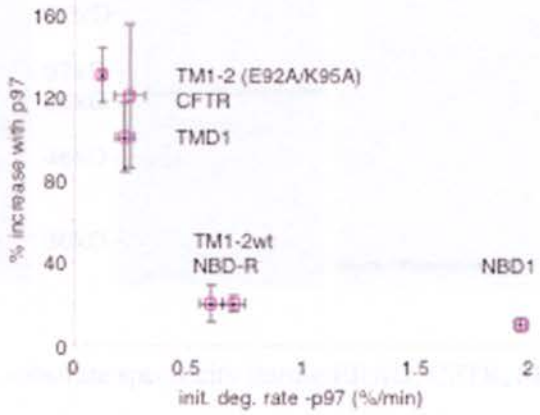

Figure A-8. P97 effect is inversely related to the rate of degradation. The stimulatory effect (% increase) of p97 on the degradation rate was plotted as a function of the initial degradation rate in the absence of p97.

Fig. Supp. A-1

Fig. Supp A-1. RRL substrate specificity during ERAD. CFTR, SRP receptor α subunit (SRPR α), bovine prolactin and human aquaporin 2 (AQP2) were synthesized in vitro in the presence of microsomal membranes and ^{35}S-methionine. Microsomes were then pelleted, resuspended, and added to degradation reactions as described in Methods. Reactions were incubated at 37. C for 4h, and aliquots were taken at the indicated time points and analyzed directly by SDS-PAGE and autoradiography. Results show marked differences in the stability between CFTR and the single-spanning, lumenal and six-spanning substrates, respectively. RRL is thus highly specific in discriminating in vitro synthesized proteins as potential ERAD substrates, even those with large cytosolic domains (SRPRα)

Fig. Supp A-2

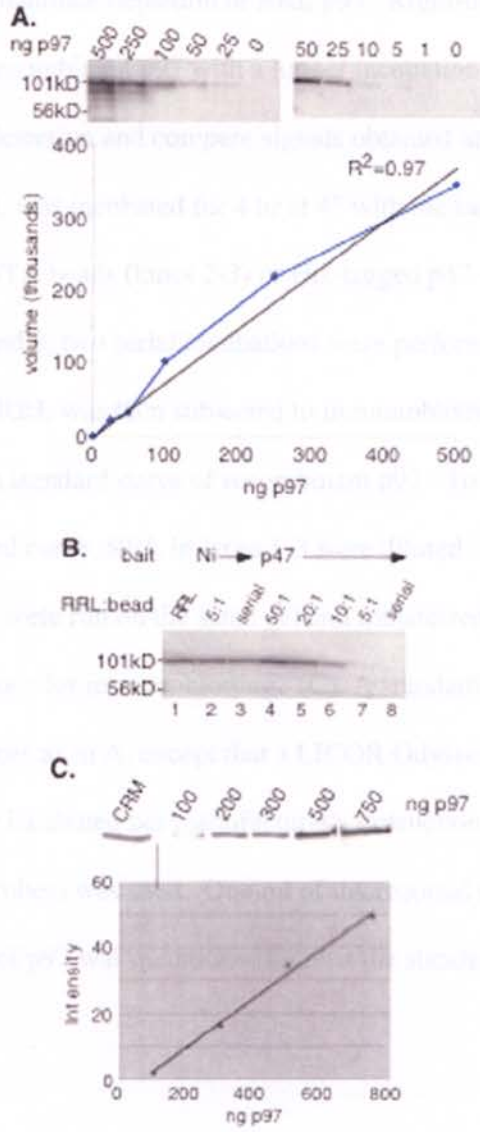

Fig. Supp. A-2 Standard curves for p97 Quantitation. (A) Immunoblots of purified recombinant His6-tagged p97 using mAb anti-p97 (1:500; BD Transduction Laboratories) and 2° anti-mouse-AP (1:2500; Promega) with ECF substrate (Amersham Biosciences). The blot was scanned on a Biorad FX phosphoimager and fluorescent

signals were quantitated using QuanityOne software. Plot shows a representative standard curve used to quantitate depletion of RRL p97. Right-hand panel shows decreasing amounts of recombinant p97 with a longer incubation in ECF substrate to determine the limits of detection and compare signals obtained at very low p97 concentrations. (B) RRL was incubated for 4 hr at 4° with the indicated ratio (RRL:beads) using Ni-NTA beads (lanes 2-3) or His-tagged p47-saturated Ni-NTA beads (lanes 4-8). In lanes 3 and 8, two serial incubations were performed using 5/1 bead volume each. Depleted RRL was then subjected to immunoblotting as in panels A and B and quantitated against a standard curve of recombinant p97. To ensure that values would fall on the standard curve, RRL in lanes 1-3 were diluted 2 fold. For each RRL depletion, p97 standards were run on the same gel and transferred to the same membrane to ensure similar conditions for immunoblotting. (C) A standard curve was developed for microsomal membranes as in A, except that a LICOR Odyssey was used for quantitation. Blots were incubated per manufacturer's instructions, and 2° anti-mouse-Alexa 680 (Molecular Probes) was used. One ml of microsomal membranes was also blotted, and the amount of p97 was quantitated against the standard curve.

Fig. Supp. A-3

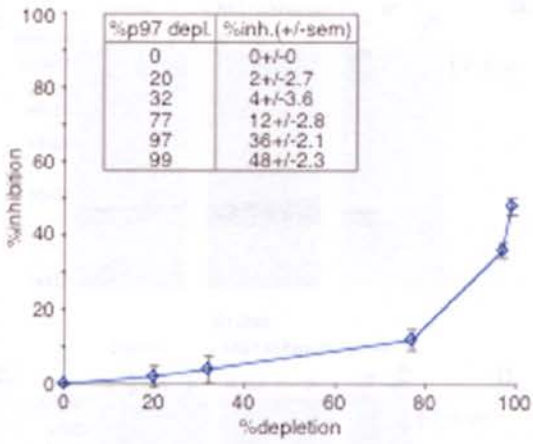

Fig. Supp. A-3 Effect of partial p97 depletion on CFTR degradation activity. RRL p97 was depleted by incubation in varying amounts of p47-saturated Ni-NTA coated beads. Residual p97 was measured by immunoblotting using a standard curve of recombinant protein (inset). CFTR degradation was then measured in depleted RRL based on conversion to TCA soluble fragments as described in Methods. The % inhibition in degradation (based on Mock-depleted RRL) was plotted as a function of the % of p97 depletion. Results show that modest p97 depletion as little effect on CFTR degradation, which likely reflects a relative excess of p97 over substrate and/or ERAD-dependent cofactors. At high levels of depletion (>95%) a linear relationship is observed (see Figure 3E in main text).

Fig. Supp. A-4

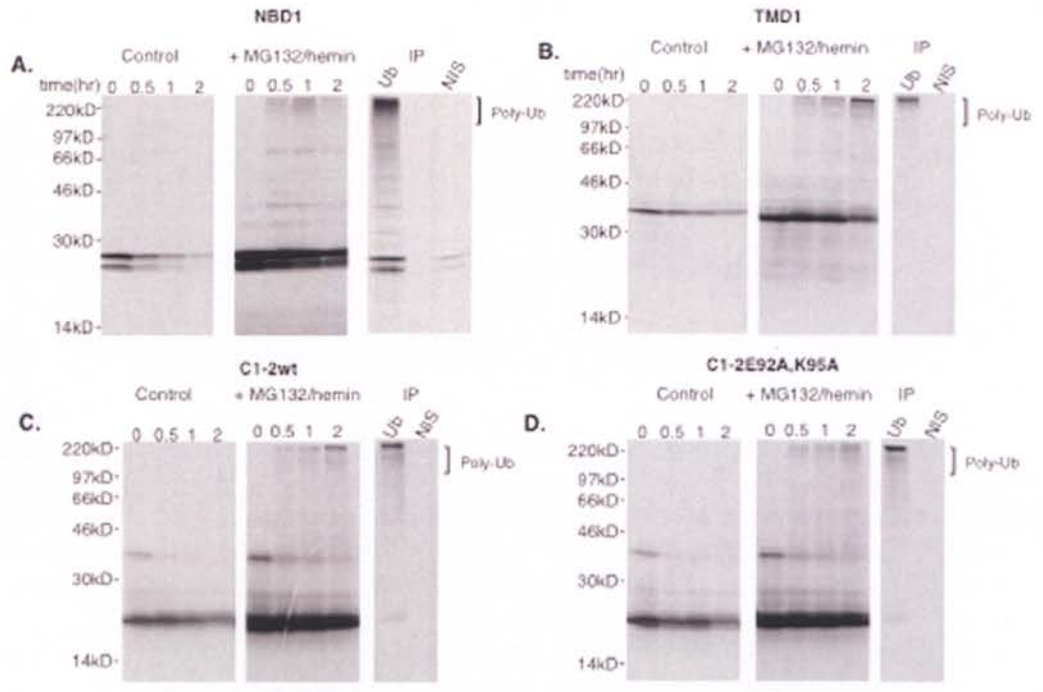

Fig. Supp A-4 Ubiquitination of CFTR cytosolic and TM domains. Degradation of indicated CFTR domains was carried out under standard conditions (as in Methods) or in the presence of proteasome inhibitors MG132 (100 μM) and hemin (40μM) as indicated. Aliquots were analyzed by SDS-PAGE and autoradiography at indicated time points. At 2 hours, remaining samples were immunoprecipitated (IP) by incubating overnight at 4∞C in 0.1% SDS, 1% NP-40, 10% glycerol, 150mM NaCl, 2mM EDTA, and 25mM Tris-Cl, pH 7.5 in the presence of FK2 anti-polyubiquitin antibody (BioMol) or non-immune serum. Protein G was added for the last hour of incubation, and beads were washed 3 times in IP buffer and analyzed by SDS-PAGE and autoradiography. To better visualize ubiquitinated products, samples containing inhibitors were exposed 46 fold longer than controls. Immunoprecipitated products were exposed an additional 10X. For

NBD1, MG132 was added directly to translation reactions and incubated at 37∞C for 2 hours.

Fig. Supp. A-5

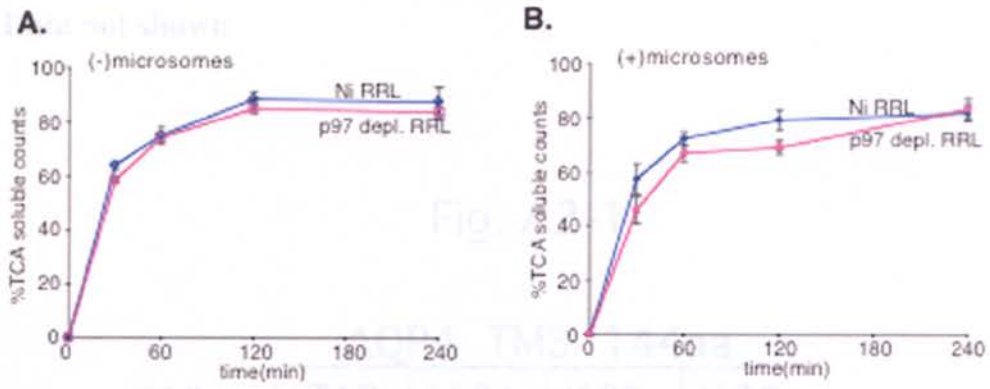

Fig. Supp. A-5 Degradation of NBD1 in presence and absence of microsomal membranes. His-tagged, radiolabeled NBD1 was translated in vitro, isolated and added to degradation reactions containing mock (Ni RRL) or p97-depleted RRL. In panel p97-depleted microsomal membranes were added to recapitulate degradation conditions for TM constructs. Aliquots were taken at the indicated time points, and degradation was determined based on conversion of NBD1 to TCA-soluble fragments. Data show that NBD1 degradation is not significantly affected by the presence or absence of microsomal membranes.

Appendix 2

Data not shown

Fig. A2-1

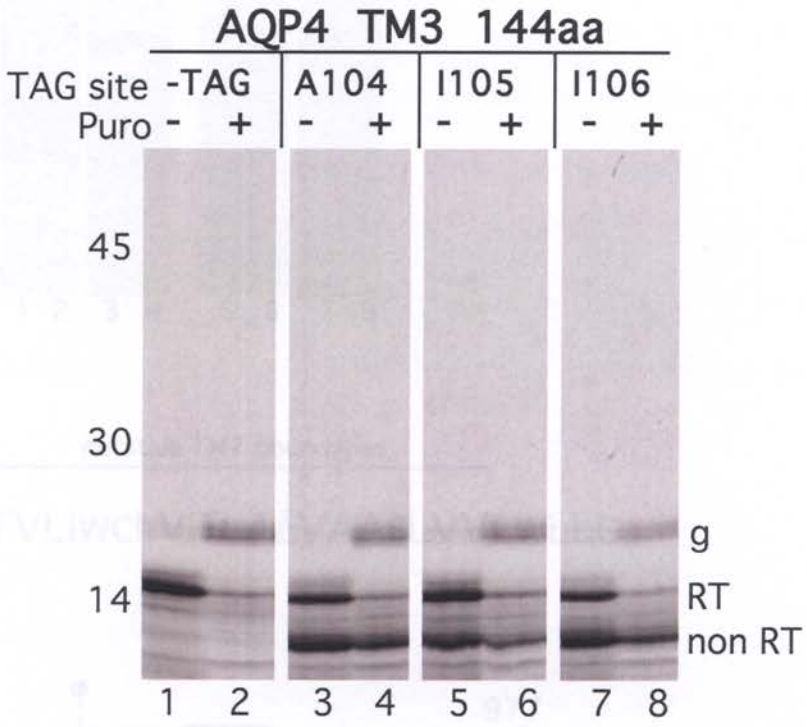

Fig. A-2-1. AQP 4 is glycosylated when released with puromycin demonstrating that the C-terminus is translocated. Integration intermediates that remain ribosome tethered are unable to rotate to a type II topology and be glycosylated (lanes 1, 3, 5, 7). Release with puromycin allows >75% of read-through (RT) polypeptide to rotate to a type II topology and be glycosylated (g).

Fig. A2-2

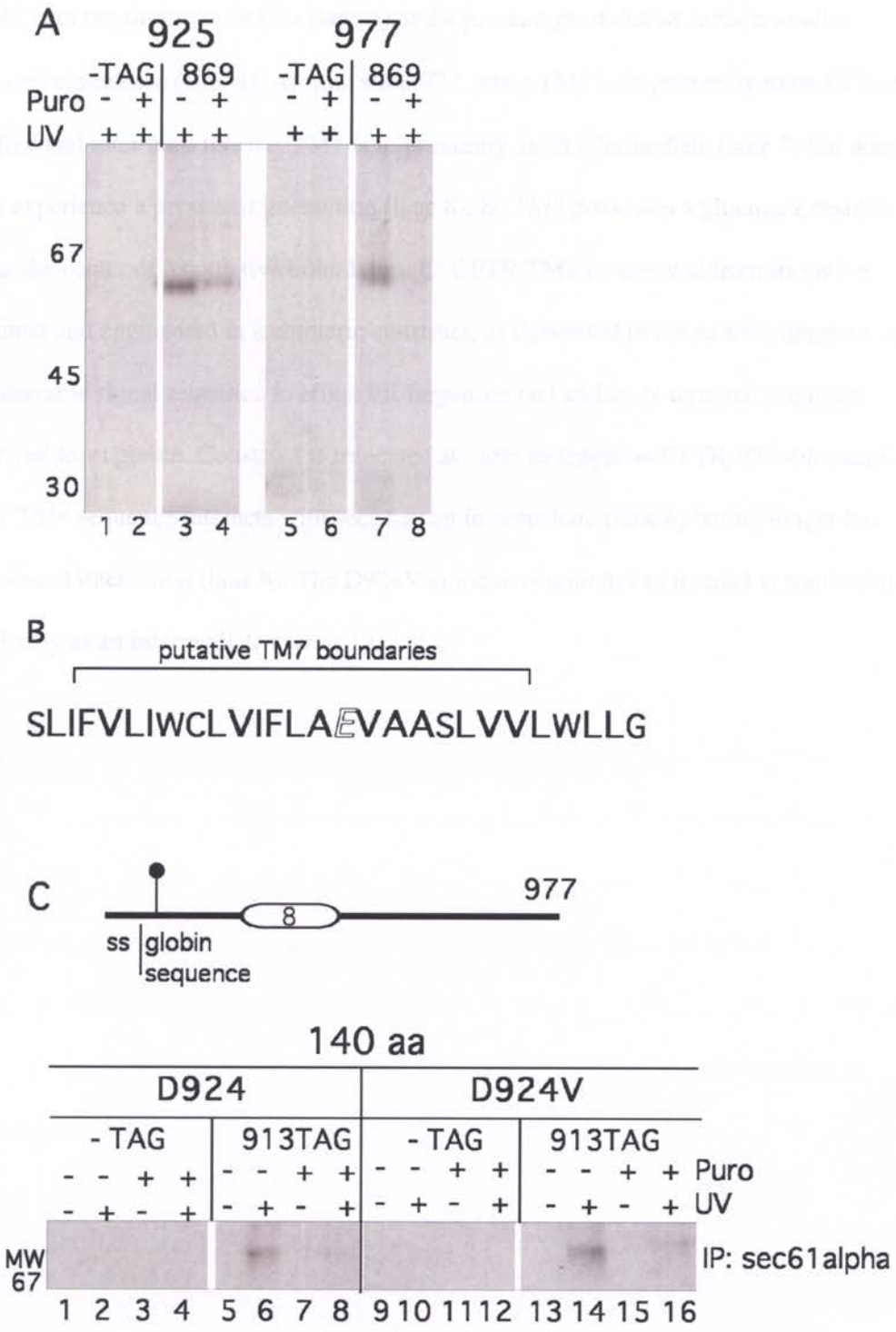
A
925
977
-TAG
869
-TAG
869
Puro
UV
67
45
30
1 2 3 4 5 6 7 8
B
putative TM7 boundaries
SLIFVLIWCLVIFLAEVAASLVVLWLLG
C
977
8
ss
globin
sequence
140 aa
D924
D924V
- TAG
913TAG
- TAG
913TAG
Puro
UV
MW
67
IP: sec61alpha
1 2 3 4 5 6 7 8 9 10 11 12 13 14 15 16

Fig. A2-2. TM7 also has a prolonged and persistent interaction with sec61α. A: ANB probe placed at residue 869 in center of TM7. At truncation 925, prior to entry of TM8, TM7 is in proximity to sec61α (lane 3) and a percentage of chains remain so after puromycin release (lane 4). At truncation 977, when TM8 is in proximity to sec61 both before and after puro release, TM7 is in proximity as an intermediate (lane 7) but does not experience a persistent interaction (lane 8). B: TM7 possesses a glutamate residue near the center of its putative boundaries. C: CFTR TM8 is removed from its native context and engineered in a chimeric construct, as illustrated in the cartoon diagram, with a cleavable signal sequence to effect ER targetting (ss) and an N-terminal sequence derived from globin. Construct is truncated at same aa length as CFTR-977 truncation. WT TM8 sequence interacts with sec61 as an intermediate (lane 6) but no longer has persistent interaction (lane 8). The D924V construct continues to interact at truncation 977 only as an intermediate (lanes 12, 14).

Fig. A2-3

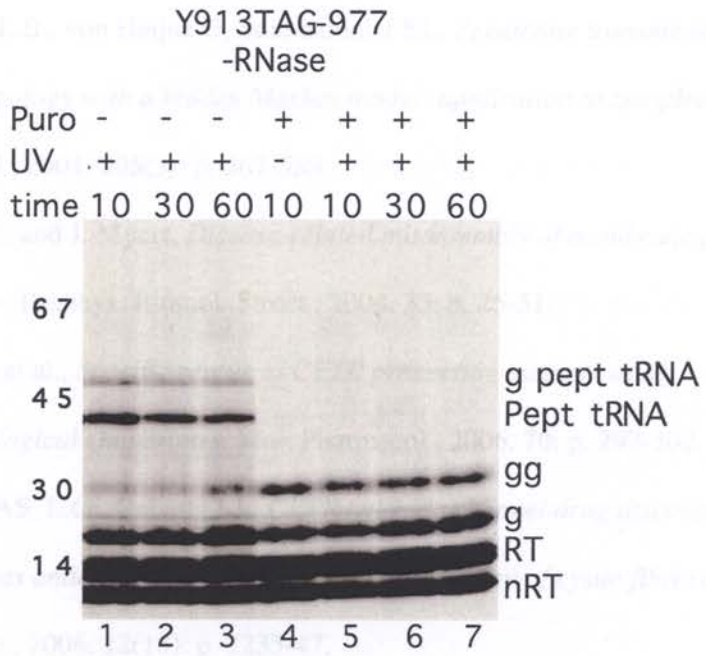

Fig. A2-3. Peptidyl-tRNA bond is stable for at least 1 hour post-translation.

Y913 TAG translated in presence of amber suppressor tRNA lacking the ANB probe. Peptidyl-tRNA is stable in RRL at 24° for at least 1 hour (lanes 1-3). Puromycin effectively releases nascent chain (lanes 4-7). No probe independent crosslinks are noted. nRT- non-read through band; RT-read-through band; g-singly glycosylated; gg-doubly glycosylated; pept tRNA- peptidyl-tRNA band; g pept tRNA- glycosylated peptidyl-tRNA band.

VI. References

1. Krogh A, L.B., von Heijne G, Sonnhammer EL, *Predicting transmembrane protein topology with a hidden Markov model: application to complete genomes.* J Mol Biol., 2001. **305**(3): p. 567-580.
2. Sanders, C. and J. Myers, *Disease-related misassembly of membrane proteins.* Annu. Rev. Biophys. Biomol. Struct., 2004. **33**: p. 25-51.
3. Wang, C., et al., *Specific rescue of CFTR processing mutants using pharmacological chaperones.* Mol. Pharmacol., 2006. **70**: p. 297-302.
4. Verkman AS, L.G., Galietta LJ., *CFTR chloride channel drug discovery--inhibitors as antidiarrheals and activators for therapy of cystic fibrosis.* Curr Pharm Des., 2006. **12**(18): p. 2235-47.
5. Dill, K., *Dominant forces in protein folding.* Biochemistry., 1990. **29**(31): p. 7133-55.
6. Acampora, *Reversible denaturation of sperm whale myoglobin. I. Dependence on temperature, pH, and composition.* J Am Chem Soc., 1967. **89**(7): p. 1543-7.
7. Popot, J.L. and D. Engelman, *Membrane protein folding and oligomerization: the two stage model.* Biochem., 1990. **29**: p. 4031-4037.
8. Popot, J. and D. Engelman, *Helical membrane protein folding, stability and evolution.* Ann. Rev. Biochem., 2000. **69**: p. 881-922.
9. Mothes, W., et al., *Molecular mechanism of membrane protein integration into the endoplasmic reticulum.* Cell, 1997. **89**: p. 523-533.

10. Martoglio, B., et al., *The protein-conducting channel in the membrane of the endoplasmic reticulum is open laterally toward the lipid bilayer*. Cell, 1995. **81**: p. 207-214.

11. Kuroiwa, T., et al., *Reinitiation of protein translocation across the endoplasmic reticulum membrane for the topogenesis of multispanning membrane proteins*. J. Biol. Chem., 1996. **271**: p. 6423-6428.

12. Skach, W., M.C. Calayag, and V. Lingappa, *Evidence for an alternate model of human P-glycoprotein structure and biogenesis*. J Biol. Chem., 1993. **268**: p. 6903-6908.

13. Wilkinson, B., A. Critchley, and C. Stirling, *Determination of the transmembrane topology of yeast Sec61p, an essential component of the endoplasmic reticulum translocation complex*. J. Biol. Chem., 1996. **271**: p. 25590-25597.

14. Heinrich, U., et al., *The Sec61p complex mediates the integration of a membrane protein by allowing lipid partitioning of the transmembrane domain*. Cell, 2000. **102**: p. 233-244.

15. Carveth, K., et al., *Cooperativity and flexibility of cytsic fibrosis transmembrane conductance regulator transmembrane segments poarticipate in membrane localization of a charged residue*. J. Biol. Chem., 2002. **277**: p. 39507-39514.

16. Frydman, J., *Folding of newly translated proteins in vivo: the role of molecular chaperones*. Annu Rev Biochem., 2001. **70**: p. 603-47.

17. Flynn, G., Pohl J, Flocco MT, Rothman JE., *Peptide-binding specificity of the molecular chaperone BiP*. Nature, 1991. **353**: p. 726-30.

18. Johnson BD, C.A., Felts SJ, Bouhouche I, Catelli MG, Toft DO., *Hsp90 chaperone activity requires the full-length protein and interaction among its multiple domains.* J Biol Chem, 2000. **275**(42): p. 32499-507.

19. Parodi, A., *Role of N-oligosaccharide endoplasmic reticulum processing reactions in glycoprotein folding and degradation.* Biochem, J, 2000. **348**(Pt 1): p. 1-13.

20. Parodi, A., *Protein glucosylation and its role in protein folding.* Annu Rev Biochem., 2000. **69**: p. 69-93.

21. Oda Y, H.N., Wada I, Nagata K., *EDEM as an acceptor of terminally misfolded glycoproteins released from calnexin.* Science, 2003. **299**: p. 1394-7.

22. Görlich, D. and T. Rapoport, *Protein translocation into proteoliposomes reconstituted from purified components of the endoplasmic reticulum membrane.* Cell, 1993. **75**: p. 615-630.

23. Keenan RJ, F.D., Stroud RM, Walter P., *The signal recognition particle.* Annu Rev Biochem., 2001. **70**: p. 755-75.

24. Crowley, K., G. Reinhart, and A. Johnson, *The signal sequence moves through a ribosomal tunnel into a noncytoplasmic aqueous environment at the ER membrane early in translocation.* Cell, 1993. **73**: p. 1101-1115.

25. Crowley, K., et al., *Secretory proteins move through the endoplasmic reticulum membrane via an aqueous, gated pore.* Cell, 1994. **78**: p. 461-471.

26. Johnson, A. and M. van Waes, *The Translocon: A dynamic gateway at the ER membrane.* Ann. Rev. Cell Dev. Biol, 1999. **15**: p. 799-842.

27. Liao, S., et al., *Both lumenal and cytosolic gating of the aqueous translocon pore are regulated from inside the ribosome during membrane protein integration.* Cell, 1997. **90**: p. 31-42.

28. Hamman, B., L. Hendershot, and A. Johnson, *BiP maintains the permeability barrier of the ER membrane by sealing the lumenal end of the translocon pore before and early in translocation.* Cell, 1998. **92**: p. 747-758.

29. Alder, N., et al., *The molecular mechanisms underlying BiP-mediated gating of the Sec61 translocon of the endoplasmic reticulum.* J. Cell. Biol., 2005. **168**: p. 389-99.

30. Matlack, K., et al., *BiP acts as a molecular ratchet during posttranslational transport of prepro-α factor across the ER membrane.* Cell, 1999. **97**: p. 553-564.

31. Mothes, W., S. Prehn, and T. Rapoport, *Systematic probing of the environment of a translocating secretory protein during translocation through the ER membrane.* EMBO J., 1994. **13**: p. 3973-3982.

32. Hegde, R., et al., *TRAM regulated the exposure of nascent secretory proteins to the cytosol during translocation into the endoplasmic reticulum.* Cell, 1998. **92**: p. 621-631.

33. Do, H., et al., *The cotranslational integration of membrane proteins into the phospholipid bilayer is a multistep process.* Cell, 1996. **85**: p. 369-378.

34. Görlich, D., et al., *A protein of the endoplasmic reticulum involved in early polypeptide translocation.* Nature, 1992. **357**: p. 47-52.

35. Voight, S., et al., *Signal sequence-dependent function of the TRAM protein during early phases of protein transport across the endoplasmic reticulum membrane.* J. Cell. Biol., 1996. **134**: p. 25-35.

36. McCormick, P., et al., *Cotranslational protein integration into the ER membrane is mediated by the binding of nascent chains to translocon proteins.* Mol. Cell, 2003. **12**: p. 329-341.

37. Fons, R., B. Bogert, and R. Hegde, *Substrate-specific function of the translocon-associated protein complex during translocation across the ER membrane.* J. Cell. Biol, 2003. **160**: p. 529-539.

38. Nagasawa K, H.T., Hosokawa N, Kaufman RJ, Nagata K., *Simultaneous induction of the four subunits of the TRAP complex by ER stress accelerates ER degradation.* EMBO J., 2007: p. 483-9.

39. Chavan M, L.W., *The molecular basis of coupling of translocation and N-glycosylation.* Trends Biochem Sci., 2006(1): p. 17-20.

40. Chavan M, Y.A., Lennarz WJ., *Subunits of the translocon interact with components of the oligosaccharyl transferase complex.* J Biol Chem., 2005. **280**(24): p. 22917-24.

41. Shibatani, T., et al., *Proteomic analysis of mammalian oligosaccharyltransferase reveals multiple subcomplexes that contain Sec61, TRAP and two potential new subunits.* Biochemistry, 2005. **44**: p. 5982-5992.

42. Jungnickel, B. and T. Rapoport, *A posttargeting signal sequence recognition event in the endoplasmic reticulum membrane.* Cell, 1995. **82**: p. 261-270.

43. Oliver, J., et al., *The Sec61 complex is essential for the insertion of proteins into the membrane of the endoplasmic reticulum.* FEBS Letters, 1995. **362**: p. 126-130.

44. Beckmann, R., et al., *Alignment of conduits for the nascent polypeptide chain in the ribosome-Sec61 complex.* Science, 1997. **278**: p. 2123-2126.

45. Snapp, E., et al., *The organization of engaged and quiescent translocons in the endoplasmic reticulum of mammalian cells.* J. Cell. Biol., 2004. **164**: p. 997-1007.

46. Menetret, J., et al., *The structure of ribosome-channel complexes engaged in protein translocation.* Mol. Cell, 2000. **6**: p. 1219-32.

47. Breyton, C., et al., *Three-dimensional structure of the bacterial protein-translocation complex SecYEG.* Nature, 2002. **418**: p. 662-665.

48. van den Berg, B., et al., *X-ray structure of a protein-conducting channel.* Nature, 2004. **427**: p. 36-44.

49. Menetret, J.-F., et al., *Architecture of the ribosome-channel complex derived from native membranes.* J. Mol. Biol., 2005. **348**: p. 445-457.

50. Mitra, K., et al., *Structure of the E. coli protein-conducting channel bound to a translating ribosome.* Nature, 2005. **438**: p. 318-324.

51. Hamman, B., et al., *The aqueous pore through the translocon has a diameter of 40-60Å during cotranslational protein translocation at the ER membrane.* Cell, 1997. **89**: p. 535-544.

52. Haigh, N. and A. Johnson, *A new role for BiP: closing the aqueous translocon pore during protein integration into the ER membrane.* J. Cell. Biol., 2002. **156**: p. 261-270.

53. Woolhead, C., A. Johnson, and H. Bernstein, *Translation arrest requires two-way communication between a nascent polypeptide and the ribosome*. Mol. Cell, 2006. **22**: p. 587-598.

54. Skach, W. and V. Lingappa, *Amino terminus assembly of human P-glycoprotein at the endoplasmic reticulum is directed by cooperative actions of two internal sequences*. J. Biol. Chem., 1993. **268**: p. 23552-23561.

55. Borel, A. and S. Simon, *Biogenesis of polytopic membrane proteins: membrane segments of P-glycoprotein sequentially translocate to span the ER membrane*. Biochemistry, 1996. **35**: p. 10587-10594.

56. Heinrich, S. and T. Rapoport, *Cooperation of transmembrane segments during integration of a double-spanning protein into the ER membrane*. EMBO J, 2003. **22**: p. 3654-3663.

57. Goder, V., T. Junne, and M. Spiess, *Sec61p contributes to signal sequence orientation according to the positive inside rule*. Mol. Biol. Cell, 2004. **15**: p. 1470-1478.

58. Goder, V., C. Bieri, and M. Spiess, *Glycosylation can influence topogenesis of membrane proteins and reveals dynamic reorientation of nascent polypeptides within the translocon*. J. Cell. Biol., 1999. **147**: p. 257-266.

59. Junne, T., et al., *The plug domain of yeast Sec61p is important for efficient protein translocation, but is not essential for cell viability*. Mol. Biol. Cell, 2006. **17**: p. 4062-4068.

60. Osborne, A.R. and T.A. Rapoport, *Protein translocation is mediated by oligomers of the SecY complex with one SecY copy forming the channel.* Cell, 2007. **129**(1): p. 97-110.

61. Tam PC, M.A., Chan KK, Duong F., *Investigating the SecY plug movement at the SecYEG translocation channel.* EMBO J., 2005. **24**(19): p. 3380-8.

62. Deutsch, C., *The birth of a channel.* Neuron, 2003. **40**(2): p. 265-76.

63. Woolhead, C., P. McCormick, and A. Johnson, *Nascent membrane and secretory proteins differ in FRET-detected folding far inside the ribosome and in their exposure to ribosomal proteins.* Cell, 2004. **116**: p. 725-736.

64. Beckmann, R., et al., *Architecture of the protein-conducting channel associated with the translating 80S ribosome.* Cell, 2001. **107**: p. 361-72.

65. Morgan, D., et al., *Structure of the mammalian ribosome-channel complex at 17A resolution.* J. Mol. Biol., 2002. **324**: p. 871-886.

66. Potter, M. and C. Nicchitta, *Endoplasmic reticulum-bound ribosomes reside in stable association with the translocon following termination of protein synthesis.* J. Biol. Chem, 2002. **277**: p. 23314-23320.

67. Neuhof A, R.M., Jungnickel B, Kalies KU, Rapoport TA., *Binding of signal recognition particle gives ribosome/nascent chain complexes a competitive advantage in endoplasmic reticulum membrane interaction.* Mol Biol Cell., 1998. **9**(1): p. 103-15.

68. Schaletzky J, R.T., *Ribosome binding to and dissociation from translocation sites of the endoplasmic reticulum membrane.* Mol Biol Cell., 2006. **9**: p. 3860-9.

69. Hessa, T., et al., *Recognition of transmembrane helices by the endoplasmic reticulum translocon.* Nature, 2005. **433**: p. 377-381.

70. Matlack KE, M.W., Rapoport TA., *Protein translocation: tunnel vision.* cell, 1998. **92**(3): p. 381-90.

71. Hessa T, M.M., von Heijne G., *Stop-transfer efficiency of marginally hydrophobic segments depends on the length of the carboxy-terminal tail.* EMBO J, 2003(2): p. 178-83.

72. Borel, A. and S. Simon, *Biogenesis of polytopic membrane proteins: Membrane segments assemble within translocation channels prior to membrane integration.* Cell, 1996. **85**: p. 379-389.

73. Hessa T, W.S., von Heijne G., *Membrane insertion of a potassium-channel voltage sensor.* Science, 2005. **308**: p. 1743.

74. Sadlish, H., et al., *Sequential triage of transmembrane segments by Sec61α during biogenesis of a native multispanning membrane protein.* Nat. Struct. Mol. Biol., 2005. **12**: p. 870-878.

75. Wilson, C., et al., *Ribophorin I associates with a subset of membrane protiens after their integration at the Sec61 translocon.* J. Biol. Chem., 2005. **280**: p. 4195-4206.

76. Adamian L, L.J., *Helix-helix packing and interfacial pairwise interactions of residues in membrane proteins.* J Mol Biol., 2001. **311**(4): p. 891-907.

77. Choma, C., et al., *Asparagine-mediated self-association of a model transmembrane helix.* Nat. Struct. Mol. Biol., 2000. **7**: p. 161-166.

78. Hermansson M, v.H.G., *Inter-helical hydrogen bond formation during membrane protein integration into the ER membrane.* J Mol Biol, 2003. **334**(4): p. 803-9.

79. Meindl-Beinker, N., et al., *Asn- and Asp-mediated interactions between transmembrane helices during translocon-mediated membrane protein assembly.* EMBO Rep., 2006. **7**: p. 1111-1116.

80. Zhou, F., et al., *Interhelical hydrogen bonding drives strong interactions in membrane proteins.* Nat. Struct. Biol., 2000. **7**: p. 154-160.

81. Zhou FX, M.H., Brunger AT, Engelman DM., *Polar residues drive association of polyleucine transmembrane helices.* Proc Natl Acad Sci U S A., 2001. **98**(5): p. 2250-5.

82. Landolt-Marticorena C, W.K., Deber CM, Reithmeier RA., *Non-random distribution of amino acids in the transmembrane segments of human type I single span membrane proteins.* J Mol Biol., 1993. **229**(3): p. 602-8.

83. Murata, K., et al., *Structural determinants of water permeation through aquaporin-1.* Nature, 2000. **407**: p. 599-605.

84. Fu, D., et al., *Structure of a glycerol-conducting channel and the basis for its selectivity.* Science, 2000. **290**: p. 481-486.

85. Sui, H., et al., *Structural basis of water specific transport through the AQP1 water channel.* Nature, 2001. **414**: p. 872-878.

86. Nielsen, S. and P. Agre, *The aquaporin family of water channels in the kidney.* Kidney Int., 1995. **48**: p. 1057-1068.

87. Fujiyoshi, Y., et al., *Structure and function of water channels.* Curr. Opin. Struc. Biol., 2002. **12**(4): p. 509-15.

88. Tajkhorshid, E., et al., *Control of the selectivity of the aquaporin water channel family by global orientational tuning*. Science, 2002. **296**: p. 525-530.

89. Agre P, L.M., Devidas S, Guggino WB., *Aquaporins and ion conductance.* Science, 1997. **275**: p. 1490.

90. Verkman, A.S., *More than just water channels: unexpected cellular roles of aquaporins*. Journal of Cell Science, 2005. **118**(15): p. 3225-3232.

91. Verkman, A., et al., *Water transport across mammalian cell membranes*. Am. J. Physiol., 1996. **270 (Cell Physiol. 39)**: p. C12-C30.

92. Knepper MA, I.T., *Regulation of aquaporin-2 water channel trafficking by vasopressin*. Curr Opin Cell Biol., 1997. **9**(4): p. 560-4.

93. Kuznetsov, G. and S. Nigam, *Folding of secretory and membrane proteins.* NEJM, 1998. **339**: p. 1688-95.

94. Tamarappoo, B.K. and A. Verkman, *Defective aquaporin-2 trafficking in nephrogenic diabetes insipidus and correction by chemical chaperones*. J. Clin. Invest., 1998. **101**: p. 2257-2267.

95. Morello, J.-P. and D. Bichet, *Nephrogenic diabetes insipidus*. Annu. Rev. Physiol., 2001. **63**: p. 607-630.

96. Agre, p., *Membrane water transport and aquaporins: looking back*. Biol Cell., 2005. **97**(6): p. 355-6.

97. Verkman, A., et al., *Three distinct roles of aquaporin-4 in brain function revealed by knockout mice*. Bioch. Biophys. Acta, 2006. **1758**: p. 1085-1093.

98. Shi, L.-B., et al., *Distinct biogenesis mechanisms for water channels MIWC and CHIP28 at the endoplasmic reticulum.* Biochemistry, 1995. **34**: p. 8250-8256.

99. Foster, W., et al., *Identification of sequence determinants that direct different intracellular folding pathways for AQP1 and AQP4.* J. Biol. Chem., 2000. **275**: p. 34157-34165.

100. Skach, W., et al., *Biogenesis and transmembrane topology of the CHIP28 water channel in the endoplasmic reticulum.* J. Cell Biol., 1994. **125**: p. 803-815.

101. Foster, W., et al., *Identification of sequence determinants responsible for different intracellular folding pathways of AQP1 and AQP4.* J. Am. Soc. Nephrology, 1998. **9**: p. A0128.

102. Buck, T., et al., *A novel tripartite structural motif involved in aquaporin topogenesis, monomer folding and tetramerization.* Nat. Struct. Mol. Biol., 2007. **14**: p. 762-769.

103. Riordan, J.R., et al., *Identification of the cystic fibrosis gene: cloning and characterization of complementary DNA.* Science, 1989. **245**: p. 1066-1072.

104. Skach, W.R., *Defects in Processing and Trafficking of CFTR.* Kidney International, 2000. **57**: p. 825-831.

105. Lu, Y., et al., *Co- and Posttranslational mechanisms direct CFTR N-terminus transmembrane assembly.* J. Biol. Chem., 1998. **273**: p. 568-576.

106. Hollenstein K, D.R., Locher KP., *Structure and mechanism of ABC transporter proteins.* Curr Opin Struct Biol., 2007. **17**(4): p. 412-8.

107. Dawson, R. and K.P. Locher, *Structure of a bacterial multidrug ABC trasnporter.* Nature, 2006. **443**: p. 180-185.

108. Lewis, H., et al., *Structure of nucleotide-binding domain 1 of the cystic fibrosis transmembrane conductance regulator.* EMBO J, 2004. **23**: p. 282-293.

109. Lewis, H.A., et al., *Impact of the deltaF508 mutation in first nucleotide-binding domain of human cystic fibrosis transmembrane conductance regulator on domain folding and structure*. J Biol Chem, 2005. **280(2)**: p. 1346-53.

110. Du, K., M. Sharma, and G. Lukacs, *The ΔF508 cystic fibrosis mutation impairs domain-domain interactions and arrests post-translational folding of CFTR*. Nature Struct. Mol. Biol., 2004. **12**: p. 17-25.

111. Thibodeau, P., et al., *Side chain and backbone contributions of Phe508 to CFTR folding*. Nature Struct. Mol. Biol., 2004. **12**: p. 10-16.

112. Dalemans W, B.P., Champigny G, Jallat S, Dott K, Dreyer D, Crystal RG, Pavirani A, Lecocq JP, Lazdunski M., *Altered chloride ion channel kinetics associated with the delta F508 cystic fibrosis mutation*. Nature, 1991. **354**: p. 503-4.

113. Gadsby, D., m.P. Vergani, and L. Csanady, *The ABC protein turned chloride channel whose failure causes cystic fibrosis*. Naature, 2006. **440**: p. 477-483.

114. Reddy MM, Q.P., *ENaC activity requires CFTR channel function independently of phosphorylation in sweat duct*. J Membr Biol., 2005. **207**: p. 23-33.

115. Guggino, W., *Outwardly rectifying chloride channels and CF: a divorce and remarriage*. J Bioenerg Biomembr., 1993. **25**(1): p. 27-35.

116. Devor DC, S.A., Lambert LC, DeLuca A, Frizzell RA, Bridges RJ., *Bicarbonate and chloride secretion in Calu-3 human airway epithelial cells*. J Gen Physiol., 1999. **113**(5): p. 743-60.

117. Wine, J., *Acid in the airways. Focus on "Hyperacidity of secreted fluid from submucosal glands in early cystic fibrosis"*. Am J Physiol Cell Physiol., 2006. **290**(3): p. C669-71.

118. Cheng, S.H., et al., *Defective intracellular transport and processing of CFTR is the molecular basis of most cystic fibrosis*. Cell, 1990. **63**: p. 827-834.

119. Yang, Y., et al., *The common variant of cystic fibrosis transmembrane conductance regulator is recognized by hsp70 and degraded in a pre-Golgi nonlysosomal compartment*. Proc. Natl. Acad. Sci. USA, 1993. **90**: p. 9480-9484.

120. Jensen, T., et al., *Multiple proteolytic systems, including the proteosome, contribute to CFTR processing*. Cell, 1995. **83**: p. 129-136.

121. Xiong, X., E. Chong, and W. Skach, *Evidence that endoplasmic reticulum (ER)-associated degradation of cystic fibrosis transmembrane conductance regulator is linked to retrograde translocation from the ER membrane*. J. Biol. Chem, 1999. **274**: p. 2616-2624.

122. Chang XB, C.L., Hou YX, Jensen TJ, Aleksandrov AA, Mengos A, Riordan JR., *Removal of multiple arginine-framed trafficking signals overcomes misprocessing of delta F508 CFTR present in most patients with cystic fibrosis*. Mol Cell, 1999. **4**(1): p. 137-42.

123. Drumm, M., et al., *Chloride conductance expressed by ΔF508 and other mutant CFTRs in Xenopus oocytes*. Science, 1991. **254**: p. 1797-17909.

124. Lukacs, G., et al., *The ΔF508 mutation decreases the stability of cystic fibrosis transmembrane conductance regulator in the plasma membrane*. J. Biol. Chem., 1993. **268**: p. 21592-21598.

125. Zhang, Y., et al., *Hsp70 molecular chaperone facilitates endoplasmic reticulum-associated protein degradation of cystic fibrosis transmembrane conductance regulator in yeast.* Mol. Biol. Cell, 2001. **12**: p. 1303-1314.

126. Amaral, M., *CFTR and chaperones: processing and degradation.* J. Mol. Neurosci., 2004. **23**: p. 41-48.

127. Loo, M., et al., *Perturbation of Hsp90 interaction with nascent CFTR prevents its maturation and accelerates its degradation by the proteasome.* EMBO J., 1998. **17**: p. 6879-6887.

128. Wang, X., et al., *Hsp90 cochaperone Aha1 rescue of the human misfolding disease cystic fibrosis.* Cell, this issue, 2006.

129. Ward, C. and R. Kopito, *Intracellular turnover of cystic fibrosis transmembrane conductance regulator.* J. Biol. Chem., 1994. **269**: p. 25710-25718.

130. Varga, K., et al., *Efficient intracellular processing of the endogenous cystic fibrosis transmembrane conductance regulator in epithelial cell lines.* J. Biol. Chem., 2004. **279(21)**: p. 22578-22584.

131. Kreda SM, M.M., Mengos A, Rochelle L, Yankaskas J, Riordan JR, Boucher R, *Characterization of wild-type and deltaF508 cystic fibrosis transmembrane regulator in human respiratory epithelia.* Mol Biol Ce;ll, 2005. **16**(5): p. 2154-67.

132. Denning, G., et al., *Localization of cystic fibrosis transmembrane conductance regulator in chloride secretory epithelia.* J. Clin. Invest., 1992. **89**: p. 339-349.

133. Egan ME, S.E., Guggino WB., *Differential expression of ORCC and CFTR induced by low temperature in CF airway epithelial cells.* Am J Physiol., 1995. **268**: p. C243-51.

134. Sharma M, B.M., Hu W, Lukacs GL., *Conformational and temperature-sensitive stability defects of the delta F508 cystic fibrosis transmembrane conductance regulator in post-endoplasmic reticulum compartments.* J Biol Chem, 2001. **276**(12): p. 8942-50.

135. Loffing-Cueni D, L.J., Shaw C, Taplin AM, Govindan M, Stanton CR, Stanton BA., *Trafficking of GFP-tagged DeltaF508-CFTR to the plasma membrane in a polarized epithelial cell line.* Am J Physiol Cell Physiol., 2001. **281**(6): p. C1889-97.

136. Sato, S., et al., *Glycerol reverses the misfolding phenotype of the most common cystic fibrosis mutation.* J. Biol. Chem., 1996. **271**: p. 635-638.

137. Pedemonte, N., et al., *Small-molecule correctors of defective DeltaF508-CFTR cellular processing identified by high-throughput screening.* J. Clin. Invest., 2005. **115**: p. 2564-71.

138. Wang Y, L.T., Bartlett MC, Clarke DM., *Correctors Promote Maturation of Cystic Fibrosis Transmembrane Conductance Regulator (CFTR)-processing Mutants by Binding to the Protein.* J Biol Chem, 2007. **282**(46): p. 33247-51.

139. Lukacs, G., et al., *Conformational maturation of CFTR but not its mutant counterpart (delta F508) occurs in the endoplasmic reticulum and requires ATP.* EMBO J., 1994. **13**: p. 6076-86.

140. Xiong, X., et al., *Structural cues involved in ER degradation of G85E and G91R mutant CFTR.* J. Clin. Invest., 1997. **100**: p. 1079-1088.

141. Nilsson, I., et al., *Photocross-linking of nascent chains to the STT3 subunit of the oligosaccharyltransferase complex.* J. Cell Biol., 2003. **161**: p. 715-725.

142. Preston, G.M. and P. Agre, *Isolation of the cDNA for erythrocyte integral membrane protein of 28-kilodaltons - member of an ancient channel family.* Proc. Natl. Acad. Sci. USA, 1991. **88**: p. 11110-11114.

143. Preston, G.M., et al., *Appearance of water channels in Xenopus oocytes expressing red cell CHIP28 protein.* Science, 1992. **256**: p. 385-387.

144. Verkman, A.S., *Mechanisms and regulation of water permeability in renal epithelia.* Am. J. Physiol., 1989. **257**: p. C837-C850.

145. Agre, P., et al., *Aquaporin CHIP - the archetypal molecular water channel.* Am. J. Phys., 1993. **265**: p. F463-F476.

146. Van Hoek, A.N., et al., *Functional unit of 30 kD for proximal tubule water channels as revealed by radiation inactivation.* J. Biol. Chem., 1991. **226**: p. 16633-16635.

147. Nielsen, S., et al., *Aquaporins in the kidney: from molecules to medicine.* Physiol. Rev., 2001. **82**: p. 205-244.

148. Agre, P., et al., *Aquaporin water channels - from atomic structure to clinical medicine.* J. Physiol., 2002. **542**: p. 3-16.

149. Verkman, A. and A. Mitra, *Structure and function of aquaporin water channels.* Am. J. Renal Phys., 2000. **278**: p. F13-F28.

150. Mitra, A., et al., *Projection structure of CHIP28 water channel in lipid bilayer membranes at 14 Angstrom resolution.* Biochemistry, 1994. **33**: p. 12735-12740.

151. Walz, T., et al., *Biologically active 2-dimensional crystals of aquaporin CHIP.* J. Biol. Chem., 1994. **269**: p. 1583-1586.

152. Walz, T., et al., *The three-dimensional structure of aquaporin-1*. Nature, 1997. **387**: p. 624-627.

153. Gonen, T., et al., *Lipid-protein interactions in double-layered two-dimensional AQP0 crystals*. Nature, 2005. **438**: p. 633-638.

154. Lieburg, A., et al., *Patients with autosomal nephrogenic diabetes insipidus homozygous for mutations in the aquaporin 2 water-channel gene*. AM. J. Hum. Genet., 1994. **55**: p. 648-652.

155. Deen, P. and N. Knoers, *Vasopressin type-2 receptor and aquaporin-2 water channel mutants in nephrogenic diapetes insipidus*. Am. J. Med. Sci., 1998. **316**: p. 300-309.

156. Deen, P., et al., *Water channels encoded by mutant aquaporin-2 genes in nephrogenic diabetes insipidus are impaired in their cellular routing*. J. Clin. Invest., 1995. **95**: p. 2291-2296.

157. Tamarappoo, B., B. Yang, and A. Verkman, *Misfolding of mutant aquaporin-2 water channels in nephrogenic diabetes insipidus*. J. Biol. Chem., 1999. **49**: p. 34825-34831.

158. Hirano, K., et al., *The proteasome is involved in the degradation of different aquaporin-2 mutants causing nephrogenic diabetes insipidus*. Am. J. Path., 2003. **163**: p. 111-120.

159. Verbavatz, J.M., et al., *Tetrameric assembly of CHIP28 water channels in liposomes and cell membranes. A freeze-fracture study*. J. Cell. Biol., 1993. **123**: p. 605-618.

160. Smith, B.L. and P. Agre, *Erythrocyte Mr 28,000 transmembrane protein exists as a multisubunit oligomer similar to channel proteins.* J. Biol. Chem., 1991. **266**: p. 6407-6415.

161. Preston, G., et al., *Membrane topology of aquaporin CHIP - analysis of functional epitope-scanning mutants by vectorial proteolysis.* J. Biol. Chem., 1994. **269**: p. 1668-1673.

162. Schnell, D. and D. Hebert, *Protein translocons: multifunctional mediators of protein translocation across membranes.* Cell, 2003. **112**: p. 491-505.

163. Gilmore, R., Blobel, G., Walter, P., *Protein translocation across the endoplasmic reticulum. I Detection in the microsomal membrane of a receptor for the signal recognition particle.* J. Cell Biol., 1982. **95**: p. 463-469.

164. Walter, P. and V.R. Lingappa, *Mechanisms of protein translocation across the endoplasmic reticulum membrane.* Annu. Rev. Cell Biol., 1986. **2**: p. 499-516.

165. Görlich, D., et al., *A mammalian homolog of SEC61p and SECYp is associated with ribosomes and nascent polypeptides during translocation.* Cell, 1992. **71**: p. 489-503.

166. Wiedmann, M., et al., *A signal sequence receptor in the endoplasmic reticulum membrane.* Nature, 1987. **328**: p. 830 - 833.

167. Song, W., et al., *Role of Sec61alpha in the regulated transfer of the ribosome-nascent chain complex from the signal recognition particle to the translocation channel.* Cell, 2000. **100**: p. 333-343.

168. Krieg, U., P. Walter, and A. Johnson, *Photocrosslinking of the signal sequence of nascent preprolactin to the 54-kilodalton polypeptide of the signal recognition particle.* Proc. Natl. Acad. Sci. USA, 1986. **83**: p. 8604 - 8608.

169. High, S., et al., *The identification of proteins in the proximity of signal-anchor sequences during their targeting to and insertion into the membrane of the ER.* J Cell Biol, 1991. **113**: p. 35-44.

170. High, S., et al., *Sec61p is adjacent to nascent type I and type II signal-anchor proteins during their membrane insertion.* J. Cell Biol., 1993. **121**: p. 743-750.

171. High, S., et al., *Site-specific photocrosslinking reveals that Sec61P and TRAM contact different regions of a membrane inserted signal sequence.* J. Biol. Chem., 1993. **268**: p. 26745-26751.

172. Chen, W. and A. Helenius, *Role of the ribosome and translocon complex during folding of influenza hemagglutinin in the endoplasmic reticulum of living cells.* Mol. Biol. Cell, 2000. **11**: p. 765-772.

173. Kowarik, M., et al., *Protein folding during cotranslational translocation in the endoplasmic reticulum.* Mol. Cell, 2003. **10**: p. 735-744.

174. Alder, N. and A. Johnson, *Cotranslational membrane protein biogenesis at the endoplasmic reticulum.* J. Biol. Chem., 2004. **279**: p. 22787-22790.

175. Anthony, V. and W. Skach, *Molecular Mechanism of P-glycoprotein into cellular membranes.* Curr. Prot. Pept. Sci., 2002. **3**: p. 485-501.

176. Sadlish, H. and W. Skach, *Biogenesis of CFTR and other polytopic membrane proteins; new roles for the ribosome-translocon complex.* J. Mem. Biol., 2004. **202**: p. 115-126.

177. Buck, T. and W. Skach, *Differential stability of biogenesis intermediates reveals a common pathway for aquaporin-1 topological maturation.* J. Biol. Chem., 2005. **280**: p. 261-269.

178. Dohke, Y. and R.J. Turner, *Evidence that the transmembrane biogenesis of aquaporin 1 is cotranslational in intact mammalian cells.* J. Biol. Chem., 2002. **277**: p. 15215-15219.

179. Lu, Y., et al., *Reorientation of Aquaporin-1 topology during maturation in the endoplasmic reticulum.* Mol. Biol. Cell, 2000. **11**: p. 2973-2985.

180. Turnbull, I., et al., *Biogenesis and folding of aquaporin water channels in the endoplasmic reticulum.* Molecular biology and physiology of water and solute transport, ed. S. Hohmann and S. Nielson. 2000, New York: Kluwer Academic/Plenum. 49-55.

181. Goder, V. and M. Spiess, *Molecular mechanism of signal sequence orientation in the endoplasmic reticulum.* EMBO J, 2004. **22**: p. 3645-3653.

182. von Heijne, G., *Analysis of the distribution of charged residues in the N-terminal region of signal sequences: implications for protein export in prokaryotic and eukaryotic cells.* EMBO J., 1984. **3**(10): p. 2315-2318.

183. von Heijne, G., *The distribution of positively charged residues in bacterial inner membrane proteins correlates with trans-membrane topology.* EMBO J., 1986. **5**(11): p. 3021-3027.

184. Goder, V. and M. Spiess, *Topogenesis of membrane proteins: determinants and dynamics.* FEBS Lett., 2001. **504**: p. 87-93.

185. Denzer, A., C. Nabholz, and M. Spiess, *Transmembrane orientation of signal-anchor proteins is affected by the folding state but not the size of the N-terminal domain.* EMBO J, 1995. **14**: p. 6311-6317.

186. Wilkinson, B., et al., *Distinct domains within yeast Sec61p involved in post-translational translocation and protein dislocation.* J. Biol. Chem., 2000. **275**: p. 521-529.

187. Bogdanov, M., P. Heacock, and W. Dowhan, *A polytopic membrane protein displays a reversible topology dependent on membrane lipid composition.* EMBO J., 2002. **21**: p. 2107-16.

188. Zhang, W., et al., *Reversible topological organization within a polytopic membrane protein is governed by a change in membrane phospholipid composition.* J. Biol. Chem., 2003. **278**: p. 50128-35.

189. Engelman, D., *Membranes are more mosaic than fluid.* Nature, 2005. **438**: p. 578-580.

190. Bowie, J., *Solving the membrane protein folding problem.* Nature, 2005. **438**: p. 581-589.

191. Clemons, W., et al., *Structural insight into the protein translocation channel.* Curr. Opin. Struct. Biol., 2004. **14**: p. 390-396.

192. Gilmore, R., Blobel, G., *Translocation of secretory proteins across the microsomal membrane occurs through an environment accessible to aqueous perturberants.* Cell, 1985. **42**: p. 497-505.

193. Audigier, Y., M. Friedlander, and G. Blobel, *Multiple topogenic sequences in bovine opsin.* Proc. Natl. Acad. Sci. USA, 1987. **84**: p. 5783-5787.

194. Lin, J. and R. Addison, *A novel integration signal that is composed of two transmembrane segments is required to integrate the Neurospora plasma membrane H+-ATPase into microsomes.* J. Biol. Chem., 1995. **270**: p. 6935-6941.

195. Krieg, U., A. Johnson, and P. Walter, *Protein translocation across the endoplasmic reticulum membrane: Identification by photocross-linking of a 39-kD integral membrane glycoprotein as part of a putative translocation tunnel.* J. Cell Biol., 1989. **109**: p. 2033 - 2043.

196. Plath, K., et al., *Signal sequence recognition in posttranslational protein transport across the yeast ER membrane.* Cell, 1998. **94**: p. 795-807.

197. Plath, K., et al., *Interactions between Sec complex and prepro-alpha-factor during posttranslational protein transport into the endoplasmic reticulum.* Mol. Biol. Cell, 2004. **15**: p. 1-10.

198. Meacock, S., et al., *Different transmembrane domains associate with distinct endoplasmic reticulum components during membrane integration of a polytopic protein.* Mol. Biol. Cell, 2002. **13**: p. 4114-4129.

199. Laird, V. and S. High, *Discrete cross-linking products identified during membrane protein biosynthesis.* J. Biol. Chem., 1997. **272**: p. 1983-1989.

200. Simon, S.M. and G. Blobel, *A protein-conducting channel in the endoplasmic reticulum.* Cell, 1991. **65**: p. 371-380.

201. Hanein, D., et al., *Oligomeric rings of the Sec61p complex induced by ligands required for protein translocation.* Cell, 1996. **87**: p. 721-732.

202. Mingarro, I., et al., *Different conformations of nascent polypeptides during translocation across the ER membrane.* BMC Cell Biology, 2000. **1**: p. www.biomedcentral.com/1471-2121/1/3.

203. Gilbert, R., et al., *Three-dimensional structures of translating ribosomes by Cryo-EM.* Mol. Cell, 2004. **14**: p. 57-66.

204. Lu, J. and C. Deutsch, *Secondary structure formation of a transmembrane segment in Kv channels.* Biochemistry, 2005. **44**: p. 8230-8243.

205. Nissen, P., et al., *The structural basis of ribosome activity in protein synthesis.* Science, 2000. **289**: p. 920-930.

206. Ban, N., et al., *The complete atomic structure of the large ribosomal subunit at 2.4 A resolution.* Science, 2000. **289**: p. 905-920.

207. Higy, M., T. Junne, and M. Spiess, *Topogenesis of membrane proteins at the endoplasmic reticulum.* Biochemistry, 2004. **43(40)**: p. 12716-22.

208. Brodsky, J., J. Goeckeler, and R. Schekman, *BiP and Sec61p are required for both co- and posttranslational protein translocation into the yeast endoplasmic reticulum.* Proc. Hatl. Acad. Sci. USA, 1995. **92**: p. 9643-9646.

209. Rapoport, T., M. Rolls, and B. Jungnickel, *Approaching the mechanism of protein transport across the ER membrane.* Curr. Opin. Cell Biol., 1996. **8**: p. 499-504.

210. Rapoport, T., et al., *Membrane-protein integration and the role of the translocation channel.* Trends Cell Biol., 2004. **14**: p. 568-575.

211. Thrift, R.N., et al., *A nascent membrane protein is located adjacent to ER membrane proteins throughout its integration and translocation.* J. Cell Biol., 1991. **112**: p. 809-821.

212. Hegde, R. and V. Lingappa, *Membrane protein biogenesis: regulated complexity at the endoplasmic reticulum.* Cell, 1997. **91**: p. 575-582.

213. Bibi, E., *The role of the ribosome-translocon complex in translation and assembly of polytopic membrane proteins.* Trends Biochem. Sci., 1998. **23**: p. 51-55.

214. Manting, E., et al., *SecYEG assembles into a tetramer to form the active protein translocation channel.* EMBO J., 2000. **19**: p. 851-861.

215. Moss, K., et al., *Coupled translocation events generate topologic heterogeneity at the endoplasmic reticulum membrane.* Mol. Biol. Cell, 1998. **9**: p. 2681-2697.

216. Hasegawa, H., et al., *Molecular cloning of a mercurial-insensitive water channel expressed in selected water-transporting tissues.* J. Biol. Chem., 1994. **269**: p. 5498-5500.

217. Hegde, R., S. Voigt, and V. Lingappa, *Regulation of Protein Topology by trans-acting factors at the endoplasmic reticulum.* Mol. Cell, 1998. **2**: p. 85-91.

218. Kim, S., et al., *Signal Sequences control gating of the protein translocation channel in a substrate-specific manner.* Dev. Cell, 2002. **2**: p. 207-217.

219. van Geest M, L.J., *Membrane topology and insertion of membrane proteins: search for topogenic signals.* Microbiol Mol Biol Rev, 2000. **64**(1): p. 13-33.

220. Cannon, K.S., et al., *Disulfide bridge formation between SecY and a translocating polypeptide localizes the translocation pore to the center of SecY.* J Cell Biol, 2005. **169(2)**: p. 219-25.

221. Saurí A, S.S., Salgado J, Johnson AE, Mingarro I., *Double-spanning plant viral movement protein integration into the endoplasmic reticulum membrane is signal*

recognition particle-dependent, translocon-mediated, and concerted. J Biol Chem., 2005. **280**(27): p. 25907-12.

222. Oda T, I.A., *Involvement of free ribosomes in the early stage of secretory protein biosynthesis in rat liver.* J Biochem (Tokyo). 1981. **89**(5): p. 1547-54.

223. Hortsch M, A.D., Meyer DI., *Characterization of secretory protein translocation: ribosome-membrane interaction in endoplasmic reticulum.* J Cell Biol., 1986. **103**(1): p. 241-53.

224. Whitley P, N.I., von Heijne G., *A nascent secretory protein may traverse the ribosome/endoplasmic reticulum translocase complex as an extended chain.* J Biol Chem., 1996. **271**(11): p. 6241-4.

225. Kleizen, B., et al., *Folding of CFTR is predominantly cotranslational.* Molecular Cell, 2005. **20**: p. 277-287.

226. Borgese N, M., W, Kreibich G, Sabatini D, *Ribosomal-membrane interaction: In vitro binding of ribosomes to microsomal membranes.* Journal of Molecular Biology, 1973. **88**(3): p. 559-580.

227. Oberdorf, J., D. Pitonzo, and W. Skach, *An energy-dependent maturation step is required for release of the cystic fibrosis transmembrane conductance regulator from early endoplasmic reticulum biosynthetic machinery.* J. Biol. Chem., 2005. **280**: p. 38193-38202.

228. Pitonzo, D. and W. Skach, *Molecular mechanisms of aquaporin biogenesis by the endoplasmic reticulum Sec61 translocon.* Bioch. Biophys. Acta, 2006. **1758**: p. 976-988.

229. Shimohata N, N.S., Akiyama Y, Kaback HR, Ito K., *SecY alterations that impair membrane protein folding and generate a membrane stress.* J Cell Biol., 2007. **176**(3): p. 307-17.

230. Walters RF, D.W., *Helix-packing motifs in membrane proteins.* Proc Natl Acad Sci U S A., 2006. **103**(37): p. 13658-63.

231. Cotten, J. and M. Melsh, *Cystic fibrosis-associated mutations at arginine 347 alter the pore architecture of CFTR: evidence for disruption of a salt bridge.* J. Biol. Chem., 1999. **274**: p. 5429-5435.

232. Hasegawa, H., et al., *A multifunctional aqueous channel formed by CFTR.* Science, 1992. **258**: p. 1477-1479.

233. Welsh, M. and A. Smith, *Molecular mechanisn of CFTR chloride channel dysfunction in cystic fibrosis.* Cell, 1993. **73**: p. 1251-1254.

234. Pasyk, E. and K. Foskett, *Mutant (ΔF508) cystic fibrosis transmembrane conductance regulator Cl- channel is functional when retained in the endoplasmic reticulum of mammalian cells.* J. Biol. Chem., 1995. **270**: p. 12347-12350.

235. Zhang, F., N. Kartner, and G. Lukacs, *Limited proteolysis as a probe for arrested conformational maturation of ΔF508 CFTR.* Nature Structural Biology, 1998. **5**: p. 180-183.

236. Ward, C., C. Omura, and R. Kopito, *Degradation of CFTR by the ubiquitin-proteosome pathway.* Cell, 1995. **83**: p. 121-128.

237. Chen, M. and J. Zhang, *Topogenesis of cystic fibrosis transmembrane conductance regulator (CFTR): regulation by the amino terminal transmembrane sequences.* Biochemistry, 1999. **38**: p. 5471-5477.

238. Tector, M. and F. Hartl, *An unstable transmembrane segment in the cystic fibrosis transmembrane conductance regulator*. EMBO J, 1999. **18**: p. 6290-6298.

239. Pind, S., J. Riordan, and D. Williams, *Participation of the endoplasmic reticulum chaperone calnexin (p88, IP90) in the biogenesis of the cystic fibrosis transmembrane conductance regulator*. J. Biol. Chem., 1994. **269**: p. 12784-8.

240. Cyr, D., T. Langer, and M. Douglas, *Dna-J-like proteins: molecular chaperones and specific regulators of Hsp70*. TIBS, 1994. **19**: p. 176-181.

241. Jiang, J., et al., *CHIP is a U-box-dependent E3 ubiquitin ligase: Identification of Hsc70 as a target for ubiquitylation*. J. Biol. Chem., 2001. **276**: p. 42938-42934.

242. Meacham, G., et al., *The Hdj-2/Hsc70 chaperone pair facilitates early steps in CFTR biogenesis*. EMBO J., 1999. **18**: p. 1492-1505.

243. Strickland, E., et al., *The molecular chaperone Hsc70 assists the in vitro folding of the N-terminal nucleotide-binding domain of the cystic fibrosis transmembrane conductance regulator*. J. Biol. Chem., 1997. **272**: p. 25421-25424.

244. Younger, J., et al., *A foldable CFTRΔF508 biogenic intermediate accumulates upon inhibition of the Hsc70-CHIP E3 ubiquitin ligase*. J. Cell BIol., 2004. **167**: p. 1075-1085.

245. Meacham, G., et al., *The Hsc70 co-chaperone CHIP targets immature CFTR for proteasomal degradation*. Nat. Cell Biol., 2001. **3**: p. 100-105.

246. Jiang, C., et al., *Partial restoration of cAMP-stimulated CFTR chloride channel activity in DeltaF508 cells by deoxyspergulin*. Am. J. Physiol., 1996. **275**: p. C171-8.

247. Zhang, H., et al., *Cysteine string protein interacts with and modulates the maturation of the cystic fibrosis transmembrane conductance regulator.* J. Biol. Chem., 2002. **277**: p. 28948-28958.

248. Youker, R., et al., *Distinct Roles for the Hsp40 and Hsp90 Molecular Chaperones during Cystic Fibrosis Transmembrane Conductance Regulator Degradation in Yeast.* Mol. Biol. Cell, 2004. **15**: p. 4787-4797.

249. Wang, X., et al., *COPII-dependent export of cystic fibrosis transmembrane conductance regulator from the ER uses a di-acidic exit code.* J. Cell. Biol., 2004. **167**: p. 65-74.

250. de Silve, A., I. Braakman, and A. Helenius, *Posttranslational folding of vesicular stomatitis virus G protein in the ER: involvement of noncovalent and covalent complexes.* J. Cell Biol., 1993. **120**: p. 647-655.

251. Marqardt, T., D. Hebert, and A. Helenius, *Post-translational folding of influenza hemagglutinin in isolated endoplasmic reticulum-derived microsomes.* J. Biol. Chem., 1993. **268**: p. 19618-19625.

252. Jansens, A., E. Duijn, and I. Braakman, *Coordinated nonvectorial folding in a newly synthesized multidomain protein.* Science, 2002. **298**: p. 2401-2403.

253. Buck, T., J. Eledge, and W. Skach, *Stabilization of Aquaporin-2 folding mutants by N-linked glycosylation in the endoplasmic reticulum.* Am. J. Physiol., 2004. **287**: p. C1292-C1299.

254. Oberdorf, J. and W. Skach, *In vitro reconstitution of CFTR biogenesis and degradation.* Cystic Fibrosis Methods and Protocols ed. Methods in Molecular Medicine, ed. W. Skach. Vol. 70. 2002, Totowa, NJ: Humana Press Inc. 295-310.

255. Jackson, R. and T. Hunt, *Preparation and use of nuclease-treated rabbit reticulocyte lysates for the translation of eukaryotic messenger RNA.* Methods in Enzymology, *1983.* ***96****: p. 50-74.*

256. Walter, P. and G. Blobel, *Preparation of microsomal membranes for cotranslational protein translocation.* Methods in Enzymology, ed. S. Fleischer and B. Fleischer. Vol. 96. 1983, New York: Academic Press, Inc. 84-93.

257. Oberdorf, J., E. Carlson, and W. Skach, *Redundancy of proteasome ß subunit function during endoplasmic reticulum associated degradation.* Biochem., 2001. **40**: p. 13397-13305.

258. Skach, W., *Topology of P-glycoproteins.* Methods in Enzymology, ed. S. Ambudkar and M. Gottesman. Vol. 292. 1998, San Diego: Academic Press Inc. 265-277.

259. Fuller, W. and A. Cuthbert, *Post-translational disruption of the delta F508 cystic fibrosis transmembrane conductance regulator (CFTR)-molecular chaperone complex with geldanamycin stabilizes delta F508 CFTR in the rabbit reticulocyte lysate.* J. Biol. Chem., 2000. **275**: p. 37462-37468.

260. Wang, L. and B. Dobberstein, *Oligomeric complexes involved in translocation of proteins across the membrane of the endoplasmic reticulum.* FEBS letters, 1999. **457**: p. 316-322.

261. Osborne, A.R., T.A. Rapoport, and B. van den Berg, *Protein translocation by the Sec61/SecY channel.* Annu. Rev. Cell. Dev. Biol., 2005. **21**: p. 529-550.

262. Ohrui, T., et al., *Radiotracer studies of CFTR expressed in Xenopus oocytes.* Am. J. Physiol. (Cell. Physiol.), 1994. **266 (Cell Physiol)**: p. C1586-C1593.

263. Patrick, T., C. Lewer, and V. Pain, *Preparation and characterization of cell-free protein synthesis systems from oocytes and egges of Xenopus laevis.* Development, 1989. **106**: p. 1-9.

264. Chen, C.-J., et al., *Internal duplication and homology with bacterial transport proteins in the mdr1 (P-glycoprotein) gene from multidrug resistant human cells.* Cell, 1986. **47**: p. 381-389.

265. Chen, M. and J. Zhang, *Membrane insertion, processing and topology of cystic fibrosis transmembrane conductance regulator in microsomal membranes.* Mol. Memb. Biol., 1996. **13**: p. 33-40.

266. Potter, M. and C. Nicchitta, *Regulation of ribosome detachment from the mammalian endoplasmic reticulum membrane.* J. Biol. Chem., 2000. **275**: p. 33828-33835.

267. Seiser, R. and C. Nicchitta, *The fate of membrane-bound ribosomes following the termination of protein synthesis.* J. Biol. Chem., 2000. **275**: p. 33820-33827.

268. Mothes, W., et al., *Signal sequence recognition in cotranslational translocation by protein components of the endoplasmic reticulum.* J. Cell Biol., 1998. **142**: p. 355-364.

269. Shi, L.-B., W. Skach, and A. Verkman, *Functional independence of monomeric CHIP28 sater channels revealed by expression of wild-type-mutant heterodimers.* J. Biol. Chem., 1994. **269**: p. 10417-10422.

270. Ostedgaard, L., et al., *Association of domains within the cystic fibrosis transmembrane conductance regulator.* Biochemistry, 1997. **36**: p. 1287-1294.

271. Therien, A., F. Grant, and C. Deber, *Interhelical hydrogen bonds in the CFTR membrane domain.* Nature Struct. Biol., 2001. **8**: p. 597-601.

272. Bear, C., et al., *CL- channel activity in Xenopus oocytes expressing the cystic fibrosis gene.* J. Biol. Chem., 1991. **266**: p. 19142-19145.

273. Loo, T. and D. Clark, *Reconstitution of drug-stimulated ATPase activity following co-expression of each half of human P-glycoprotein as separate polypeptides.* J. Biol. Chem., 1994. **269**: p. 7750-7755.

274. Ismail, N., S. Crawshaw, and S. High, *Active and passive displacement of transmembrane domains during opsin biogenesis at the Sec61 translocon.* J. Cell Sci., 2006. **119**: p. 2826-2836.

275. Okiyoneda T, H.K., Takeya M, Yamahira K, Wada I, Shuto T, Suico MA, Hashimoto Y, Kai H., *Delta F508 CFTR pool in the endoplasmic reticulum is increased by calnexin overexpression.* Mol Biol Cell., 2004. **15**(2): p. 563-74.

276. Wessels, H. and M. Spiess, *Insertion of a multispanning membrane protein occurs sequentially and requires only one signal sequence.* Cell, 1988. **55**: p. 61-70.

277. Ogura T, W.A., *AAA+ superfamily ATPases: common structure--diverse function.* Genes Cells., 2001. **6**(7): p. 575-97.

278. Mayer, T., T. Braun, and S. Jentsch, *Role of the proteasome in membrane extraction of a short-lived ER-transmembrane protein.* EMBO J, 1998. **17**: p. 3251-3257.

279. Plemper, R., et al., *Endoplasmic reticulum degradation of a mutated ATP-binding cassette transporter Pdr5 proceeds in a conserted action of Sec61 and the proteasome.* J. Biol. Chem, 1998. **273**: p. 32848-856.

280. Ye, Y., H. Meyer, and T. Rapoport, *The AAA-ATPase Cdc48/p97 and its partners transport proteins from the ER into the cytosol.* Nature, 2001. **414**: p. 652-656.

281. McCracken, A. and J. Brodsky, *Evolving questions and paradigm shifts in endoplasmic-reticulum-associated degradation (ERAD).* BioEssays, 2003. **25**: p. 868-877.

282. Pickart CM, C.R., *Proteasomes and their kin: proteases in the machine age.* Nat Rev Mol Cell Biol., 2004. **5**(3): p. 177-87.

283. Glickman MH, R.D., Fried VA, Finley D., *The regulatory particle of the Saccharomyces cerevisiae proteasome.* Mol Cell Biol., 1998. **18**(6): p. 3149-62.

284. Bays, N. and R. Hampton, *Cdc48-Ufd1-Npl4: Stuck in the middle with Ub.* Current Biol., 2002. **12**: p. R366-371.

285. Dai RM, C.E., Longo DL, Gorbea CM, Li CC., *nvolvement of valosin-containing protein, an ATPase Co-purified with IkappaBalpha and 26 S proteasome, in ubiquitin-proteasome-mediated degradation of IkappaBalpha.* J Biol Chem., 1998. **273**(6): p. 3562-3573.

286. Kalies KU, A.S., Sergeyenko T, Kröger H, Römisch K., *The protein translocation channel binds proteasomes to the endoplasmic reticulum membrane.* EMBO J., 2005. **24**(13): p. 2284-93.

287. Schuberth C, B.A., *Membrane-bound Ubx2 recruits Cdc48 to ubiquitin ligases and their substrates to ensure efficient ER-associated protein degradation.* Nat Cell Biol., 2005. **7**(10): p. 999-1006.

288. Neuber, O., et al., *Ubx2 links the Cdc48 complex to ER-associated protein degradation.* Nat. Cell Biol., 2005. **7**: p. 993-998.

289. Zhong X, S.Y., Ballar P, Apostolou A, Agami R, Fang S., *AAA ATPase p97/valosin-containing protein interacts with gp78, a ubiquitin ligase for endoplasmic reticulum-associated degradation.* J Biol Chem., 2004. **279**(44): p. 45676-84.

290. Lilley BN, P.H., *A membrane protein required for dislocation of misfolded proteins from the ER.* Nature., 2004. **429**: p. 834-40.

291. Ye, Y., et al., *A membrane protein complex mediates retro-translocation from the ER lumen into the cytosol.* Nature, 2004. **429**: p. 841-847.

292. Köhler A, C.P., Leggett DS, Woo KM, Goldberg AL, Finley D., *The axial channel of the proteasome core particle is gated by the Rpt2 ATPase and controls both substrate entry and product release.* Mol Cell., 2001. **7**(6): p. 1143-52.

293. Braun, B., et al., *The base of the proteasome regulatory particle exhibits chaperone-like activity.* Nature Cell Biol., 1999. **1**: p. 221-226.

294. Liu Z, T.V., Akoev V, Zolkiewski M., *Conserved amino acid residues within the amino-terminal domain of ClpB are essential for the chaperone activity.* J Mol Biol, 2002. **321**: p. 111-20.

295. Babbitt SE, K.A., Deffenbaugh AE, Chang YH, Bailly E, Erdjument-Bromage H, Tempst P, Buranda T, Sklar LA, Baumler J, Gogol E, Skowyra D., *ATP*

hydrolysis-dependent disassembly of the 26S proteasome is part of the catalytic cycle. Cell., 2005. **12**(4): p. 553-65.

296. Navon, A. and A. Goldberg, *Proteins are unfolded on the surface of the ATPase ring before transport into the proteasome.* Molecular Cell, 2001. **8**: p. 1339-1349.

297. Ortega J, S.S., Ishikawa T, Maurizi MR, Steven AC., *Visualization of substrate binding and translocation by the ATP-dependent protease, ClpXP.* Mol Cell., 2000. **6**(6): p. 1515-21.

298. Lee, R., et al., *Uncouupling retro-translocation and degradation in the ER-associated degradation of a soluble protein.* EMBO J., 2004. **23**: p. 2206-2215.

299. Verma R, O.R., Graumann J, Deshaies RJ., *Multiubiquitin chain receptors define a layer of substrate selectivity in the ubiquitin-proteasome system.* Cell, 2004. **118**(1): p. 99-110.

300. Richly H, R.M., Braun S, Rumpf S, Hoege C, Jentsch S., *A series of ubiquitin binding factors connects CDC48/p97 to substrate multiubiquitylation and proteasomal targeting.* Cell, 2005. **120**(1): p. 73-84.

301. Gnann, A., J. Riordan, and D. Wolf, *Cystic fibrosis transmembrane conductance regulator degradation depends on the lectins Htmm1p/EDEM and the cdc48 complex in yeast.* Mol. Biol. Cell, 2004. **15**: p. 4125-4135.

302. Huyer G, P.W., Fansler Z, Kreft SG, Hochstrasser M, Brodsky JL, Michaelis S., *Distinct machinery is required in Saccharomyces cerevisiae for the endoplasmic reticulum-associated degradation of a multispanning membrane protein and a soluble luminal protein.* J Biol Chem., 2004. **279**(37): p. 38369-78.

303. Bays, N., et al., *HRD4/NPL4 is required for the proteasomal processing of ubiquitinated ER proteins*. Mol. Biol. Cell, 2001. **12**: p. 4114-4128.

304. Rabinovich, E., et al., *AAA-ATPase p97/Cdc48p, a cytosolic chaperone required for endoplasmic reticulum-associated protein degradation*. Mol. Cell Biol., 2002. **22**: p. 626-634.

305. Rape, M., et al., *Mobilization of processed, membrane -tethered SPT23 transcription factor by CDC48(Ufd1/Npl4), a ubiquitin-selective chaperone*. Cell, 2001. **107**: p. 667-677.

306. Hitchcock AL, K.H., Frietze S, Lin A, Latterich M, Silver PA., *The conserved npl4 protein complex mediates proteasome-dependent membrane-bound transcription factor activation*. Mol Biol Cell., 2001. **12**(10): p. 3226-41.

307. Jarosch, E., et al., *Protein dislocation from the ER requires polyubiquitination and the AAA-ATPase Cdc48*. Nature Cell Biol., 2002. **4**: p. 134-139.

308. Elkabetz Y, S.I., Rabinovich E, Bar-Nun S., *Distinct steps in dislocation of luminal endoplasmic reticulum-associated degradation substrates: roles of endoplamic reticulum-bound p97/Cdc48p and proteasome*. J Biol Chem., 2004. **279**(6): p. 3980-9.

309. Dalal S, R.M., Cyr DM, Hanson PI., *Distinct roles for the AAA ATPases NSF and p97 in the secretory pathway*. Mol Biol Cell., 2004. **15**(2): p. 637-48.

310. Giaever, G., et al, *Functional profiling of the Saccharomyces cerevisiae genome*. Nature, 2002. **418**: p. 387-391.

311. Moir D, S.S., Osmond BC, Botstein D., *Cold-sensitive cell-division-cycle mutants of yeast: isolation, properties, and pseudoreversion studies.* Genetics, 1982. **100**(4): p. 547-63.

312. Wójcik C, Y.M., DeMartino GN., *RNA interference of valosin-containing protein (VCP/p97) reveals multiple cellular roles linked to ubiquitin/proteasome-dependent proteolysis.* J Cell Sci., 2004. **117**(pt 2): p. 281-92.

313. Gusarova V, C.A., Brodsky JL, Fisher EA., *Apoprotein B degradation is promoted by the molecular chaperones hsp90 and hsp70.* J Biol Chem., 2001. **276**(27): p. 24891-900.

314. Qu, D., et al., *Degradation of a mutant secretory protein, alpha1-antitrypsin Z, in the endoplasmic reticulum requires proteasome activity.* J. Biol. Chem, 1996. **271**: p. 22971-22975.

315. Oberdorf, J., et al., *Uncoupling proteasome peptidase and ATPase activities results in cytosolic release of an ER polytopic protein.* J Cell Sci, 2006. **119(Pt) 2**: p. 303-13.

316. Kondo H, R.C., Newman R, Levine TP, Pappin D, Freemont P, Warren G., *p47 is a cofactor for p97-mediated membrane fusion.* Nature, 1997. **388**: p. 75-8.

317. Johnson ES, M.P., Ota IM, Varshavsky A., *A proteolytic pathway that recognizes ubiquitin as a degradation signal.* J Biol Chem., 1995. **270**(29): p. 17442-56.

318. Baumeister, W., et al., *The proteasome: paradigm of a self-compartmentalizing protease.* Cell, 1998. **92**: p. 367-380.

319. Lee, C., et al., *ATP-dependent proteases degrade their substrates by processively unraveling them from the degradation signal.* Mol. Cell, 2001. **7**: p. 627-637.

311. Moir D, S.S., Osmond BC, Botstein D., *Cold-sensitive cell-division-cycle mutants of yeast: isolation, properties, and pseudoreversion studies.* Genetics, 1982. **100**(4): p. 547-63.

312. Wójcik C, Y.M., DeMartino GN., *RNA interference of valosin-containing protein (VCP/p97) reveals multiple cellular roles linked to ubiquitin/proteasome-dependent proteolysis.* J Cell Sci., 2004. **117**(pt 2): p. 281-92.

313. Gusarova V, C.A., Brodsky JL, Fisher EA., *Apoprotein B degradation is promoted by the molecular chaperones hsp90 and hsp70.* J Biol Chem., 2001. **276**(27): p. 24891-900.

314. Qu, D., et al., *Degradation of a mutant secretory protein, alpha1-antitrypsin Z, in the endoplasmic reticulum requires proteasome activity.* J. Biol. Chem, 1996. **271**: p. 22971-22975.

315. Oberdorf, J., et al., *Uncoupling proteasome peptidase and ATPase activities results in cytosolic release of an ER polytopic protein.* J Cell Sci, 2006. **119(Pt) 2**: p. 303-13.

316. Kondo H, R.C., Newman R, Levine TP, Pappin D, Freemont P, Warren G., *p47 is a cofactor for p97-mediated membrane fusion.* Nature, 1997. **388**: p. 75-8.

317. Johnson ES, M.P., Ota IM, Varshavsky A., *A proteolytic pathway that recognizes ubiquitin as a degradation signal.* J Biol Chem., 1995. **270**(29): p. 17442-56.

318. Baumeister, W., et al., *The proteasome: paradigm of a self-compartmentalizing protease.* Cell, 1998. **92**: p. 367-380.

319. Lee, C., et al., *ATP-dependent proteases degrade their substrates by processively unraveling them from the degradation signal.* Mol. Cell, 2001. **7**: p. 627-637.

320. White, S. and W. Wimley, *Membrane protein folding and stability: physical principles*. Annu. Rev. Biophys. Biomol. Struct., 1999. **28**: p. 319-365.

321. DeLaBarre B, B.A., *Complete structure of p97/valosin-containing protein reveals communication between nucleotide domains.T.* Nat Struct Biol., 2003. **10**(10): p. 856-63.

322. Hartmann-Petersen R, G.C., *Proteins interacting with the 26S proteasome.* Cell Mol Life Sci., 2004. **61**(13): p. 1589-95.

323. Du K, S.M., Lukacs GL., *The DeltaF508 cystic fibrosis mutation impairs domain-domain interactions and arrests post-translational folding of CFTR.* Nat Struct Mol Biol., 2005. **12**(1): p. 17-25.

324. Qu, B., E. Strickland, and P. Thomas, *Localization and suppression of a kinetic defect in cystic fibrosis transmembrane conductance regulator folding.* J. Biol. Chem., 1997. **272**: p. 15739-15744.

325. Kenniston, J.A., et al., *Linkage between ATP consumption and mechanical unfolding during the protein processing reactions of an AAA+ degradation machine.* Cell, 2003. **114**(4): p. 511-20.

326. Kenniston, J.A., T.A. Baker, and R.T. Sauer, *Partitioning between unfolding and release of native domains during ClpXP degradation determines substrate selectivity and partial processing.* Proceedings of the National Academy of Sciences of the United States of America, 2005. **102**(5): p. 1390-5.

327. Carlson, E., et al., *Reticulocyte lysate as a model system to study ER membrane protein degradation.* Methods in Molecular Biology: Ubiquitin proteasome

protocol, ed. C. Patterson and D. Cyr. Vol. In Press. 2005, Totowa, NJ: Humana Press Inc. In Press.